



for geotechnics & structures

DYNAMICS IN ZSOIL

Report 100101

(revised 02.01.2021)

A. Truty

Th. Zimmermann

GeoDev.

PO Box CH-1001 Lausanne
Switzerland
<https://zsoil.com>

Contents

1	INTRODUCTION	7
2	THEORY	9
2.1	Equations of motion for single phase media	9
2.1.1	Nonlinear algorithms for arbitrary dynamic input for single phase media	9
2.1.2	Absorbing boundaries for single-phase media	12
2.2	Equations of motion for dynamic consolidation of two-phase fully or partially saturated media	13
2.2.1	Nonlinear algorithms for arbitrary dynamic input for two-phase media	15
2.2.2	Absorbing boundaries for dynamic consolidation of two-phase media .	17
2.3	Mesh size and time stepping	19
2.4	Seismic input	19
2.4.1	Rigid base model	20
2.4.2	Compliant base model	21
3	SOIL-STRUCTURE INTERACTION PROBLEMS	25
3.1	Domain Reduction Method (DRM) for single-phase media	25
3.2	DRM metod for two-phase media	30
4	CONSTITUTIVE MODELS FOR DYNAMIC APPLICATIONS	35
4.1	HS-s model	35
4.2	Densification model	37
4.2.1	Sawicki's model for time domain applications	38
4.2.2	User interface for densification model	41
5	USER INTERFACE	45
5.1	Transient dynamic driver	45
5.2	Eigenvalue and eigenmodes driver	51
5.3	Seismic input	53

5.3.1	Baseline correction to ground motion acceleration time histories . . .	56
5.3.2	Linear deconvolution of seismic records	58
5.4	Absorbing boundaries	61
5.5	DRM modeling components	63
5.5.1	Setting boundary and external layers in the preprocessor	63
5.5.2	Running DRM models with preprocessed free field motion	64
5.6	Initial conditions	65
5.7	Boundary conditions	66
5.7.1	Solid BC	66
5.7.2	Periodic BC	67
6	BENCHMARKS	69
6.1	Eigenvalues and eigenmodes	69
6.1.1	Natural vibrations of cantilever beam	69
6.1.1.1	Simulations using 2-node linear beam elements	69
6.1.1.2	Simulations using quadrilateral 4-node shell elements	71
6.1.1.3	Simulations using quadrilateral 4-node continuum elements	71
6.1.1.4	Simulations using brick 8-node continuum elements	71
6.1.2	Natural vibrations of a bar	72
6.1.2.1	Simulations using truss elements	72
6.1.2.2	Simulations using linear 2-node beam elements	73
6.1.2.3	Simulations using 2D 4-node continuum elements	73
6.1.2.4	Simulations using 3D 8-node continuum elements	74
6.1.2.5	Simulations using shell elements	74
6.1.3	Natural vibrations of shear layer	74
6.2	Baseline correction and Butterworth filtering of earthquake records	75
6.3	1D dynamic consolidation	75
6.4	Absorbing boundaries	81
6.4.1	Absorbing boundaries for single-phase media	81
6.4.2	Absorbing boundaries for dynamic consolidation	84
6.5	Soil-structure interaction via DRM method	89
6.5.1	Beam-subsoil interaction via DRM method, 1D example	89
6.5.2	Beam-subsoil interaction via DRM method, 2D example	96
6.6	Application of densification model	105
6.6.1	Cyclic simple shear test with strain control	105

6.6.2	Static liquefaction problem	106
6.6.3	Cyclic undrained triaxial test	107
6.6.4	Dynamic shear layer problem (dry medium)	110
6.6.5	Layer subject to San Fernando earthquake (dry medium)	112
6.6.6	Liquefaction of sand layer subject to San Fernando earthquake (two-phase consolidation)	113
6.7	Baseline correction and Butterworth filtering	115
6.7.1	Example of baseline correction and Butterworth filtering	115
6.8	Linear deconvolution	117
6.8.1	Convolution analysis for undamped soil layer on rigid base	117
6.8.2	Deconvolution analysis for undamped soil layer on rigid base	120
6.8.3	Convolution analysis for damped soil layer on rigid base	124
6.8.4	Deconvolution analysis for damped soil layer on rigid base	127
6.8.5	Convolution analysis for damped soil layer on compliant base	131
6.8.6	Rigid vs compliant base models	134

List of modifications

1. An extra cosine taper filter was removed from Butterworth filtering; it is not needed anymore
2. Linear deconvolution to transfer signals from control point to the base has been added
3. A compliant base model has been added in menu for seismic input; this helps to cancel standing waves in cases when assumed damping is insufficient
4. Benchmarks concerning convolution/deconvolution analysis have been added

Chapter 1

INTRODUCTION

The current development in the field of dynamics is limited to the time history analysis. This procedure, as the most versatile one for nonlinear applications, was extended to soil-structure interaction problems for both single-phase and two-phase partially saturated media. In addition extraction of eigenmodes and eigenvalues were added. The theoretical background, implementation schemes, user interface and finally applications and benchmarks will be presented in the following chapters.

Chapter 2

THEORY

2.1 Equations of motion for single phase media

In the time history analysis, for given solution for accelerations, velocities and displacements at time t_n , we seek for the solution at time t_{n+1} by solving the following discretized (in time and space) equations of motion

$$\mathbf{M}\mathbf{a} + \mathbf{C}\mathbf{v} + \mathbf{N}(\mathbf{d}) = \mathbf{F}_{\text{ext}} \quad (2.1)$$

where nodal accelerations, velocities and displacements are denoted by \mathbf{a} , \mathbf{v} and \mathbf{d} respectively. The $\mathbf{N}(\mathbf{d})$ is a nonlinear vector of internal forces, the \mathbf{F}_{ext} is the external force vector, \mathbf{M} is the mass matrix (lumped or consistent) and \mathbf{C} is the damping matrix. The Rayleigh damping [2] is used here, i.e.:

$$\mathbf{C} = \alpha_o \mathbf{M} + \beta_o \mathbf{K} \quad (2.2)$$

where α_o and β_o are obtained by imposing damping rates at two different modal frequencies (i, j): For information about applicable damping rates see e.g. [Bachmann]

$$\begin{Bmatrix} \xi_i \\ \xi_j \end{Bmatrix} = 0.5 \begin{bmatrix} 1/\omega_i & \omega_j \\ 1/\omega_j & \omega_i \end{bmatrix} \begin{Bmatrix} \alpha_o \\ \beta_o \end{Bmatrix} \quad (2.3)$$

Remarks:

1. \mathbf{C} takes into account minor nonlinearities ignored in $\mathbf{N}(\mathbf{d})$
2. \mathbf{K} can be the initial or a tangent stiffness matrix

2.1.1 Nonlinear algorithms for arbitrary dynamic input for single phase media

Newmark algorithm is one of the most common in transient dynamics. The following implementation scheme is given by Hughes [4]. Let us consider equilibrium state at any time instance $t_{n+1} = (n + 1) \cdot \Delta t$

Window 2-1: Nonlinear Newmark algorithm

ZSoil®

The algorithm consists of the following 3 equations:

$$\mathbf{M}\mathbf{a}_{n+1} + \mathbf{C}\mathbf{v}_{n+1} + \mathbf{N}(\mathbf{d}_{n+1}) = \mathbf{F}_{n+1}$$

with

$$\begin{aligned}\mathbf{d}_{n+1} &= \mathbf{d}_n + \Delta t \mathbf{v}_n + \frac{\Delta t^2}{2} [(1 - 2\beta)\mathbf{a}_n + 2\beta\mathbf{a}_{n+1}] \\ \mathbf{v}_{n+1} &= \mathbf{v}_n + \Delta t [(1 - \gamma)\mathbf{a}_n + \gamma\mathbf{a}_{n+1}]\end{aligned}$$

where subscripts n and $n + 1$ indicate values at instances t_n and t_{n+1} , respectively. The algorithm is completed by the following predictors

$$\begin{aligned}\tilde{\mathbf{d}}_{n+1} &= \mathbf{d}_n + \Delta t \mathbf{v}_n + \frac{\Delta t^2}{2} (1 - 2\beta)\mathbf{a}_n \\ \tilde{\mathbf{v}}_{n+1} &= \mathbf{v}_n + (1 - \gamma)\Delta t \mathbf{a}_n\end{aligned}$$

and correctors:

$$\begin{aligned}\mathbf{d}_{n+1} &= \tilde{\mathbf{d}}_{n+1} + \beta \Delta t^2 \mathbf{a}_{n+1} \\ \mathbf{v}_{n+1} &= \tilde{\mathbf{v}}_{n+1} + \gamma \Delta t \mathbf{a}_{n+1}\end{aligned}$$

Window 2-1

As the problem to be solved is nonlinear, an iterative procedure is needed; Newton-Raphson procedure is used here to linearize the problem. Let's consider the static procedure first.

Window 2-2: Static Newton-Raphson procedure

ZSoil®

Let superscript $(i + 1)$ indicates iteration, in the vicinity of the displacement \mathbf{d}_{n+1}^{i+1}

$$\begin{aligned}\mathbf{N}(\mathbf{d}_{n+1}^{i+1}) &\cong \mathbf{N}(\mathbf{d}_{n+1}^i) + \frac{d\mathbf{N}}{d\mathbf{d}} \Delta \mathbf{d} = \mathbf{N}(\mathbf{d}_{n+1}^i) + \mathbf{K}_T \Delta \mathbf{d} \\ \mathbf{d}_{n+1}^{i+1} &= \mathbf{d}_{n+1}^i + \Delta \mathbf{d}\end{aligned}$$

hence:

$$\begin{cases} \mathbf{K}_T \Delta \mathbf{d} = \mathbf{F}_{n+1} - \mathbf{N}(\mathbf{d}_{n+1}^i) \\ \mathbf{d}_{n+1}^{i+1} = \mathbf{d}_{n+1}^i + \Delta \mathbf{d} \end{cases} \quad (\text{with } \mathbf{d}_{n+1}^0 = \mathbf{d}_n)$$

Convergence is reached when:

$$\|\mathbf{F}_{n+1} - \mathbf{N}(\mathbf{d}_{n+1}^{i+1})\| < \text{TOLERANCE}$$

Remarks:

The following algorithmic alternatives are possible:

1. Update \mathbf{K} at each step and iteration: full Newton-Raphson
2. Update \mathbf{K} at certain time steps and/or iterations: modified Newton-Raphson
3. $\mathbf{K}_T = \mathbf{K}_0$: constant stiffness algorithm

Window 2-2

Let's now consider the corresponding DYNAMIC PROCEDURE in terms of incremental displacements $\Delta \mathbf{d}$

Window 2-3: Nonlinear dynamic Newton-Raphson-Newmark procedure

ZSoil®

Equivalent static formulation

Let's define an equivalent static problem:

$$\mathbf{N}^*(\mathbf{d}) = \mathbf{M}\mathbf{a} + \mathbf{C}\mathbf{v} + \mathbf{N}(\mathbf{d})$$

$$\mathbf{K}^* = \left(\frac{d\mathbf{N}^*}{d\mathbf{d}} \right) = \frac{\mathbf{M}}{\Delta t^2 \beta} + \frac{\gamma}{\Delta t \beta} \mathbf{C}_T + \mathbf{K}_T$$

1. Initialization

$$\mathbf{d}_0 = \mathbf{d}(0)$$

$$\mathbf{v}_0 = \mathbf{v}(0)$$

 2. For each Δt

A: Compute predictors

$$\tilde{\mathbf{d}}_{n+1} = \mathbf{d}_n + \Delta t \mathbf{v}_n + (1 - 2\beta) \frac{\Delta t^2}{2} \mathbf{a}_n$$

$$\tilde{\mathbf{v}}_{n+1} = \mathbf{v}_n + (1 - \gamma) \Delta t \mathbf{a}_n$$

$$\mathbf{d}_{n+1}^{i=0} = \tilde{\mathbf{d}}_{n+1}$$

$$\mathbf{v}_{n+1}^{i=0} = \tilde{\mathbf{v}}_{n+1}$$

$$\mathbf{a}_{n+1}^{i=0} = \mathbf{0}$$

B: For each $\Delta \mathbf{d}$

i. Solve

$$\Delta \mathbf{F}_{n+1}^i = \mathbf{F}_{n+1} - \mathbf{N}^*(\mathbf{d}_{n+1}^i)$$

$$\mathbf{K}^* \Delta \mathbf{d} = \Delta \mathbf{F}_{n+1}^i$$

$$\mathbf{d}_{n+1}^{i+1} = \mathbf{d}_{n+1}^i + \Delta \mathbf{d}$$

ii. Compute correctors

$$\mathbf{a}_{n+1}^{i+1} = \frac{\mathbf{d}_{n+1}^{i+1} - \tilde{\mathbf{d}}_{n+1}}{\Delta t^2 \beta}$$

$$\mathbf{v}_{n+1}^{i+1} = \tilde{\mathbf{v}}_{n+1} + \Delta t \gamma \mathbf{a}_{n+1}^{i+1}$$

iii. Next iteration if $\|\Delta \mathbf{F}_{n+1}^i\| > TOLERANCE \Rightarrow i = i + 1$

C: Next time step

$$\text{if } t < T_{max} \Rightarrow n = n + 1$$

Remarks: The following algorithmic alternative are possible:

1. Update \mathbf{K}_T at each step and iteration: full Newton-Raphson
2. Update \mathbf{K} at certain time steps and/or iterations: modified Newton-Raphson
3. $\mathbf{K}_T = \mathbf{K}_0$: constant stiffness algorithm
4. The algorithm does not work for $\beta = 0$. A similar algorithm, expressed in terms of incremental accelerations $\Delta \mathbf{a}$, can be derived which supports $\beta = 0$.

Window 2-3

High frequencies introduce noise into the numerical solution. To overcome this problem a Nonlinear HHT- α algorithm [3] for arbitrary dynamic input is developed in ZSoil.

Window 2-4: HHT- α algorithm

ZSoil®

The original **linear** form of the algorithm is written:

$$\mathbf{M}\mathbf{a}_{n+1} + (1 + \alpha)\mathbf{C}\mathbf{v}_{n+1} - \alpha\mathbf{C}\mathbf{v}_n + (1 + \alpha)\mathbf{K}\mathbf{d}_{n+1} - \alpha\mathbf{K}\mathbf{d}_n = \mathbf{F}_{n+\alpha}$$

with

$$[*]_{n+\alpha} = (1 + \alpha)[*]_{n+1} - \alpha[*]_n$$

thus

$$\mathbf{F}_{n+\alpha} = (1 + \alpha)\mathbf{F}_{n+1} - \alpha\mathbf{F}_n$$

The corresponding nonlinear statement can be written as

$$\mathbf{M}\mathbf{a}_{n+1} + \mathbf{C}\mathbf{v}_{n+\alpha} + \mathbf{N}(\mathbf{d}_{n+\alpha}) = \mathbf{F}_{n+\alpha}$$

with

$$\begin{aligned}\mathbf{d}_{n+1} &= \mathbf{d}_n + \Delta t \mathbf{v}_n + \frac{\Delta t^2}{2} [(1 - 2\beta)\mathbf{a}_n + 2\beta\mathbf{a}_{n+1}] \\ \mathbf{v}_{n+1} &= \mathbf{v}_n + \Delta t [(1 - \gamma)\mathbf{a}_n + \gamma\mathbf{a}_{n+1}]\end{aligned}$$

Remarks:

1. Hilber proposes: $-0.3 < \alpha < 0$, $\gamma = \frac{(1 - 2\alpha)}{2}$, $\beta = \frac{(1 - \alpha)^2}{4}$
2. $\alpha = 0$ corresponds to Newmark's algorithm
3. For unexperienced user the HHT- α algorithm with $\alpha = -0.3$, is certainly the safest way to go. The choice of a time-step, small enough to correctly represent the load, and a proper mesh refinement is then the only question left.

Window 2-4

2.1.2 Absorbing boundaries for single-phase media

One of the simplest ways to avoid reflections of waves outgoing from the domain is to use Lysmer type dashpots.

Window 2-5: Absorbing boundaries (single-phase): viscous force vector

ZSoil®

The resulting damping force vector that is added to the right hand side is defined as follows

$$\mathbf{F}^v = - \int_{\Gamma} \mathbf{N}^T \boldsymbol{\sigma}^s d\Gamma$$

In the above equation \mathbf{N} is a matrix of standard shape functions and $\boldsymbol{\sigma}^s$ is a viscous stress defined as

$$\boldsymbol{\sigma} = - \left\{ \frac{1}{c_p} (\lambda_s + 2\mu_s) \mathbf{nn}^T + \frac{\mu_s}{c_s} (\mathbf{t}_1 \mathbf{t}_1^T + \mathbf{t}_2 \mathbf{t}_2^T) \right\} \mathbf{v}^s$$

The corresponding shear and dilatational wave velocities are denoted by

$$c_s = \sqrt{\frac{G}{\rho}}$$

$$c_p = \sqrt{\frac{\lambda + 2G}{\rho}}$$

while solid velocity vector at a given point by \mathbf{v}^s .

The normalized normal and tangential vectors are denoted by \mathbf{n} and $\mathbf{t}_1, \mathbf{t}_2$ respectively.

Window 2-5

2.2 Equations of motion for dynamic consolidation of two-phase fully or partially saturated media

In the current development the $u - p$ formulation is adopted. It allows to analyze real world problems concerning earthquake engineering. In this approach the relative fluid acceleration with respect to the solid skeleton is neglected. Presence of the inertial term in the Darcy law is left to the user's choice (by default we assume that it is present).

Window 2-6: Governing equations for two-phase dynamic consolidation

ZSoil®

The two-phase dynamic consolidation of fully or partially saturated media is governed by two balance equations

- Balance of the momentum: $\frac{\partial \sigma_{ij}}{\partial x_j} + \gamma b_i = \rho \ddot{u}_i$
- Balance of the mass for the fluid: $\tilde{S} \dot{\epsilon}_{kk} - v_{i,i}^F - c\dot{p} = 0$

supplied by the corresponding initial and boundary conditions. In the above equations the total stress is expressed via Bishop's effective stress principle

$$\sigma_{ij} = \sigma'_{ij} + \tilde{\alpha} \tilde{S} \delta_{ij} p$$

and relative fluid velocity is governed by the Darcy's law

$$v_i^F = k_{ij} k_r(S) \left(\frac{1}{\gamma^F} p_{,j} + b_j - \frac{1}{g} \ddot{u}_j \right)$$

Remarks:

1. $\tilde{\alpha}$ is the elastic Biot coefficient ($\tilde{\alpha} = 1 - \frac{K_t}{K_s}$) (K_t is the elastic bulk modulus while K_s is the elastic grains bulk modulus)
2. \tilde{S} can be selected as the standard saturation ratio S or corrected effective saturation $S_e^{1/(nm)} = \left(\frac{S - S_r}{1 - S_r} \right)^{1/(nm)}$
3. term $\frac{1}{g} \ddot{u}_j$ in the Darcys law is optional
4. the k_r function can be defined using formula by Irmay ($k_r = \left(\frac{S - S_r}{1 - S_r} \right)^3$) or by Mualem ($k_r = S_e^{1/2} \left(1 - \left(1 - S_e^{1/m} \right)^m \right)^2$)
5. storage coefficient $c = c(p) = n \left(\frac{S}{K_w} - \frac{dS}{dp} \right) + \frac{\tilde{\alpha} - n}{K_s} S \left(S - \frac{dS}{dp} p \right)$
6. K_w is the water-air mixture bulk modulus defined as $\frac{1}{K_w} = \frac{S}{K_f} + \frac{1 - S}{K_a}$
7. K_f is the fluid bulk modulus and K_a is the air bulk modulus at the atmospheric pressure ($K_a = 100$ kPa)

Window 2-6

2.2.1 Nonlinear algorithms for arbitrary dynamic input for two-phase media

In the following derivations the HHT– α scheme will be used. The standard Newmark method is easily recovered from HHT– α assuming $\alpha=0$.

Window 2-7: Integration scheme for kinematic quantities and pore pressure

ZSoil®

Expressions for solid displacements and velocities [12]:

$$\begin{aligned}\mathbf{u}_{n+1} &= \mathbf{u}_n + \dot{\mathbf{u}}_n \Delta t + \frac{\Delta t^2}{2} [(1 - 2\beta) \ddot{\mathbf{u}}_n + 2\beta \ddot{\mathbf{u}}_{n+1}] \\ \dot{\mathbf{u}}_{n+1} &= \dot{\mathbf{u}}_n + \Delta t [(1 - \gamma) \ddot{\mathbf{u}}_n + \gamma \ddot{\mathbf{u}}_{n+1}]\end{aligned}$$

Expression for pore pressure:

$$p_{n+1} = p_n + (1 - \theta) \dot{p}_n \Delta t + \theta \Delta t \dot{p}_{n+1}$$

In the HHT scheme

$$\begin{aligned}p_{n+\alpha} &= (1 + \alpha)p_{n+1} - \alpha p_n \\ \dot{p}_{n+\alpha} &= (1 + \alpha)\dot{p}_{n+1} - \alpha \dot{p}_n \\ \mathbf{u}_{n+\alpha} &= (1 + \alpha)\mathbf{u}_{n+1} - \alpha \mathbf{u}_n \\ \dot{\mathbf{u}}_{n+\alpha} &= (1 + \alpha)\dot{\mathbf{u}}_{n+1} - \alpha \dot{\mathbf{u}}_n \\ \ddot{\mathbf{u}}_{n+\alpha} &= (1 + \alpha)\ddot{\mathbf{u}}_{n+1} - \alpha \ddot{\mathbf{u}}_n\end{aligned}$$

Hence variation of one of the above quantities is expressed as follows

$$\delta(\dots)_{n+\alpha} = (1 + \alpha)\delta(\dots)$$

Window 2-7

Window 2-8: Balance equations in matrix form

ZSoil®

Balance of momentum (HHT scheme)

$$\mathbf{M}\ddot{\mathbf{u}}_{n+1} + \mathbf{C}\dot{\mathbf{u}}_{n+\alpha} + \mathbf{F}'_{INT}(\mathbf{u}_{n+\alpha}) + \mathbf{C}^F \mathbf{p}_{n+\alpha} = \mathbf{F}_{EXTn+\alpha}$$

Balance of the mass for fluid phase written at time step $n + \alpha$

$$\left(\tilde{\mathbf{C}}^F\right)^T \dot{\mathbf{u}}_{n+\alpha} - \frac{1}{\gamma^F} \mathbf{H}^F \mathbf{p}_{n+\alpha} + \mathbf{R}^F \ddot{\mathbf{u}}_{n+\alpha} - \mathbf{h}^F - \mathbf{M}^F \dot{\mathbf{p}}_{n+\alpha} + \mathbf{Q}^F - \mathbf{P}^F \mathbf{p}_{n+\alpha} + \mathbf{P}^F \mathbf{p}_{\text{ext}n+\alpha} = \mathbf{0}$$

where

$$\begin{aligned} \mathbf{F}'_{INT}(\mathbf{u}_{n+\alpha}) &= \int_{\Omega} \mathbf{B}^T \boldsymbol{\sigma}(\mathbf{u}_{n+\alpha}) d\Omega \\ \mathbf{C}^F &= \int_{\Omega} \mathbf{N}^T \tilde{\alpha} \tilde{S}_{n+\alpha} \mathbf{1}^T \\ \tilde{\mathbf{C}}^F &= \int_{\Omega} \mathbf{N}^T \tilde{\alpha} S_{n+\alpha} \mathbf{1}^T \\ \mathbf{H}^F &= \int_{\Omega} \nabla \mathbf{N}^T \mathbf{k} \nabla \mathbf{N} d\Omega \\ \mathbf{M}^F &= \int_{\Omega} \mathbf{N}^T c_{n+\alpha} \mathbf{N} d\Omega \\ \mathbf{P}^F &= \int_{\Gamma_s} \mathbf{N}^T k_v \mathbf{N} d\Gamma \\ \mathbf{R}^F &= \int_{\Omega} \nabla \mathbf{N}^T \mathbf{k} \frac{1}{g} \nabla \mathbf{N} d\Omega \\ \mathbf{h}^F &= \int_{\Omega} \nabla \mathbf{N}^T \mathbf{k} b d\Omega \\ \mathbf{Q}^F &= \int_{\Gamma_q} \mathbf{N}^T \bar{q} d\Omega \end{aligned}$$

Meaning of the parameters appearing in the integrals

$$c_{n+\alpha} = c(p_{n+\alpha})$$

k_v - penalty factor for seepage element

g - earth acceleration ($g=9.81 \text{ m/s}^2$)

\bar{q} - imposed fluid flux at boundary Γ_q

Window 2-8

Window 2-9: Linearization of balance equations in the HHT format

ZSoil®

In this derivation we assume that current saturation ratio S and storage function value c are kept constant and equal to their values at previous step.

Linearization of the matrix form of balance equations of the momentum and fluid mass yields the following result

$$\left[\begin{array}{cc} \mathbf{M} + \mathbf{K}(1 + \alpha)\beta\Delta t^2 + \mathbf{C}(1 + \alpha)\gamma\Delta t & \mathbf{C}^F(1 + \alpha)\theta\Delta t \\ \left(\tilde{\mathbf{C}}^F\right)^T(1 + \alpha)\theta\Delta t + \frac{\theta}{\gamma}(1 + \alpha)\mathbf{R}^F & \frac{\theta}{\gamma}(1 + \alpha)\left(-\frac{1}{\gamma^F}\mathbf{H}^F\theta\Delta t - \mathbf{M}^F - \mathbf{P}^F\theta\Delta t\right) \end{array} \right] \left\{ \begin{array}{c} \delta\ddot{\mathbf{u}} \\ \delta\dot{\mathbf{p}} \end{array} \right\} =$$

$$\left\{ \begin{array}{c} \mathbf{F}_{EXTn+\alpha} - \mathbf{M}\ddot{\mathbf{u}}_{n+\alpha} - \mathbf{C}\dot{\mathbf{u}}_{n+\alpha} - \mathbf{F}'_{INT} - \mathbf{C}^F\mathbf{p}_{n+\alpha} \\ \frac{1}{\gamma\Delta t}\left(-\mathbf{Q}^F + \mathbf{h}^F - \left(\tilde{\mathbf{C}}^F\right)^T\dot{\mathbf{u}}_{n+\alpha} + \frac{1}{\gamma^F}\mathbf{H}^F\mathbf{p}_{n+\alpha} - \mathbf{R}^F\ddot{\mathbf{u}}_{n+\alpha} + \mathbf{M}^F\dot{\mathbf{p}}_{n+\alpha} + \mathbf{P}^F\mathbf{p}_{n+\alpha} - \mathbf{P}^F\mathbf{p}_{extn+\alpha}\right) \end{array} \right\}$$

Remarks:

1. The system of equations is solved for solid accelerations $\delta\ddot{\mathbf{u}}$ and pore pressure rates $\delta\dot{\mathbf{p}}$
2. The resulting system of linearized equations is nonsymmetric in general
3. To eliminate spurious spatial pressure oscillations a stabilization procedure based on pressure Laplacian is used (same as for the standard static consolidation problems)

Window 2-9

2.2.2 Absorbing boundaries for dynamic consolidation of two-phase media

In the current development the zeroth-order paraxial formulation by Modaressi and Bonzenati [8] is adopted. It is coherent with the $u - p$ type formulation. The viscous force and flux vectors are defined in the following Window.

Window 2-10: Absorbing boundaries (two-phase): viscous force and flux vectors

ZSoil®

The resulting viscous force and flux vectors that are added to the right hand side are defined as follows

$$\mathbf{F}_u^v = - \int_{\Gamma} \mathbf{N}^T \boldsymbol{\sigma}^s d\Gamma$$

$$\mathbf{F}_p^v = - \int_{\Gamma} \mathbf{N}^T \Phi d\Gamma$$

In the above equation \mathbf{N} is a matrix of standard shape functions, $\boldsymbol{\sigma}^s$ is a total viscous stress and Φ is a fluid flux transferred through paraxial boundary defined as

$$\boldsymbol{\sigma}^s = - \left\{ \rho \frac{c_p^2}{V_{p1}} (\lambda_s + 2\mu_s) \mathbf{nn}^T + \rho c_s (\mathbf{t}_1 \mathbf{t}_1^T + \mathbf{t}_2 \mathbf{t}_2^T) \right\} \mathbf{v}^s + \mathbf{n} \left(\tilde{\alpha} \tilde{S} p - \tilde{\alpha}_o \tilde{S}_o p_o \right)$$

$$\Phi = k \left[\rho \left(1 - \frac{c_p^2}{V_{p1}^2} - \rho^F \right) \right] \mathbf{n}^T \mathbf{a}^s$$

The corresponding shear and dilatational wave velocities for solid phase are expressed as follows

$$c_s = \sqrt{\frac{G}{\rho}} \quad c_p = \sqrt{\frac{\lambda + 2G}{\rho}}$$

The approximate first dilatational wave velocity for saturated medium is defined as

$$V_{p1}^2 = c_p^2 \left(1 + \frac{Q}{\lambda + 2G} \right)$$

and

$$\frac{1}{Q} = c(p)$$

Solid velocity and acceleration vectors are denoted by \mathbf{v}^s and \mathbf{a}^s .

The normalized normal and tangential vectors are denoted by \mathbf{n} and $\mathbf{t}_1, \mathbf{t}_2$ respectively.

Remarks:

1. The $S_o p_o$ term reflects the initial saturation/pressure condition prior dynamic time history analysis
2. k is the permeability value along \mathbf{n} direction; it can be computed as $k = \mathbf{n}^T \mathbf{kn}$
3. ρ value is computed as $\rho = \rho_D + n S \rho^F$

Window 2-10

2.3 Mesh size and time stepping

To trace wave propagation in the medium we need approximately 10 nodes per wavelength. The mesh size depends on the maximum frequency f_{\max} that is to be represented. For typical seismic application f_{\max} is limited up to 10 Hz. Hence the maximum mesh size should be smaller than

$$h^e \leq \frac{\lambda}{10} = \frac{v}{10 f_{\max}} \quad (2.4)$$

In the above expression v is the lowest wave velocity that is to be considered in the analyzed problem. In most cases v is taken as shear wave velocity.

Size of the applied time step, even for implicit integration schemes, is limited to a certain value too. This is so due to the fact that the smallest fundamental period of vibration needs to be represented by at least 10 points (same amount as for the spatial discretization). Hence the time step limitation can be formulated as follows

$$\Delta t \leq \frac{h^e}{v} \quad (2.5)$$

and v is the highest wave velocity.

2.4 Seismic input

The seismic input can be applied

- in the absolute format for rigid base model; here certain nodal displacements/velocities/accelerations are imposed and driven by an associated load time function (this is so-called rigid base model because waves are reflected by this boundary); this definition can be made through the acceleration/velocity/displacement boundary conditions
- in the absolute format for compliant base model; here seismic input is given as an imposed acceleration $\mathbf{a}_g = \ddot{\mathbf{u}}_g$ that is integrated to velocities (via Newmark method) and applied at the base of the model where viscous dashpots are added; this way the acceleration record is converted to the traction time history and applied to the bottom boundary of the model (the bottom boundary is identified as a line segment (2D) or surface (3D), shared by viscous boundary located at $y = y_{MIN} = \text{const}$) (this is compliant base model that circumvents waves reflections)
- in the relative format for rigid base model; here seismic input is given as an imposed acceleration $\mathbf{a}_g = \ddot{\mathbf{u}}_g$ of the ground that is global to the whole structure; the corresponding inertia forces are shifted to the right hand side

$$\mathbf{F}(t) = -\mathbf{M}\mathbf{a}_g(t) \quad (2.6)$$

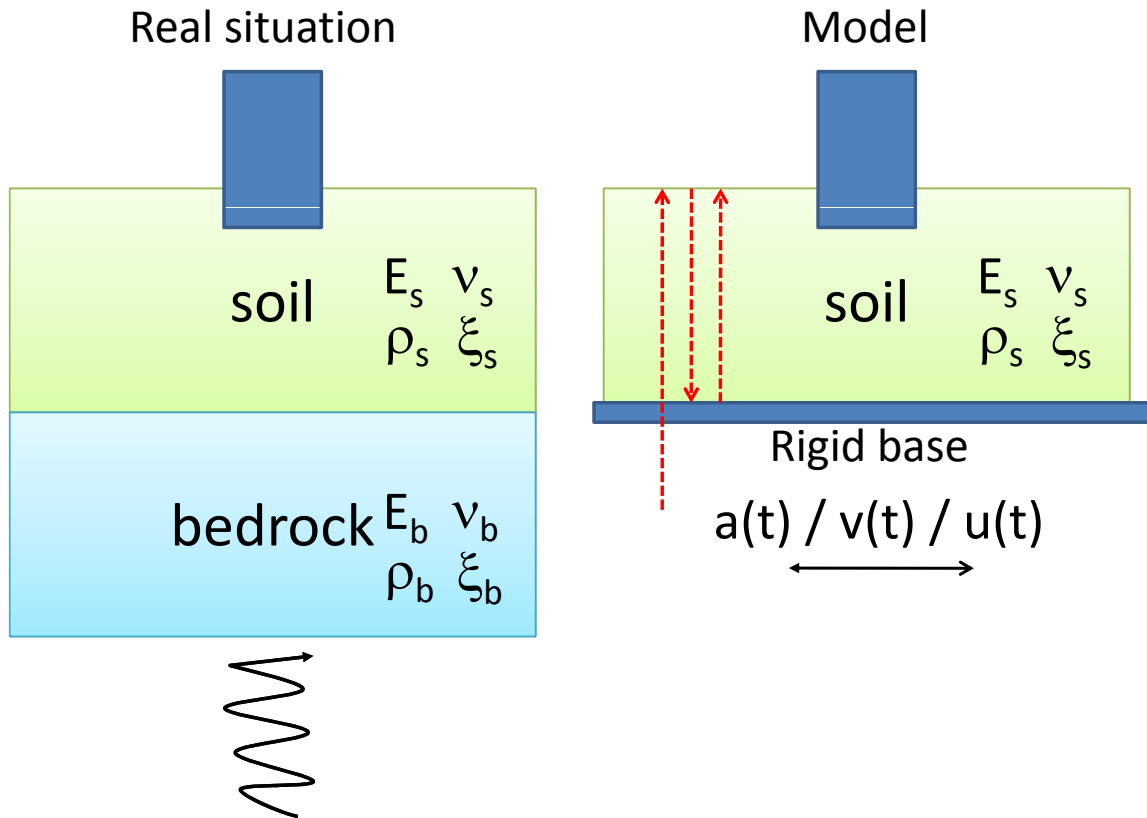
In the absolute format displacements are total ones, referred to inertial coordinate system while in the relative one, displacements are relative ones with respect to the fixed nodes, and are referred to noninertial coordinate system ("shaking table approach")

2.4.1 Rigid base model

Window 2-11: Rigid base model and seismic input

ZSoil®

The idea of application of the acceleration record to the rigid base model is shown in the figure



$$\text{Impedance ratio } \alpha_z = \frac{\rho_s v_{ss}}{\rho_r v_{sr}} \rightarrow 0 \text{ (complex for nonzero damping)}$$

In the rigid base model the following assumptions are made

- Nodes at the bottom are fixed
- (a) Motion is imposed by displacement/velocity/acceleration boundary conditions (absolute format)
 - ★ Output: absolute displacements/velocities/accelerations
- (b) Motion is imposed by application of global acceleration to the whole domain (relative format)
 - ★ Output: relative displacements/velocities/accelerations (with respect to the rigid base)

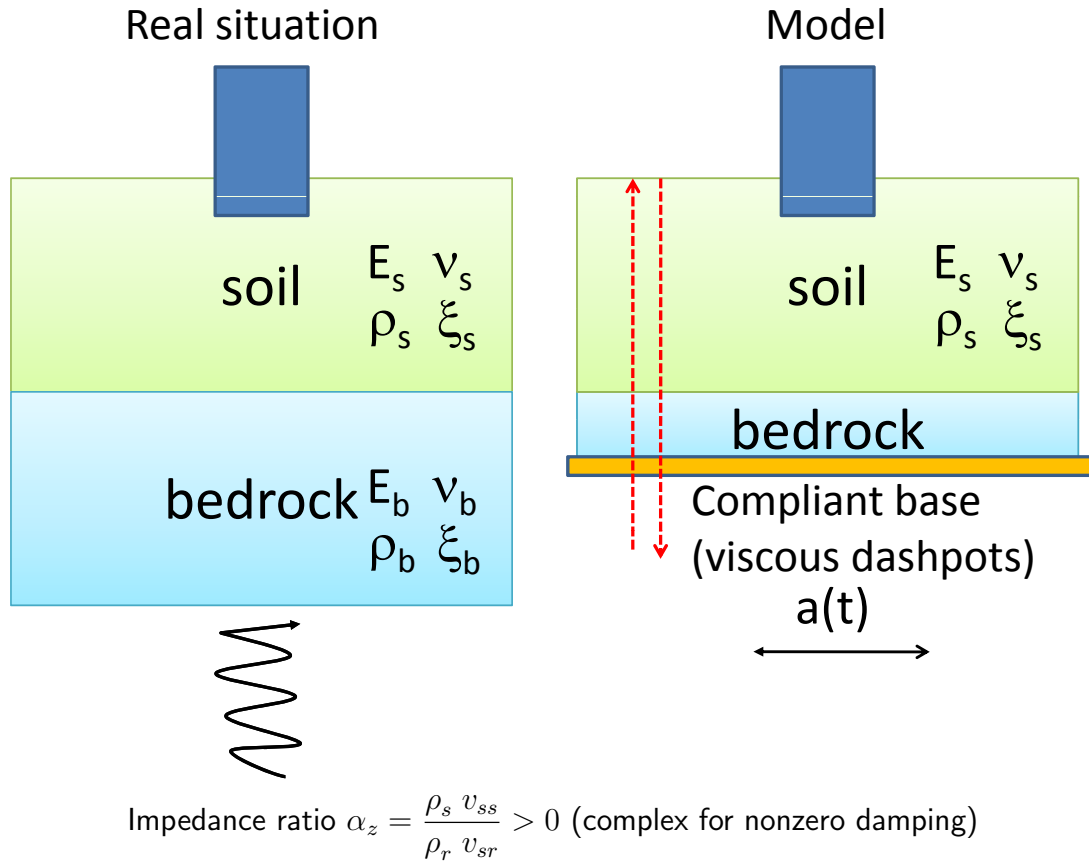
Window 2-11

2.4.2 Compliant base model

Window 2-12: Compliant base model and seismic input

ZSoil®

The idea of application of the acceleration record to the compliant base model is shown in the figure [7].



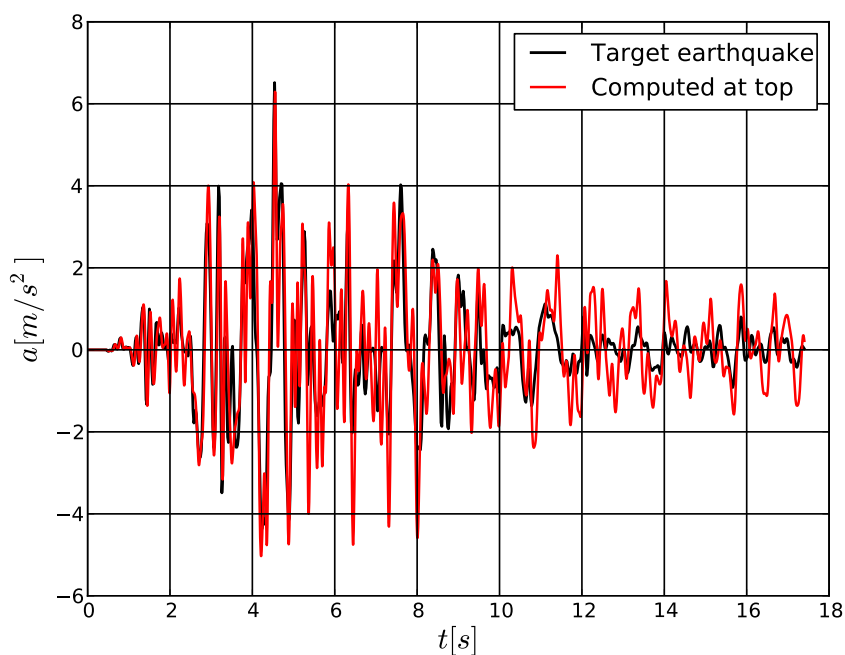
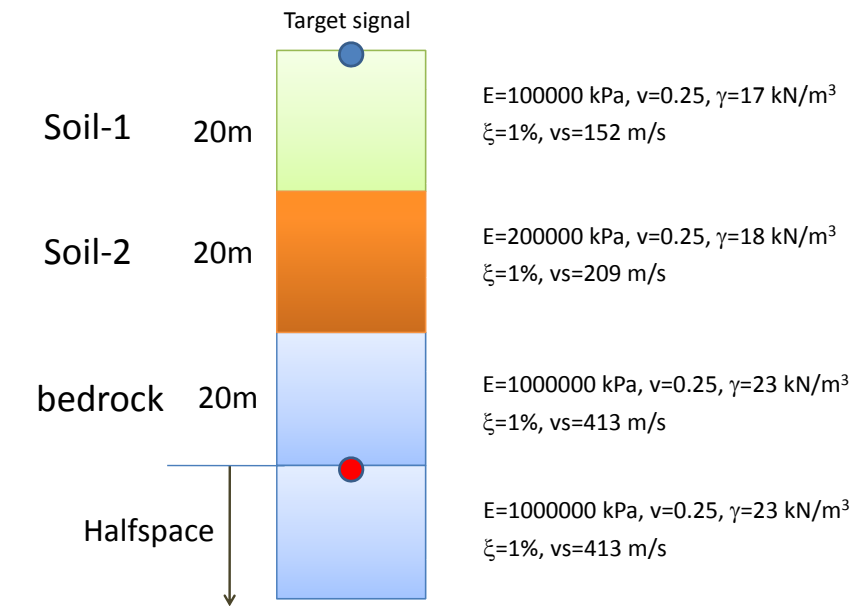
- Nodes at the bottom may freely move
- Viscous dashpots are added to the base (with bedrock parameters !)
- Motion can exclusively be applied through the acceleration record (seismic input)
 1. Output: absolute displacements/velocities/accelerations
- Accelerations are integrated to velocities via Newmark method ($a(t) \rightarrow v_{su}(t)$)
- Viscous shear tractions are computed and applied to the base
- The input $a(t)$ does not need to be compatible with $a(t)$ computed at the base (!)

Window 2-12

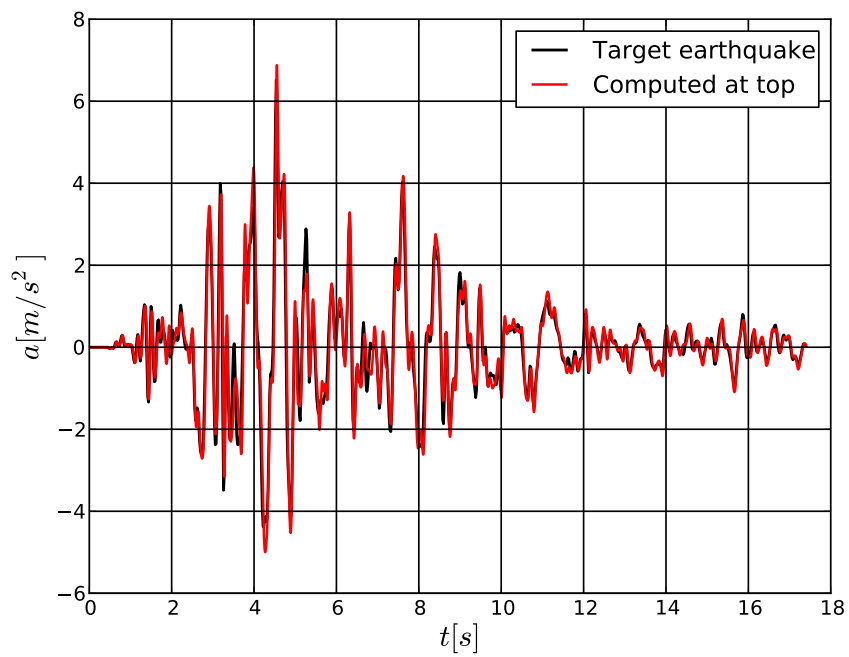
Window 2-13: Why compliant base model is better than rigid one ?

ZSoil®

In order to show why compliant base model is usually better than the rigid base one let us consider a simple example of a shear layer problem for subsoil as shown in the figure. The target acceleration record is given at the surface therefore we need to transfer it to the base of the FE model using linear deconvolution procedure (described in section 5.3.2). After linear deconvolution we will compute response of the rigid and compliant base models for deconvoluted signal perturbing shear wave velocity v_s in the first soil layer by 5%.



Result for rigid base



Result for compliant base

The two results show that the compliant base model (especially for low material damping) is insensitive to the introduced error.

Window 2-13

Chapter 3

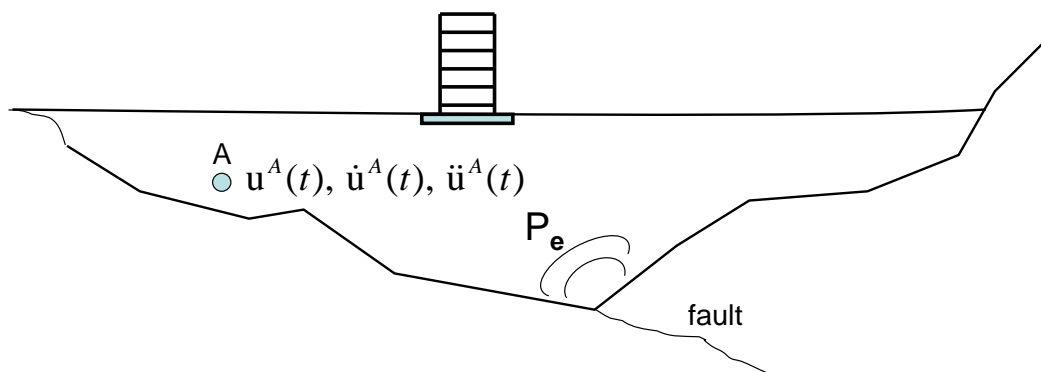
SOIL-STRUCTURE INTERACTION PROBLEMS

3.1 Domain Reduction Method (DRM) for single-phase media

The Domain Reduction Method was proposed by Bielak et al. [1], [11]. The main goal of this method is to analyze the computational model that concerns the structure and a small adjacent part of subsoil. This way the size of the problem to be solved is substantially reduced. The basic assumptions and theory are shown in the following Windows.

Window 3-1: DRM method: general idea

ZSoil®



Full model of subsoil and structure, and source of the loading $P_e(t)$

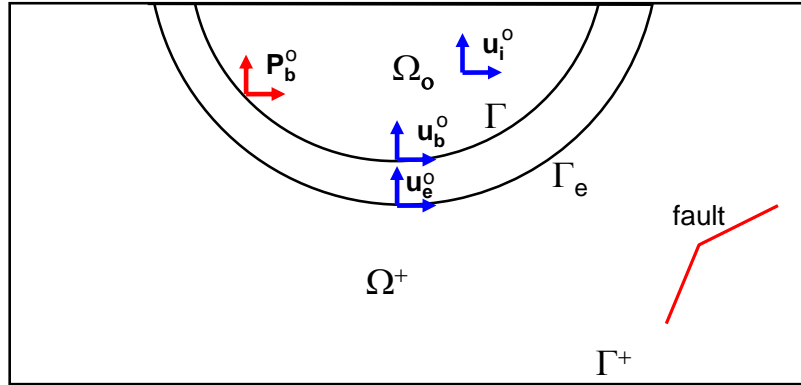
Remarks:

1. At any point displacements, velocities and accelerations induced by $P_e(t)$ are denoted by $u(t)$, $\dot{u}(t)$, $\ddot{u}(t)$
2. The complex model with a large subsoil zone and source of load $P_e(t)$ is split into background model (see Win.3-2) and a reduced model (see Win.3-3)

Window 3-1

Window 3-2: DRM method: background model

ZSoil®



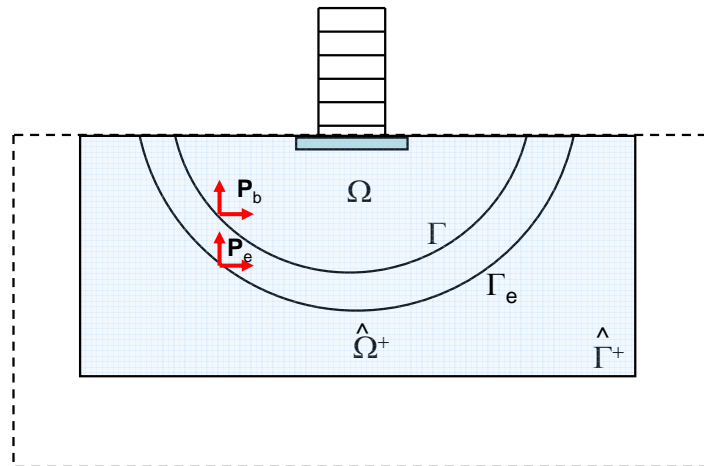
Remarks:

1. In the background model the structure is removed and free field motion is analyzed
2. Displacements, velocities and accelerations induced by $P_e(t)$ are denoted by $u^0(t)$, $\dot{u}^0(t)$, $\ddot{u}^0(t)$

Window 3-2

Window 3-3: DRM method: reduced model

ZSoil®



Remarks:

1. The interior domain is denoted by Ω while exterior one by Ω^+
2. Γ is the boundary that separates interior and exterior domains
3. Γ^+ is a boundary where viscous damping elements are to be put to cancel wave reflections
4. Kinematic quantities at any point in the interior domain will be denoted with the lower index $()_i$, at boundary Γ with index $()_b$ and in the exterior domain with index $()_e$
5. In the exterior domain the following displacement decomposition is used:

$$\mathbf{u}_e = \mathbf{u}_e^0 + \hat{\mathbf{u}}_e$$

6. Nodal points that belong to the boundary Γ are denoted as *boundary* (*b*), nodes that are in the Ω^+ domain and do not belong to the boundary Γ are denoted as *exterior* (*e*), the remaining ones are denoted as *interior* (*i*)

Window 3-3

Window 3-4: DRM method: governing equations

ZSoil®

After partitioning of the whole domain into Ω and Ω^+ one may write equations of motion, neglecting viscous damping terms, in Ω and Ω^+ respectively

$$\begin{bmatrix} \mathbf{M}_{ii}^{\Omega} & \mathbf{M}_{ib}^{\Omega} \\ \mathbf{M}_{bi}^{\Omega} & \mathbf{M}_{bb}^{\Omega} \end{bmatrix} \begin{Bmatrix} \ddot{\mathbf{u}}_i \\ \ddot{\mathbf{u}}_b \end{Bmatrix} + \begin{bmatrix} \mathbf{K}_{ii}^{\Omega} & \mathbf{K}_{ib}^{\Omega} \\ \mathbf{K}_{bi}^{\Omega} & \mathbf{K}_{bb}^{\Omega} \end{bmatrix} \begin{Bmatrix} \mathbf{u}_i \\ \mathbf{u}_b \end{Bmatrix} = \begin{Bmatrix} \mathbf{0} \\ \mathbf{P}_b \end{Bmatrix} \quad (1)$$

$$\begin{bmatrix} \mathbf{M}_{bb}^{\Omega^+} & \mathbf{M}_{be}^{\Omega^+} \\ \mathbf{M}_{eb}^{\Omega^+} & \mathbf{M}_{ee}^{\Omega^+} \end{bmatrix} \begin{Bmatrix} \ddot{\mathbf{u}}_b \\ \ddot{\mathbf{u}}_e \end{Bmatrix} + \begin{bmatrix} \mathbf{K}_{bb}^{\Omega^+} & \mathbf{K}_{be}^{\Omega^+} \\ \mathbf{K}_{eb}^{\Omega^+} & \mathbf{K}_{ee}^{\Omega^+} \end{bmatrix} \begin{Bmatrix} \mathbf{u}_b \\ \mathbf{u}_e \end{Bmatrix} = \begin{Bmatrix} -\mathbf{P}_b \\ \mathbf{P}_e \end{Bmatrix} \quad (2)$$

The two above sets of equations can be written in the global form as follows:

$$\begin{bmatrix} \mathbf{M}_{ii}^{\Omega} & \mathbf{M}_{ib}^{\Omega} & \mathbf{0} \\ \mathbf{M}_{bi}^{\Omega} & \mathbf{M}_{bb}^{\Omega} + \mathbf{M}_{bb}^{\Omega^+} & \mathbf{M}_{be}^{\Omega^+} \\ \mathbf{0} & \mathbf{M}_{eb}^{\Omega^+} & \mathbf{M}_{ee}^{\Omega^+} \end{bmatrix} \begin{Bmatrix} \ddot{\mathbf{u}}_i \\ \ddot{\mathbf{u}}_b \\ \ddot{\mathbf{u}}_e \end{Bmatrix} + \begin{bmatrix} \mathbf{K}_{ii}^{\Omega} & \mathbf{K}_{ib}^{\Omega} & \mathbf{0} \\ \mathbf{K}_{bi}^{\Omega} & \mathbf{K}_{bb}^{\Omega} + \mathbf{K}_{bb}^{\Omega^+} & \mathbf{K}_{be}^{\Omega^+} \\ \mathbf{0} & \mathbf{K}_{eb}^{\Omega^+} & \mathbf{K}_{ee}^{\Omega^+} \end{bmatrix} \begin{Bmatrix} \mathbf{u}_i \\ \mathbf{u}_b \\ \mathbf{u}_e \end{Bmatrix} = \begin{Bmatrix} \mathbf{0} \\ \mathbf{0} \\ \mathbf{P}_e \end{Bmatrix} \quad (3)$$

Let us decompose displacement vector in the exterior domain \mathbf{u}_e into free field displacement \mathbf{u}_e^0 and residual one $\hat{\mathbf{u}}_e$ as follows:

$$\mathbf{u}_e = \mathbf{u}_e^0 + \hat{\mathbf{u}}_e \quad (4)$$

Substituting eq.(4) into eq.(3) modifies eq.(3) to the following form:

$$\begin{bmatrix} \mathbf{M}_{ii}^{\Omega} & \mathbf{M}_{ib}^{\Omega} & \mathbf{0} \\ \mathbf{M}_{bi}^{\Omega} & \mathbf{M}_{bb}^{\Omega} + \mathbf{M}_{bb}^{\Omega^+} & \mathbf{M}_{be}^{\Omega^+} \\ \mathbf{0} & \mathbf{M}_{eb}^{\Omega^+} & \mathbf{M}_{ee}^{\Omega^+} \end{bmatrix} \begin{Bmatrix} \ddot{\mathbf{u}}_i \\ \ddot{\mathbf{u}}_b \\ \ddot{\mathbf{w}}_e \end{Bmatrix} + \begin{bmatrix} \mathbf{K}_{ii}^{\Omega} & \mathbf{K}_{ib}^{\Omega} & \mathbf{0} \\ \mathbf{K}_{bi}^{\Omega} & \mathbf{K}_{bb}^{\Omega} + \mathbf{K}_{bb}^{\Omega^+} & \mathbf{K}_{be}^{\Omega^+} \\ \mathbf{0} & \mathbf{K}_{eb}^{\Omega^+} & \mathbf{K}_{ee}^{\Omega^+} \end{bmatrix} \begin{Bmatrix} \mathbf{u}_i \\ \mathbf{u}_b \\ \mathbf{w}_e \end{Bmatrix} = \begin{Bmatrix} \mathbf{0} \\ \mathbf{0} \\ \mathbf{P}_e - \mathbf{M}_{ee}^{\Omega^+} \ddot{\mathbf{u}}_e^0 - \mathbf{K}_{ee}^{\Omega^+} \mathbf{u}_e^0 \end{Bmatrix} \quad (5)$$

The \mathbf{P}_e term can now be derived from eq.(2) assuming that it is solved for a simpler problem that does not include the structure

$$\mathbf{P}_e = \mathbf{M}_{eb}^{\Omega^+} \ddot{\mathbf{u}}_b^0 + \mathbf{M}_{ee}^{\Omega^+} \ddot{\mathbf{u}}_e^0 + \mathbf{K}_{eb}^{\Omega^+} \mathbf{u}_b^0 + \mathbf{K}_{ee}^{\Omega^+} \mathbf{u}_e^0 \quad (6)$$

By substituting the above \mathbf{P}_e term to the eq.(5) the following form of the right hand side term is obtained:

$$\mathbf{P}^{eff} = \begin{Bmatrix} \mathbf{0} \\ -\mathbf{M}_{be}^{\Omega^+} \ddot{\mathbf{u}}_e^0 - \mathbf{K}_{be}^{\Omega^+} \mathbf{u}_e^0 \\ \mathbf{M}_{eb}^{\Omega^+} \ddot{\mathbf{u}}_b^0 + \mathbf{K}_{eb}^{\Omega^+} \mathbf{u}_b^0 \end{Bmatrix} \quad (7)$$

Remark: For lumped mass matrix terms $\mathbf{M}_{be}^{\Omega^+} \ddot{\mathbf{u}}_e^0$, $\mathbf{M}_{eb}^{\Omega^+} \ddot{\mathbf{u}}_b^0$ disappear

Window 3-4

Window 3-5: DRM method: seismic input in the relative format (rigid base model)

ZSoil®

Seismic input is given as an imposed acceleration \mathbf{a}_g of the ground, common to the whole structure. In this case the external force vector can be written as follows:

$$\mathbf{F}(t) = -\mathbf{M}\mathbf{a}_g(t) + \mathbf{F}_{ext}(t) \quad (1)$$

In this approach the displacements are relative ones with respect to the fixed nodes and are referred to noninertial coordinate system ("shaking table approach").

In the Domain Reduction Method the inertia force term $-\mathbf{M}\mathbf{a}_g(t)$ on the right hand side must be modified for nodal points which are in the exterior domain Ω^+ (this forces are not present in the exterior domain). By partitioning it into interior, boundary and exterior nodes it takes the following form:

$$-\mathbf{M}\mathbf{a}_g(t) = \begin{Bmatrix} -\mathbf{M}_{ii}^{\Omega}\mathbf{a}_g - \mathbf{M}_{ib}^{\Omega}\mathbf{a}_g \\ -\mathbf{M}_{bi}^{\Omega}\mathbf{a}_g - \mathbf{M}_{bb}^{\Omega}\mathbf{a}_g - \mathbf{M}_{bb}^{\Omega^+}\mathbf{a}_g - \mathbf{M}_{be}^{\Omega^+}\mathbf{a}_g \\ \mathbf{0} \end{Bmatrix} \quad (2)$$

Remark: The $\mathbf{M}_{ie} = \mathbf{0}$, $\mathbf{M}_{ei} = \mathbf{0}$

Window 3-5

3.2 DRM metod for two-phase media

Window 3-6: DRM method for two-phase media: governing equations

ZSoil®

After partitioning of the whole domain into Ω and Ω^+ one may write equations of motion and fluid mass balance in Ω and Ω^+ respectively

Overall equilibrium in Ω

$$\begin{bmatrix} \mathbf{M}_{ii}^{\Omega} & \mathbf{M}_{ib}^{\Omega} \\ \mathbf{M}_{bi}^{\Omega} & \mathbf{M}_{bb}^{\Omega} \end{bmatrix} \begin{Bmatrix} \ddot{\mathbf{u}}_i \\ \ddot{\mathbf{u}}_b \end{Bmatrix} + \begin{bmatrix} \mathbf{K}_{ii}^{\Omega} & \mathbf{K}_{ib}^{\Omega} \\ \mathbf{K}_{bi}^{\Omega} & \mathbf{K}_{bb}^{\Omega} \end{bmatrix} \begin{Bmatrix} \mathbf{u}_i \\ \mathbf{u}_b \end{Bmatrix} + \begin{bmatrix} \mathbf{C}_{ii}^{\Omega} & \mathbf{C}_{ib}^{\Omega} \\ \mathbf{C}_{bi}^{\Omega} & \mathbf{C}_{bb}^{\Omega} \end{bmatrix} \begin{Bmatrix} \dot{\mathbf{u}}_i \\ \dot{\mathbf{u}}_b \end{Bmatrix} + \begin{bmatrix} \mathbf{C}_{ii}^{\mathbf{F}\Omega} & \mathbf{C}_{ib}^{\mathbf{F}\Omega} \\ \mathbf{C}_{bi}^{\mathbf{F}\Omega} & \mathbf{C}_{bb}^{\mathbf{F}\Omega} \end{bmatrix} \begin{Bmatrix} \mathbf{p}_i \\ \mathbf{p}_b \end{Bmatrix} = \begin{Bmatrix} \mathbf{0} \\ \mathbf{P}_b \end{Bmatrix} \quad (1)$$

Overall equilibrium in Ω^+

$$\begin{bmatrix} \mathbf{M}_{bb}^{\Omega^+} & \mathbf{M}_{be}^{\Omega^+} \\ \mathbf{M}_{eb}^{\Omega^+} & \mathbf{M}_{ee}^{\Omega^+} \end{bmatrix} \begin{Bmatrix} \ddot{\mathbf{u}}_b \\ \ddot{\mathbf{u}}_e \end{Bmatrix} + \begin{bmatrix} \mathbf{K}_{bb}^{\Omega^+} & \mathbf{K}_{be}^{\Omega^+} \\ \mathbf{K}_{eb}^{\Omega^+} & \mathbf{K}_{ee}^{\Omega^+} \end{bmatrix} \begin{Bmatrix} \mathbf{u}_b \\ \mathbf{u}_e \end{Bmatrix} + \begin{bmatrix} \mathbf{C}_{bb}^{\Omega^+} & \mathbf{C}_{be}^{\Omega^+} \\ \mathbf{C}_{eb}^{\Omega^+} & \mathbf{C}_{ee}^{\Omega^+} \end{bmatrix} \begin{Bmatrix} \dot{\mathbf{u}}_b \\ \dot{\mathbf{u}}_e \end{Bmatrix} + \begin{bmatrix} \mathbf{C}_{bb}^{\mathbf{F}\Omega^+} & \mathbf{C}_{be}^{\mathbf{F}\Omega^+} \\ \mathbf{C}_{eb}^{\mathbf{F}\Omega^+} & \mathbf{C}_{ee}^{\mathbf{F}\Omega^+} \end{bmatrix} \begin{Bmatrix} \mathbf{p}_b \\ \mathbf{p}_e \end{Bmatrix} = \begin{Bmatrix} -\mathbf{P}_b \\ \mathbf{P}_e \end{Bmatrix} \quad (2)$$

Fluid mass balance in Ω

$$\begin{bmatrix} \mathbf{R}_{ii}^{\mathbf{F}\Omega} & \mathbf{R}_{ib}^{\mathbf{F}\Omega} \\ \mathbf{R}_{bi}^{\mathbf{F}\Omega} & \mathbf{R}_{bb}^{\mathbf{F}\Omega} \end{bmatrix} \begin{Bmatrix} \ddot{\mathbf{u}}_i \\ \ddot{\mathbf{u}}_b \end{Bmatrix} + \begin{bmatrix} \left(\tilde{\mathbf{C}}_{ii}^{\mathbf{F}\Omega}\right)^{\top} & \left(\tilde{\mathbf{C}}_{ib}^{\mathbf{F}\Omega}\right)^{\top} \\ \left(\tilde{\mathbf{C}}_{bi}^{\mathbf{F}\Omega}\right)^{\top} & \left(\tilde{\mathbf{C}}_{bb}^{\mathbf{F}\Omega}\right)^{\top} \end{bmatrix} \begin{Bmatrix} \dot{\mathbf{u}}_i \\ \dot{\mathbf{u}}_b \end{Bmatrix} - \frac{1}{\gamma^{\mathbf{F}}} \begin{bmatrix} \mathbf{H}_{ii}^{\mathbf{F}\Omega} & \mathbf{H}_{ib}^{\mathbf{F}\Omega} \\ \mathbf{H}_{bi}^{\mathbf{F}\Omega} & \mathbf{H}_{bb}^{\mathbf{F}\Omega} \end{bmatrix} \begin{Bmatrix} \mathbf{p}_i \\ \mathbf{p}_b \end{Bmatrix} - \begin{bmatrix} \mathbf{M}_{ii}^{\mathbf{F}\Omega} & \mathbf{M}_{ib}^{\mathbf{F}\Omega} \\ \mathbf{M}_{bi}^{\mathbf{F}\Omega} & \mathbf{M}_{bb}^{\mathbf{F}\Omega} \end{bmatrix} \begin{Bmatrix} \dot{\mathbf{p}}_i \\ \dot{\mathbf{p}}_b \end{Bmatrix} = \begin{Bmatrix} -\mathbf{Q}_i^{\mathbf{F}} + \mathbf{h}_i^{\mathbf{F}\Omega} \\ -\mathbf{Q}_b^{\mathbf{F}} + \mathbf{h}_b^{\mathbf{F}\Omega} \end{Bmatrix} \quad (3)$$

Fluid mass balance in Ω^+

$$\begin{bmatrix} \mathbf{R}_{bb}^{\mathbf{F}\Omega^+} & \mathbf{R}_{be}^{\mathbf{F}\Omega^+} \\ \mathbf{R}_{eb}^{\mathbf{F}\Omega^+} & \mathbf{R}_{ee}^{\mathbf{F}\Omega^+} \end{bmatrix} \begin{Bmatrix} \ddot{\mathbf{u}}_b \\ \ddot{\mathbf{u}}_e \end{Bmatrix} + \begin{bmatrix} \left(\tilde{\mathbf{C}}_{bb}^{\mathbf{F}\Omega^+}\right)^{\top} & \left(\tilde{\mathbf{C}}_{be}^{\mathbf{F}\Omega^+}\right)^{\top} \\ \left(\tilde{\mathbf{C}}_{eb}^{\mathbf{F}\Omega^+}\right)^{\top} & \left(\tilde{\mathbf{C}}_{ee}^{\mathbf{F}\Omega^+}\right)^{\top} \end{bmatrix} \begin{Bmatrix} \dot{\mathbf{u}}_b \\ \dot{\mathbf{u}}_e \end{Bmatrix} - \frac{1}{\gamma^{\mathbf{F}}} \begin{bmatrix} \mathbf{H}_{bb}^{\mathbf{F}\Omega^+} & \mathbf{H}_{be}^{\mathbf{F}\Omega^+} \\ \mathbf{H}_{eb}^{\mathbf{F}\Omega^+} & \mathbf{H}_{ee}^{\mathbf{F}\Omega^+} \end{bmatrix} \begin{Bmatrix} \mathbf{p}_b \\ \mathbf{p}_e \end{Bmatrix} - \begin{bmatrix} \mathbf{M}_{bb}^{\mathbf{F}\Omega^+} & \mathbf{M}_{be}^{\mathbf{F}\Omega^+} \\ \mathbf{M}_{eb}^{\mathbf{F}\Omega^+} & \mathbf{M}_{ee}^{\mathbf{F}\Omega^+} \end{bmatrix} \begin{Bmatrix} \dot{\mathbf{p}}_b \\ \dot{\mathbf{p}}_e \end{Bmatrix} = \begin{Bmatrix} \mathbf{Q}_b^{\mathbf{F}} + \mathbf{h}_b^{\mathbf{F}\Omega^+} \\ -\mathbf{Q}_e^{\mathbf{F}} + \mathbf{h}_e^{\mathbf{F}\Omega^+} \end{Bmatrix} \quad (4)$$

The overall equilibrium and fluid mass balance can be written in the global form as follows:

Overall equilibrium

$$\begin{aligned}
 & \begin{bmatrix} \mathbf{M}_{ii}^{\Omega} & \mathbf{M}_{ib}^{\Omega} & \mathbf{0} \\ \mathbf{M}_{bi}^{\Omega} & \mathbf{M}_{bb}^{\Omega} + \mathbf{M}_{bb}^{\Omega+} & \mathbf{M}_{be}^{\Omega+} \\ \mathbf{0} & \mathbf{M}_{eb}^{\Omega+} & \mathbf{M}_{ee}^{\Omega+} \end{bmatrix} \begin{Bmatrix} \ddot{\mathbf{u}}_i \\ \ddot{\mathbf{u}}_b \\ \ddot{\mathbf{u}}_e \end{Bmatrix} + \begin{bmatrix} \mathbf{K}_{ii}^{\Omega} & \mathbf{K}_{ib}^{\Omega} & \mathbf{0} \\ \mathbf{K}_{bi}^{\Omega} & \mathbf{K}_{bb}^{\Omega} + \mathbf{K}_{bb}^{\Omega+} & \mathbf{K}_{be}^{\Omega+} \\ \mathbf{0} & \mathbf{K}_{eb}^{\Omega+} & \mathbf{K}_{ee}^{\Omega+} \end{bmatrix} \begin{Bmatrix} \mathbf{u}_i \\ \mathbf{u}_b \\ \mathbf{u}_e \end{Bmatrix} + \\
 & \begin{bmatrix} \mathbf{C}_{ii}^{\Omega} & \mathbf{C}_{ib}^{\Omega} & \mathbf{0} \\ \mathbf{C}_{bi}^{\Omega} & \mathbf{C}_{bb}^{\Omega} + \mathbf{C}_{bb}^{\Omega+} & \mathbf{C}_{be}^{\Omega+} \\ \mathbf{0} & \mathbf{C}_{eb}^{\Omega+} & \mathbf{C}_{ee}^{\Omega+} \end{bmatrix} \begin{Bmatrix} \dot{\mathbf{u}}_i \\ \dot{\mathbf{u}}_b \\ \dot{\mathbf{u}}_e \end{Bmatrix} + \begin{bmatrix} \mathbf{C}_{ii}^{\mathbf{F}\Omega} & \mathbf{C}_{ib}^{\mathbf{F}\Omega} & \mathbf{0} \\ \mathbf{C}_{bi}^{\mathbf{F}\Omega} & \mathbf{C}_{bb}^{\mathbf{F}\Omega} + \mathbf{C}_{bb}^{\mathbf{F}\Omega+} & \mathbf{C}_{be}^{\mathbf{F}\Omega+} \\ \mathbf{0} & \mathbf{C}_{eb}^{\mathbf{F}\Omega+} & \mathbf{C}_{ee}^{\mathbf{F}\Omega+} \end{bmatrix} \begin{Bmatrix} \mathbf{p}_i \\ \mathbf{p}_b \\ \mathbf{p}_e \end{Bmatrix} = \\
 & \begin{Bmatrix} \mathbf{0} \\ \mathbf{0} \\ \mathbf{P}_e \end{Bmatrix} \quad (5)
 \end{aligned}$$

Fluid mass balance

$$\begin{aligned}
 & \begin{bmatrix} \mathbf{R}_{ii}^{\mathbf{F}\Omega} & \mathbf{R}_{ib}^{\mathbf{F}\Omega} & \mathbf{0} \\ \mathbf{R}_{bi}^{\mathbf{F}\Omega} & \mathbf{R}_{bb}^{\mathbf{F}\Omega} + \mathbf{R}_{bb}^{\mathbf{F}\Omega+} & \mathbf{R}_{be}^{\mathbf{F}\Omega+} \\ \mathbf{0} & \mathbf{R}_{eb}^{\mathbf{F}\Omega+} & \mathbf{R}_{ee}^{\mathbf{F}\Omega+} \end{bmatrix} \begin{Bmatrix} \ddot{\mathbf{u}}_i \\ \ddot{\mathbf{u}}_b \\ \ddot{\mathbf{u}}_e \end{Bmatrix} + \\
 & \begin{bmatrix} (\tilde{\mathbf{C}}_{ii}^{\mathbf{F}\Omega})^{\top} & (\tilde{\mathbf{C}}_{ib}^{\mathbf{F}\Omega})^{\top} & \mathbf{0} \\ (\tilde{\mathbf{C}}_{bi}^{\mathbf{F}\Omega})^{\top} & (\tilde{\mathbf{C}}_{bb}^{\mathbf{F}\Omega})^{\top} + (\tilde{\mathbf{C}}_{bb}^{\mathbf{F}\Omega+})^{\top} & (\tilde{\mathbf{C}}_{be}^{\mathbf{F}\Omega+})^{\top} \\ \mathbf{0} & (\tilde{\mathbf{C}}_{eb}^{\mathbf{F}\Omega+})^{\top} & (\tilde{\mathbf{C}}_{ee}^{\mathbf{F}\Omega+})^{\top} \end{bmatrix} \begin{Bmatrix} \dot{\mathbf{u}}_i \\ \dot{\mathbf{u}}_b \\ \dot{\mathbf{u}}_e \end{Bmatrix} - \\
 & \frac{1}{\gamma^{\mathbf{F}}} \begin{bmatrix} \mathbf{H}_{ii}^{\mathbf{F}\Omega} & \mathbf{H}_{ib}^{\mathbf{F}\Omega} & \mathbf{0} \\ \mathbf{H}_{bi}^{\mathbf{F}\Omega} & \mathbf{H}_{bb}^{\mathbf{F}\Omega} + \mathbf{H}_{bb}^{\mathbf{F}\Omega+} & \mathbf{H}_{be}^{\mathbf{F}\Omega+} \\ \mathbf{0} & \mathbf{H}_{eb}^{\mathbf{F}\Omega+} & \mathbf{H}_{ee}^{\mathbf{F}\Omega+} \end{bmatrix} \begin{Bmatrix} \mathbf{p}_i \\ \mathbf{p}_b \\ \mathbf{p}_e \end{Bmatrix} - \\
 & \begin{bmatrix} \mathbf{M}_{ii}^{\mathbf{F}\Omega} & \mathbf{M}_{ib}^{\mathbf{F}\Omega} & \mathbf{0} \\ \mathbf{M}_{bi}^{\mathbf{F}\Omega} & \mathbf{M}_{bb}^{\mathbf{F}\Omega} + \mathbf{M}_{bb}^{\mathbf{F}\Omega+} & \mathbf{M}_{be}^{\mathbf{F}\Omega+} \\ \mathbf{0} & \mathbf{M}_{eb}^{\mathbf{F}\Omega+} & \mathbf{M}_{ee}^{\mathbf{F}\Omega+} \end{bmatrix} \begin{Bmatrix} \dot{\mathbf{p}}_i \\ \dot{\mathbf{p}}_b \\ \dot{\mathbf{p}}_e \end{Bmatrix} = \begin{Bmatrix} -\mathbf{Q}_i^{\mathbf{F}} + \mathbf{h}_i^{\mathbf{F}} \\ \mathbf{0} + \mathbf{h}_b^{\mathbf{F}\Omega} + \mathbf{h}_b^{\mathbf{F}\Omega+} \\ -\mathbf{Q}_e^{\mathbf{F}} + \mathbf{h}_e^{\mathbf{F}} \end{Bmatrix} \quad (6)
 \end{aligned}$$

Let us decompose displacement \mathbf{u}_e and pressure \mathbf{p}_e vectors, in the exterior domain, into free field ones \mathbf{u}_e^0 and \mathbf{p}_e^0 and residual $\hat{\mathbf{u}}_e$ and $\hat{\mathbf{p}}_e$ as follows:

$$\mathbf{u}_e = \mathbf{u}_e^0 + \hat{\mathbf{u}}_e \quad (7)$$

$$\mathbf{p}_e = \mathbf{p}_e^0 + \hat{\mathbf{p}}_e \quad (8)$$

Substituting terms (7) and (8) into eq.(3) and (6) yields

Overall equilibrium

$$\begin{aligned}
 & \begin{bmatrix} \mathbf{M}_{ii}^{\Omega} & \mathbf{M}_{ib}^{\Omega} & \mathbf{0} \\ \mathbf{M}_{bi}^{\Omega} & \mathbf{M}_{bb}^{\Omega} + \mathbf{M}_{bb}^{\Omega+} & \mathbf{M}_{be}^{\Omega+} \\ \mathbf{0} & \mathbf{M}_{eb}^{\Omega+} & \mathbf{M}_{ee}^{\Omega+} \end{bmatrix} \begin{Bmatrix} \ddot{\mathbf{u}}_i \\ \ddot{\mathbf{u}}_b \\ \ddot{\mathbf{u}}_e \end{Bmatrix} + \begin{bmatrix} \mathbf{K}_{ii}^{\Omega} & \mathbf{K}_{ib}^{\Omega} & \mathbf{0} \\ \mathbf{K}_{bi}^{\Omega} & \mathbf{K}_{bb}^{\Omega} + \mathbf{K}_{bb}^{\Omega+} & \mathbf{K}_{be}^{\Omega+} \\ \mathbf{0} & \mathbf{K}_{eb}^{\Omega+} & \mathbf{K}_{ee}^{\Omega+} \end{bmatrix} \begin{Bmatrix} \mathbf{u}_i \\ \mathbf{u}_b \\ \hat{\mathbf{u}}_e \end{Bmatrix} + \\
 & \begin{bmatrix} \mathbf{C}_{ii}^{\Omega} & \mathbf{C}_{ib}^{\Omega} & \mathbf{0} \\ \mathbf{C}_{bi}^{\Omega} & \mathbf{C}_{bb}^{\Omega} + \mathbf{C}_{bb}^{\Omega+} & \mathbf{C}_{be}^{\Omega+} \\ \mathbf{0} & \mathbf{C}_{eb}^{\Omega+} & \mathbf{C}_{ee}^{\Omega+} \end{bmatrix} \begin{Bmatrix} \dot{\mathbf{u}}_i \\ \dot{\mathbf{u}}_b \\ \dot{\mathbf{u}}_e \end{Bmatrix} + \begin{bmatrix} \mathbf{C}_{ii}^{\mathbf{F}\Omega} & \mathbf{C}_{ib}^{\mathbf{F}\Omega} & \mathbf{0} \\ \mathbf{C}_{bi}^{\mathbf{F}\Omega} & \mathbf{C}_{bb}^{\mathbf{F}\Omega} + \mathbf{C}_{bb}^{\mathbf{F}\Omega+} & \mathbf{C}_{be}^{\mathbf{F}\Omega+} \\ \mathbf{0} & \mathbf{C}_{eb}^{\mathbf{F}\Omega+} & \mathbf{C}_{ee}^{\mathbf{F}\Omega+} \end{bmatrix} \begin{Bmatrix} \mathbf{p}_i \\ \mathbf{p}_b \\ \hat{\mathbf{p}}_e \end{Bmatrix} = \\
 & \begin{Bmatrix} \mathbf{0} \\ -\mathbf{M}_{be}^{\Omega+} \ddot{\mathbf{u}}_e^0 - \mathbf{K}_{be}^{\Omega+} \mathbf{u}_e^0 - \mathbf{C}_{be}^{\Omega+} \dot{\mathbf{u}}_e^0 - \mathbf{C}_{be}^{\mathbf{F}\Omega+} \mathbf{p}_e^0 \\ \mathbf{P}_e - \mathbf{M}_{ee}^{\Omega+} \ddot{\mathbf{u}}_e^0 - \mathbf{K}_{ee}^{\Omega+} \mathbf{u}_e^0 - \mathbf{C}_{ee}^{\Omega+} \dot{\mathbf{u}}_e^0 - \mathbf{C}_{ee}^{\mathbf{F}\Omega+} \mathbf{p}_e^0 \end{Bmatrix} \quad (9)
 \end{aligned}$$

Fluid mass balance

$$\begin{aligned}
 & \begin{bmatrix} \mathbf{R}_{ii}^{\mathbf{F}\Omega} & \mathbf{R}_{ib}^{\mathbf{F}\Omega} & \mathbf{0} \\ \mathbf{R}_{bi}^{\mathbf{F}\Omega} & \mathbf{R}_{bb}^{\mathbf{F}\Omega} + \mathbf{R}_{bb}^{\mathbf{F}\Omega+} & \mathbf{R}_{be}^{\mathbf{F}\Omega+} \\ \mathbf{0} & \mathbf{R}_{eb}^{\mathbf{F}\Omega+} & \mathbf{R}_{ee}^{\mathbf{F}\Omega+} \end{bmatrix} \begin{Bmatrix} \ddot{\mathbf{u}}_i \\ \ddot{\mathbf{u}}_b \\ \ddot{\mathbf{u}}_e \end{Bmatrix} + \\
 & \begin{bmatrix} \left(\tilde{\mathbf{C}}_{ii}^{\mathbf{F}\Omega}\right)^{\top} & \left(\tilde{\mathbf{C}}_{ib}^{\mathbf{F}\Omega}\right)^{\top} & \mathbf{0} \\ \left(\tilde{\mathbf{C}}_{bi}^{\mathbf{F}\Omega}\right)^{\top} & \left(\tilde{\mathbf{C}}_{bb}^{\mathbf{F}\Omega}\right)^{\top} + \left(\tilde{\mathbf{C}}_{bb}^{\mathbf{F}\Omega+}\right)^{\top} & \left(\mathbf{C}_{be}^{\mathbf{F}\Omega+}\right)^{\top} \\ \mathbf{0} & \left(\tilde{\mathbf{C}}_{eb}^{\mathbf{F}\Omega+}\right)^{\top} & \left(\tilde{\mathbf{C}}_{ee}^{\mathbf{F}\Omega+}\right)^{\top} \end{bmatrix} \begin{Bmatrix} \dot{\mathbf{u}}_i \\ \dot{\mathbf{u}}_b \\ \dot{\mathbf{u}}_e \end{Bmatrix} - \\
 & \frac{1}{\gamma^F} \begin{bmatrix} \mathbf{H}_{ii}^{\mathbf{F}\Omega} & \mathbf{H}_{ib}^{\mathbf{F}\Omega} & \mathbf{0} \\ \mathbf{H}_{bi}^{\mathbf{F}\Omega} & \mathbf{H}_{bb}^{\mathbf{F}\Omega} + \mathbf{H}_{bb}^{\mathbf{F}\Omega+} & \mathbf{H}_{be}^{\mathbf{F}\Omega+} \\ \mathbf{0} & \mathbf{H}_{eb}^{\mathbf{F}\Omega+} & \mathbf{H}_{ee}^{\mathbf{F}\Omega+} \end{bmatrix} \begin{Bmatrix} \mathbf{p}_i \\ \mathbf{p}_b \\ \hat{\mathbf{p}}_e \end{Bmatrix} - \\
 & \begin{bmatrix} \mathbf{M}_{ii}^{\mathbf{F}\Omega} & \mathbf{M}_{ib}^{\mathbf{F}\Omega} & \mathbf{0} \\ \mathbf{M}_{bi}^{\mathbf{F}\Omega} & \mathbf{M}_{bb}^{\mathbf{F}\Omega} + \mathbf{M}_{bb}^{\mathbf{F}\Omega+} & \mathbf{M}_{be}^{\mathbf{F}\Omega+} \\ \mathbf{0} & \mathbf{M}_{eb}^{\mathbf{F}\Omega+} & \mathbf{M}_{ee}^{\mathbf{F}\Omega+} \end{bmatrix} \begin{Bmatrix} \dot{\mathbf{p}}_i \\ \dot{\mathbf{p}}_b \\ \dot{\hat{\mathbf{p}}}_e \end{Bmatrix} = \\
 & \begin{Bmatrix} -\mathbf{Q}_i^{\mathbf{F}} + \mathbf{h}_i^{\mathbf{F}} \\ \mathbf{h}_b^{\mathbf{F}\Omega} \\ \mathbf{0} \end{Bmatrix} + \begin{Bmatrix} \mathbf{0} \\ \mathbf{h}_b^{\mathbf{F}\Omega+} - \mathbf{R}_{be}^{\mathbf{F}\Omega+} \ddot{\mathbf{u}}_e^0 - \left(\tilde{\mathbf{C}}_{be}^{\mathbf{F}\Omega+}\right)^{\top} \dot{\mathbf{u}}_e^0 + \frac{1}{\gamma^F} \mathbf{H}_{be}^{\mathbf{F}\Omega+} \mathbf{p}_e^0 + \mathbf{M}_{be}^{\mathbf{F}\Omega+} \dot{\mathbf{p}}_e^0 \\ -\mathbf{Q}_e^{\mathbf{F}} + \mathbf{h}_e^{\mathbf{F}} - \mathbf{R}_{ee}^{\mathbf{F}\Omega+} \ddot{\mathbf{u}}_e^0 - \left(\tilde{\mathbf{C}}_{ee}^{\mathbf{F}\Omega+}\right)^{\top} \dot{\mathbf{u}}_e^0 + \frac{1}{\gamma^F} \mathbf{H}_{ee}^{\mathbf{F}\Omega+} \mathbf{p}_e^0 + \mathbf{M}_{ee}^{\mathbf{F}\Omega+} \dot{\mathbf{p}}_e^0 \end{Bmatrix} \quad (10)
 \end{aligned}$$

The \mathbf{P}_e and \mathbf{Q}_e terms can now be derived from eq.(2), and eq.(4) respectively, assuming that these are solved for a simpler problem that does not include the structure

$$\mathbf{P}_e = \mathbf{M}_{eb}^{\Omega^+} \ddot{\mathbf{u}}_b^0 + \mathbf{M}_{ee}^{\Omega^+} \ddot{\mathbf{u}}_e^0 + \mathbf{K}_{eb}^{\Omega^+} \mathbf{u}_b^0 + \mathbf{K}_{ee}^{\Omega^+} \mathbf{u}_e^0 + \mathbf{C}_{eb}^{\Omega^+} \dot{\mathbf{u}}_b^0 + \mathbf{C}_{ee}^{\Omega^+} \dot{\mathbf{u}}_e^0 + \mathbf{C}_{eb}^{\mathbf{F}\Omega^+} \mathbf{p}_b^0 + \mathbf{C}_{ee}^{\mathbf{F}\Omega^+} \mathbf{p}_e^0 \quad (11)$$

$$-\mathbf{Q}_e + \mathbf{h}^{\mathbf{F}}_e = \mathbf{R}_{eb}^{\mathbf{F}\Omega^+} \ddot{\mathbf{u}}_b^0 + \mathbf{R}_{ee}^{\mathbf{F}\Omega^+} \ddot{\mathbf{u}}_e^0 + \left(\tilde{\mathbf{C}}_{eb}^{\mathbf{F}\Omega^+} \right)^{\top} \dot{\mathbf{u}}_b^0 + \left(\tilde{\mathbf{C}}_{ee}^{\mathbf{F}\Omega^+} \right)^{\top} \dot{\mathbf{u}}_e^0 - \frac{1}{\gamma^{\mathbf{F}}} \mathbf{H}_{eb}^{\mathbf{F}\Omega^+} \mathbf{p}_b^0 - \frac{1}{\gamma^{\mathbf{F}}} \mathbf{H}_{ee}^{\mathbf{F}\Omega^+} \mathbf{p}_e^0 - \mathbf{M}_{eb}^{\mathbf{F}\Omega^+} \dot{\mathbf{p}}_b^0 - \mathbf{M}_{ee}^{\mathbf{F}\Omega^+} \dot{\mathbf{p}}_e^0 \quad (12)$$

By substituting the \mathbf{P}_e term to the eq.(5) the following form of the right hand side term is obtained:

$$\mathbf{P}^{eff} = \begin{Bmatrix} 0 \\ -\mathbf{M}_{be}^{\Omega^+} \ddot{\mathbf{u}}_e^0 - \mathbf{K}_{be}^{\Omega^+} \mathbf{u}_e^0 - \mathbf{C}_{be}^{\Omega^+} \dot{\mathbf{u}}_e^0 - \mathbf{C}_{be}^{\mathbf{F}\Omega^+} \mathbf{p}_e^0 \\ \mathbf{M}_{eb}^{\Omega^+} \ddot{\mathbf{u}}_b^0 + \mathbf{K}_{eb}^{\Omega^+} \mathbf{u}_b^0 + \mathbf{C}_{eb}^{\Omega^+} \dot{\mathbf{u}}_b^0 + \mathbf{C}_{eb}^{\mathbf{F}\Omega^+} \mathbf{p}_b^0 \end{Bmatrix} \quad (13)$$

$$\begin{aligned} & \begin{bmatrix} \mathbf{M}_{ii}^{\Omega} & \mathbf{M}_{ib}^{\Omega} & \mathbf{0} \\ \mathbf{M}_{bi}^{\Omega} & \mathbf{M}_{bb}^{\Omega} + \mathbf{M}_{bb}^{\Omega^+} & \mathbf{M}_{be}^{\Omega^+} \\ \mathbf{0} & \mathbf{M}_{eb}^{\Omega^+} & \mathbf{M}_{ee}^{\Omega^+} \end{bmatrix} \begin{Bmatrix} \ddot{\mathbf{u}}_i \\ \ddot{\mathbf{u}}_b \\ \ddot{\mathbf{u}}_e \end{Bmatrix} + \begin{bmatrix} \mathbf{K}_{ii}^{\Omega} & \mathbf{K}_{ib}^{\Omega} & \mathbf{0} \\ \mathbf{K}_{bi}^{\Omega} & \mathbf{K}_{bb}^{\Omega} + \mathbf{K}_{bb}^{\Omega^+} & \mathbf{K}_{be}^{\Omega^+} \\ \mathbf{0} & \mathbf{K}_{eb}^{\Omega^+} & \mathbf{K}_{ee}^{\Omega^+} \end{bmatrix} \begin{Bmatrix} \mathbf{u}_i \\ \mathbf{u}_b \\ \mathbf{u}_e \end{Bmatrix} + \\ & \begin{bmatrix} \mathbf{C}_{ii}^{\Omega} & \mathbf{C}_{ib}^{\Omega} & \mathbf{0} \\ \mathbf{C}_{bi}^{\Omega} & \mathbf{C}_{bb}^{\Omega} + \mathbf{C}_{bb}^{\Omega^+} & \mathbf{C}_{be}^{\Omega^+} \\ \mathbf{0} & \mathbf{C}_{eb}^{\Omega^+} & \mathbf{C}_{ee}^{\Omega^+} \end{bmatrix} \begin{Bmatrix} \dot{\mathbf{u}}_i \\ \dot{\mathbf{u}}_b \\ \dot{\mathbf{u}}_e \end{Bmatrix} + \begin{bmatrix} \mathbf{C}_{ii}^{\mathbf{F}\Omega} & \mathbf{C}_{ib}^{\mathbf{F}\Omega} & \mathbf{0} \\ \mathbf{C}_{bi}^{\mathbf{F}\Omega} & \mathbf{C}_{bb}^{\mathbf{F}\Omega} + \mathbf{C}_{bb}^{\mathbf{F}\Omega^+} & \mathbf{C}_{be}^{\mathbf{F}\Omega^+} \\ \mathbf{0} & \mathbf{C}_{eb}^{\mathbf{F}\Omega^+} & \mathbf{C}_{ee}^{\mathbf{F}\Omega^+} \end{bmatrix} \begin{Bmatrix} \mathbf{p}_i \\ \mathbf{p}_b \\ \mathbf{p}_e \end{Bmatrix} = \mathbf{P}^{eff} \end{aligned} \quad (14)$$

Similarly substituting the \mathbf{Q}_e term to the eq.(10) yields the following form of the right hand side term

$$\mathbf{Q}^{eff} = \begin{Bmatrix} \mathbf{h}_b^{\mathbf{F}\Omega^+} - \mathbf{R}_{be}^{\mathbf{F}\Omega^+} \ddot{\mathbf{u}}_e^0 - \left(\tilde{\mathbf{C}}_{be}^{\mathbf{F}\Omega^+} \right)^{\top} \dot{\mathbf{u}}_e^0 + \frac{1}{\gamma^{\mathbf{F}}} \mathbf{H}_{be}^{\mathbf{F}\Omega^+} \mathbf{p}_e^0 + \mathbf{M}_{be}^{\mathbf{F}\Omega^+} \dot{\mathbf{p}}_e^0 \\ \mathbf{R}_{eb}^{\mathbf{F}\Omega^+} \ddot{\mathbf{u}}_b^0 + \left(\tilde{\mathbf{C}}_{eb}^{\mathbf{F}\Omega^+} \right)^{\top} \dot{\mathbf{u}}_b^0 - \frac{1}{\gamma^{\mathbf{F}}} \mathbf{H}_{eb}^{\mathbf{F}\Omega^+} \mathbf{p}_b^0 - \mathbf{M}_{eb}^{\mathbf{F}\Omega^+} \dot{\mathbf{p}}_b^0 \end{Bmatrix} \quad (15)$$

$$\begin{aligned}
 & \begin{bmatrix} \mathbf{R}^{\mathbf{F}\Omega}_{ii} & \mathbf{R}^{\mathbf{F}\Omega}_{ib} & \mathbf{0} \\ \mathbf{R}^{\mathbf{F}\Omega}_{bi} & \mathbf{R}^{\mathbf{F}\Omega}_{bb} + \mathbf{R}^{\mathbf{F}\Omega+}_{bb} & \mathbf{R}^{\mathbf{F}\Omega+}_{be} \\ \mathbf{0} & \mathbf{R}^{\mathbf{F}\Omega+}_{eb} & \mathbf{R}^{\mathbf{F}\Omega+}_{ee} \end{bmatrix} \begin{Bmatrix} \ddot{\mathbf{u}}_i \\ \ddot{\mathbf{u}}_b \\ \ddot{\mathbf{u}}_e \end{Bmatrix} + \\
 & \begin{bmatrix} \left(\tilde{\mathbf{C}}^{\mathbf{F}\Omega}_{ii}\right)^{\top} & \left(\tilde{\mathbf{C}}^{\mathbf{F}\Omega}_{ib}\right)^{\top} & \mathbf{0} \\ \left(\tilde{\mathbf{C}}^{\mathbf{F}\Omega}_{bi}\right)^{\top} & \left(\tilde{\mathbf{C}}^{\mathbf{F}\Omega}_{bb}\right)^{\top} + \left(\tilde{\mathbf{C}}^{\mathbf{F}\Omega+}_{bb}\right)^{\top} & \left(\tilde{\mathbf{C}}^{\mathbf{F}\Omega+}_{be}\right)^{\top} \\ \mathbf{0} & \left(\tilde{\mathbf{C}}^{\mathbf{F}\Omega+}_{eb}\right)^{\top} & \left(\tilde{\mathbf{C}}^{\mathbf{F}\Omega+}_{ee}\right)^{\top} \end{bmatrix} \begin{Bmatrix} \dot{\mathbf{u}}_i \\ \dot{\mathbf{u}}_b \\ \dot{\mathbf{u}}_e \end{Bmatrix} - \\
 & \frac{1}{\gamma^F} \begin{bmatrix} \mathbf{H}^{\mathbf{F}\Omega}_{ii} & \mathbf{H}^{\mathbf{F}\Omega}_{ib} & \mathbf{0} \\ \mathbf{H}^{\mathbf{F}\Omega}_{bi} & \mathbf{H}^{\mathbf{F}\Omega}_{bb} + \mathbf{H}^{\mathbf{F}\Omega+}_{bb} & \mathbf{H}^{\mathbf{F}\Omega+}_{be} \\ \mathbf{0} & \mathbf{H}^{\mathbf{F}\Omega+}_{eb} & \mathbf{H}^{\mathbf{F}\Omega+}_{ee} \end{bmatrix} \begin{Bmatrix} \mathbf{p}_i \\ \mathbf{p}_b \\ \hat{\mathbf{p}}_e \end{Bmatrix} - \\
 & \begin{bmatrix} \mathbf{M}^{\mathbf{F}\Omega}_{ii} & \mathbf{M}^{\mathbf{F}\Omega}_{ib} & \mathbf{0} \\ \mathbf{M}^{\mathbf{F}\Omega}_{bi} & \mathbf{M}^{\mathbf{F}\Omega}_{bb} + \mathbf{M}^{\mathbf{F}\Omega+}_{bb} & \mathbf{M}^{\mathbf{F}\Omega+}_{be} \\ \mathbf{0} & \mathbf{M}^{\mathbf{F}\Omega+}_{eb} & \mathbf{M}^{\mathbf{F}\Omega+}_{ee} \end{bmatrix} \begin{Bmatrix} \dot{\mathbf{p}}_i \\ \dot{\mathbf{p}}_b \\ \dot{\mathbf{p}}_e \end{Bmatrix} = \begin{Bmatrix} -\mathbf{Q}^{\mathbf{F}}_i + \mathbf{h}^{\mathbf{F}}_i \\ \mathbf{h}^{\mathbf{F}}_b \\ \mathbf{0} \end{Bmatrix} + \mathbf{Q}^{eff} \quad (16)
 \end{aligned}$$

Window 3-6

Chapter 4

CONSTITUTIVE MODELS FOR DYNAMIC APPLICATIONS

4.1 HS-s model

The small strain version (HSs) of HS model can be used to model soil behavior in dynamic simulations. It includes stress/strain dependent stiffness moduli varying from the initial value E_o at very low strains through E_{ur} up to E_{50} and less for larger strain amplitudes. The assumed hypo-elastic Hardin-Drnevich law used at low strains allows to model hysteretic damping fairly well. The main drawback of the model in dynamic simulations is such that it cannot reproduce well the effect of progressive densification due to cyclic shearing with constant stress amplitude. Behavior of the model in drained and undrained triaxial test conditions is shown in figures below. One may notice that in the drained case all stress cycles of same amplitude will produce plastic straining and variation of position of the internal shear mechanism only in the first cycle. Densification/dilation is produced only by shear plastic mechanisms. In the undrained case the excess of pore water pressure is generated only when volumetric irreversible strains are produced. For constant stress amplitudes the excess of pore pressure will be observed only in the first cycle and then it will stabilize. Hence this model cannot be used for loose sands that may liquefy due to cyclic straining and another one, called densification model (see 4.2) is recommended.

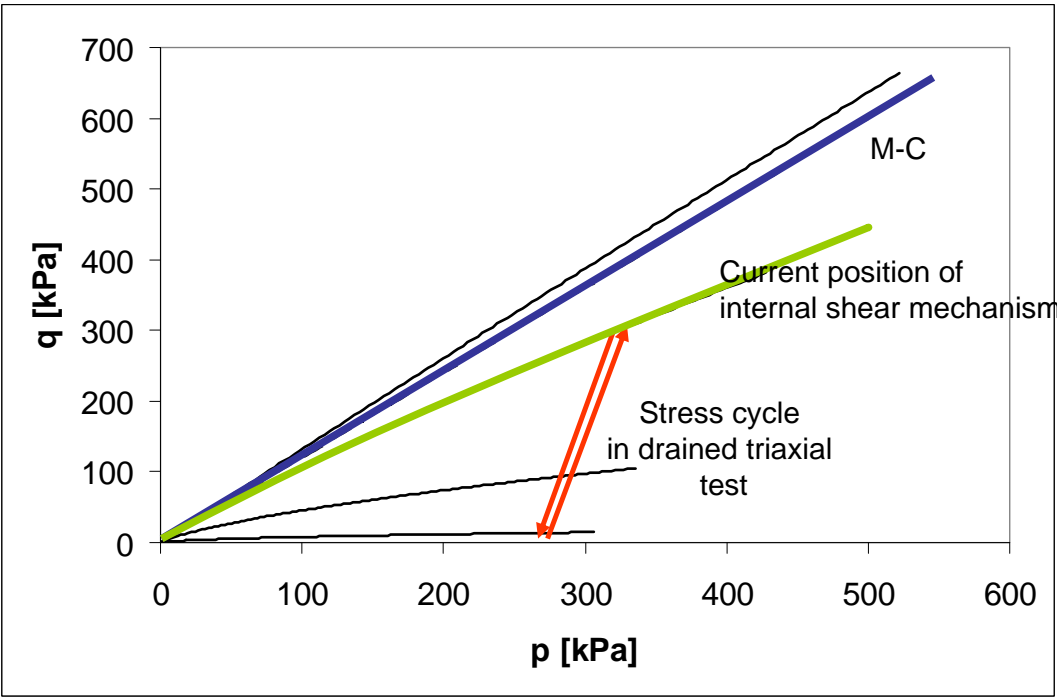


Figure 4.1: HSs model in drained triaxial test

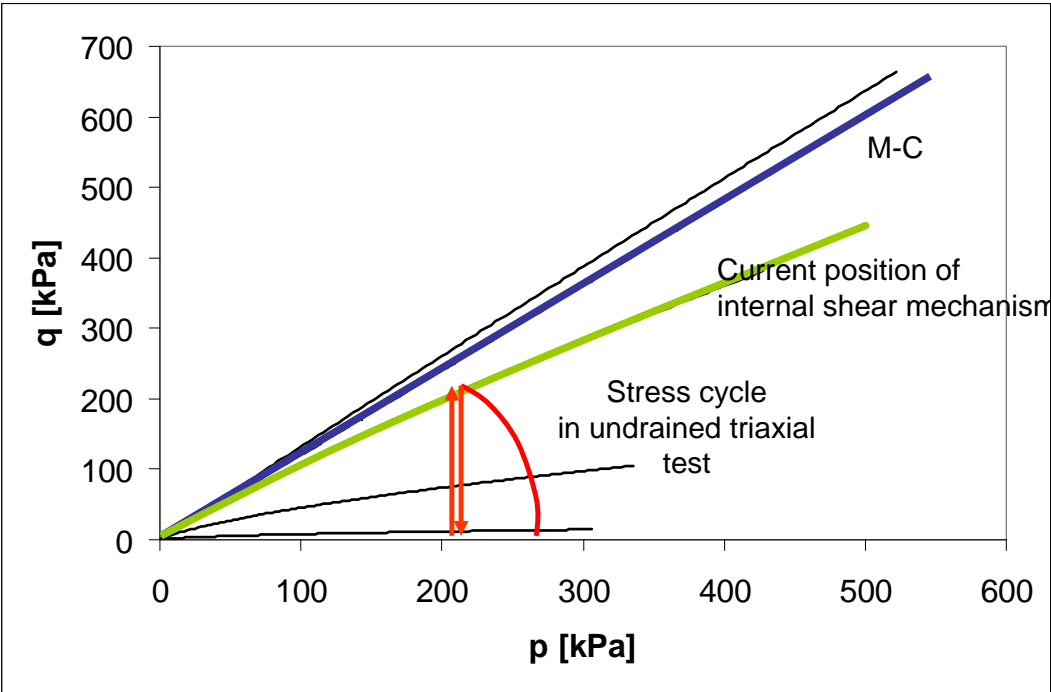


Figure 4.2: HSs model in undrained triaxial test

4.2 Densification model

Densification model, designed to reproduce behavior of loose sandy soils was derived directly from the HSs model by adding an extra explicit densification mechanism. Hence it belongs to the class of elasto-plastic models with shear strain hardening (this mechanism can be canceled in the user interface) controlled in addition by the Mohr-Coulomb criterion (see the corresponding report on HSs model). As the densification mechanism is defined by an explicit formula the purely deviatoric plastic flow rule is assumed for both current shear yield surface and, if needed, the MC one (dilatancy angle $\psi = 0^\circ$). Moreover, the volumetric (cap) mechanism is canceled. As in the HSs model, small strain stiffness variation in the range of low strains can be activated. However, contrary to the HSs model all formula for the unloading-reloading E_{ur} and initial E_o stiffness formula depend on effective mean pressure p' rather than on σ_3 , and are expressed as follows:

$$E_{ur} = E_{ur}^{ref} \left(\frac{p^*}{\sigma_{ref}} \right)^m \quad E_o = E_o^{ref} \left(\frac{p^*}{\sigma_{ref}} \right)^m \quad (4.1)$$

where: $p^* = \max(p', \sigma_L)$

σ_L is usually assumed to be of order of few kPa (5 kPa for instance) to avoid zero stiffness for vanishing mean effective stress.

The small strain stiffness variation in the range of small strains, described by the Hardin-Drnevich formula, will help to include the effect of hysteretic damping in dynamic simulations.

The incremental stress-strain relation can be written in the form

$$d\sigma = \mathbf{D}^e (d\epsilon - d\epsilon^p - d\epsilon^{acc}) \quad (4.2)$$

where the infinitesimally small increment of accumulated volumetric strain $d\epsilon^{acc}$ in the Zienkiewicz's model is defined as follows

$$d\epsilon_{ij}^{acc} = -\frac{A}{1+B} \frac{d\kappa}{\kappa} m_{ij} \quad (4.3)$$

$$d\kappa = \exp(-\gamma \tilde{\eta}) d\xi \quad (4.4)$$

$$d\xi = \sqrt{de_{ij} de_{ij}} \quad (4.5)$$

$$de_{ij} = d\epsilon_{ij} - d\epsilon_m \delta_{ij} \quad (4.6)$$

$$(4.7)$$

The two densification laws are considered in the current version i.e. Zienkiewicz's [12] and Sawicki's one [10].

In original formulations of both densification laws the mapping tensor m_{ij} is defined as $m_{ij} = \frac{1}{3} \delta_{ij}$ and δ_{ij} denotes the Kronecker's symbol. The stress ratio $\tilde{\eta}$, in Zienkiewicz's model, is defined as $\tilde{\eta} = \frac{q(\sigma_{ij})}{p}$ or $\tilde{\eta} = \frac{q(\tilde{\sigma}_{ij} - \sigma_{ij}^o)}{p}$ (here the initial stress state is denoted by σ_{ij}^o). The latter definition was used by Zienkiewicz to solve the problem of liquefaction of San Fernando dam. It is also used in the current implementation.

4.2.1 Sawicki's model for time domain applications

The main finding of Sawicki and Świdziński, derived from cyclic simple shear tests, is such that there exists so called common compaction curve representing given loose sand, no matter how big are the shear strain cycles. In the original version of Sawicki's model the densification law is insensitive to the mean stress variation. With this assumption the accumulated volumetric strain produced in N cycles of cyclic shear test, run at constant given shear strain amplitude γ_o , is defined by the following expression

$$\varepsilon^{acc} = e_o C_1 \ln(1 + C_2 z) \quad (4.8)$$

where z parameter, corresponding to the accumulated deviatoric straining, is defined as $z = \frac{1}{4} N \gamma_o^2$

The main drawback of this model is such that it cannot be directly used in standard FE calculations in time domain because of presence of the term N that is equal to the number of the uniform shear strain cycles.

It is however possible to adapt Sawicki's model to time domain applications using a similar densification law as the one proposed by Zienkiewicz. It can easily be shown that Zienkiewicz's model, even for constant mean stress, cannot reproduce the common compaction curve. To achieve this goal let us formulate the modified densification law as a set of the following equations:

$$d\kappa = \tilde{\eta} d\xi \quad (4.9)$$

$$d\varepsilon_v^{acc} = -\frac{A}{1 + B\kappa} d\kappa \quad (4.10)$$

$$\tilde{\eta} = \frac{q(\tilde{\sigma}_{ij})}{p} \quad (4.11)$$

$$\tilde{\sigma}_{ij} = \sigma_{ij} - \sigma_{ij}^o \quad (4.12)$$

In the above equations the stress level $\tilde{\eta}$ is computed based on q invariant of the stress difference measured between the current configuration and the one at the initial state. Let us now examine this law in the context of strain driven simple shear test that generates stress paths within the elastic domain. If we assume that the mean stress remains constant during the test (this is not possible when isotropic mapping vector is used in the definition of accumulated strain) then the elastic stiffness remains constant, and the stress ratio $\tilde{\eta}$ is computed as:

$$\tilde{\eta} = \frac{|\tau_{xy}|}{p_o} = \frac{G(p_o) |\gamma_{xy}|}{p_o} \quad (4.13)$$

$$d\xi = \sqrt{d e_{ij} d e_{ij}} = \sqrt{2} |d\varepsilon_{xy}| = \frac{\sqrt{2}}{2} |d\gamma_{xy}| \quad (4.14)$$

$$d\kappa = \tilde{\eta} d\xi = \frac{G(p_o) |d\gamma_{xy}| \sqrt{2}}{p_o} \frac{\sqrt{2}}{2} |d\gamma_{xy}| \quad (4.15)$$

After 1/4 of full shear strain cycle with constant strain amplitude $\gamma_{xy} = \gamma_o$ the accumulated κ value is equal to $\kappa^{1/4} = \frac{\sqrt{2}}{2} \frac{G(p_o)}{p_o} \frac{1}{2} \gamma_o^2$. Hence after N cycles it is equal to

$$\kappa(N) = 4N \frac{1}{2} \frac{\sqrt{2}}{2} \frac{G(p_o)}{p_o} \gamma_o^2 = \sqrt{2} N \frac{G(p_o) \gamma_o^2}{p_o} \quad (4.16)$$

Let us now assume that in Zienkiewicz's model we fix the C parameter to zero what allows us to integrate the accumulated strain in the closed form. The closed form expressions for accumulated volumetric strain produced by the two models can be written as follows

$$\text{Sawicki's model : } \varepsilon_v^S = e_o C_1 \ln \left(1 + C_2 \frac{1}{4} N \gamma_o^2 \right) \quad (4.17)$$

$$\text{modified Zienkiewicz's model : } \varepsilon_v^Z = \frac{A}{B} \ln \left(1 + B \sqrt{2} N \frac{G(p_o)}{p_o} \gamma_o^2 \right) \quad (4.18)$$

From the above expressions one can deduce that by adding $\tilde{\eta}$ function to the Zienkiewicz's densification law, and fixing parameter C to zero, one may obtain in the accumulated volumetric strain value the term $N \gamma_o^2$. This yields the following relations between C_1, C_2 parameters of original Sawicki's model and A, B of the corresponding modified Zienkiewicz's one

$$B = \frac{1}{4\sqrt{2}} C_2 \frac{p_o}{G(p_o)} \quad (4.19)$$

$$A = e_o C_1 B \quad (4.20)$$

$$(4.21)$$

where stress dependent shear modulus $G(p_o)$ is expressed by the formula

$$G(p_o) = G_o^{ref} \left(\frac{p_o}{\sigma^{ref}} \right)^m \quad (4.22)$$

After replacing the term $G(p_o)$ by the formula 4.22 in expression 4.19 one gets the following definition of B parameter

$$B = \frac{1}{4\sqrt{2}} C_2 \frac{p_o}{G_o^{ref} \left(\frac{p_o}{\sigma^{ref}} \right)^m} = \frac{1}{4\sqrt{2}} C_2 \frac{\sigma^{ref}}{G_o^{ref}} \frac{1}{\sigma^{ref}} \frac{p_o}{\left(\frac{p_o}{\sigma^{ref}} \right)^m} = \underbrace{\frac{1}{4\sqrt{2}} C_2 \frac{\sigma^{ref}}{G_o^{ref}}}_{B_o} \underbrace{\left(\frac{p_o}{\sigma^{ref}} \right)^{1-m}}_{f_1\left(\frac{p_o}{\sigma^{ref}}\right)} \quad (4.23)$$

The corresponding A parameter can be expressed as follows:

$$A = e_o C_1 B_o f_1 \left(\frac{p_o}{\sigma^{ref}} \right) \quad (4.24)$$

This densification law, that is a time domain equivalent of Sawicki's model, will not reproduce the common compaction curve for shear strain amplitudes that yield plastic straining. In that case the stress ratio $\tilde{\eta}$ tends to some asymptotic value and therefore the resulting accumulated

strain amplitude will significantly be underestimated. To remedy this problem a modification of evolution law for shear straining history parameter κ was proposed

$$d\kappa = \tilde{\eta} f_2 \left(\frac{\xi^{pl}}{\xi} \right) d\xi \quad (4.25)$$

and the newly introduced function f_2 is expressed as follows

$$f_2 \left(\frac{\xi^p}{\xi} \right) = 1 + C \left(\frac{\xi^p}{\xi} \right)^D \quad (4.26)$$

where C and D are the parameters derived from optimization procedure based on given C_1 and C_2 values. It has been found that C and D parameters are insensitive to the mean stress value. Therefore one may optimize them for a given reference mean stress.

The history of plastic straining is represented by ξ^p parameter integrated in time using the following expression

$$\xi^p = \int_{t_o}^t \sqrt{\dot{e}_{ij}^p \dot{e}_{ij}^p} dt \quad (4.27)$$

It has to be emphasized here that in the M-C plastic mechanism the purely deviatoric plastic flow rule ($\psi = 0^\circ$) is adopted. This way all volumetric plastic changes are described by the densification law.

To summarize the densification law that is equivalent to the Sawicki's model one has to define the 2 parameters C_1 and C_2 . For given C_1 , C_2 and assumed level of the mean stress p_o the C and D parameters are derived by minimizing the following functional

$$\sum_{i=1}^M \sum_{j=1}^N \left(\frac{e_o C_1 \ln \left(1 + C_2 \frac{1}{4} j \gamma_o^2 \right) - \varepsilon_v^{acc}(\gamma_{oi}, j)}{e_o C_1 \ln \left(1 + C_2 \frac{1}{4} j \gamma_o^2 \right)} \right)^2 \rightarrow \min \quad (4.28)$$

where i is the number of all considered values of shear strain amplitudes γ_o (all must generate plastic straining), N is the maximum number of strain cycles, j is the current cycle index, γ_{oi} is the current shear strain amplitude and ε_v^{acc} is obtained by numerical integration of eq. 4.10 for problem of cyclic simple shear test.

An example of the optimization procedure is shown in figure 4.3

The evolution of the accumulated volumetric strain fairly well approximates Sawicki's common compaction curve expressed as a function of ε_v^{acc} with respect to the z parameter.

In the above simulations we assume that mean stress p does not vary during drained simple shear test. To achieve this goal one cannot assume the mapping tensor to be expressed as $m_{ij} = \frac{1}{3} \delta_{ij}$. In the current implementation m_{ij} may have nonzero terms exclusively on normal strain directions but only those that are not constrained by the boundary conditions. In the practical boundary value problems this setting is made once the increment of the strains is given $\Delta \varepsilon_{ij}$

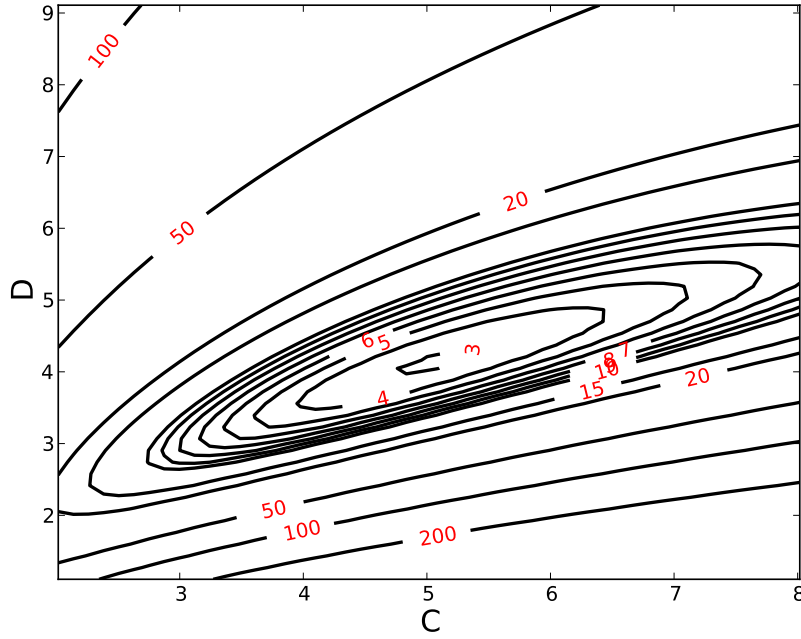


Figure 4.3: Result of optimization of C and D parameters

$$m_{ij} = \frac{|\varepsilon_{ij}|}{\sqrt{\sum_{i=1}^3 \varepsilon_{ii}^2}} \delta_{ij} \quad (4.29)$$

However, it may vary from iteration to iteration for more complex problems.

This procedure, in case of a simple shear test, yields the m_{ij} tensor with only one nonzero value that corresponds to the vertical strain component.

Several examples showing all capabilities of the model are given in the benchmark section devoted to densification model.

4.2.2 User interface for densification model

The user interface specific to this model consists of the two group of parameters located in parameter groups *Elastic* and *Nonlinear*.

All parameters in group *Elastic* are basically the same as those for the HSs model with the only difference such that stiffness moduli are functions of mean effective stress p' and not σ_3 (see Fig.(4.5) below). In the advanced setup one may activate small strain option and set the E_o^{ref} and $\gamma_{0.7}$ values. In the basic version (small strain is canceled) the E_{ur}^{ref} modulus must represent the equivalent small strain stiffness E at the reference stress σ_{ref} and strain amplitude of order 10^{-4} .

The user interface for parameters collected in group *Nonlinear* is shown in Fig.(4.6). By setting proper values of the parameters user may cancel several effects that can be described by this model. The three major effects can be switched ON/OFF:

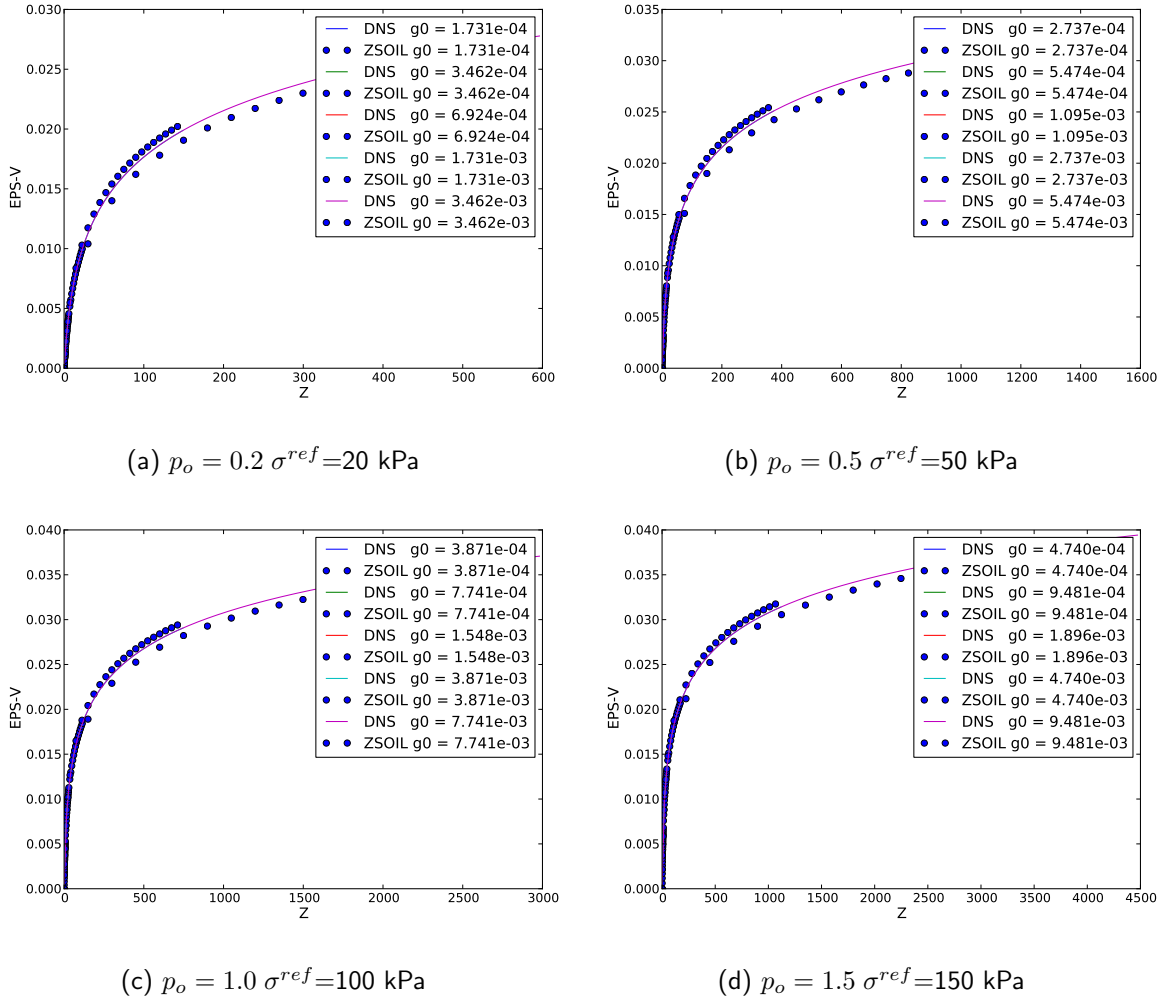
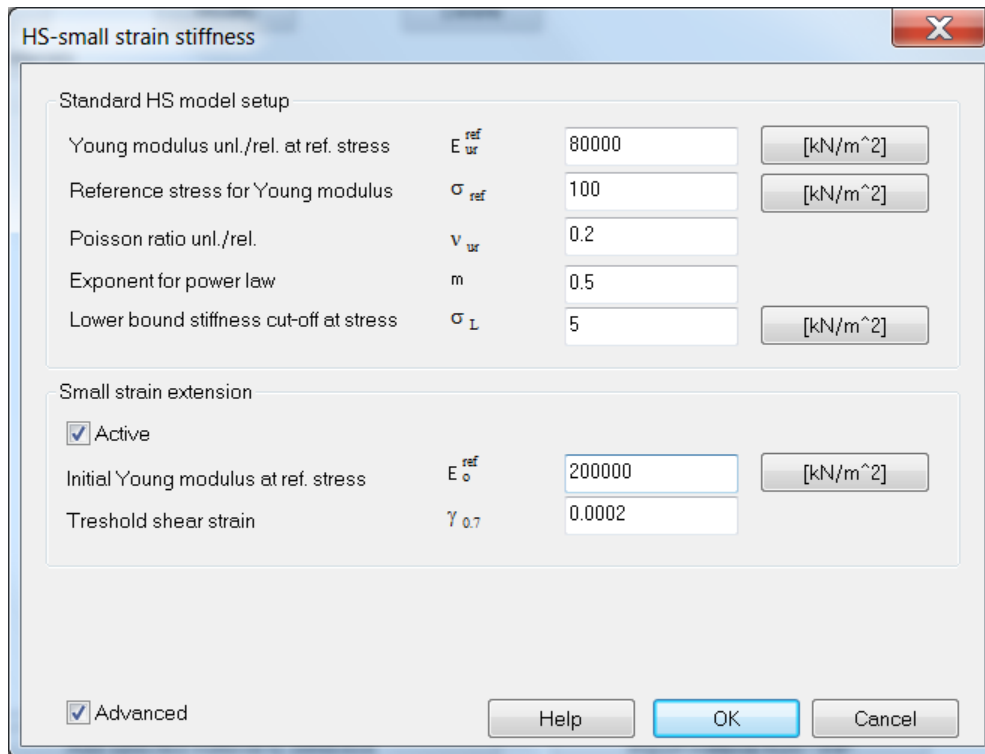


Figure 4.4: Comparison of compaction curves for original Sawicki's model and its modified time domain version

1. Shear hardening plasticity within the MC envelope (☒ **Shear plastic mechanism**)
2. MC envelope (by setting very large values of strength parameters)
3. Densification mechanism (☒ **Densification mechanism**)

It has to be mentioned that by deactivating the MC plasticity the shear hardening mechanism should be deactivated too.

Densification mechanism is responsible for modeling progressive densification during straining (not necessarily plastic). User may use the two densifications laws i.e. by Zienkiewicz or by Sawicki. Activation of shear hardening plasticity allows to reproduce static liquefaction with the phase transition line located below the MC line in the $p - q$ plane. It also allows to reproduce hyperbolic form of the $q - \varepsilon_1$ curves in the drained triaxial test in similar manner as in the HSs model. The MC yield surface controls plastic admissibility of the resulting stress state. The accumulated strain mapping set to ☒ **Isotropic** will impose isotropic projection of the accumulated volumetric strain increment on all three normal directions while the ☒ **Extended** will impose nonproportional projection described by the formula 4.29.



HS-small strain stiffness

Standard HS model setup

Young modulus unl./rel. at ref. stress	E_{ur}^{ref}	80000	[kN/m ²]
Reference stress for Young modulus	σ_{ref}	100	[kN/m ²]
Poisson ratio unl./rel.	ν_{ur}	0.2	
Exponent for power law	m	0.5	
Lower bound stiffness cut-off at stress	σ_L	5	[kN/m ²]

Small strain extension

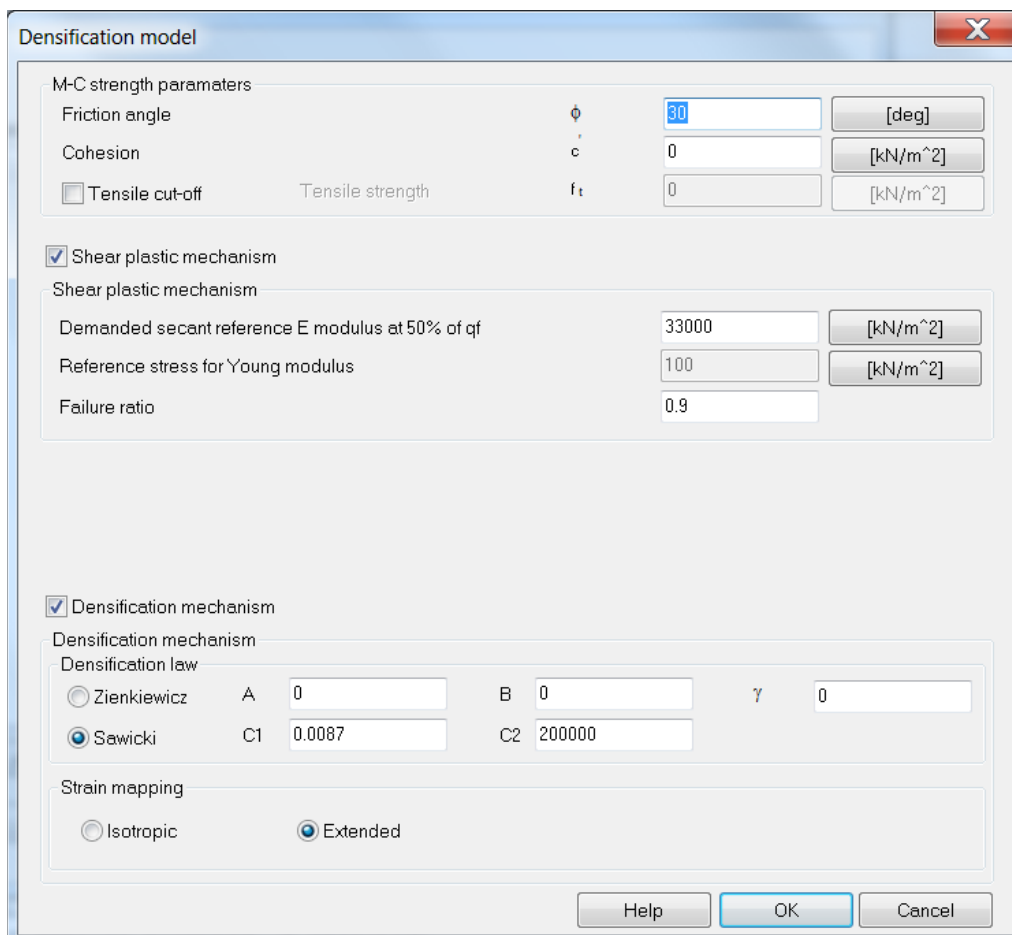
☒ Active

Initial Young modulus at ref. stress	E_o^{ref}	200000	[kN/m ²]
Threshold shear strain	$\gamma_{0.7}$	0.0002	

☒ Advanced

Help OK Cancel

Figure 4.5: User interface for elastic stiffness parameters



Densification model

M-C strength parameters

Friction angle	ϕ	30	[deg]
Cohesion	c	0	[kN/m ²]
<input type="checkbox"/> Tensile cut-off	Tensile strength	f_t	0 [kN/m ²]

☒ Shear plastic mechanism

Shear plastic mechanism

Demanded secant reference E modulus at 50% of q_f	33000	[kN/m ²]
Reference stress for Young modulus	100	[kN/m ²]
Failure ratio	0.9	

☒ Densification mechanism

Densification mechanism

Densification law

<input type="radio"/> Zienkiewicz	A	0	B	0	γ	0
<input checked="" type="radio"/> Sawicki	C1	0.0087	C2	200000		

Strain mapping

☐ Isotropic ☒ Extended

Help OK Cancel

Figure 4.6: Strength and densification law parameters in group *Nonlinear*

Chapter 5

USER INTERFACE

5.1 Transient dynamic driver

Window 5-1: Dynamics for single-phase soil-structure interaction problems

ZSoil®

- A. Problem type: Deformation
- B. Analysis type: any
- C. Driver: Dynamics
- C1. Driver type: Driven load

This driver can be used for solving a transient dynamic soil-structure interaction problems for single-phase media. The domain reduction method (DRM) can be used to reduce size of the computational model by setting DRM boundary layer of elements in the preprocessor and declaring the free field motion project in the edit field under Associated preprocessed projects

Driver	Type	Time start	Time end	Increment	Multiplier	Nonl. solver settings	Dyn. anal. settings	Store restart
Initial State		0.5	1	0.1		Default	--	<input type="checkbox"/>
Dynamics	Driven Load	1 [s]	10 [s]	0.01 [s]	1	Default	Default	<input type="checkbox"/>

Project properties

☒ Settings

Version type: Advanced

Units: STANDARD

KN-m-rad-s-C

☒ Analysis and problem type

Analysis type: Plane Strain

Problem type: Deformation

☒ Project description

Project title: Zsoil example

Model description:

Author: ZACE

Company: ZACE

☒ Associated preprocessed projects

Heat project:

Humidity project:

Free field motion project:

☒ Large displacements/rotations/strains

Large displacements/rotations: False

Update coordinates during const.: False

Control data of the driver are:

<i>Key</i>	<i>Option</i>	<i>Comment</i>	<i>Default</i>	<i>Remarks</i>
C1				1,,3,5,6
C1.1	Time start	Initial time value	(0.0)	2,3
C1.2	Time end	Final time value	(1.0)	2,3
C1.3	Time increment	Initial time step	(0.01)	3, 8
C1.4	Multiplier	Time step multiplier	(1.0)	
C1.5	Nonl. Solver	Control data		
C1.6	Dyn. Solver	Control data		9C

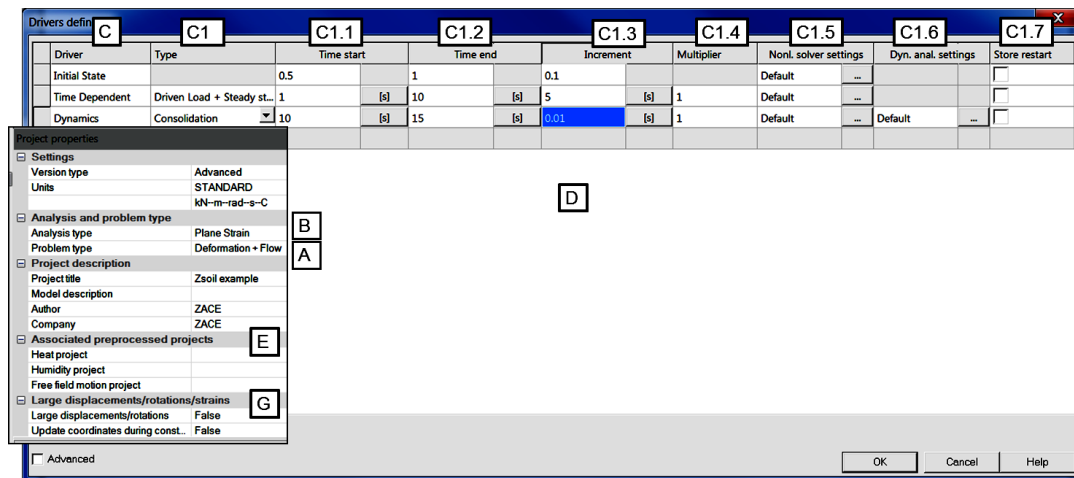
Window 5-1

Window 5-2: Dynamics for two-phase soil-structure interaction problems

ZSoil®

- A.** Problem type: Deformation+Flow
B. Analysis type: Plane Strain, 3D
C. Driver: Dynamics
C1. Driver type: Consolidation

This driver can be used for solving a coupled transient dynamic soil-structure interaction problems for two-phase media. In the current version the domain reduction method (DRM) for the two-phase problems is not yet supported.



Control data of the driver are:

Key	Option	Comment	Default	Remarks
C1				1,,3,5,6
C1.1	Time start	Initial time value	(0.0)	2,3
C1.2	Time end	Final time value	(1.0)	2,3
C1.3	Time increment	Initial time step	(0.01)	3, 8
C1.4	Multiplier	Time step multiplier	(1.0)	
C1.5	Nonl. Solver	Control data		
C1.6	Dyn. Solver	Control data		

Window 5-2

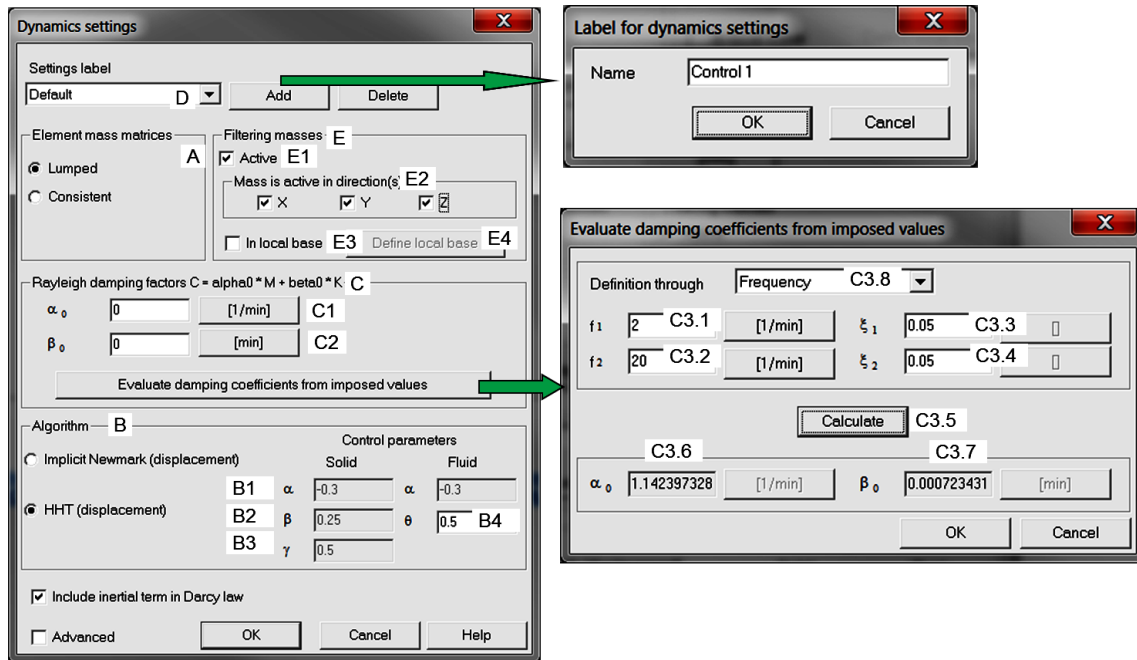
Remarks:

1. Driver type: Driven Load is the only available driver for single-phase media, for two-phase both Driven Load and Consolidation are available although the first one does not seem to be meaningful
2. Time is treated as a physical parameter (consistently with material data)
3. It is recommended to use seconds ([s]) as default time units
4. Time parameter is used as a common argument of all existence and load time functions.
5. A sequence of Dynamic Drivers can be defined, with different time step specification.
6. Within a sequence of Dynamic, Driven Load Drivers, an intermediate Time Dependent (i.e. concerning statics) or Stability Driver can be added.

7. In the sequence of drivers the state of the structure at the start of subsequent driver takes into account results (e.g. plastic status, stresses, deformation) of previous dynamic driver(s).
8. Additional time steps will be automatically enforced by load and existence time functions, at all their characteristic points
9. There are two possible methods of imposing seismic input to the structure:
 - A: by setting time dependent displacement /velocity / acceleration at support node(s) and solving for total motion
 - B: as an imposed global acceleration $\mathbf{a}_g = \ddot{\mathbf{u}}_g$ of the ground, common to the whole structure, and solving for relative motion.
 - C: Detailed description of control data for dynamic driver is given in Win.(5-3)

Window 5-3: Transient dynamics settings

ZSoil®



- A.** sets which type of the mass matrix is to be used; only lumped masses are supported
- B.** sets the time history analysis algorithm type (Newmark or Hilber-Hughes-Taylor (HHT))
- B1.** sets α parameter for HHT algorithm (default -0.3), $\alpha = 0$ corresponds to Newmark alg.
- B2.** sets β parameter for HHT (depends on α) and Newmark (default 0.25)
- B3.** sets γ parameter for HHT (depends on α) and Newmark (default 0.50)
- B4.** sets θ parameter for integration scheme for pore pressure (default 0.50)
- C.** sets Rayleigh damping factors α_o (applies to the mass) and β_o (applies to the stiffness)
- C1.** sets directly Rayleigh damping factor α_o
- C1.** sets directly Rayleigh damping factor β_o
- C3.** runs Rayleigh damping factors calculator and puts results in **C1.** and **C2.** edits
- C3.1** sets 1-st angular frequency ω_1 , frequency f_1 , or period T_1 depending on the state of the combo-box C3.8
- C3.2** sets 2-nd angular frequency ω_2 , frequency f_2 , or period T_2 depending on the state of the combo-box C3.8
- C3.3** sets percentage of the critical damping for ω_1 , f_1 or T_1
- C3.4** sets percentage of the critical damping for ω_2 , f_2 or T_2
- C3.5** runs α_o and β_o calculation
- C3.6** shows calculated α_o
- C3.7** shows calculated β_o
- C3.8** switch from angular frequency to frequency, or period
- D.** adds current dynamic settings to the list of control settings to be used later in conjunction with a selected driver Dynamics in Analysis & Drivers dialog box
- E.** sets filtering of mass matrix for selected global or local directions
- E1.** switches ON/OFF filtering of mass matrix
- E2.** selects active directions for mass matrix
- E3.** selects local or global coordinate system to filter mass matrix along selected directions

- E4.** activates a dialog box to set up the local coordinate system for mass filtering (note that for local systems defined through the vector in 3D only filtering in the local X direction (vector direction) is meaningful as the other two directions are not defined in a unique manner)

Remark:

Assumed damping factors apply to all materials unless overwritten locally in Materials

Window 5-3

5.2 Eigenvalue and eigenmodes driver

The Eigenvalue and eigenmodes driver can be used for Deformation and Deformation+Flow analyses. In the latter case mass density depends on the current saturation ratio.

Window 5-4: Eigenvalues and eigenmodes

ZSoil®

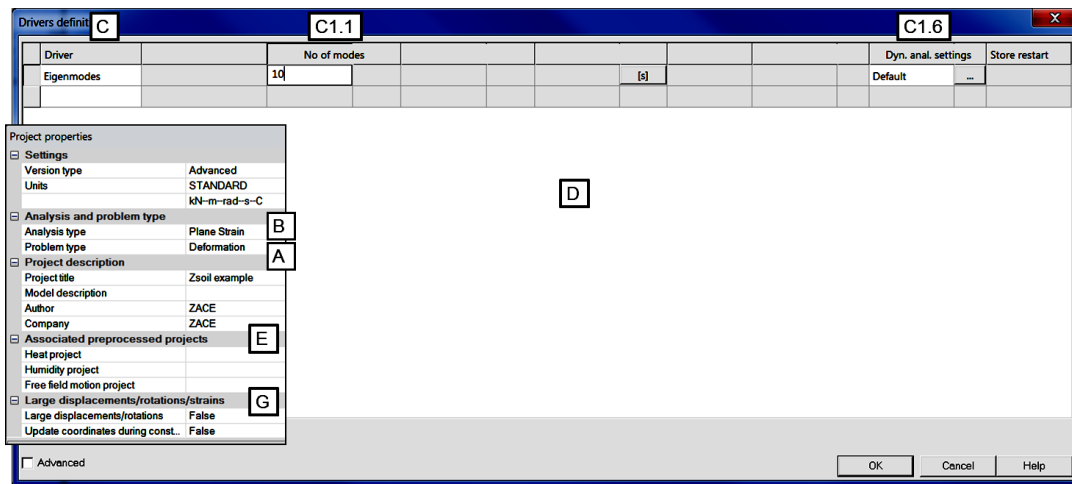
A. Problem type: Deformation

B. Analysis type: any

C. Driver: Eigenvalues

C1. Driver type:

In the Deformation mode this driver can be used for detection of declared number of eigenvalues and corresponding eigenmodes for single-phase media including structural elements.



Control data of the driver are:

Key	Option	Comment	Default	Remarks
C1.1	No of modes			1, 2
C1.6	Dyn. Solver	Control data		

Remarks:

1. Number of detected eigenvalues is limited by total number of free degrees of freedom
2. For each eigenmode mass participation factors are computed for all directions

Window 5-4

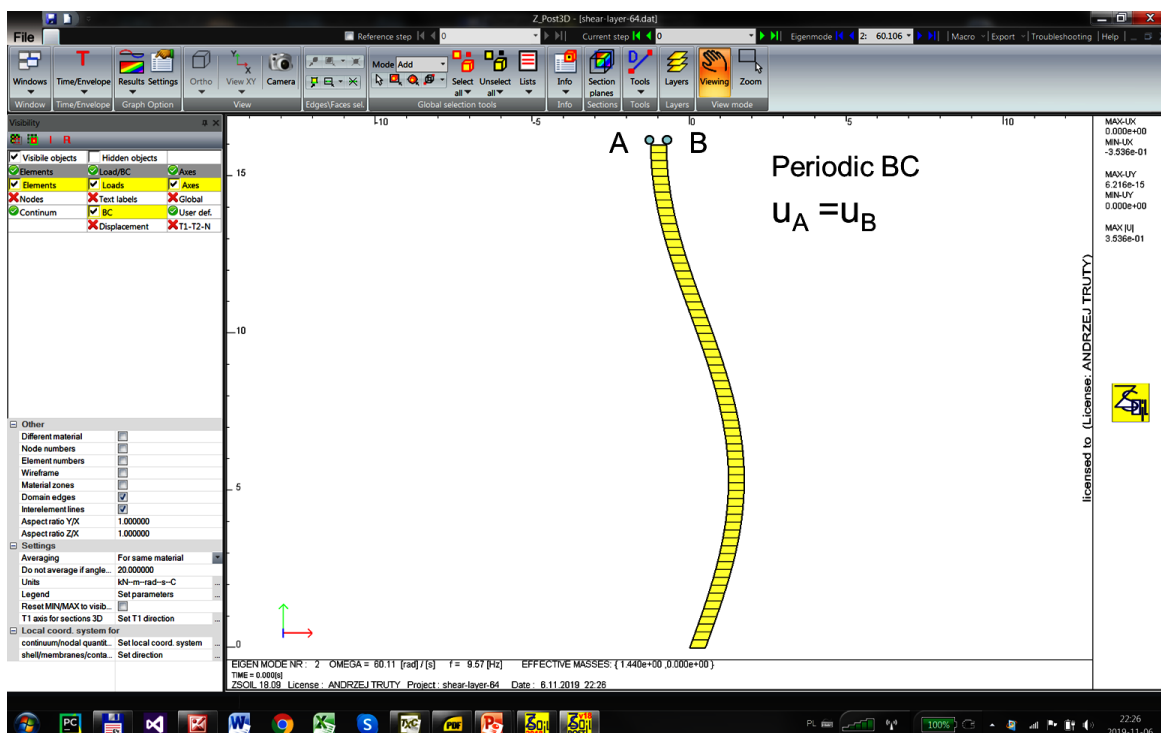
Window 5-5: Eigenvalues and eigenmodes: Vibration modes for shear layer

ZSoil®

Data: BENCHMARKS/DYNAMICS/EIGENMODES/shear-layer-64.INP

- A.** Problem type: Deformation
B. Analysis type: Plane Strain
C1. Driver type: Eigenvalues

This example concerns eigenvalue analysis of shear layer. To analyze such a problem one can set periodic boundary conditions that helps to tie selected degrees of freedom on two opposite boundaries. In the considered case we assume that $\mathbf{u}_A = \mathbf{u}_B$. The computed eigenvalues, eigenmodes and mass participation factors are given in the postprocessor. The computed eigenvalues are also stored in the *.log file.



Window 5-5

A. Problem type: Deformation+Flow
B. Analysis type: any
C. Driver: Eigenvalues
C1. Driver type:

Driver	No. of modes	Dyn. anal. settings	Store restart
Initial State	0.5	Default	Default
Eigenmodes	1	Default	Store restart
	0.1		

Project description

Project title: Zsol example

Model description: ZACE

Company: ZACE

Associated preprocessed projects:

Heat project

Humidity project

Free field motion pr...

Advanced

Key	Option	Comment	Default	Remarks
C1.1	No of modes			1, 2
C1.6	Dyn. Solver	Control data		

1. Number of detected eigenvalues is limited by total number of free degrees of freedom
2. For each eigenmode mass participation factors are computed for all directions

Window 5-6

5.3 Seismic input

Window 5-7: Seismic input

This option is available from the main menu Assembly/Seismic input. Seismic input option allows the user to apply the earthquake in the finite element model

- in the relative format for rigid base model; here seismic input is given as an imposed acceleration $\mathbf{a}_g = \ddot{\mathbf{u}}_g$ of the ground that is global to the whole structure; the corresponding inertia forces are shifted to the right hand side $\mathbf{F}(t) = -\mathbf{M}\mathbf{a}_g(t)$ (set \odot **Rigid base model** ON)
- in the absolute format for compliant base model; here seismic input is given as an imposed acceleration $\mathbf{a}_g = \ddot{\mathbf{u}}_g$ that is integrated to velocities (via Newmark method) and applied at the base of the model where viscous dashpots must be added; this way the acceleration record is converted to the traction time history and applied to the bottom boundary of the model (the bottom boundary is identified as a line segment (2D) or surface (3D), shared by viscous boundary located at $y = y_{MIN} = \text{const}$) (compliant base model circumvents waves reflections) (set \odot **Compliant base model** ON)

Seismic input dialog window

Remarks:

- Each acceleration record describes a time dependent acceleration vector that can be set in one of global X , Y or Z directions, or in the direction defined by a given vector
 - for global X direction : $\mathbf{a}_g(t) = a_o (1, 0, 0)^T \cdot LTF(t)$
 - for global Y direction : $\mathbf{a}_g(t) = a_o (0, 1, 0)^T \cdot LTF(t)$
 - for global Z direction : $\mathbf{a}_g(t) = a_o (0, 0, 1)^T \cdot LTF(t)$
 - for given vector \mathbf{v} : $\mathbf{a}_g(t) = a_o \mathbf{v} \cdot LTF(t)$

where a_o is the value set in the edit field **Acceleration** []
- Acceleration values can be set as:
 - A: relative to gravity acceleration $g = 9.81[m/s^2]$
 - B: absolute
- Seismic input may consist of collection of acceleration records. At given time instance global acceleration will be created as a sum of all records
- Each record may have a different Load Function

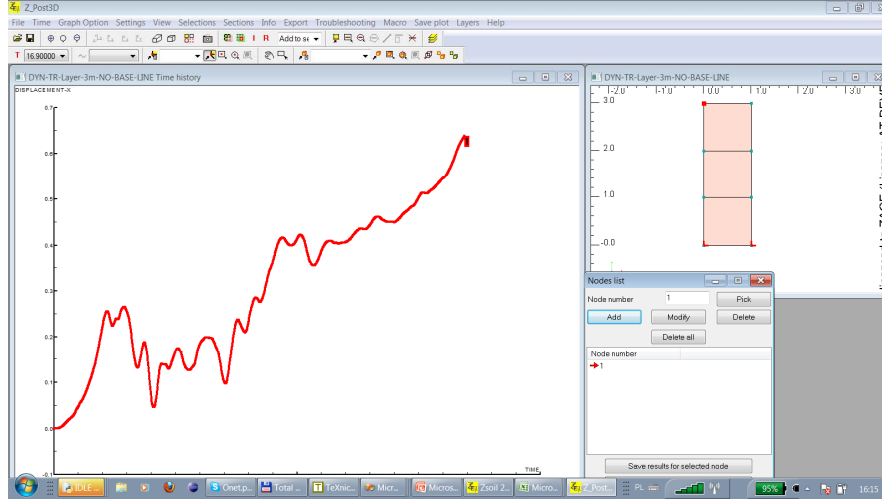
5. To perform baseline correction/Butterworth filtering or linear deconvolution of the given record use acceleration time history toolbox that can be activated at the Load time function level
6. Activate ☐ **Compliant base model** option if seismic signal was transformed by linear deconvolution procedure
7. ☐ **Compliant base model** / ☐ **Rigid base model** switch is common for all applied earthquake records

Window 5-7

5.3.1 Baseline correction to ground motion acceleration time histories

Window 5-8: Major goal of baseline correction

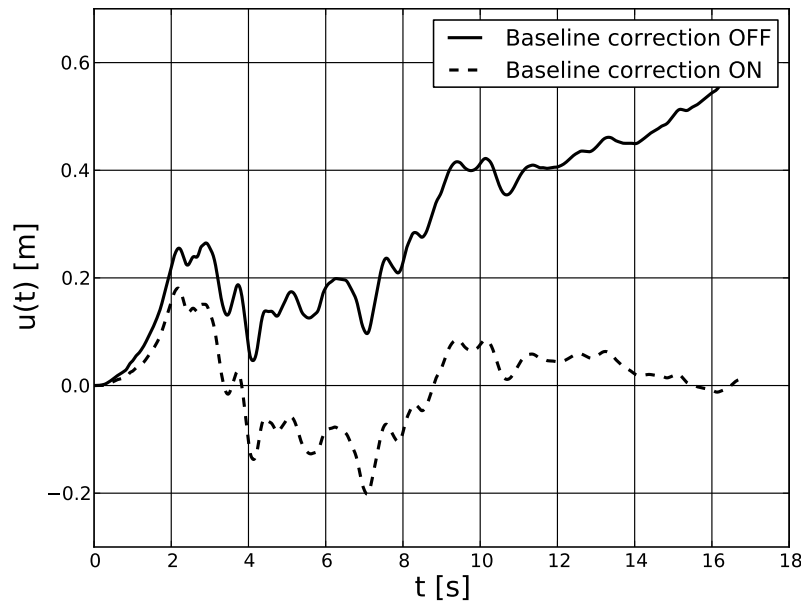
ZSoil®



Displacement time history (baseline correction inactive) for shear layer problem driven by imposed acceleration applied at the base

The baseline correction procedure can be summarized as follows

- Given: set of points: $a_i(t_i)$
- Goal: remove trend line from $a_i(t_i)$ (use cubic polynomial)
- Method: solve optimization problem: $\sum_i^n \{a_i - \tilde{a}(t_i)\}^2 \rightarrow MIN$
- Trend line equation: $\tilde{a}(t_i) = a_o + a_1 * t_i + a_2 * t_i^2 + a_3 * t_i^3$



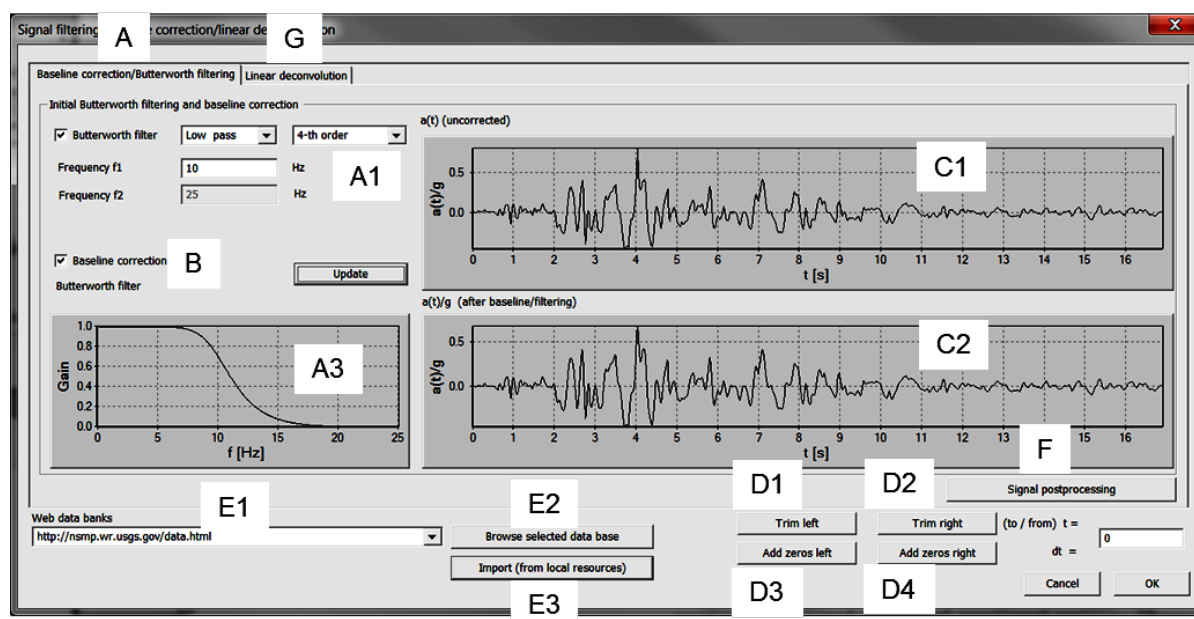
Displacement time history after baseline correction

Window 5-8

Window 5-9: User interface for baseline correction and filtering the acceleration time history

ZSoil®

To apply the acceleration time histories as a seismic input, or imposed BC expressed in terms of accelerations, a special toolbox was designed that allows to filter given $a(t)$ signal using one of the high pass, low pass, band pass or band stop (combo box (A)), 2-nd, 3-rd or 4-th order Butterworth filters. This toolbox performs also so called baseline correction (3-rd order polynomial is used) that eliminates the drift effect in the computed displacement time histories. It may also export uncorrected/corrected acceleration time histories but also acceleration, velocity and displacement undamped/damped Fourier spectra to the Excel.

**Remarks:**

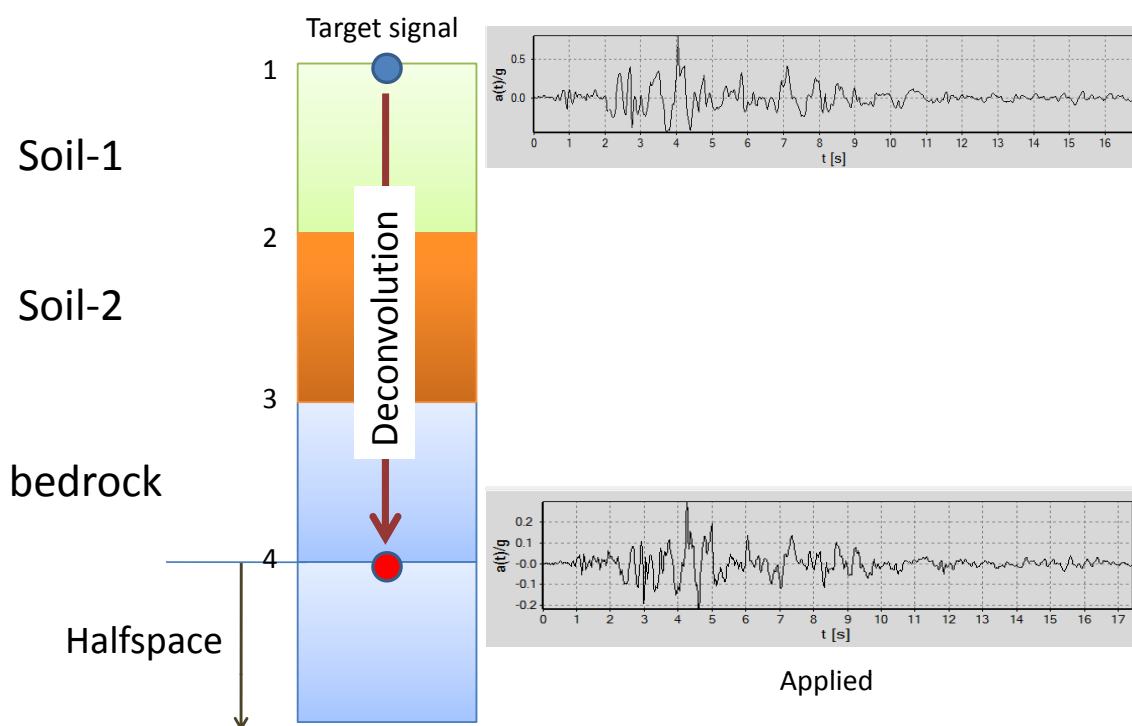
1. To perform baseline correction press button **Update**; the result of the correction will be shown in diagram (C2)
2. To add an additional signal filtering one may use a Butterworth filter; for low pass filter set value f_1 that will cancel frequencies higher than f_1 (the gain function (A3) shows how the Fourier amplitudes are scaled); for high pass set again value f_1 that will cancel frequencies lower than f_1 , and for band pass and band stop set values f_1 and f_2 that give the range of frequencies that are to be maintained or canceled.
3. Three formats of data bases can be imported: the US data bank published at <http://nsmmp.wr.usgs.gov/data.html>, the European one published at <http://www.isesd.hi.is/ESD.Local/frameset.htm> and the free format where pairs $(t, a(t))$ are stored (E1); user may browse one of the mentioned data banks by pressing button **Browse..**
4. One may trim the acceleration record from the left and right side (use buttons (D1), (D2))
5. After downloading the acceleration records user may store them at his own directory; by clicking the button (E3) user may select one of the stored records
6. To export filtered, uncorrected/corrected (through baseline correction) acceleration time histories, and corresponding undamped/damped Fourier spectra, to the Excel, press button (F)

Window 5-9

5.3.2 Linear deconvolution of seismic records

Window 5-10: Idea of linear deconvolution procedure

ZSoil®



- Signal is measured at control point (target signal)
- In finite element model we need to have a signal at the base
- The goal of the deconvolution procedure is to transfer the target signal to the base of the FE model

Window 5-10

Window 5-11: Theoretical basis for linear deconvolution procedure

ZSoil®

The theoretical bases for linear deconvolution procedure can be found in textbooks on soil dynamics (see Kramer [6]).

- Shear wave equation for harmonic motion with frequency ω :

$$u(x, t) = A e^{i(kx+\omega t)} + B e^{-i(kx-\omega t)}$$
- First term represents upward propagating wave and second the reflected downward propagating one
- If we know amplitudes at one point, all other can easily be computed using the following recursion:
 - $A_{m+1} = \frac{1}{2} A_m (1 + \alpha_m) e^{i k_m h_m} + \frac{1}{2} B_m (1 - \alpha_m) e^{-i k_m h_m}$
 - $B_{m+1} = \frac{1}{2} A_m (1 - \alpha_m) e^{i k_m h_m} + \frac{1}{2} B_m (1 + \alpha_m) e^{-i k_m h_m}$
 - $G^* = G (1 + 2 i \xi)$, $v_s^* = \sqrt{\frac{G^*}{\rho}}$, $k_m^* = \frac{\omega}{v_s^*}$, h_m - layer depth
- At top of the layer the following boundary condition is assumed: $\tau_{xy} = 0 \rightarrow A_1 = B_1$

For given set of soil layers and acceleration record at the control point the linear deconvolution procedure consists of the following steps

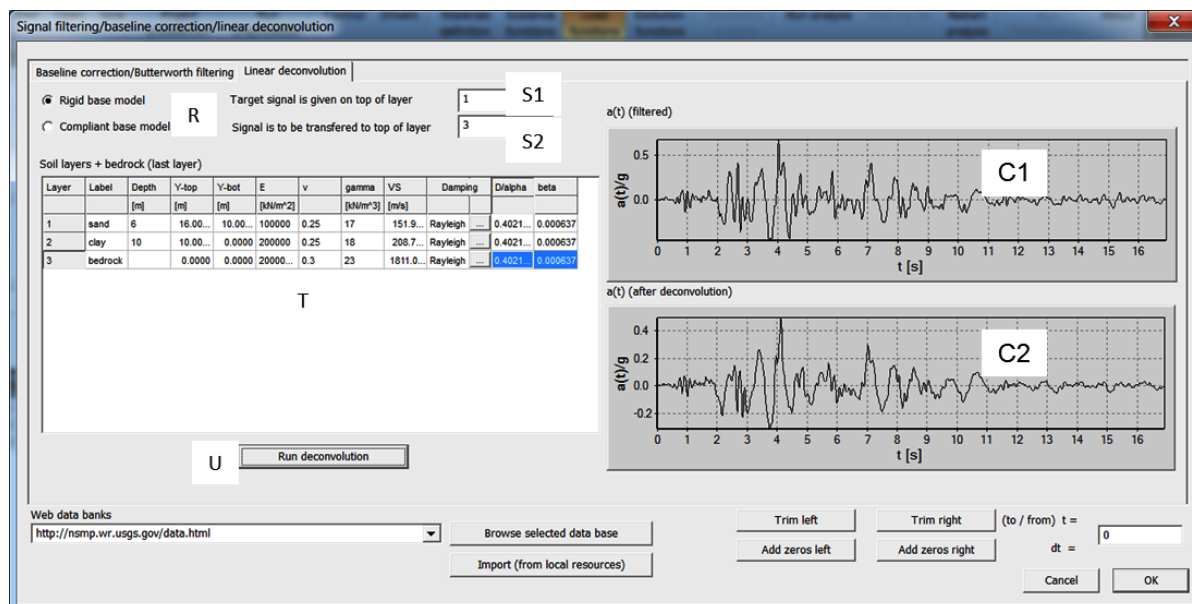
1. Filter the original signal with Butterworth filter
2. Perform FFT procedure on earthquake record (note that input is real but output is complex valued)
3. For each frequency and given set of layers find a transfer function $F_{ij}(\omega)$ (it is different for the rigid base model and compliant base one)
4. Multiply result of FFT by transfer functions for each ω_i
5. Perform an inverse FFT (input is complex but output will be real valued again)

Window 5-11

Window 5-12: User interface for linear deconvolution of seismic signals

ZSoil®

The linear deconvolution toolbox allows the user to transfer given acceleration time history record from the control point to the base of the finite element model. The two base models may be used, the rigid base and compliant base model.


Remarks:

1. Prior running deconvolution procedure one may need to add a quiet zone to the initial part of the input signal (waves traveling upward need a certain time to hit the control point)
2. Input signal is shown in (C1) field
3. To perform linear deconvolution select type of the model to be used (rigid base or compliant one) (R)
4. Fill the grid with the data for each soil layer (label, depth, Young modulus, Poisson ratio, bulk unit weight, damping properties) (T); note that the last layer is reserved for bedrock that is modeled as an elastic halfspace (depth is not meaningful for halfspace layer)
5. Define on top of which layer signal is given (S1)
6. Define on top of which layer signal is to be transferred (S2)
7. Press button **Run deconvolution** to run the procedure
8. Output signal will be shown in (C2) field
9. After deconvolution user is asked whether deconvoluted signal is to be taken as the input one when switching to the Baseline correction/Butterworth option in the dialog box (if one wants to use it please answer YES)
10. Characterization of soil layers is not memorized (!); one may select all fields of the grid and copy it to the Excel sheet for later use; the inverse action (copying whole data set from Excel sheet to the grid) is possible

Window 5-12

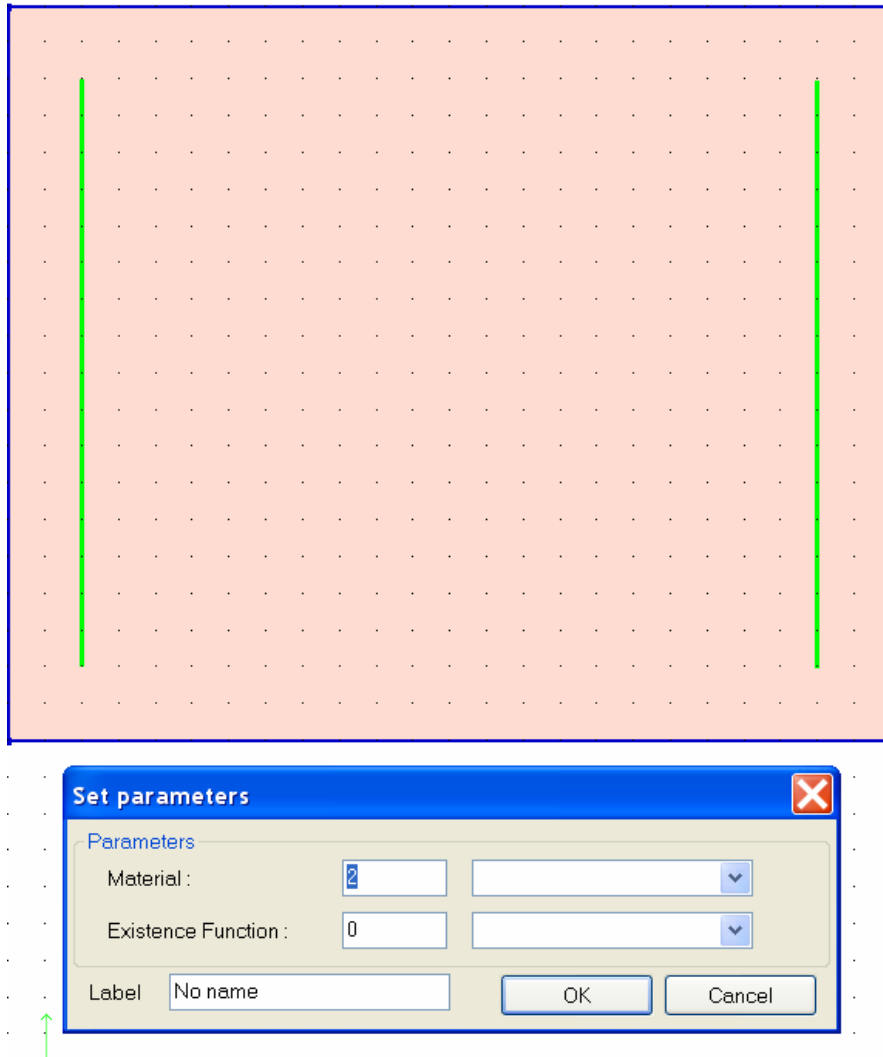
5.4 Absorbing boundaries

Viscous dampers can be generated at the macromodeling or FE level. In the 2D applications dampers are generated on selected subdomain or continuum finite element edges while in the 3D on faces.

Window 5-13: Viscous damper:On Subdomain edges

ZSoil®

A new 2D viscous damper macro-element(s) is(are) created on selected subdomain edge(s).



Remarks:

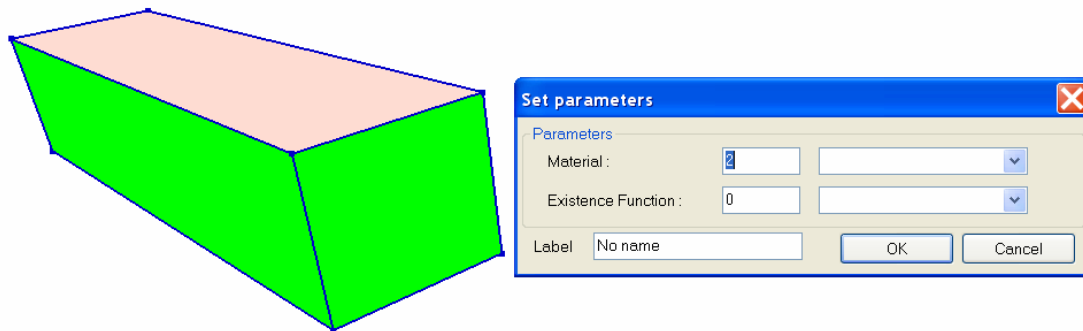
1. This macro-element is meaningful for Deformation or Deformation+Flow analyses when running Transient dynamics driver
2. Viscous damper elements will be created on edges of the mesh of continuum elements once the virtual and then the real mesh in the continuum subdomain is created
3. Any mesh refinement in the adjacent continuum automatically enforces mesh refinement in the damper macro-element
4. Viscous dampers may inherit material data from adjacent continuum elements; this setting can be made at the material level

Window 5-13

Window 5-14: Viscous damper:On Subdomain faces

ZSoil®

A new 3D viscous damper macro-element(s) is(are) created by selecting face(s) in the existing continuum 3D subdomains. See remarks given in Win.(5-13).



Window 5-14

5.5 DRM modeling components

The obligatory components for running DRM models are given in the following subsections. However, it can be very useful for the user to study the dedicated tutorial on DRM modeling included in the Tutorials manual.

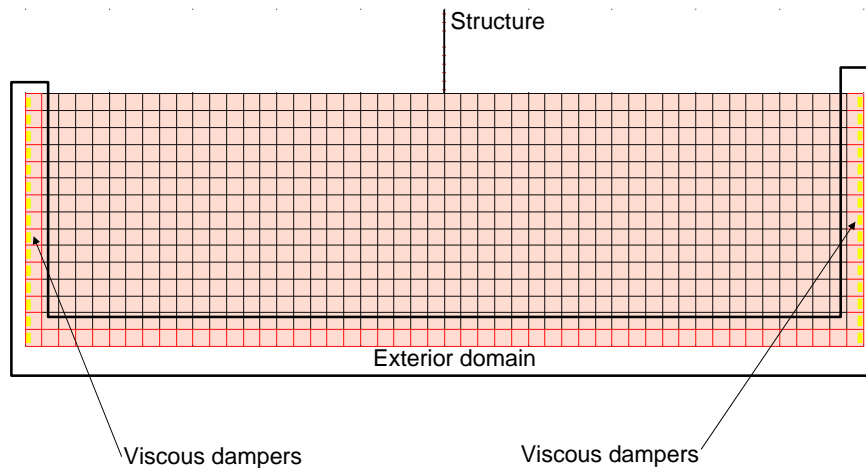
5.5.1 Setting boundary and external layers in the preprocessor

Setting the external and boundary layers for DRM models can be made exclusively at the FE level through the menu FE model/DRM domains/....

Window 5-15: DRM domains>Create: Exterior domain on element(s)

ZSoil®

This option allows the user to define the exterior domain in Domain Reduction Method (DRM) for the set of selected continuum elements. This domain must not overlap with the boundary DRM layer.



Remarks:

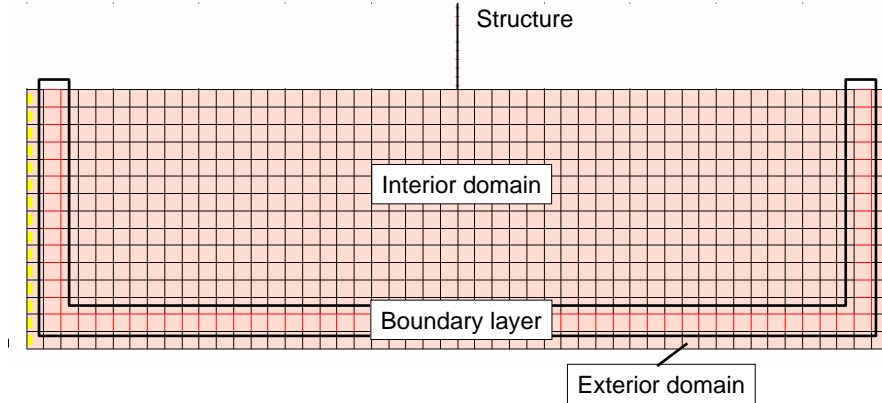
1. On the external edges/faces viscous dampers should be generated to avoid spurious reflections from finite boundaries

Window 5-15

Window 5-16: DRM domains>Create: Boundary domain on element(s)

ZSoil®

This option allows the user to define the boundary layer of elements in Domain Reduction Method (DRM) for the set of selected continuum elements. This domain must not overlap with the exterior DRM layer.



Remarks:

1. The interior domain is detected automatically once the boundary and exterior domains are selected
2. In the boundary domain continuum must behave in the elastic manner; this is enforced by the calculation module in an automatic manner for any constitutive model for continuum

Window 5-16

5.5.2 Running DRM models with preprocessed free field motion

To run the DRM models we need to define, in the FE mesh, the nonoverlapping external and boundary layers of continuum elements and to select the preprocessed (already computed) transient dynamic project that will represent the motion of a simplified model. In most of the applications this simplified model reduces to the shear layer model. It is important that any nodal point in the boundary layer must have its projection on the mesh of a simplified model. Browsing the project for a simplified model can be made at the dialog box for definition of drivers (Control/Analysis and drivers/Free field motion []). To perform this operation one has to activate the flag ☒ **Domain Reduction for transient dynamics** first and then browse the free field motion project by pressing button **Browse**.

5.6 Initial conditions

The initial conditions may consist of initial displacements/velocities and initial pore pressures in dynamic consolidation problems.

Window 5-17: Initial displacement/velocity:Create on node

ZSoil®

Using this option one may define the initial displacement and/or velocity on a single picked nodal point or set of selected nodal points.

Translational		
	Value	EF
<input checked="" type="checkbox"/> UX	0.01 [m]	0
<input type="checkbox"/> UY	0 [m]	0
<input type="checkbox"/> UZ	0 [m]	0
<input type="checkbox"/> VX	0 [m/day]	0
<input type="checkbox"/> VY	0 [m/day]	0
<input type="checkbox"/> VZ	0 [m/day]	0

Rotational		
	Value	EF
<input type="checkbox"/> RX	0 [deg]	0
<input type="checkbox"/> RY	0 [deg]	0
<input type="checkbox"/> RZ	0 [deg]	0
<input type="checkbox"/> WX	0 [deg/day]	0
<input type="checkbox"/> WY	0 [deg/day]	0
<input type="checkbox"/> WZ	0 [deg/day]	0

Label: No name

Cancel OK

Remarks:

1. This initial condition is meaningful only for dynamic driver which can be run in Deformation or Deformation+Flow mode
2. The existence function is needed to handle the case when dynamic driver is run after Driven load driver(s); in such case the initial displacement is understood as an increment of the displacement by which the structure will be excited
3. The applied initial condition may have a label

Window 5-17

Window 5-18: Initial displacement/velocity:Create on element node

ZSoil®

This option is equivalent to the one described in Window 5-17 but in this case the initial condition is applied to a single picked element node. This way in case when at a given geometrical point few nodes appear (due to contact interface for instance) one may apply the initial condition to the proper node.

Window 5-18

5.7 Boundary conditions

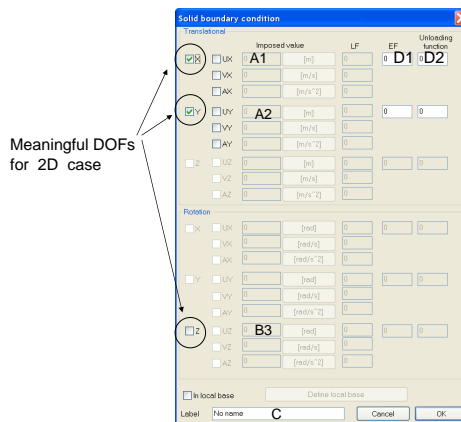
5.7.1 Solid BC

Window 5-19: Solid BC:Create:On node

ZSoil®

Using this option one may fix the translational or rotational degrees of freedom at a single picked node or group of selected nodes (if current selection list for nodes is not empty).

The dialog box used for setting these conditions is shown in figure below.

**Remarks:**

1. Solid BC may be set in the local coordinate system
2. Nodes can be fixed at a certain time period and then relaxed according to the applied existence function
3. For dynamic driver one may impose displacements, velocities or accelerations at fixed nodes (corresponding displacements are integrated via time integration schemes: Newmark or HHT)
4. For dynamic drivers imposed velocity/acceleration BC has a higher priority if both displacement and velocity/acceleration BC are simultaneously active
5. To switch from rigid to viscous boundary user may define an unloading function for relaxed translational degree of freedom ; this allows to deactivate the fixities but maintain the static reactions that will preserve static equilibrium

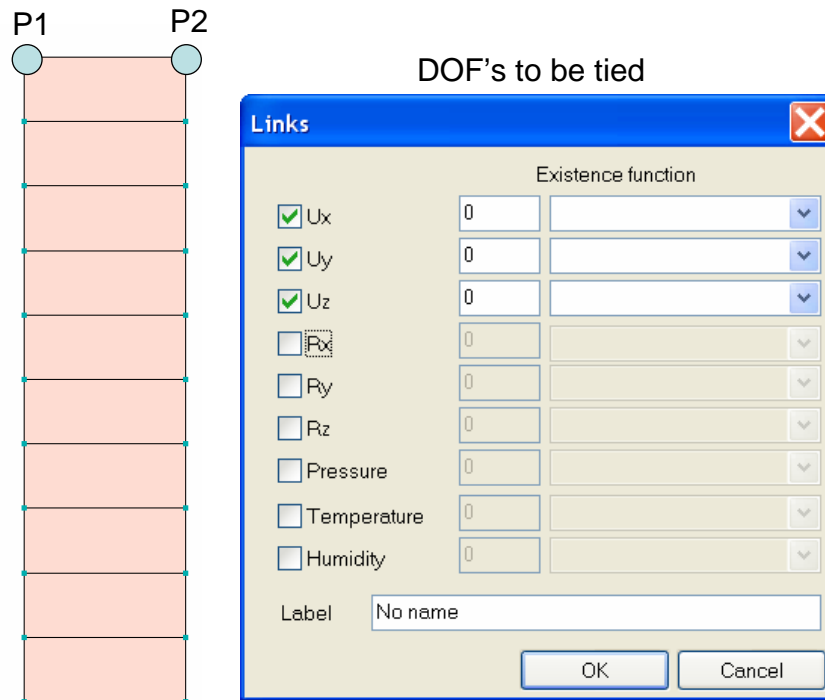
Window 5-19

5.7.2 Periodic BC

Window 5-20: Periodic BC:Create:2 nodes

ZSoil®

This option allows to tie selected degrees of freedom at two picked nodal points. It may concern any type of the degree of freedom (displacement, pressure, temperature, humidity). It is mainly used in dynamic applications to simulate motion of shear layer. The dialog box used for setting these conditions is shown in the figure below.



Remarks:

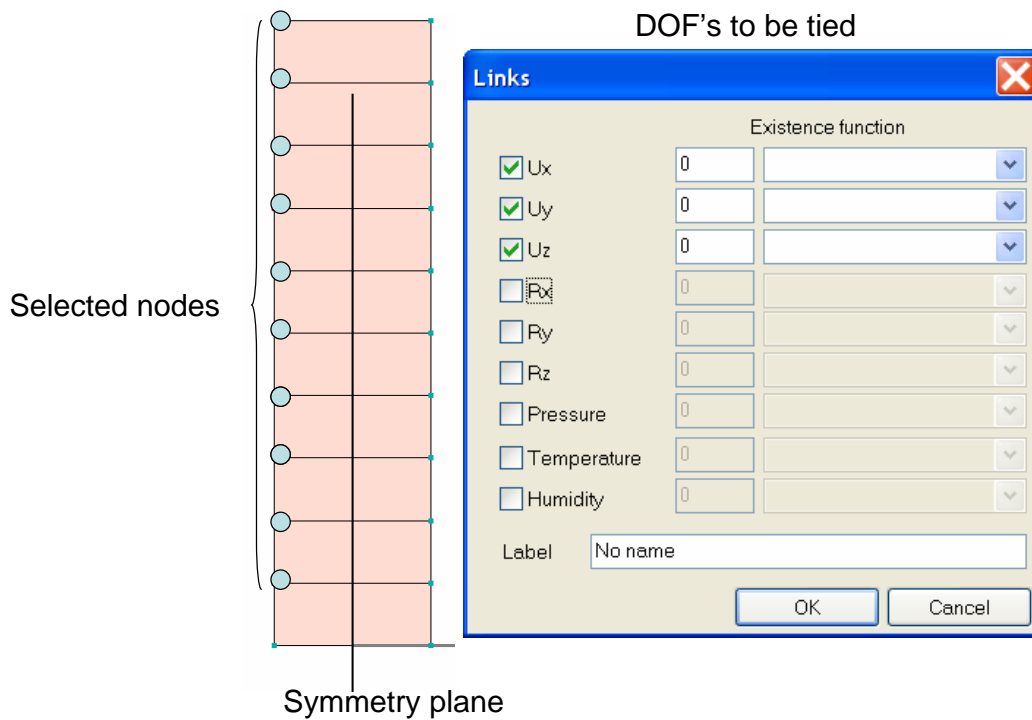
1. The tying can be made only in the global coordinate system
2. **This option does not apply to the fixed degree of freedom**
3. Each degree of freedom can be tied according to the declared existence function

Window 5-20

Window 5-21: Periodic BC:Create:Nodes & plane

ZSoil®

This option allows to tie selected degrees of freedom at the two opposite boundaries located symmetrically with respect to the indicated auxiliary plane. This option helps to generate this type of the boundary conditions for large computational models. The dialog box used for setting these conditions is shown in the figure below.

**Remarks:**

1. The tying can be made only in the global coordinate system
2. **This option does not apply to the fixed degree of freedom**
3. Each degree of freedom can be tied according to the declared existence function

Window 5-21

Chapter 6

BENCHMARKS

6.1 Eigenvalues and eigenmodes

6.1.1 Natural vibrations of cantilever beam

$$\omega_n = (a_n L)^2 \sqrt{\frac{EJ}{\bar{m}L^4}} \quad (6.1)$$

where a_n is a solution of the transcendental equation and $\bar{m} = \rho A$ (A is a cross section area)

$$1 + \cos(a_n L) \cosh(a_n L) = 0 \quad (6.2)$$

$$\phi_n(x) = A_1 \left[\sin(a_n x) - \sinh(a_n x) + \frac{\sin(a_n L) + \sinh(a_n L)}{\cos(a_n L) + \cosh(a_n L)} (\cosh(a_n x) - \cos(a_n x)) \right] \quad (6.3)$$

In this benchmark the analyzed cantilever beam (see Fig.6.1) of length $L = 4$ m has a rectangular cross section with dimensions $b = 1.0$ m, $h = 0.1$ m. It is discretized with 36 elements along the L dimension assuming that the mass matrix is lumped. All translational and rotational DOFs are fixed along edge 1-2 (see Fig.6.1). Mass filtering is activated with the only active direction set along global Y axis to consider bending modes only. The material properties are $E = 20000000$ kN/m², $\nu = 0.0$, $\gamma = 24.5166$ kN/m³ and corresponding $\rho = 2500$ kg/m³. Simulations were carried out using beam, shell and continuum elements.

6.1.1.1 Simulations using 2-node linear beam elements

File:

cantilever-beam-vibrations.inp

n	1	2	3	4	5
ω_n (analytical)	17.94	112.44	314.87	616.97	1019.90
ω_n (computed)	17.93	112.20	313.48	612.58	1009.20

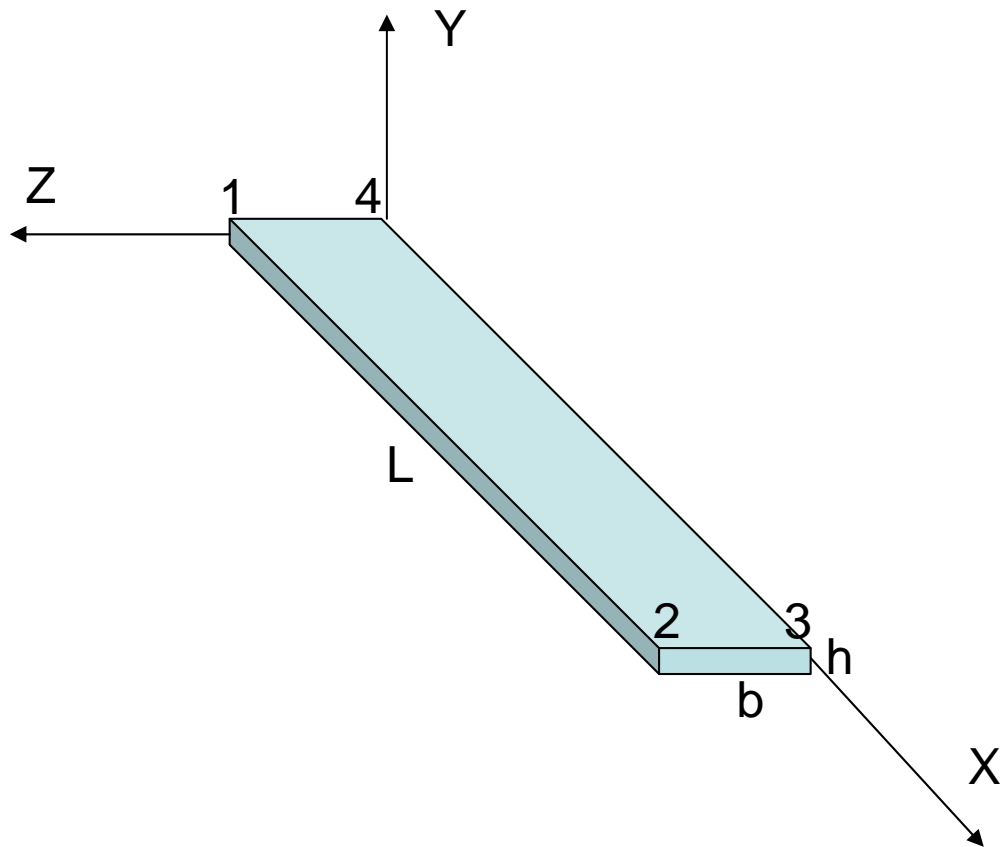


Figure 6.1: Cantilever beam

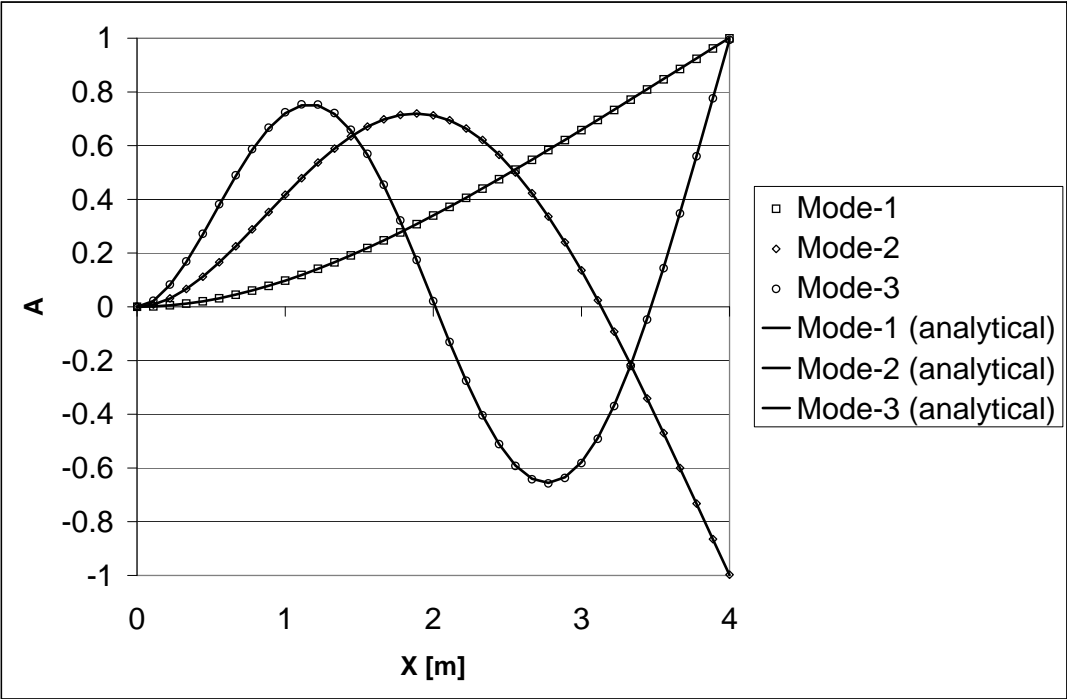


Figure 6.2: Shapes of natural vibrations of cantilever beam for first 5 frequencies

6.1.1.2 Simulations using quadrilateral 4-node shell elements

File:

cantilever-shell-vibrations.inp

In this model rotational DOFs along edges 1-2 and 3-4 along global X and Y axes are fixed to enforce cylindrical bending mode only.

Results:

n	1	2	3		
ω_n (analytical)	17.94	112.44	314.87	616.97	1019.90
ω_n (computed)	17.93	112.20	313.48	612.58	1009.20

6.1.1.3 Simulations using quadrilateral 4-node continuum elements

Files:

cantilever-continuum-2D-vibrations.inp

cantilever-continuum-2D-vibrations-dense.inp

The cantilever beam is discretized with 36x2 and then 72x2 elements (2 elements across the thickness). The eigenvalue problem is solved using standard fully integrated Q4 elements, Q4-BBAR, Q4-EAS (2 enhanced modes for normal strains only) and Q4-EAS elements with enhanced shear/bending behavior (using *Continuum for structures* instead of *Continuum* option at the material level). Switch from BBAR to EAS or standard fully integrated elements can be made under menu Control/Finite elements. To enforce pure cylindrical bending mode all translational DOFs in global Z direction along edges 1-2 and 3-4 are fixed.

Results:

n	1	2	3	4	5
ω_n (analytical)	17.94	112.44	314.87	616.97	1019.90
ω_n (computed Q4-EAS-enhanced)(36x2)	17.93	112.23	313.73	613.49	1011.59
ω_n (computed Q4-EAS-enhanced (72x2)	17.94	112.25	313.62	612.69	1008.88
ω_n (computed Q4-BBAR)(36x2)	21.91	136.99	382.50	746.71	1228.61
ω_n (computed Q4-BBAR)(72x2)	18.20	113.88	318.15	621.48	1023.21
ω_n (computed Q4-EAS)(36x2)	22.80	142.58	397.99	776.64	1277.17
ω_n (computed Q4-EAS)(72x2)	19.27	120.57	336.75	657.53	1081.99
ω_n (computed Q4-standard)(36x2)	22.80	142.58	397.99	776.64	1277.17
ω_n (computed Q4-standard (72x2)	19.27	120.57	336.75	657.53	1081.99

6.1.1.4 Simulations using brick 8-node continuum elements

The cantilever beam is discretized 36x2x1 and then 72x2x1 elements. The eigenvalue problem is solved once using standard B8-BBAR elements and B8-EAS elements with enhanced shear/bending behavior (using option *Continuum for structures*) **File: cantilever-continuum-3D-vibrations.inp**

Results:

n	1	2	3	4	5
ω_n (analytical)	17.94	112.44	314.87	616.97	1019.90
ω_n (computed B8-EAS-enhanced)(36x2)	17.93	112.23	313.73	613.49	1011.59
ω_n (computed B8-EAS-enhanced (72x2)	17.94	112.25	313.62	612.69	1008.88
ω_n (computed B8-BBAR)(36x2)	22.21	138.88	387.73	756.83	1245.04
ω_n (computed B8-BBAR)(72x2)	18.56	116.15	324.47	633.74	1043.21
ω_n (computed B8-EAS)(36x2)	22.80	142.58	397.99	776.64	1277.17
ω_n (computed B8-EAS)(72x2)	19.27	120.57	336.75	657.53	1081.99
ω_n (computed B8-standard)(36x2)	22.80	142.58	397.99	776.64	1277.17
ω_n (computed B8-standard (72x2)	19.27	120.57	336.75	657.53	1081.99

6.1.2 Natural vibrations of a bar

Analytical solution:

$$\omega_n = \frac{2n-1}{2} \pi \sqrt{\frac{EA}{mL^2}} \quad (6.4)$$

$$\phi_n(x) = A_1 \sin\left(\frac{2n-1}{2} \pi \frac{x}{L}\right) \quad (6.5)$$

The analyzed bar has length $L = 4$ m and is discretized with 36 linear elements assuming that the mass matrix is lumped.

6.1.2.1 Simulations using truss elements

File: truss-vibrations.inp, truss-vibrations-add-ele-mass, truss-vibrations-add-node-mass.inp

In the first data file mass matrix is generated from given mass density specified at the material level ($\rho = 2500$ [kg/m³]) while in the second and third data files mass matrix is generated from added masses defined via mass distributed along the element ($\rho^* = 2500 * 0.1 = 250$ [kg/m]) and nodal masses (at middle nodes $m_{add} = 250 * \frac{4}{36}$ [kg] = 27.778 [kg] while at the boundary nodes $m_{add} = \frac{1}{2} 250 * \frac{4}{36}$ [kg] = 13.889 [kg])

Material	Model	Data group	Properties	Unit	Value
1 truss	Elastic	Elastic	E	[kN/m ²]	20000000
		Density	γ	[kN/m ³]	24.5166
		Density	ρ	[kg/m ³]	2500

Results:

n	1	2	3	4	5
ω_n (analytical)	1110.72	3332.16	5553.60	7775.05	9996.49
ω_n (computed)	1110.63	3329.78	5542.59	7744.86	9932.38

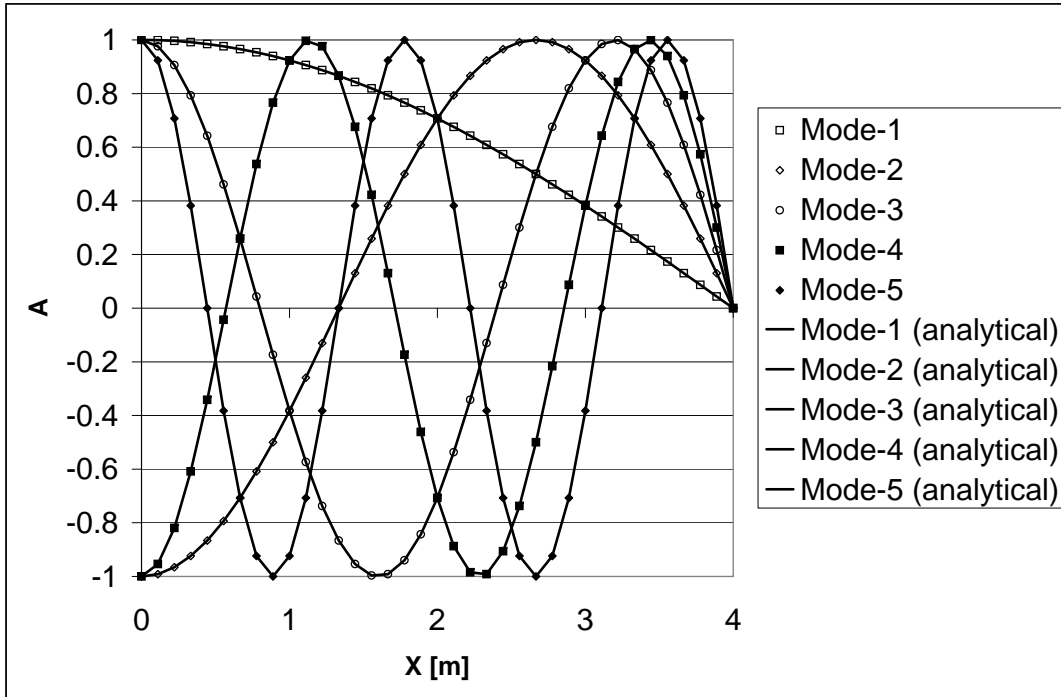


Figure 6.3: Shapes of natural vibrations for first 5 frequencies

6.1.2.2 Simulations using linear 2-node beam elements

Files:

beam-vibrations.inp
 beam-vibrations-add-ele-mass.inp
 beam-vibrations-add-node-mass.inp
 beam-vibrations-mass-filtering.inp
 beam-axial-vibrations-mass-filtering-rotated.inp

In the first data file mass matrix is generated from given mass density specified at the material level ($\rho = 2500 \text{ [kg/m}^3\text{]}$) while in the second and third data files mass matrix is generated from added masses defined via mass distributed along the element ($\rho^* = 2500 * 0.1 = 250 \text{ [kg/m]}$) and nodal masses (at middle nodes $m_{add} = 250 * \frac{4}{36} \text{ [kg]} = 27.778 \text{ [kg]}$ while at the boundary nodes $m_{add} = \frac{1}{2} * 250 * \frac{4}{36} \text{ [kg]} = 13.889 \text{ [kg]}$). In the fourth data file all fixities at internal nodes are cancelled and mass filtering is activated with the only active direction set along Y axis. The fifth data file is equivalent to the first one but whole mesh is rotated by 30 degrees and mass filtering is defined at the local rotated coordinate system.

n	1	2	3	4	5
ω_n (analytical)	1110.72	3332.16	5553.60	7775.05	9996.49
ω_n (computed)	1110.63	3329.78	5542.59	7744.86	9932.38

6.1.2.3 Simulations using 2D 4-node continuum elements

Files:

continuum-2D-axial-vibrations.inp

continuum-2D-axial-vibrations-mass-filtering.inp

The first data set consists of a column of 36 Q4 elements with fixed all DOFs in the global X direction. In the second data file we apply periodic boundary conditions (this option is available under boundary conditions menu in the preprocessor) that help to enforce displacement compatibility (u_x and u_y) for pairs of nodes placed on both vertical walls of the domain and, in addition, mass filtering is activated with the only active direction set along global Y axis.

n	1	2	3	4	5
ω_n (analytical)	1110.72	3332.16	5553.60	7775.05	9996.49
ω_n (computed)	1110.63	3329.78	5542.59	7744.86	9932.38

6.1.2.4 Simulations using 3D 8-node continuum elements

File: **continuum-3D-axial-vibrations.inp**

n	1	2	3	4	5
ω_n (analytical)	1110.72	3332.16	5553.60	7775.05	9996.49
ω_n (computed)	1110.63	3329.78	5542.59	7744.86	9932.38

6.1.2.5 Simulations using shell elements

File: **shell-axial-vibrations.inp**

n	1	2	3	4	5
ω_n (analytical)	1110.72	3332.16	5553.60	7775.05	9996.49
ω_n (computed)	1110.63	3329.78	5542.59	7744.86	9932.38

6.1.3 Natural vibrations of shear layer

Files:

shear-layer-64.inp

The analytical solution for eigenfrequencies for a shear layer resting on a rigid base is as follows

$$\omega_n = \frac{(2n - 1) \pi v_s}{2 H} \quad (6.6)$$

In the above formula the depth of the layer is denoted by H and shear wave velocity by v_s . The depth of the model is assumed $H = 16$ m while width $B = 0.5$ m (although it does not play any role). The layer is discretized along the depth with 64 plane strain Q4 elements (1 element in the horizontal direction) and 2 nodes, at the base, are fully fixed. To cancel vertical dilatational eigenmodes the periodic boundary conditions are enforced ($u_x(x = 0) = u_x(x = B)$, $u_y(x = 0) = u_y(x = B)$). The set of material properties is given in the following table.

6.2. BASELINE CORRECTION AND BUTTERWORTH FILTERING OF EARTHQUAKE RECORDS

Material	Model	Data group	Properties	Unit	Value
1 truss	Elastic	Elastic	E	[kN/m ²]	20000000
		Density	γ	[kN/m ³]	19.6133
		Density	ρ	[kg/m ³]	2000

The shear wave velocity is computed using the formula

$$c_s = \sqrt{\frac{G}{\rho}} \quad (6.7)$$

and it yields $v_s = 204.145$ m/s in the considered case.

The comparizon of analytical and computed first 8 eigenfrequencies is summarized in the table below

n	1	2	3	4	5	6	7	8
ω_n (analytical)	20.05	60.14	100.23	140.32	180.41	220.50	260.59	300.68
ω_n (computed)	20.04	60.11	100.14	140.11	179.99	219.77	259.41	298.90

6.2 Baseline correction and Butterworth filtering of earthquake records

Files:

DYN-TR-BF-BASELINE-Layer-3m-no-damp-LomaPrieta,
DYN-TR-Layer-3m-no-damp-LomaPrieta

A dynamic time history analysis of 3m high soil-column, subject to Loma Prieta earthquake (Loma-Prieta 18.10.1989, Station Corralitos) is considered in this section. The effect of baseline correction procedure and Butterworth filters will be presented. Duration of the earthquake record takes 16.9 s and it is digitized at every 0.02s. The soil-column is discretized by 3 quadrilateral elements (3×1 m) representing an elastic medium characterized by $E = 512000$ kPa, $\nu = 0.22625$, $\gamma = 20$ kN/m³ (resulting shear wave velocity is 320 m/s). To trace dynamic response of the system the time step $\Delta t = 0.01$ s is used and case of zero damping is considered (HHT method with $\alpha = -0.3$ is used). The accelaration record is applied as a boundary condition to the pair of nodes at the bottom, while remaining nodes placed along vertical walls are constrained using periodic BC in order to represent shear layer motion. The data setup is shown in the figure below. To cancel body forces the body force mutiplier (defined at the material level (under Unit weights)) is set to zero.

6.3 1D dynamic consolidation

Files:

Column-1D-Pi1_01_Pi2_01-dyn-ex.inp,
Column-1D-Pi1_01_Pi2_01-dyn.inp,
Column-1D-Pi1_01_Pi2_1-dyn-ex.inp,
Column-1D-Pi1_01_Pi2_1-dyn.inp,
Column-1D-Pi1_10_Pi2_01-dyn-ex.inp,
Column-1D-Pi1_10_Pi2_01-dyn.inp,

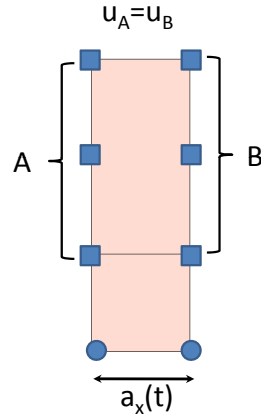


Figure 6.4: Geometry and BC for 1D time history analysis of shallow shear layer

Column-1D-Pi1_1_Pi2_01-dyn-ex.inp,
Column-1D-Pi1_1_Pi2_01-dyn.inp,
Column-1D-Pi1_1_Pi2_1-dyn-ex.inp,
Column-1D-Pi1_1_Pi2_1-dyn.inp

A 10m high soil-column subject to a harmonic surface load $q = q_o \sin(\omega t)$ ($q_o = 1\text{kN/m}^2$) is considered in this section. The soil-column is discretized with 400 quadrilateral elements (400×1). Nodes at the base are fully fixed while nodes along vertical walls can freely move in the vertical direction only. At the top of the column pressure boundary condition $p = 0$ is assumed. Solution of this problem, although in the frequency domain, can be found in the textbook by Zienkiewicz et al [13] and PhD thesis by Kantoe [5].

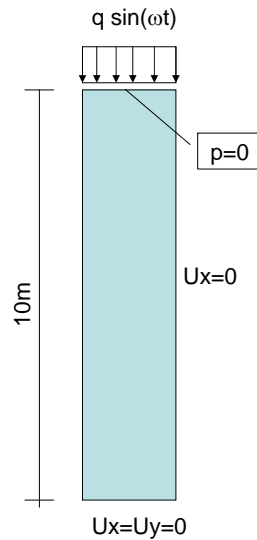


Figure 6.5: Geometry of 1D consolidation test

To achieve steady state harmonic solution more than 20 cycles of the loading are applied. Solution of this problem depends on some nondimensional parameters Π_1 and Π_2 defined as follows

$$\Pi_2 = \pi^2 \left(\frac{\hat{T}}{T_o} \right)^2$$

The natural period of vibration \hat{T} and dilataional wave velocity v_c are defined as

$$\hat{T} = \frac{2H}{v_c}$$

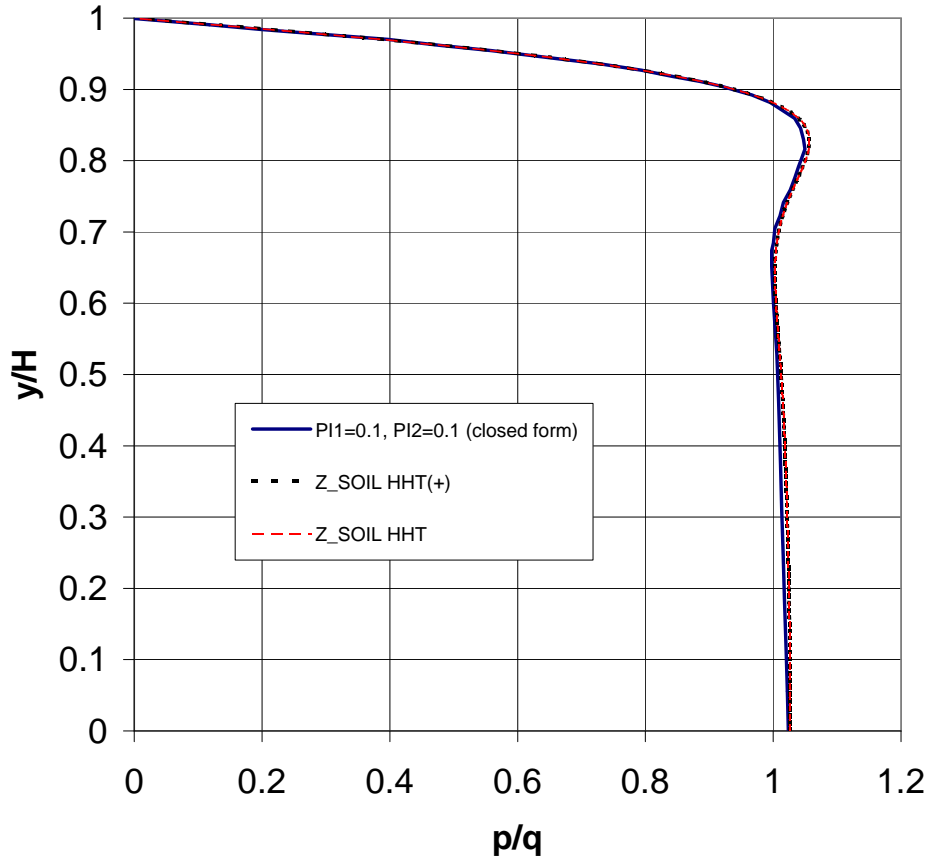
$$v_c = \sqrt{\frac{E_{oed} + K^F/n}{\rho}}$$

Parameter $\beta = \rho^F/\rho$, g is the gravitational acceleration, K^F is the fluid bulk modulus, k is permeability of soil, T_o is the period of excitation and oedometric stiffness modulus E_{oed} can be computed using the expression

$$E_{oed} = \frac{E(1 - \nu)}{(1 - 2\nu)(1 + \nu)}$$

The material data used in the simulation (see Kantoe [4]) is given in the following table

Material	Model	Data group	Properties	Unit	Value
1	Elastic	Elastic	E	[kN/m ²]	67500
			ν	[-]	0.25
		Density	γ	[kN/m ³]	26.1511
			e_o	[-]	0.5
		Flow	K^F	[kN/m ²]	973000
			k	[m/s]	depends on Π_2
			S_r	[-]	1.0
			α	[m ⁻¹]	2.0
			$\tilde{\alpha}$	[-]	1.0

Figure 6.6: Excess pore pressure distribution for $\Pi_1 = 0.1$ and $\Pi_2 = 0.1$

Five tests were carried out (see table below) for 5 different pairs of Π_1 and Π_2 . For each pair of Π_1 and Π_2 a corresponding ω (for given $\omega T_o = \frac{2\pi}{\omega}$) and k parameters were derived using the aforementioned expressions. The time step for dynamic driver was assumed as $\Delta t = T_o/40$.

No	Π_1	Π_2	k [m/s]	ω [rad/s]	Δt
1	0.1	0.1	0.001033711674	31.62277660	0.00496729
2	0.1	1.0	0.003268883333	100	0.0015708
3	1.0	1.0	0.032688833330	100	0.0015708
4	1.0	0.1	0.01033711674	31.62277660	0.00496729
5	10.0	0.1	0.1033711674	31.62277660	0.00496729

Table 6.4: k and ω values

In all cases the standard HHT integration scheme ($\alpha = -0.3$, $\beta = 0.4225$, $\gamma = 0.8$) was used and integration coefficient for the pore pressures was assumed $\theta = 0.5$. In the following results presence of the inertial term in Darcy's law was tested. Results denoted by HHT⁺ correspond to the case of active inertial term. In the following five figures distributions of the excess pore pressure are presented.

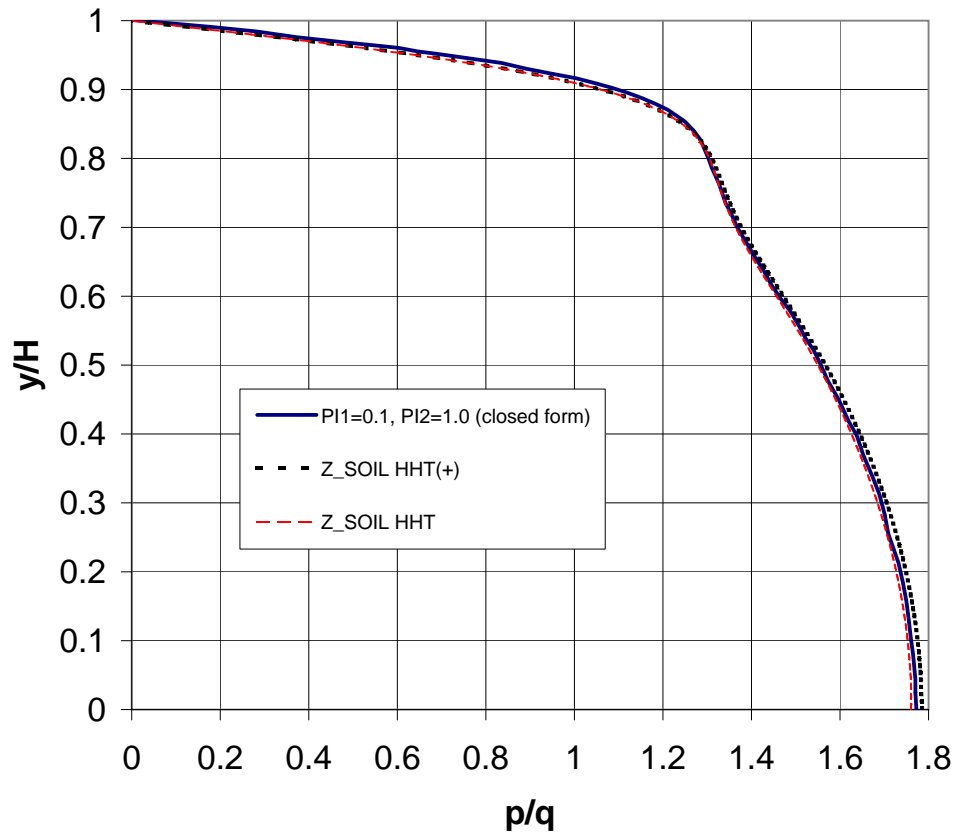


Figure 6.7: Excess pore pressure distribution for $\Pi_1 = 0.1$ and $\Pi_2 = 1.0$

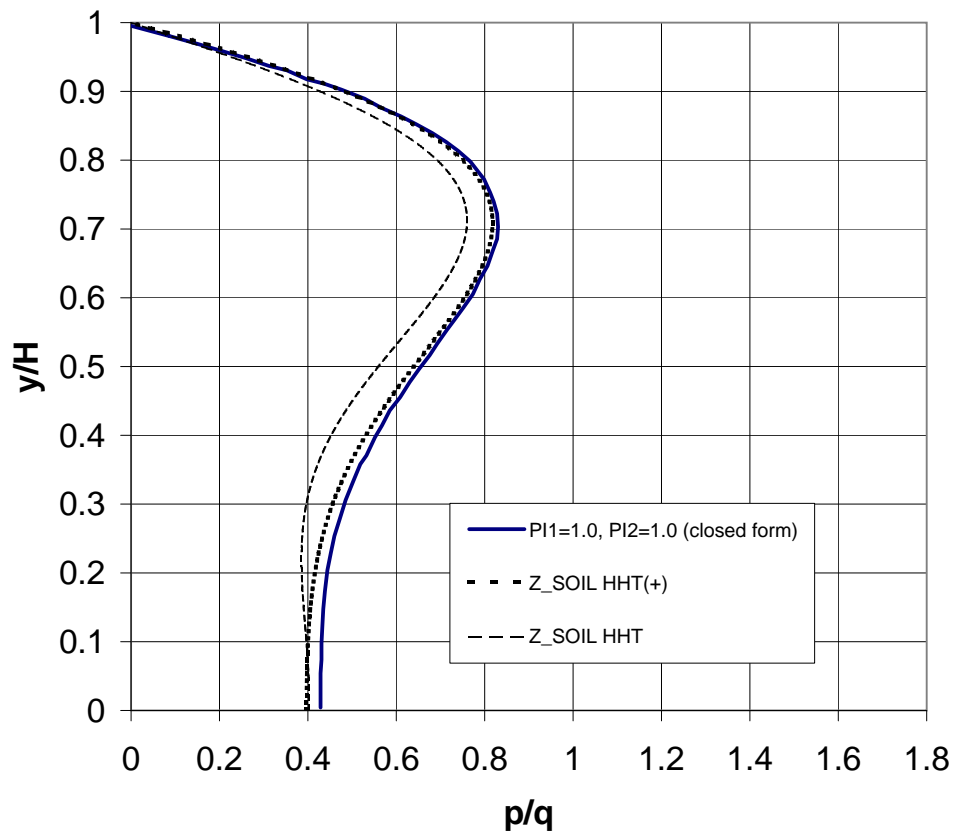


Figure 6.8: Excess pore pressure distribution for $\Pi_1 = 1.0$ and $\Pi_2 = 1.0$

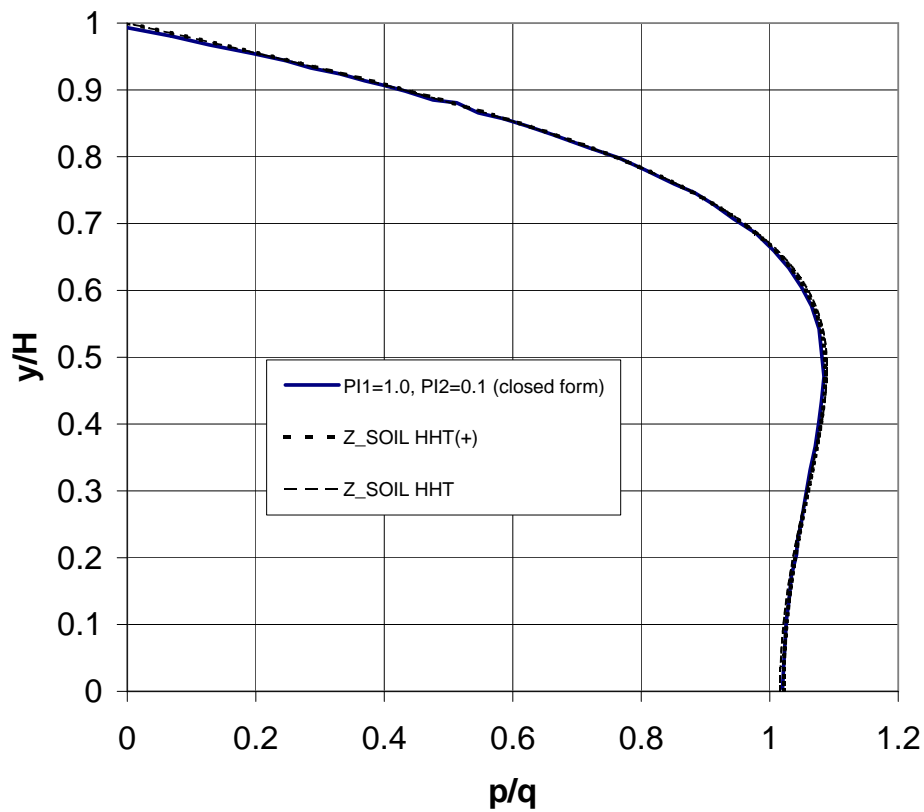


Figure 6.9: Excess pore pressure distribution for $\Pi_1 = 1.0$ and $\Pi_2 = 0.1$

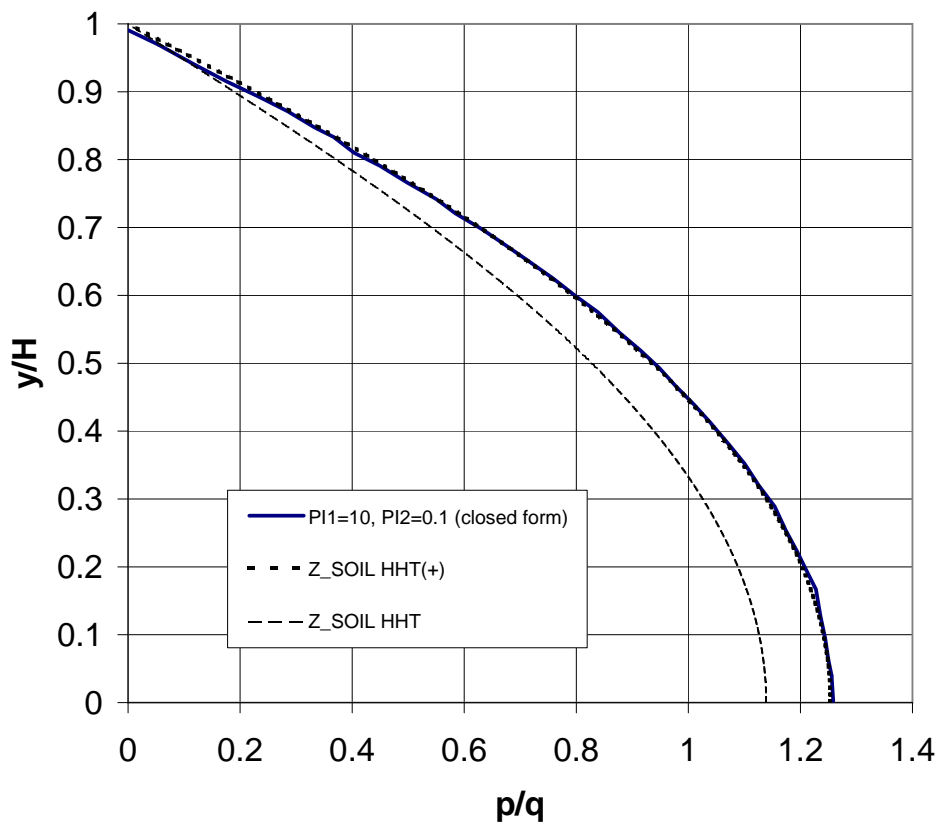


Figure 6.10: Excess pore pressure distribution for $\Pi_1 = 10$ and $\Pi_2 = 0.1$

6.4 Absorbing boundaries

6.4.1 Absorbing boundaries for single-phase media

Files:

1D-transmitting-boundary-no-dashpots-40-Q4.inp

1D-transmitting-boundary-with-dashpots-40-Q4.inp

A 10m long bar, discretized with aid of 40 plane strain quadrilateral elements, is subject to an imposed vertical ($\ddot{u}_y(t)$) and horizontal ($\ddot{u}_x(t)$) acceleration applied to nodal points A and B. The geometry, boundary conditions and load time function, common for both imposed accelerations, are shown in the figure given below. To avoid shear and dilatational waves reflection from the bottom boundary, Lysmer type viscous dashpot is added along the edge C-D.

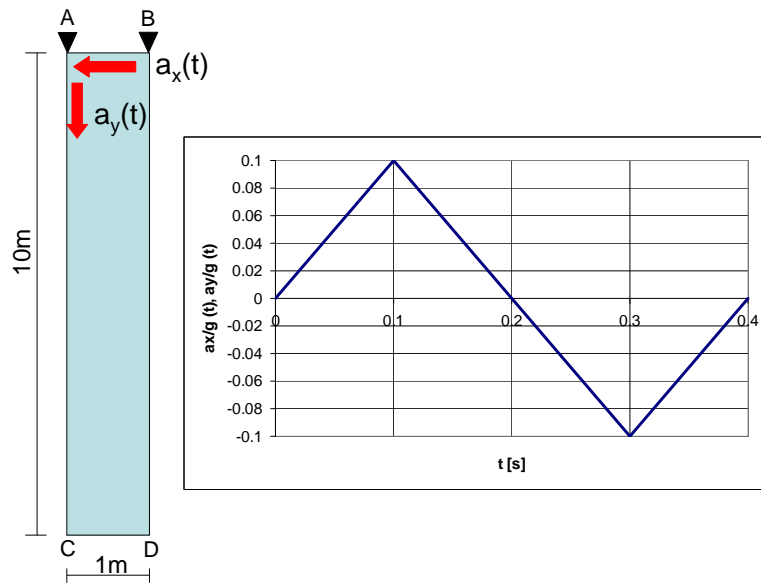


Figure 6.11: Soil layer subject to excitation applied to the boundary A-B

Material properties, common for the continuum and viscous damper, are given in the table 6.5 (note that one may declare automatic inheritance of viscous damper properties from the adjacent continuum element).

Material	Model	Data group	Properties	Unit	Value
1 Continuum	Elastic	Elastic	E	[kN/m ²]	100000
			ν	[-]	0.25
		Density	γ	[kN/m ³]	9.80665
		Density	ρ	[kg/m ³]	1000

Table 6.5: Material properties

The above values yield: $G = 40000$ kPa, $\lambda = 40000$ kPa, shear wave velocity $c_s = 200$ m/s and dilatational wave velocity $c_p = 346.41$ m/s. It means that the horizontal velocity at points C,D should vanish after time $t = 0.4 + \frac{10}{200} = 0.45$ s while the vertical one after time $t = 0.4 + \frac{10}{346.41} = 0.429$. In the following figures we can see the vertical and horizontal velocity time history at node C.

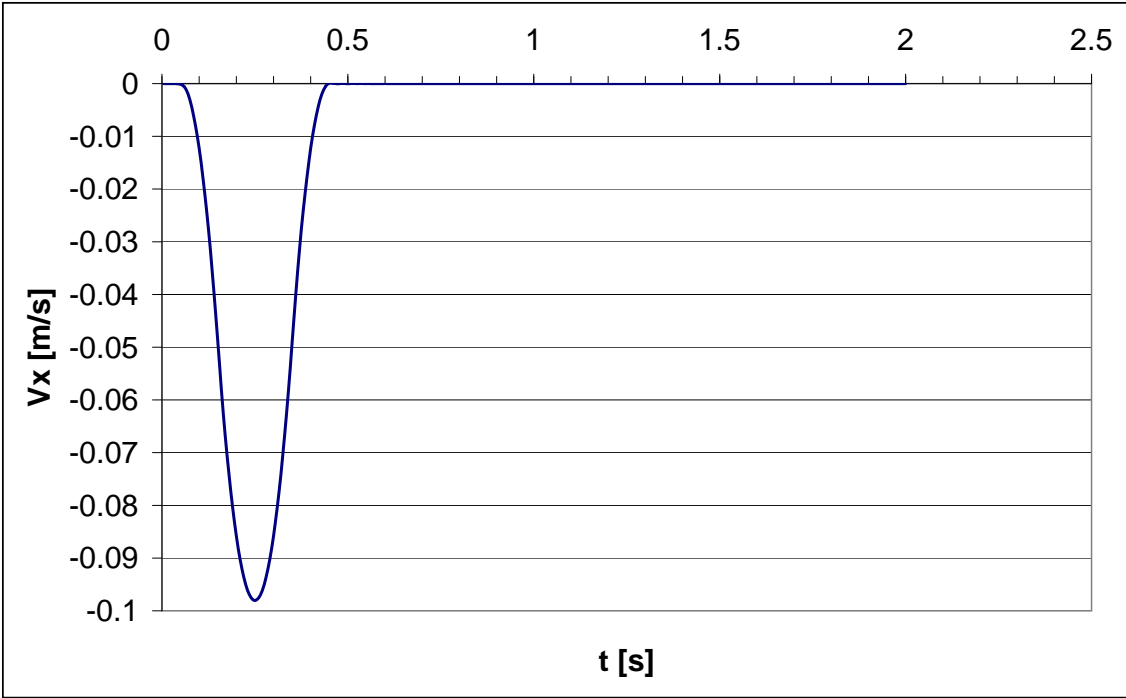


Figure 6.12: Solid velocity $v_x(t)$ at point C

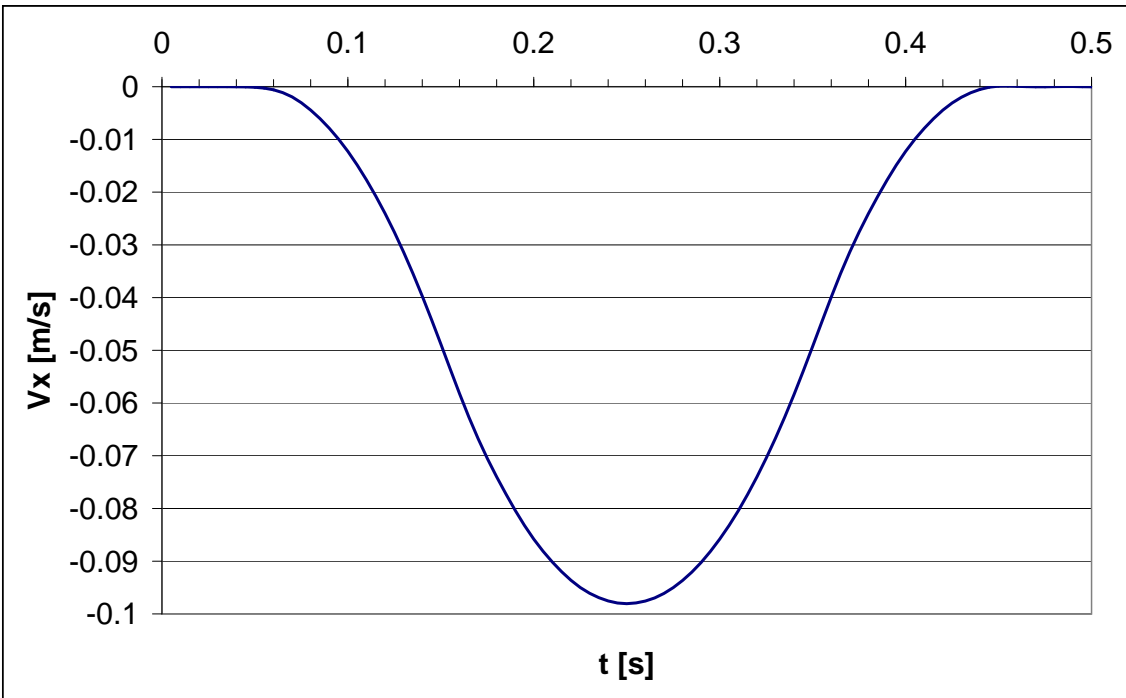
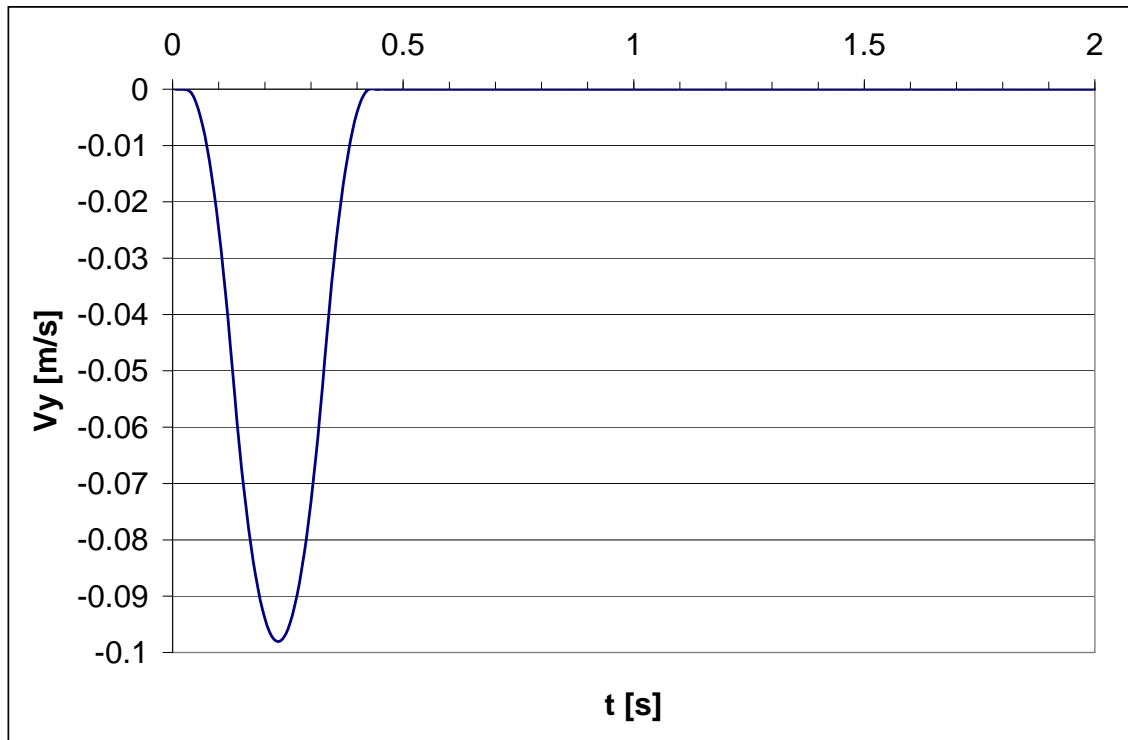
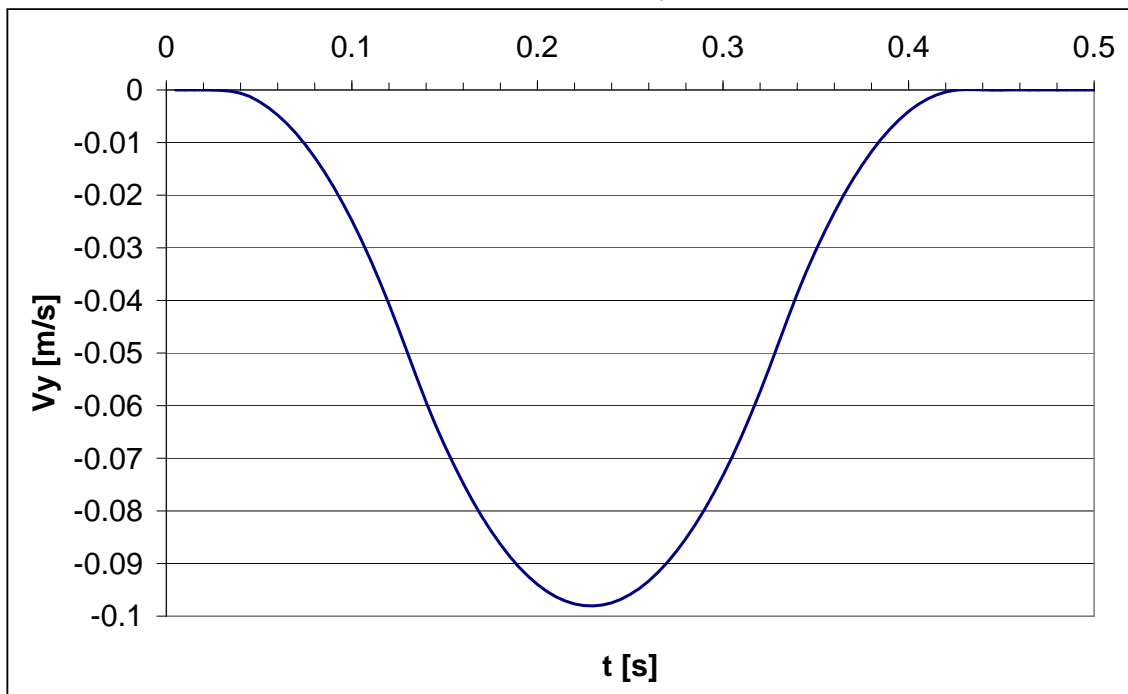


Figure 6.13: Solid velocity $v_x(t)$ (zoom) at point C

Figure 6.14: Solid velocity $v_y(t)$ at point CFigure 6.15: Solid velocity $v_y(t)$ (zoom) at point C

6.4.2 Absorbing boundaries for dynamic consolidation

Files:

Semi_Inf_Col_300m.inp,

Semi_Inf_Col_100m.inp,

Semi_Inf_Col_100m-paraxial.inp

A one-dimensional test problem of a soil column subject to Heaviside type surface load 1000 kN/m², applied to the top boundary, is analyzed (see Modaressi [5]). The material properties used in this test are given in the table 6.6.

Material	Model	Data group	Properties	Unit	Value
1 Continuum	Elastic	Elastic	E	[kN/m ²]	400000
			ν	[-]	0.3
		Density	γ_D	[kN/m ³]	12.9675
			e_o	[-]	0.423856
		Flow	K^F	[kN/m ²]	1000
			$k_x = k_y$	[m/s]	10^{-7}
			S_r	[-]	1.0
			α	[m ⁻¹]	2.0
			$\tilde{\alpha}$	[-]	1.0

Table 6.6: Material properties

To test the paraxial approach three models were constructed (see figure below). The first one, 300m long, the second, 100m long without paraxial element and the third one, again 100 m long, with paraxial element. The first model plays a role of a reference one as the duration time of the analysis is equal 0.35s. Within this time period signal does not reach the bottom boundary. The major difference among the models appear in the setting the boundary conditions. In the first model fixities at the bottom edge remain permanently active while in the 100m long models they become inactive just after 1s. The vertical fixities are released with an unloading function that is equal to 1.0 (all the time). This means that fixities are inactive but reaction forces remain active. In the third model paraxial element is added just after time instance $t=1s$.

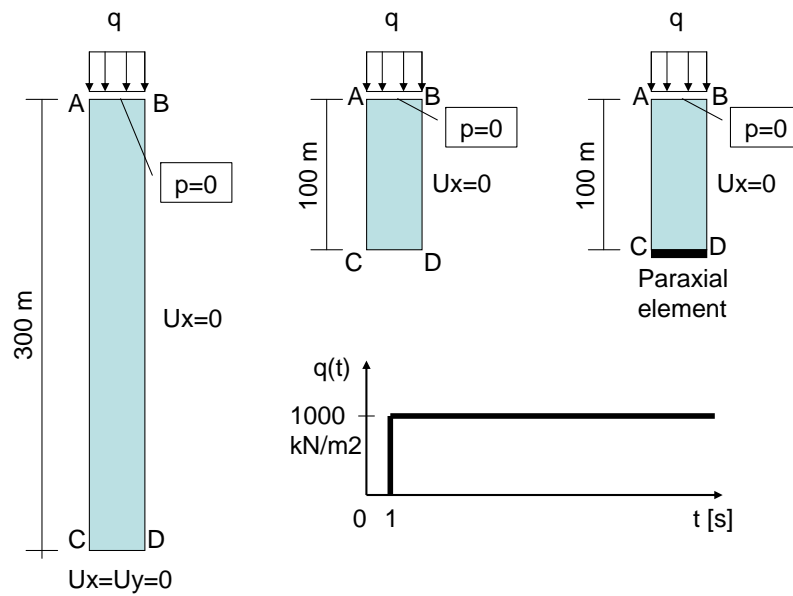


Figure 6.16: Soil layer subject to vertical surface load

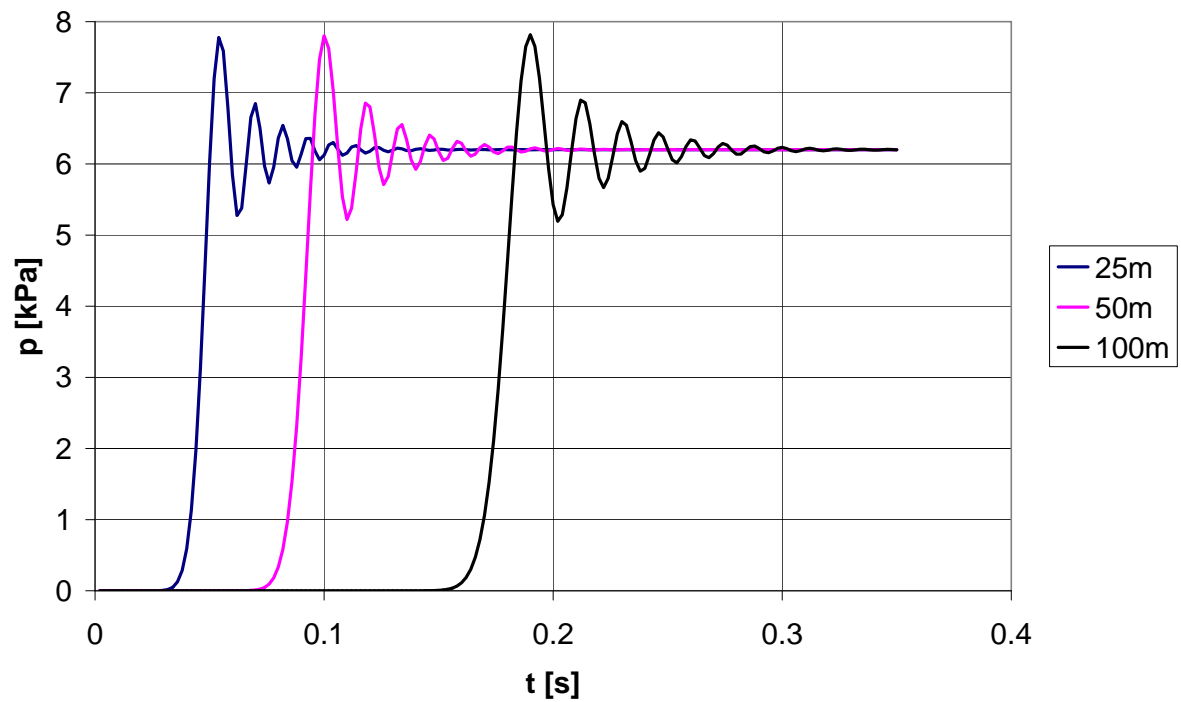


Figure 6.17: Pore pressure for semi-infinite column

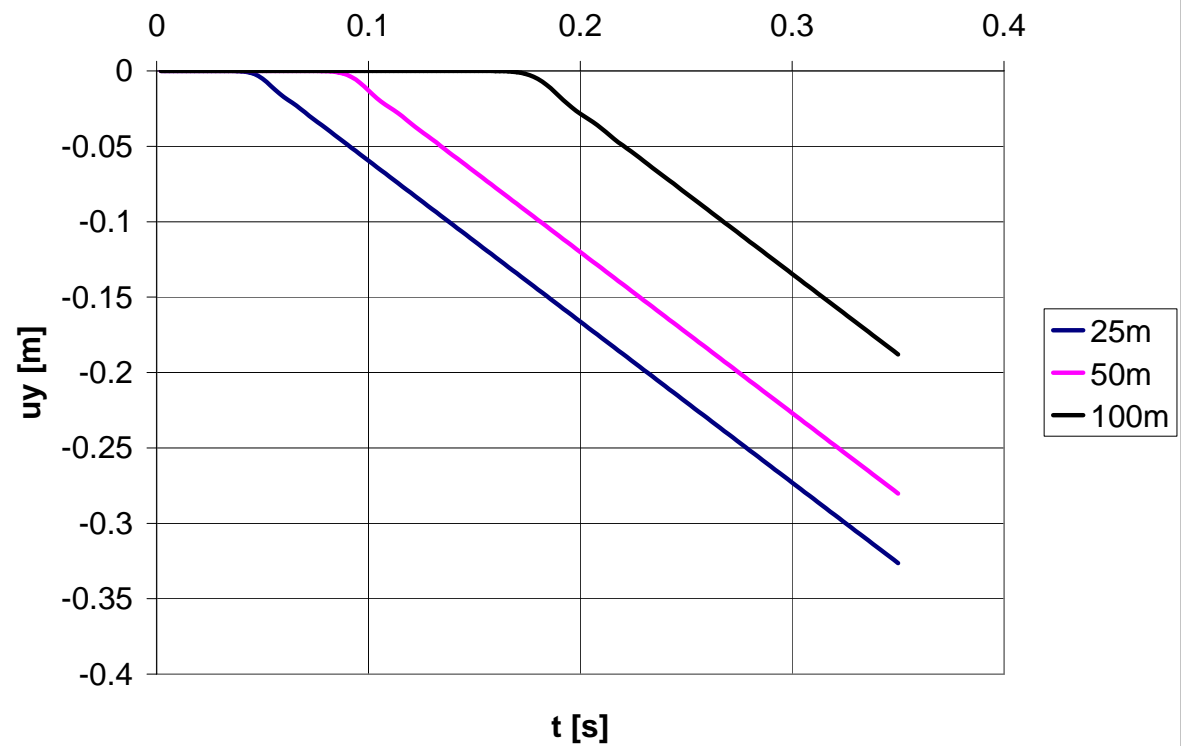


Figure 6.18: Vertical displacement for semi-infinite column

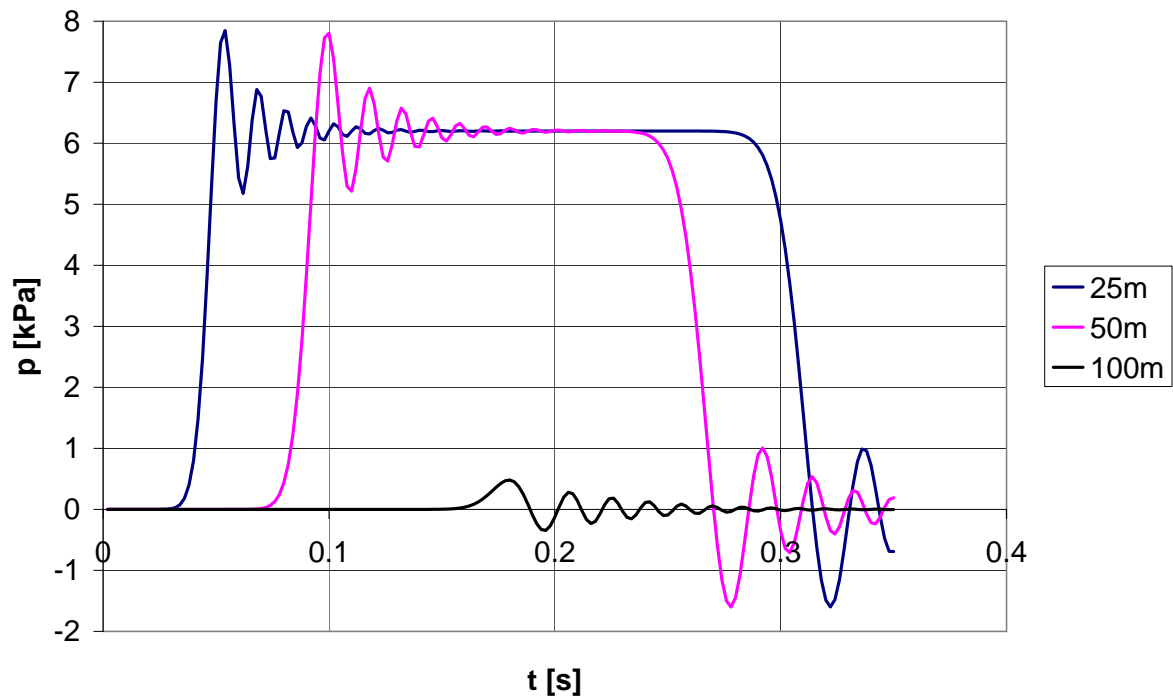


Figure 6.19: Pore pressure for finite column without paraxial elements

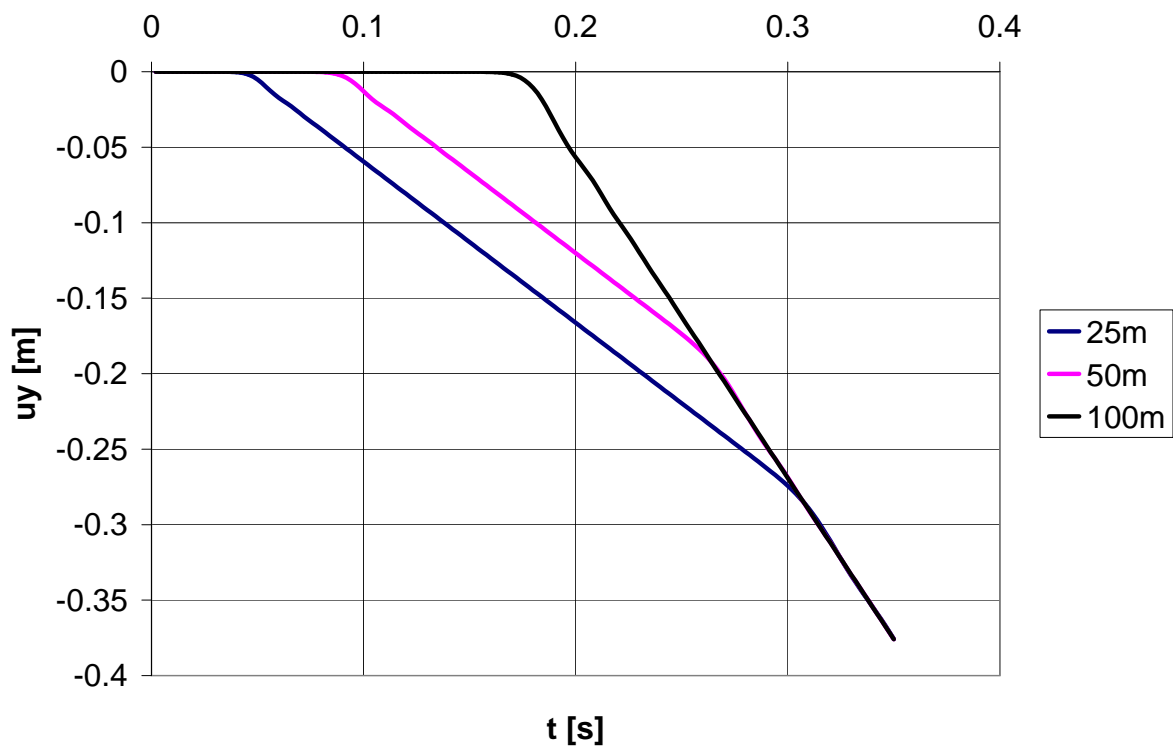


Figure 6.20: Vertical displacement for finite column without paraxial elements

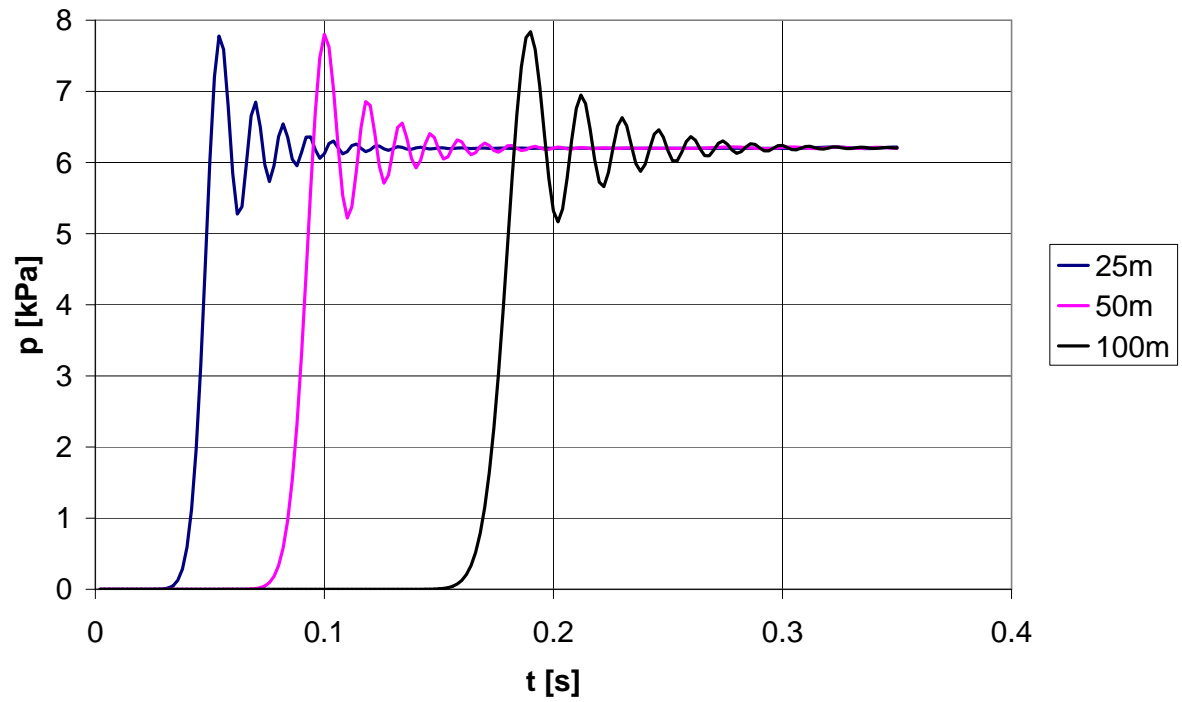


Figure 6.21: Pore pressure for finite column with paraxial elements

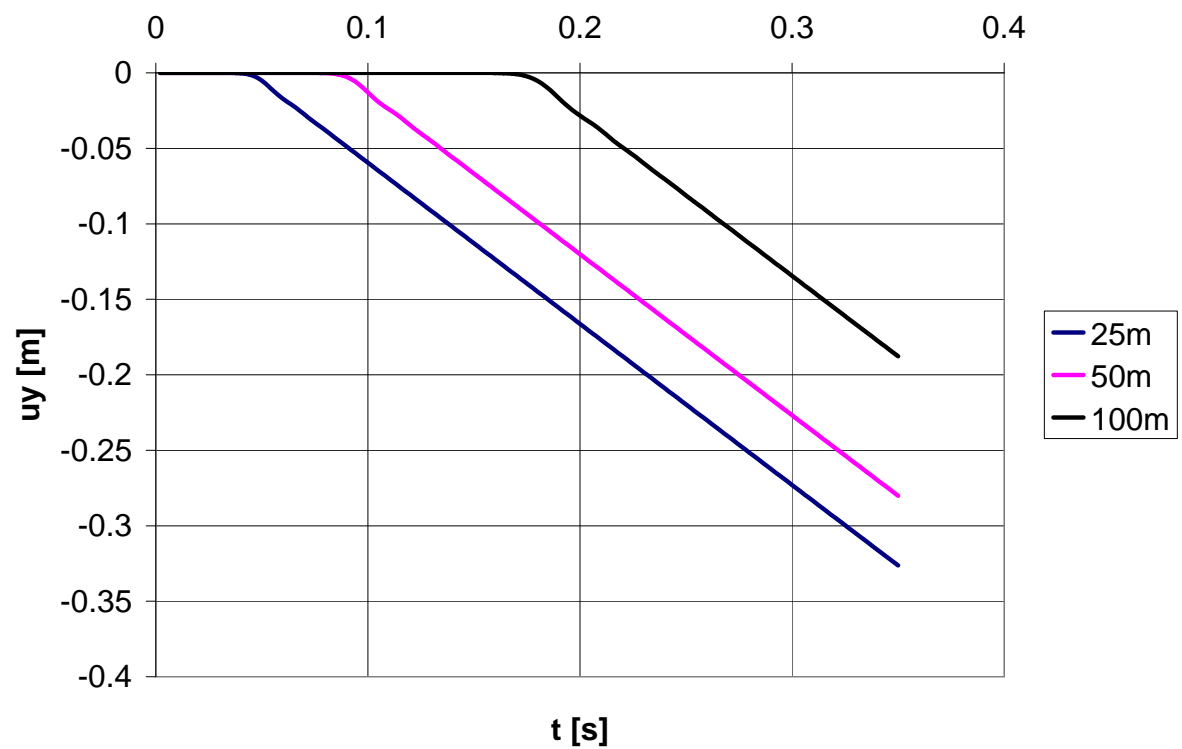


Figure 6.22: Vertical displacement for finite column with paraxial elements

6.5 Soil-structure interaction via DRM method

6.5.1 Beam-subsoil interaction via DRM method, 1D example

Files:

1D-column.inp,

1D-column-plus-beam.inp,

1D-column-plus-mass-DRM-FF-full.inp,

1D-column-plus-mass-DRM-FF-shl.inp

A 1D column-subsoil interaction problem is analyzed here using the Domain Reduction Method [9]. Model consists of 13m deep elastic soil layer and 4m long elastic beam. On top of the beam an extra mass $M = 2000$ kg is added. Thirteen plane strain quadrilateral elements are used to discretize the subsoil while six elements to discretize the beam. The system is subject to base excitation defined in terms of imposed harmonic horizontal displacements with unit amplitude and period $T = 1$ s. System is excited in the first 6s while the whole time history analysis takes 12s. As far as boundary conditions are concerned, all degrees of freedom on opposite vertical walls are tied using Periodic BC option.

To test the approach two different DRM models are considered. In the first one the free field motion is taken from the full model including beam and added mass (see fig.(6.23)) and in the second one (see fig.(6.24)) a free field motion, resulting from shear layer model, is taken as a background model. The simplified shear layer and full models, with harmonic excitation applied at the base, are included in the 1D-column.inp and 1D-column-plus-beam.inp files respectively. It has to be emphasized that in the external domain we seek for the residual motion and hence at the base of both DRM models imposed displacement must be equal to zero during the analysis. The standard validation procedure for DRM method is to substitute as a free-field the motion obtained from full model that includes both subsoil and the structure. In that case the residual field should vanish to zero.

Results of these simulations, given in form of displacement time histories at selected points, are shown in the following figures.

Material properties for continuum and beam are given in Table 6.7.

Material	Model	Data group	Properties	Unit	Value
1 Continuum	Elastic	Elastic	E	[kN/m ²]	48600
			ν	[-]	0.35
		Density	γ_D	[kN/m ³]	17.652
			e_o	[-]	0.0
2 Beam	Elastic	Elastic	E	[kN/m ²]	20000000
			ν	[-]	0.2
		Density	γ	[kN/m ³]	0.0
		Geometry	Rectangular		
			b	[m]	1.0
			h	[m]	1.0

Table 6.7: Material properties

Background model

DRM-FF-FULL

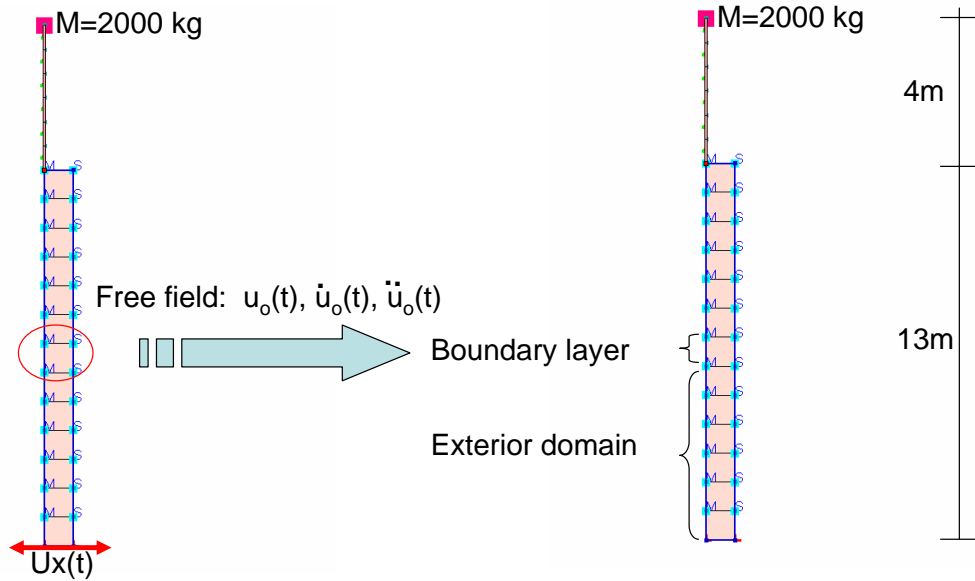


Figure 6.23: DRM model 1: free field motion is taken from full model (1D-column-plus-mass-DRM-FF-full.inp)

Background model

DRM-FF-SHL

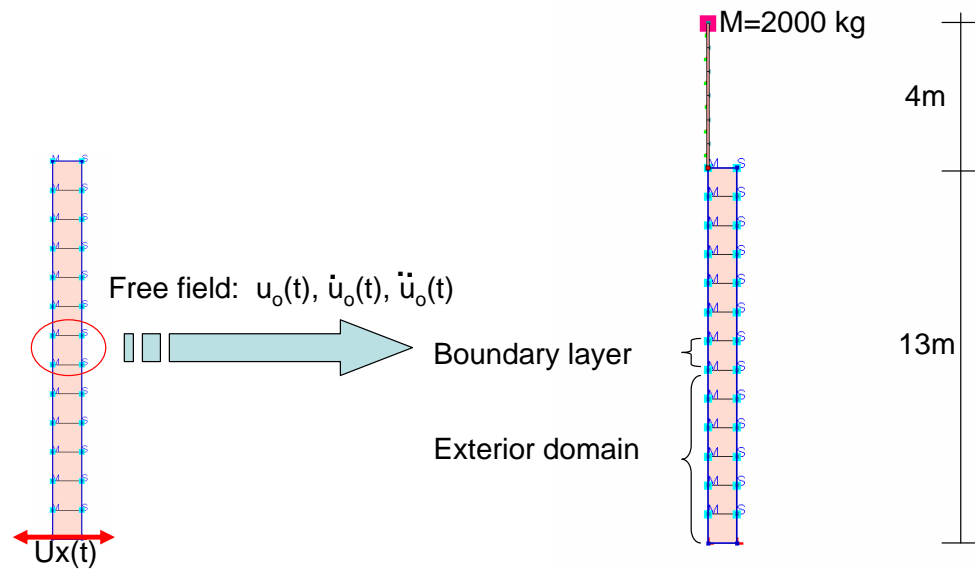


Figure 6.24: DRM model 1: free field motion is taken from simple model (1D-column-plus-mass-DRM-FF-shl.inp)

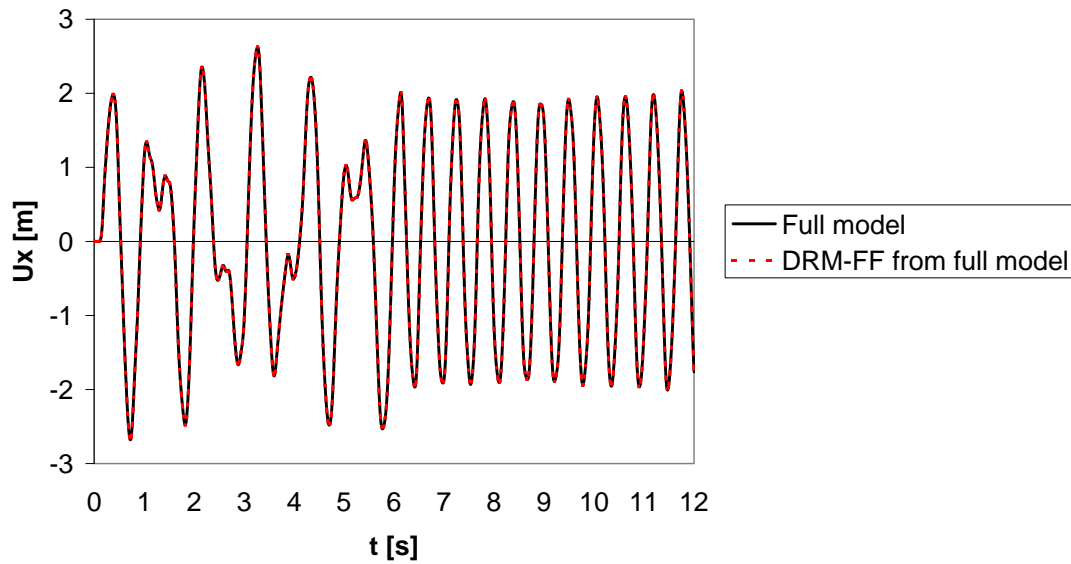


Figure 6.25: $u_x(t)$ at $y=17\text{m}$ (free field motion from full model)

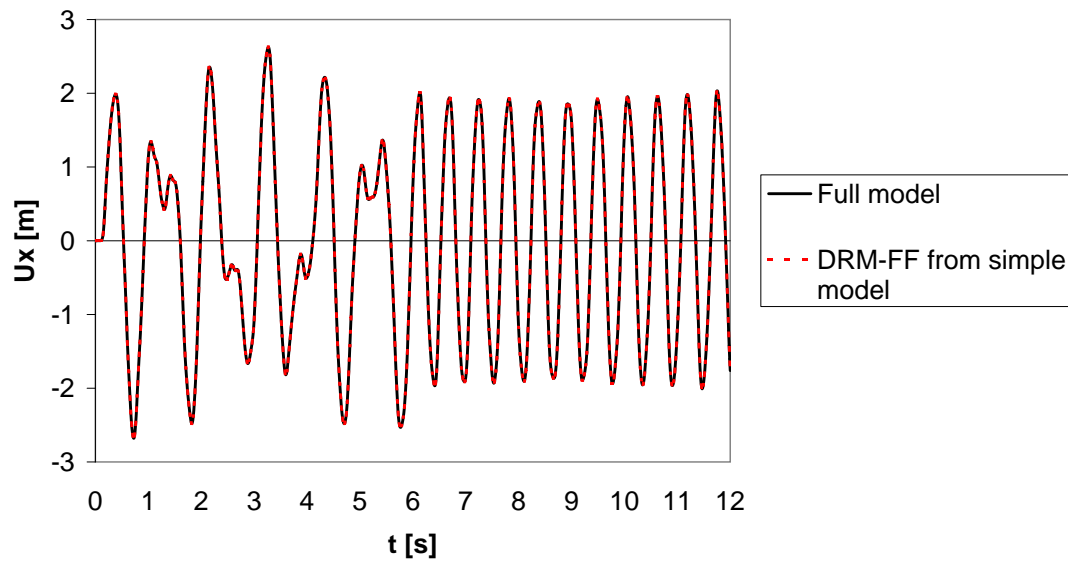


Figure 6.26: $u_x(t)$ at $y=17\text{m}$ (free field motion from simple model)

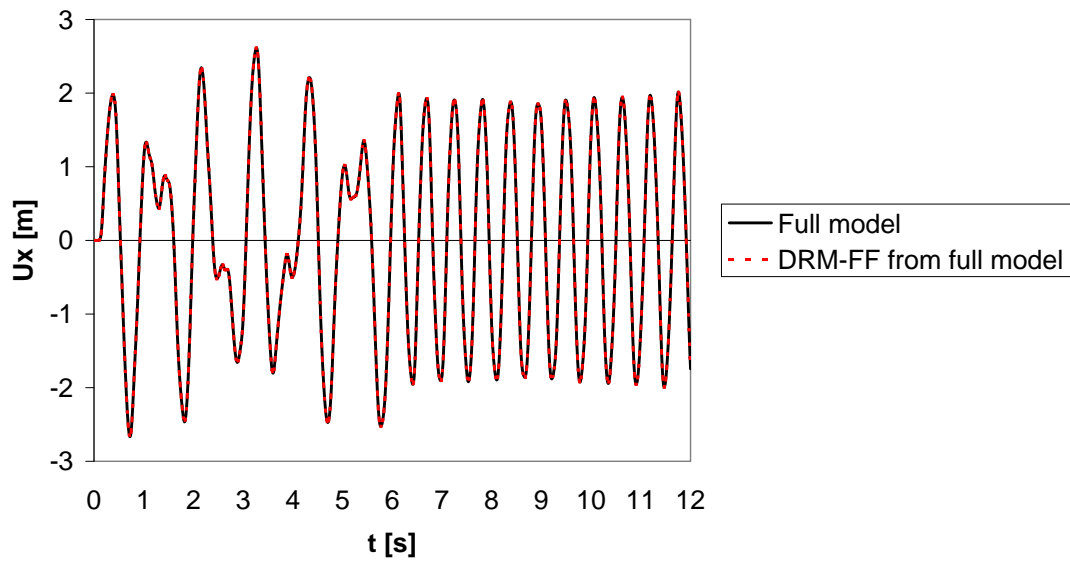


Figure 6.27: $u_x(t)$ at $y=13\text{m}$ (free field motion from full model)

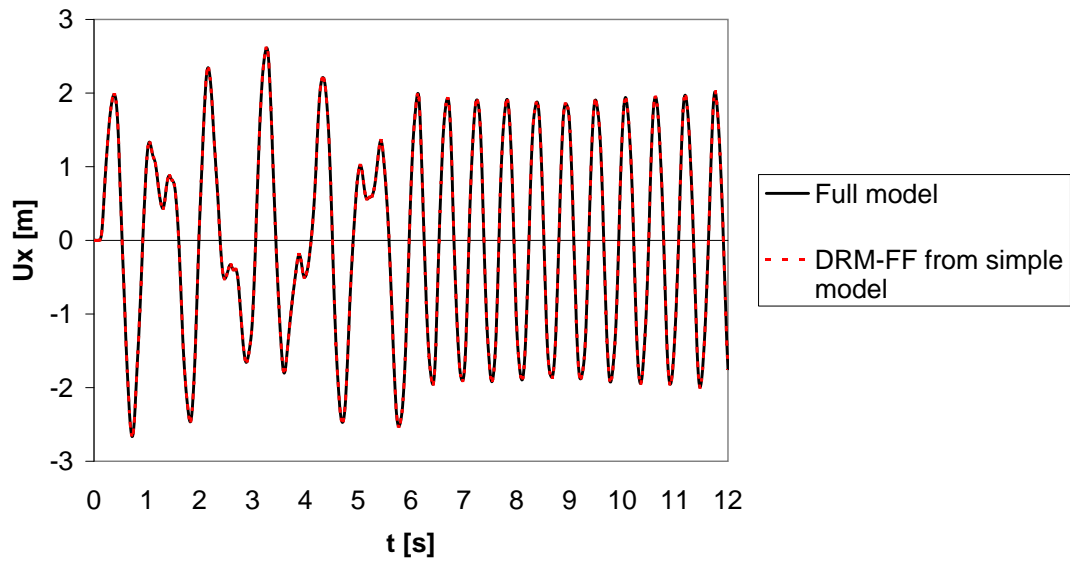


Figure 6.28: $u_x(t)$ at $y=13\text{m}$ (free field motion from simple model)

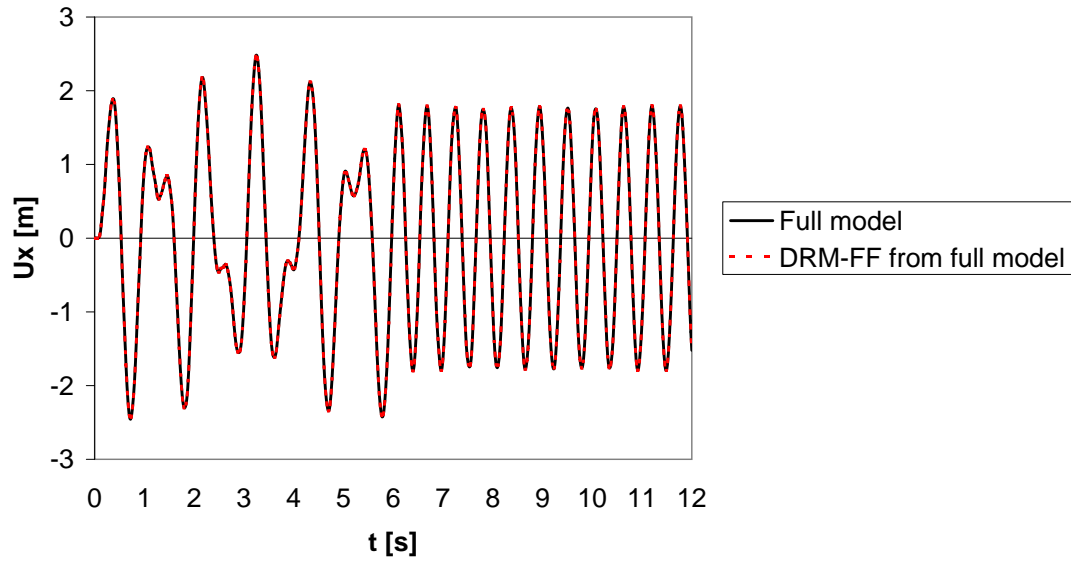


Figure 6.29: $u_x(t)$ at $y=10\text{m}$ (free field motion from full model)

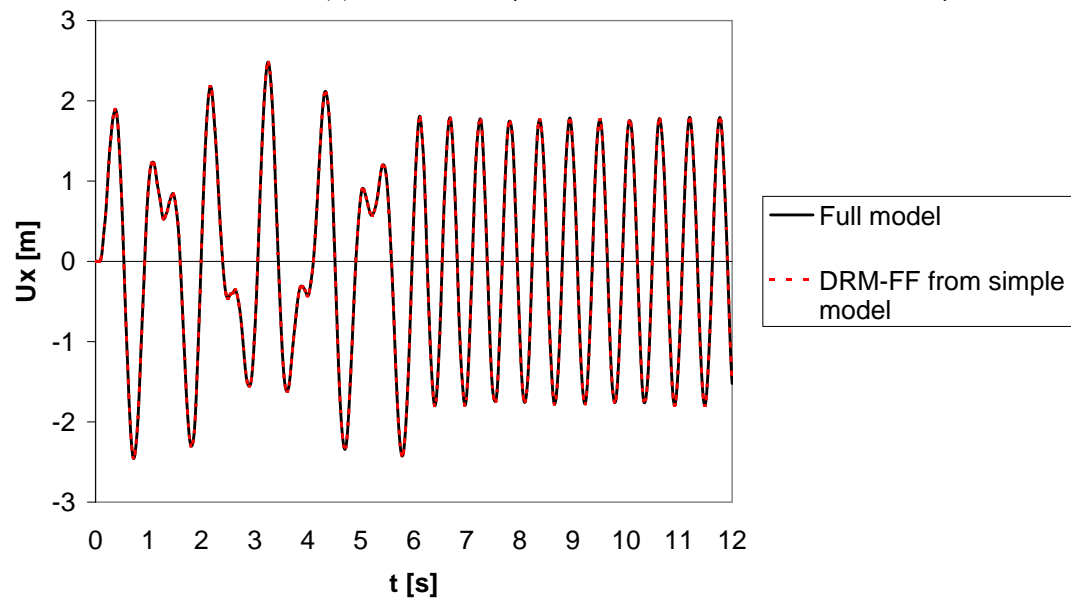


Figure 6.30: $u_x(t)$ at $y=10\text{m}$ (free field motion from simple model)

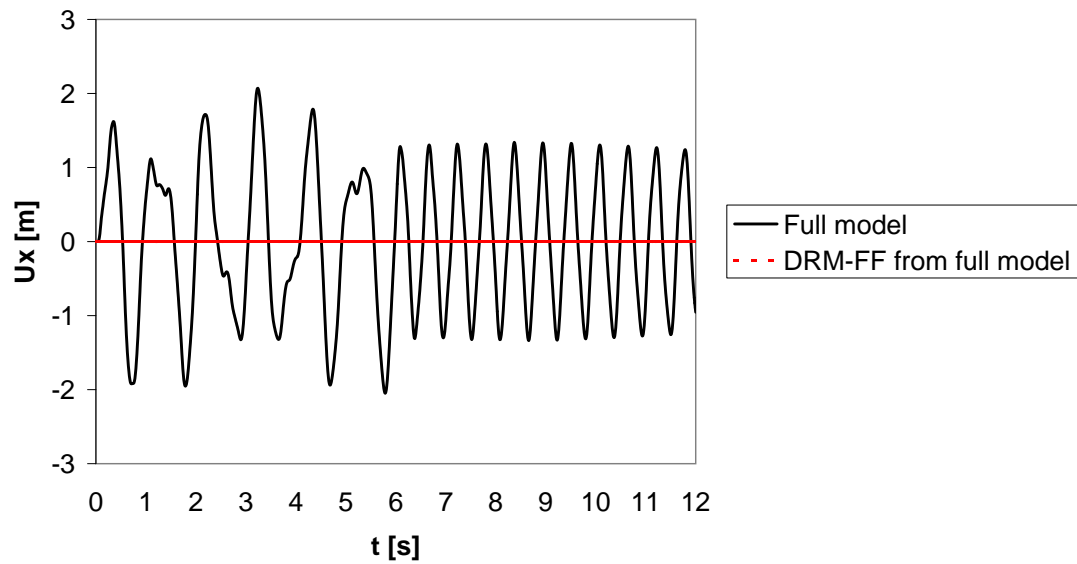


Figure 6.31: $u_x(t)$ at $y=6\text{m}$ (external node of boundary layer)(free field motion from full model)

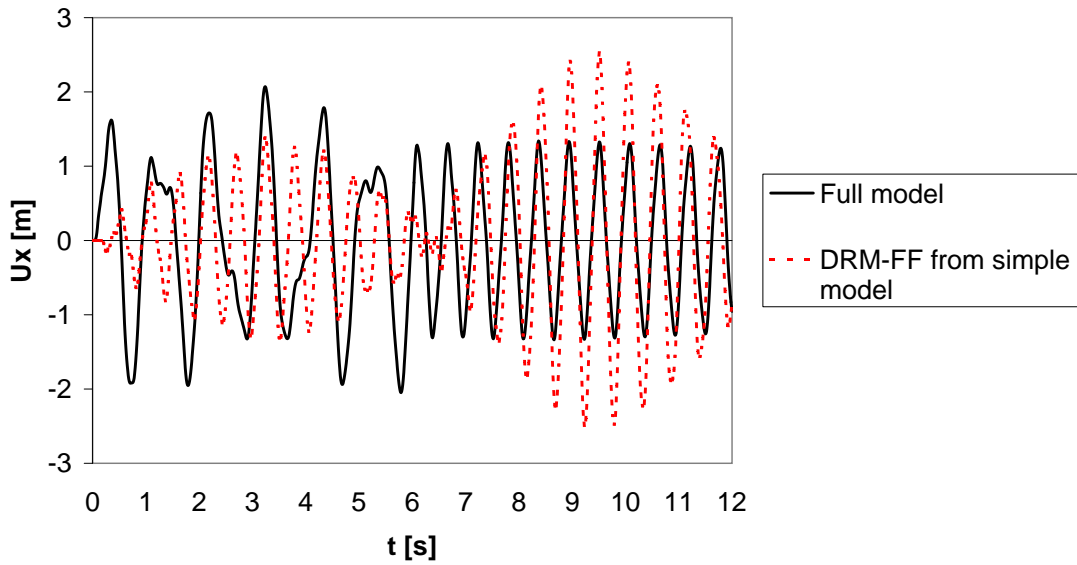


Figure 6.32: $u_x(t)$ at $y=6\text{m}$ (external node of boundary layer)(free field motion from simple model)

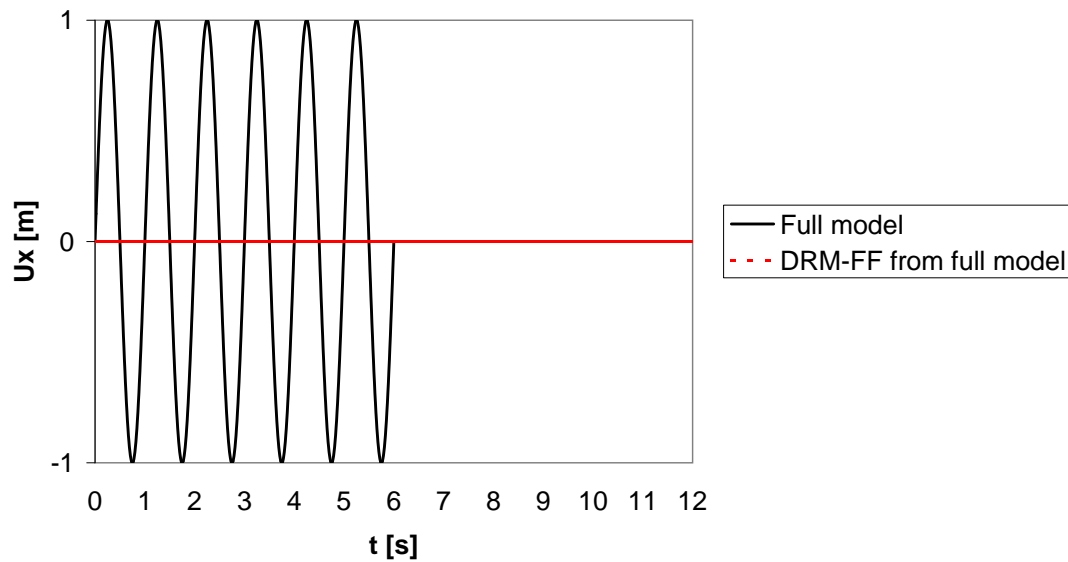


Figure 6.33: $u_x(t)$ at $y=0$ m (base node)(free field motion from full model)

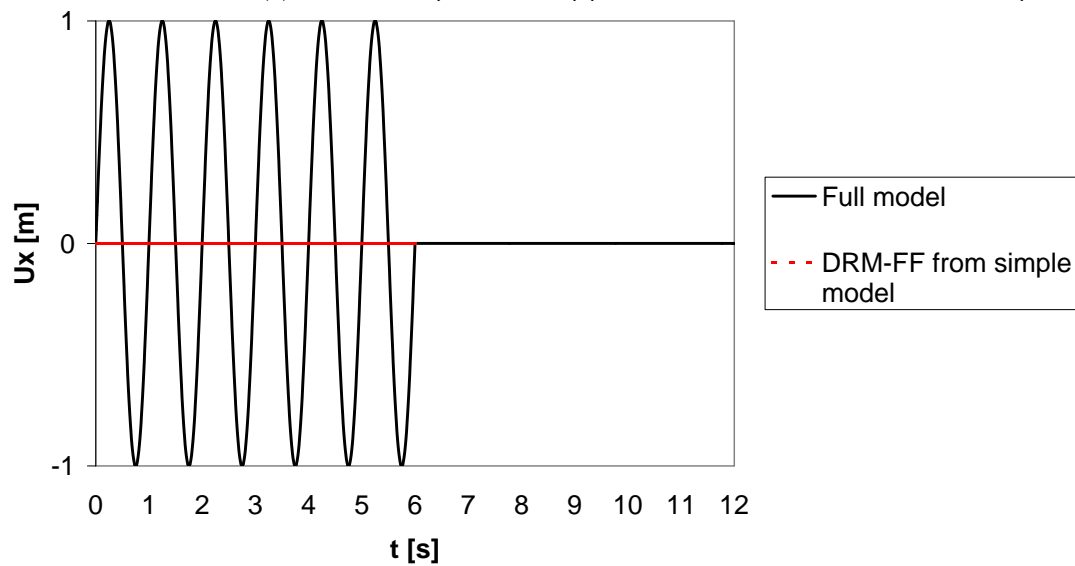


Figure 6.34: $u_x(t)$ at $y=0$ m (base node)(free field motion from simple model)

6.5.2 Beam-subsoil interaction via DRM method, 2D example

Files:

SOIL-COLUMN.inp

FF-SHL.inp,

DRM-S-FF-L.inp,

DRM-S-FF-SHL.inp,

DRM-S-V-WALL-FF-L.inp,

DRM-S-V-WALL-FF-SHL.inp,

A two-dimensional column-subsoil interaction problem is analyzed here using the DRM method. Model consists of 30m deep elastic soil layer, and 10m long elastic beam, subject to harmonic ($f = 2$ Hz) base excitation defined in terms of imposed horizontal displacements.

To obtain a reference solution a large two-dimensional model ($3600\text{m} \times 30\text{m}$) (SOIL-COLUMN.inp) was solved first assuming periodic boundary conditions at left and right vertical boundaries. The initial state was generated first for the box-type BC. In the later stage horizontal fixities, at both vertical walls, were released, but corresponding static reactions were left using unloading procedure for BC (unloading function associated with the horizontal fixities is equal to 1.0 for any time instance). Duration of time history analysis was 5s in the period $t = 1..6$ s and time step $\Delta t = 0.01$ s was selected. The setup of this model is shown in fig.(6.35).

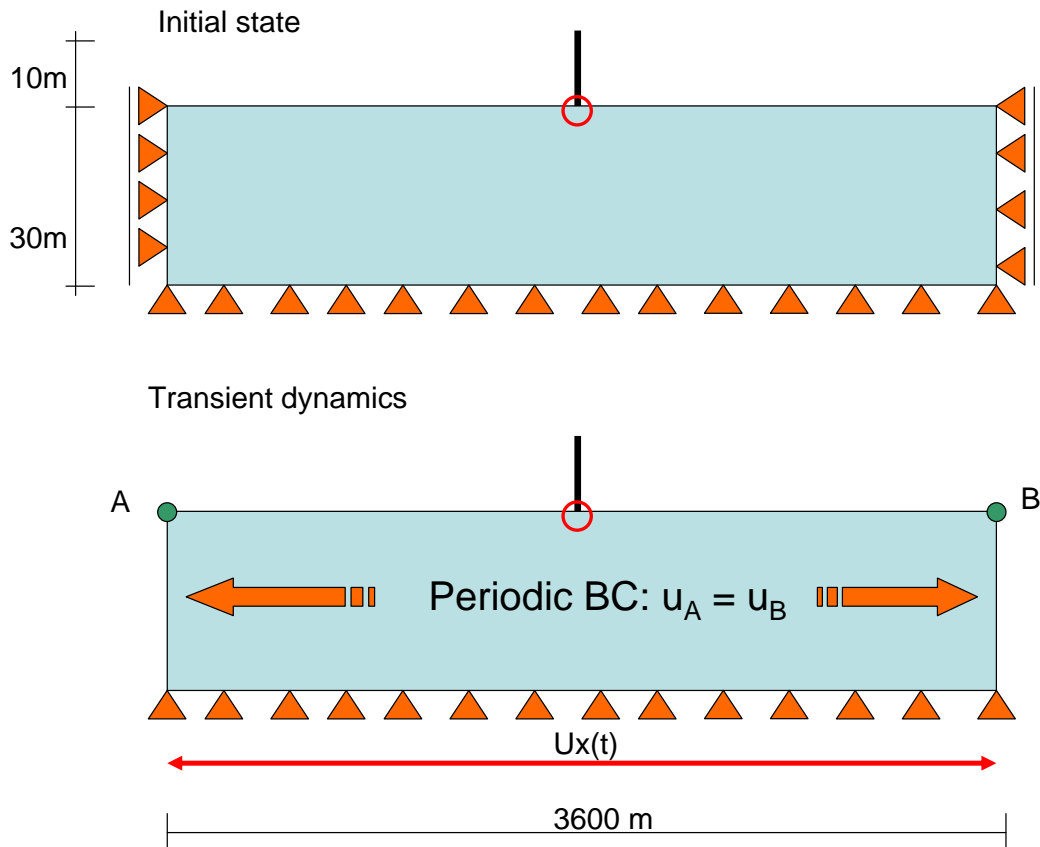


Figure 6.35: Soil-beam interaction problem (full model)

To test the approach two different DRM models were considered. In the first one (DRM-1) the boundary and external layer take U-letter form (see fig.(6.36)) while in the second one (DRM-2) the boundary and external layers are placed exclusively along vertical walls (see fig.(6.37)). In both

cases free field motions taken from the full (SOIL-COLUMN.inp) and simplified shear layer (FF-SHL.inp) models were considered. In the latter case the shear layer domain must fully cover (in the geometrical sense) the domain of the DRM finite element models. In addition in DRM models viscous dampers were added along the vertical edges of external domain (as the model is extended up to the rigid base). As in the external domain we seek for the residual motion, in the DRM-1 model, during dynamic analysis, imposed displacements, at base nodes that belong to the external domain, must be equal to zero. Contrary to DRM-1, in the DRM-2 model at all base nodes, that do not belong to the external domain, we have to apply the nonzero harmonic excitation with 2Hz frequency. Results of these simulations, given in form of horizontal displacement time histories, at certain points, are shown in the following figures. One may notice very little deviations in time histories produced by full and DRM models. This deviation is caused by the fact that presence of the beam, even in such a large model, generates deviation from pure shear layer motion at nodes placed far from the structure (see fig.(6.53)).

Material properties for continuum and beam are given in Table 6.8. Properties for viscous dashpots used in the DRM models are the same as for the continuum.

Material	Model	Data group	Properties	Unit	Value
1 Continuum	Elastic	Elastic	E	[kN/m ²]	192000
			ν	[-]	0.2
		Density	γ_D	[kN/m ³]	19.6133
			e_o	[-]	0.0
2 Beam	Elastic	Elastic	E	[kN/m ²]	20000000
			ν	[-]	0.2
		Density	γ	[kN/m ³]	24.5166
		Geometry	Rectangular		
			b	[m]	1.0
			h	[m]	1.0

Table 6.8: Material properties

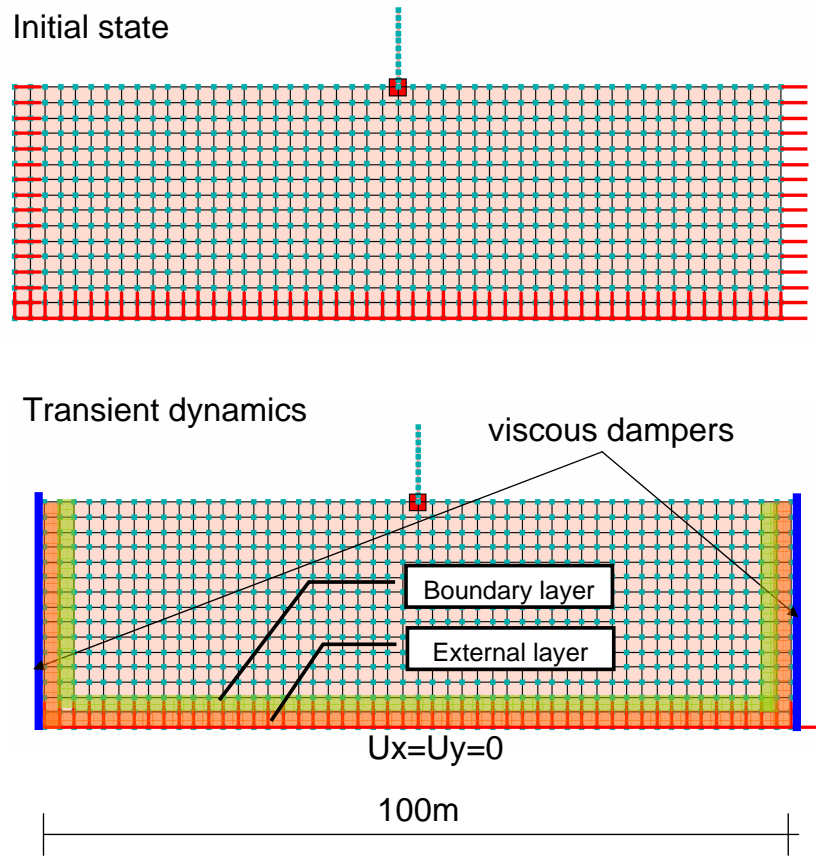


Figure 6.36: DRM-1 model: continuos boundary and external layer

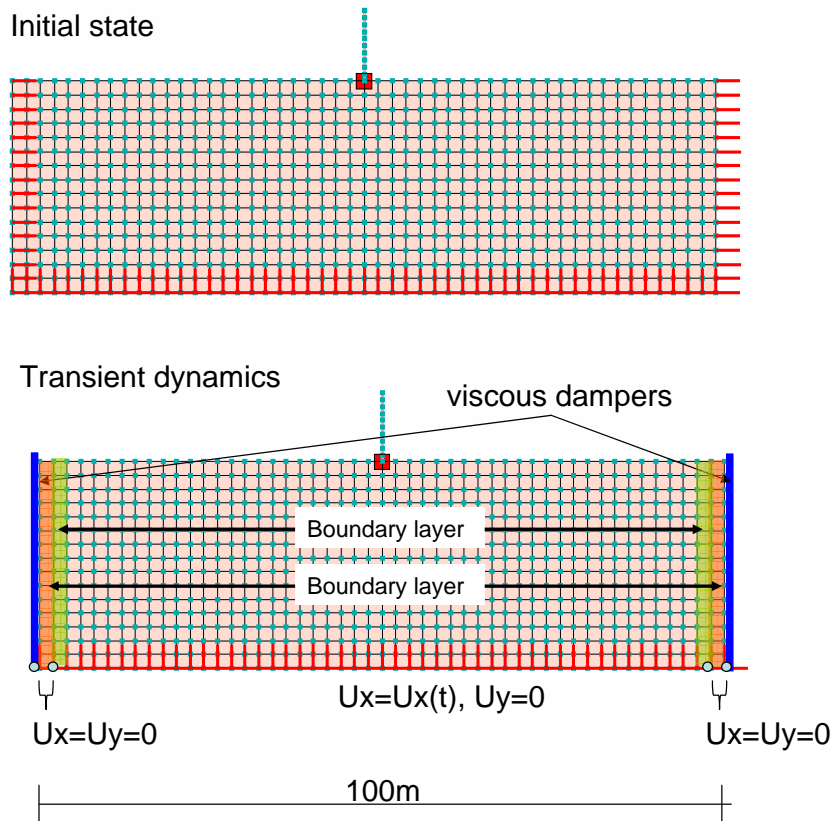


Figure 6.37: DRM-2 model: boundary and external layers placed along vertical walls

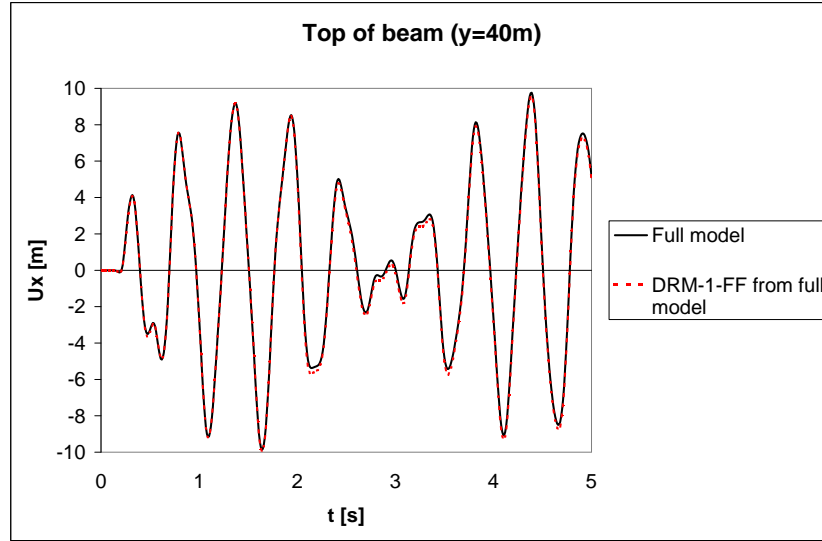


Figure 6.38: $u_x(t)$ at $y=40\text{m}$ (top of the beam)(free field motion from full model)

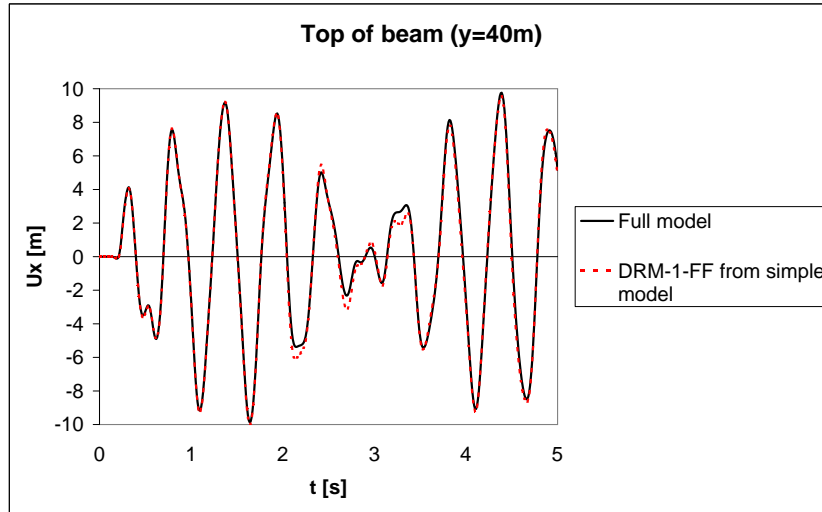


Figure 6.39: $u_x(t)$ at $y=0\text{m}$ (top of the beam)(free field motion from simple model)

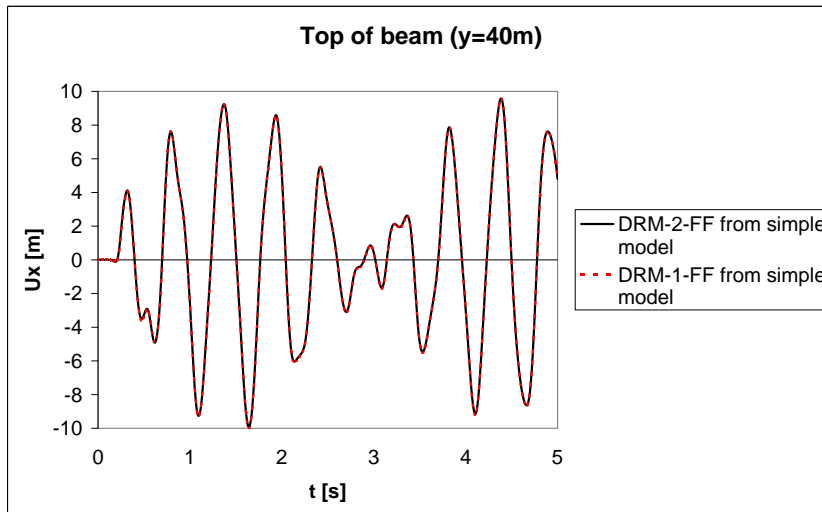


Figure 6.40: $u_x(t)$ at $y=0\text{m}$ (top of the beam)(free field motion from simple model)

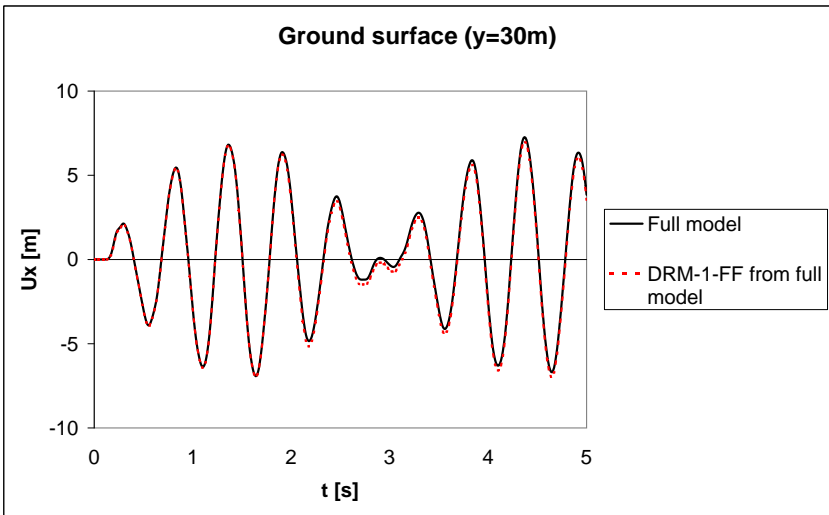


Figure 6.41: $u_x(t)$ at $y=30\text{m}$ (ground surface)(free field motion from full model)

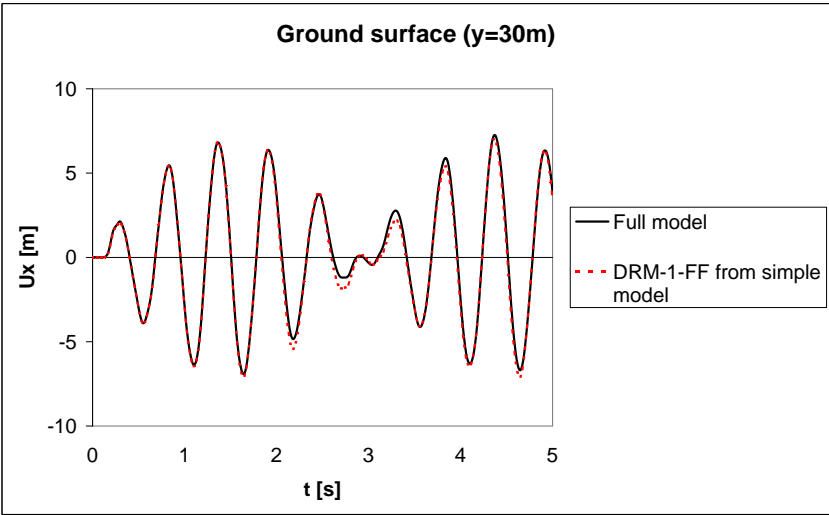


Figure 6.42: $u_x(t)$ at $y=30\text{m}$ (ground surface)(free field motion from simple model)

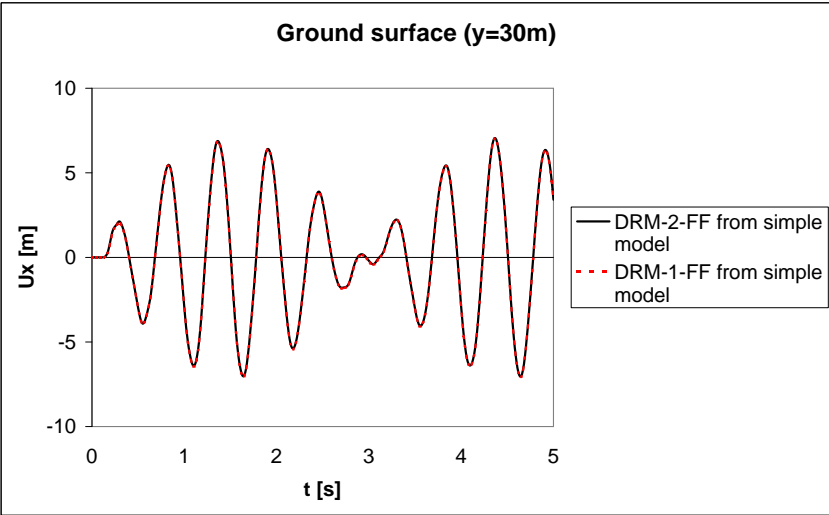


Figure 6.43: $u_x(t)$ at $y=30\text{m}$ (ground surface)(free field motion from simple model)

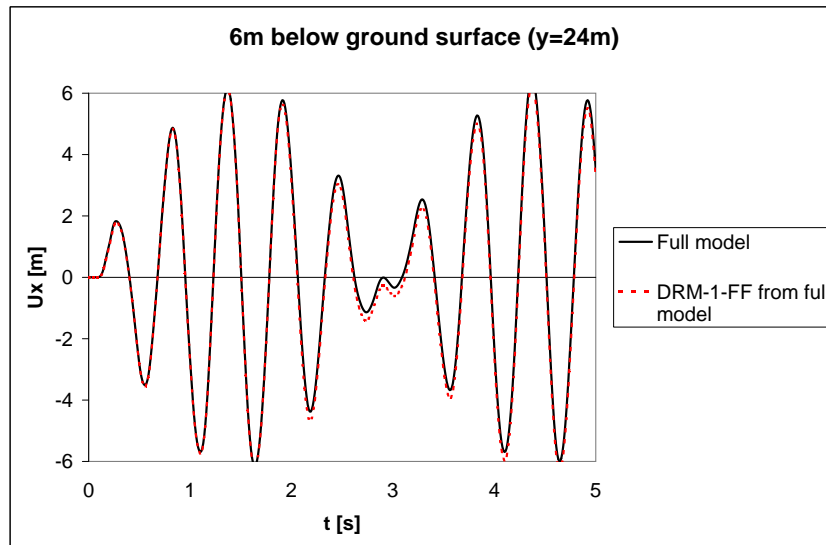


Figure 6.44: $u_x(t)$ at $y=24\text{m}$ (free field motion from full model)

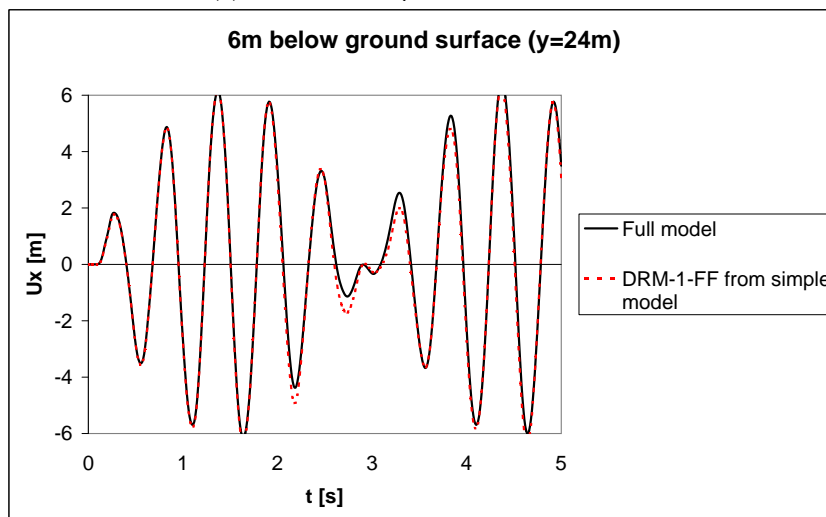


Figure 6.45: $u_x(t)$ at $y=24\text{m}$ (free field motion from simple model)

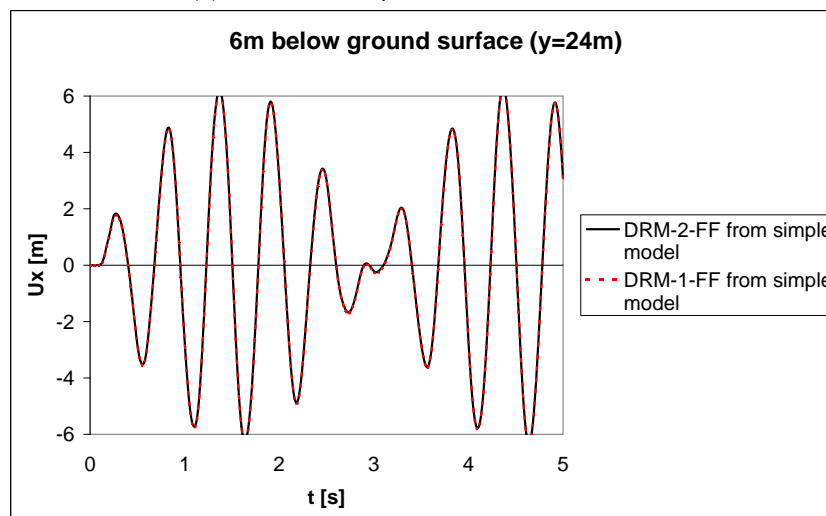


Figure 6.46: $u_x(t)$ at $y=24\text{m}$ (free field motion from simple model)

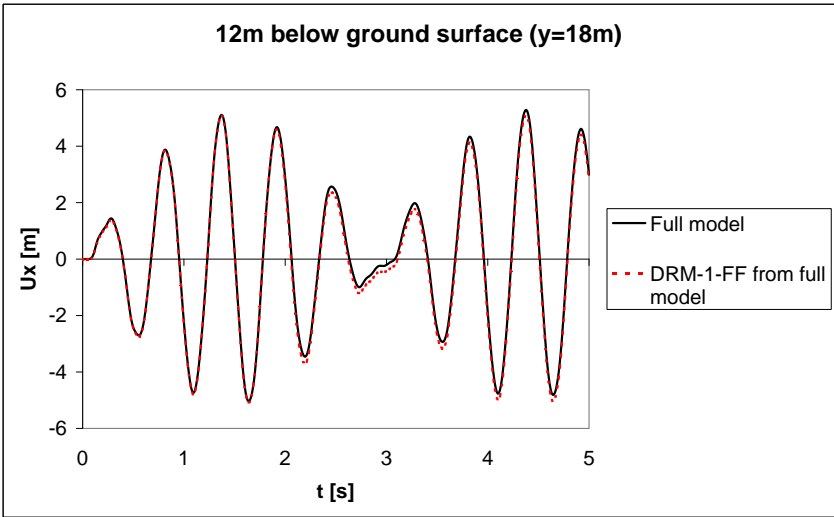


Figure 6.47: $u_x(t)$ at $y=18\text{m}$ (free field motion from full model)

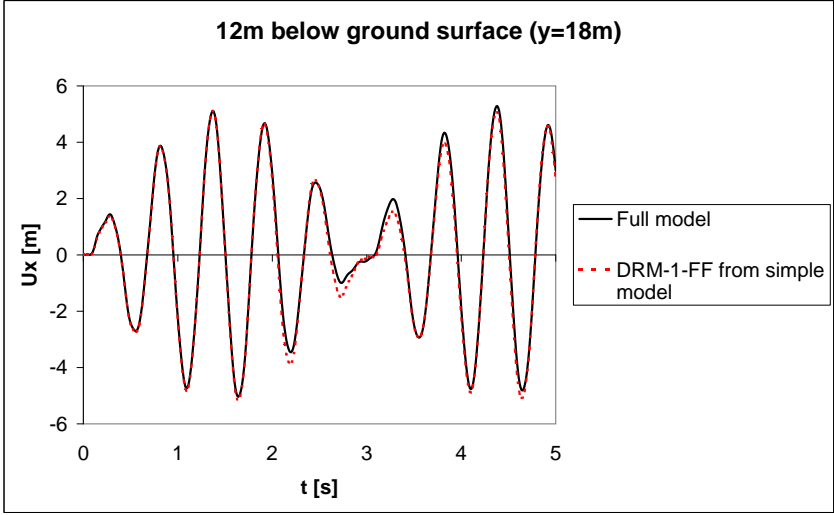


Figure 6.48: $u_x(t)$ at $y=18\text{m}$ (free field motion from simple model)

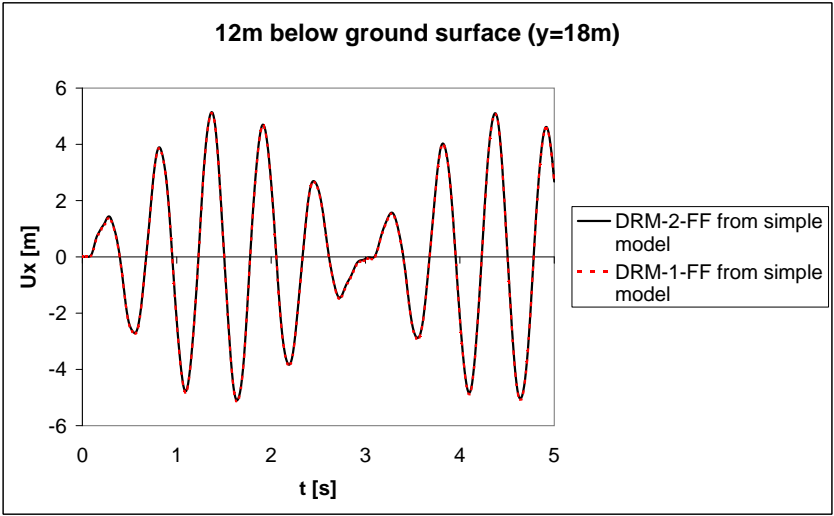


Figure 6.49: $u_x(t)$ at $y=18\text{m}$ (free field motion from simple model)

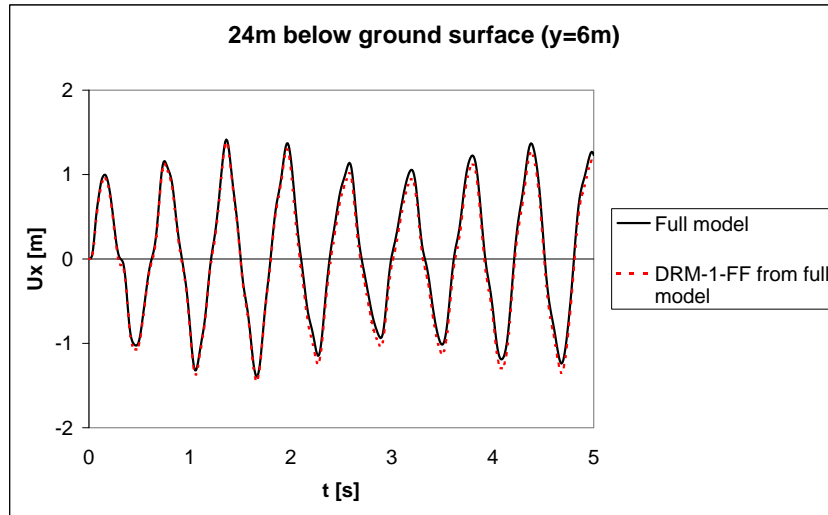


Figure 6.50: $u_x(t)$ at $y=6\text{m}$ (free field motion from full model)

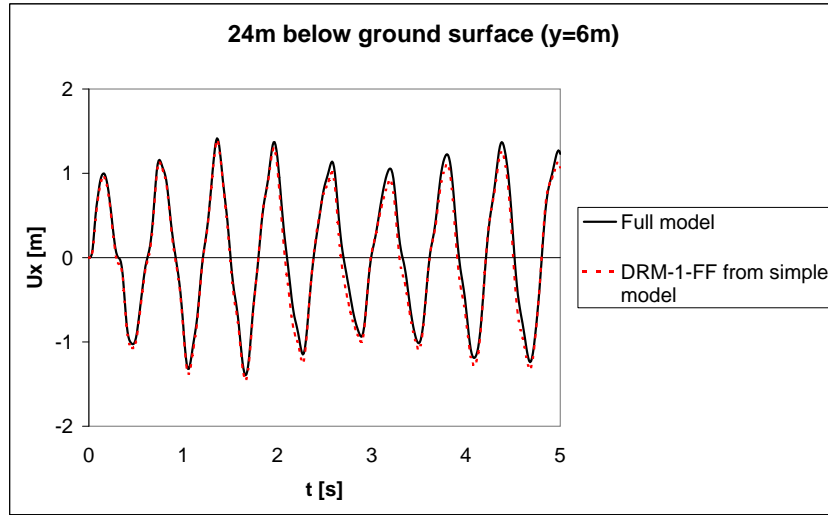


Figure 6.51: $u_x(t)$ at $y=6\text{m}$ (free field motion from simple model)

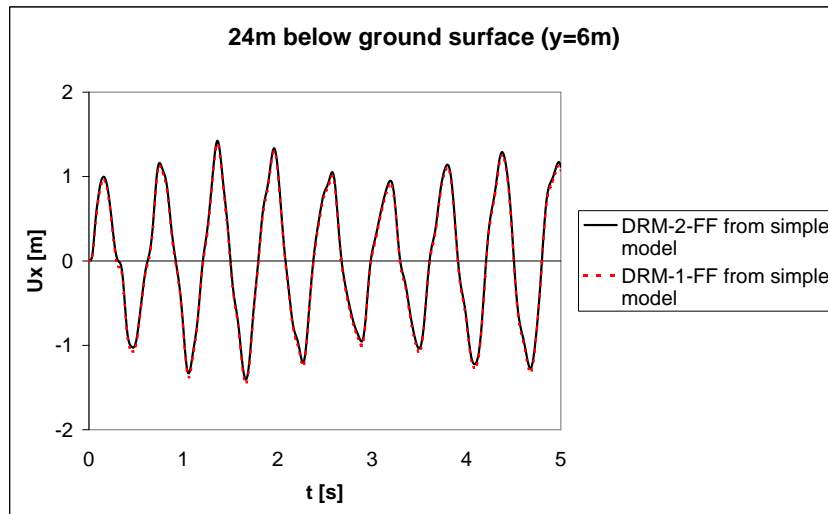


Figure 6.52: $u_x(t)$ at $y=6\text{m}$ (free field motion from simple model)

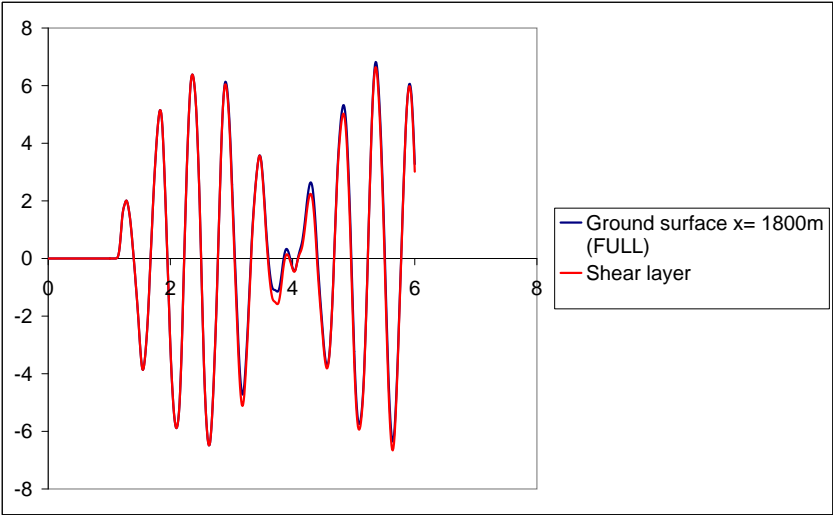


Figure 6.53: $u_x(t)$ time histories for full model (at $x = 1800\text{m}$) and shear layer at $y = 30\text{ m}$

6.6 Application of densification model

6.6.1 Cyclic simple shear test with strain control

File:simple-shear-cyclic.inp

In this example we will simulate cyclic simple shear test under drained conditions (mode : Deformation). The displacement boundary conditions are as follows $u_x^C = u_x^D = 0$, $u_y^C = u_y^D = 0$, $u_x^A = u_x^B = 10^{-3} \sin(2 * \pi * t)$ and an additional periodic boundary condition is assumed $u_y^A = u_y^B$ (see Fig.(6.54)). The imposed horizontal displacement (that yields the strain amplitude $\gamma_o(t)$) is generated inside dialog box designed for load time functions where we can introduce the following expression $10^{-3} \sin(6.283185307179586 * t)$ in time range 0..100s with step 0.25s. The meaningful material data used in this simulation is set as follows: $E_{ur}^{ref} = 100000$ kPa, $\nu_{ur} = 0.25$, $\sigma_{ref} = 100$ kPa, $\sigma_L = 5$ kPa, $m = 0.5$, small strain option is inactive, $e_o = 0.5$, $\phi = 30^\circ$, $c = 0$ kPa, shear mechanism is inactive, Sawicki's densification law is assumed with $C_1 = 8.7 * 10^{-3}$, $C_2 = 2 * 10^5$, an extended strain mapping is used (in this case accumulated strain will develop only in the vertical direction). The constant time step is used in this simulation with $\Delta t = 0.025$ s (10 strain increments per 1/4 cycle).

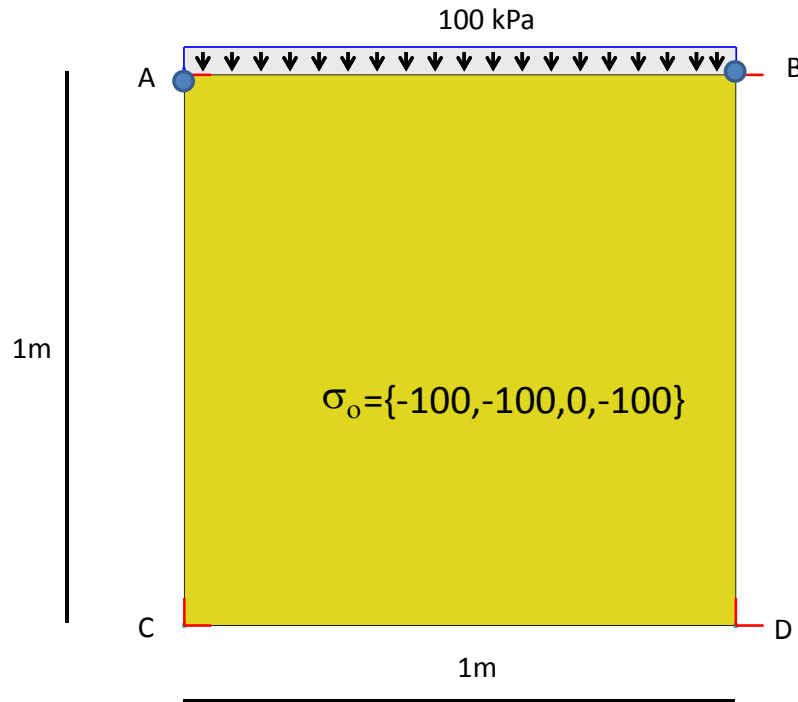


Figure 6.54: Single element setup

The comparison of the analytical solution by Sawicki ($\varepsilon_v = e_o C_1 \ln(1 + C_2 z)$) and the numerical one is shown in Fig.(6.55). In Fig.(6.56) we can take a look to the zoomed part of the analytical and numerical solution. As we can see the analytical solution is cycling along the common compaction curve.

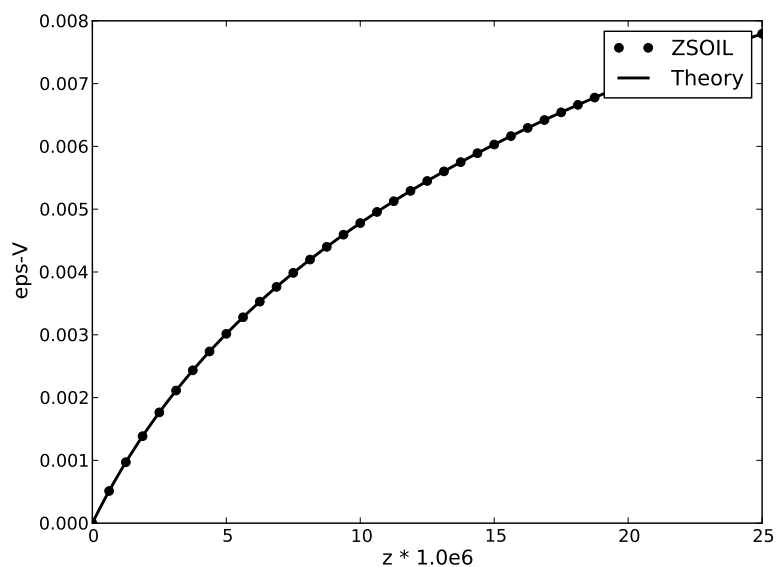


Figure 6.55: Evolution of volumetric strain with z parameter $\varepsilon_v(z)$

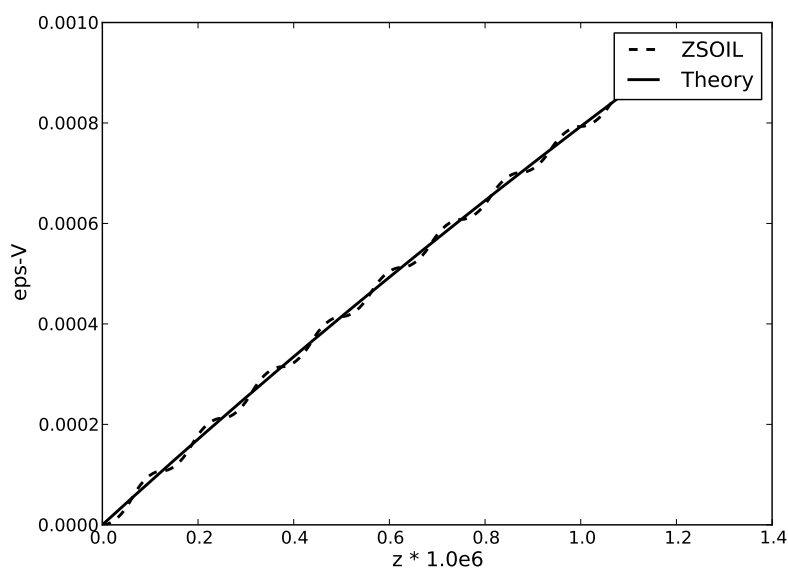


Figure 6.56: Zoom of $\varepsilon_v(z)$

6.6.2 Static liquefaction problem

Files:

simple-shear-mono-undr-100kPa.inp,
 simple-shear-mono-undr-200kPa.inp,
 simple-shear-mono-undr-300kPa.inp,
 simple-shear-mono-undr-100kPa-ex.inp,
 simple-shear-mono-undr-200kPa-ex.inp,
 simple-shear-mono-undr-300kPa-ex.inp

In this example we will simulate monotonic simple shear test under undrained conditions (mode: Deformation+Flow). The displacement boundary conditions are as follows $u_x^C = u_x^D = 0$, $u_y^C = u_y^D = 0$, $u_x^A = u_x^B = f(t)$ and an additional periodic boundary condition is assumed $u_y^A = u_y^B$ (see Fig.(6.54)). The imposed horizontal displacement is defined via load time function that consists of 5 characteristic points $\{0.0, 0.0\}, \{1.0, 0.00001\}, \{2.0, 0.0001\}, \{3.0, 0.001\}, \{4.0, 0.01\}, \{5.0, 0.1\}$. The meaningful material data used in this simulation is set as follows: $E_{ur}^{ref} = 100000$ kPa, $\nu_{ur} = 0.25$, $\sigma_{ref} = 100$ kPa, $\sigma_L = 5$ kPa, $m = 0.5$, small strain option is inactive, $e_o = 0.5$, $\phi = 30^\circ$, $c = 0$ kPa, shear mechanism is once active and then inactive, Sawicki's densification law is assumed with $C_1 = 8.7 * 10^{-3}$, $C_2 = 2 * 10^5$, an extended strain mapping is used (in this case accumulated strain will develop only in the vertical direction). In the time range $t = 0..3$ s the time step $\Delta t = 0.025$ s is used, and for the remaining period $\Delta t = 0.01$ s was assumed. In this case the undrained behavior is modeled by means of the *Driven Load (undrained)* driver. In this case in group *Flow* the gravity term in Darcy law was canceled (to avoid pore pressure build up due to fluid dead weight). This test is reproduced for three different initial confining stresses 100 kPa, 200 kPa and 300 kPa. As we can observe the descending branch of effective stress path in $p - q$ plane (see Fig.(6.57a, 6.57a)), for model with inactive shear mechanism, follows the M-C limit line while for model with the active shear mechanism one may observe existence of the phase transition line below the M-C line. For simulations with shear mechanism active the $E_{50}^{ref} = 33000$ kPa secant reference Young moduli was assumed. The evolution of deviatoric stress q with respect to the imposed shear strain is shown in Fig.(6.57c, 6.57d).

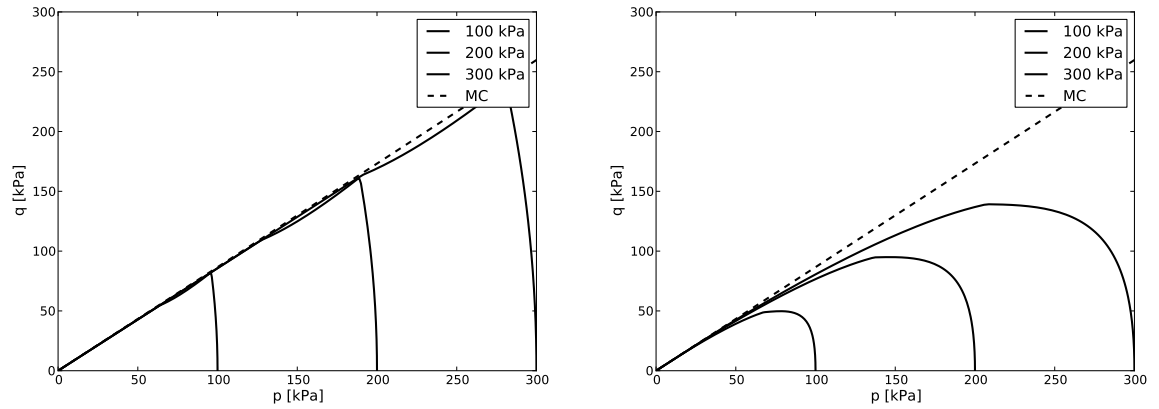
6.6.3 Cyclic undrained triaxial test

Files:

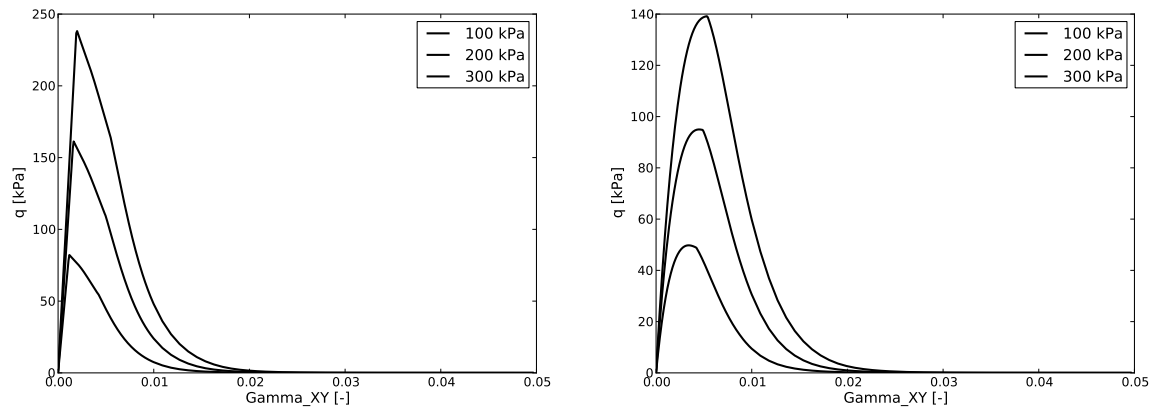
triax-cyclic-undr-stress-ctrl-30kPa.inp,
triax-cyclic-undr-stress-ctrl-40kPa.inp,
triax-cyclic-undr-stress-ctrl-50kPa.inp

In this example we will simulate an axisymmetric cyclic undrained triaxial test (mode: Deformation+Flow) using *Driven Load (undrained)* driver., for three values of the deviatoric stress amplitude 30 kPa, 40 kPa and 50 kPa. This test is stress controlled hence the displacement boundary conditions are as follows $u_x^C = 0$, $u_y^C = u_y^D = 0$, $u_x^A = u_x^B$ (see Fig.(6.54)). Sample is consolidated up to 100 kPa and then subject to cyclic vertical loading driven by the load time function defined using the expression $q \sin(6.283185307179586 * t)$, in time range 0..100s with step 0.25s (q is the applied stress amplitude). The meaningful material data used in this simulation is as follows: $E_{ur}^{ref} = 100000$ kPa, $\nu_{ur} = 0.25$, $\sigma_{ref} = 100$ kPa, $\sigma_L = 5$ kPa, $m = 0.5$, small strain option is inactive, $e_o = 0.5$, $\phi = 30^\circ$, $c = 0$ kPa, shear mechanism is inactive, Sawicki's densification law is assumed with $C_1 = 8.7 * 10^{-3}$, $C_2 = 2 * 10^5$, an extended strain mapping is used. The cyclic loading is run until failure state is achieved. Constant time step $\Delta t = 0.01$ s is used (25 increments per single 1/4 cycle). In this case the undrained behavior is modeled by means of the *Driven Load (undrained)* driver. In this case in group *Flow* the gravity term in Darcy law was canceled (to avoid pore pressure build up due to fluid dead weight) and water specific weight is set to very small value (10^{-12}) to cancel an additional body forces resulting from the water content.

The effective stress paths for three values of the applied vertical stress amplitude are shown in Fig.(6.58a, 6.58b, 6.58c).

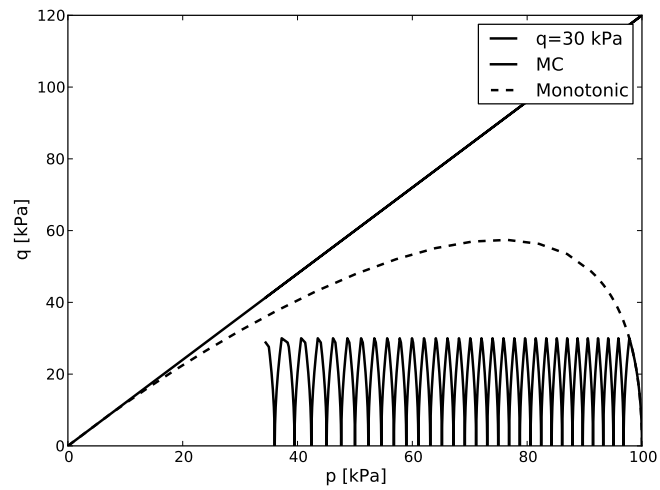


(a) Effective stress paths for model with inactive shear mechanism (b) Effective stress paths for model with active shear mechanism

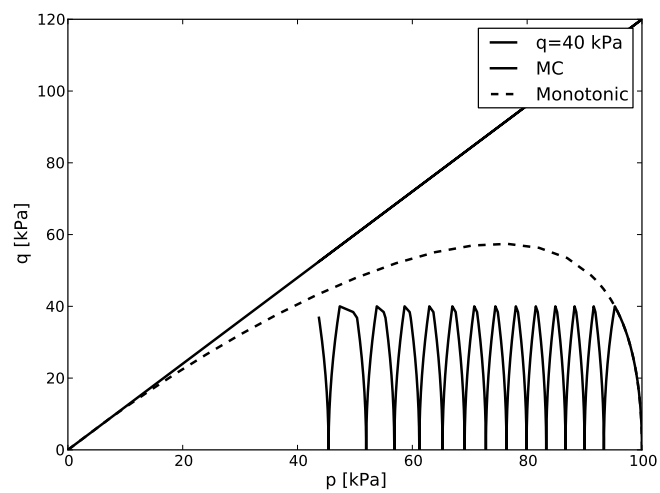


(c) $q - \gamma_{xy}$ curves for model with inactive shear mechanism (d) $q - \gamma_{xy}$ curves for model with active shear mechanism

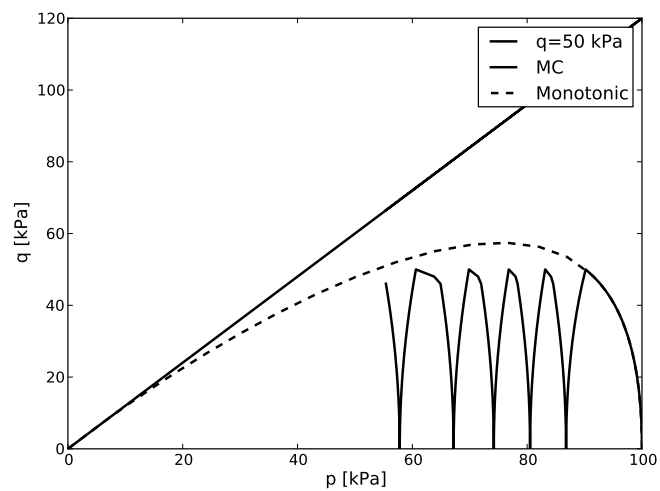
Figure 6.57: Static liquefaction problem



(a) $q = 30$ kPa



(b) $q = 40$ kPa



(c) $q = 50$ kPa

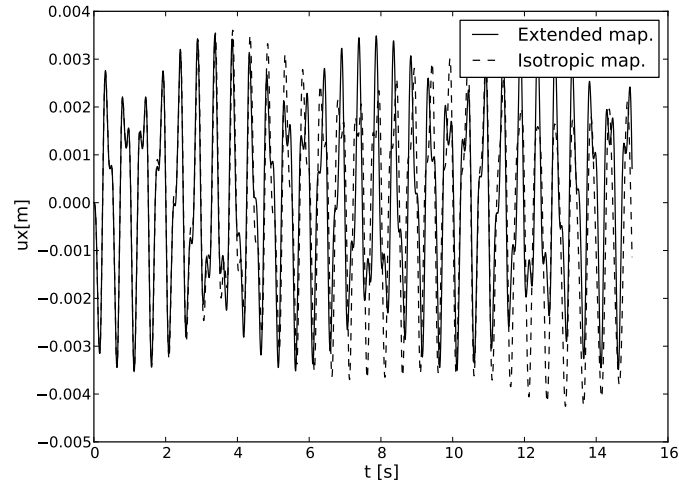
Figure 6.58: Effective stress paths for cyclic undrained triaxial test

6.6.4 Dynamic shear layer problem (dry medium)

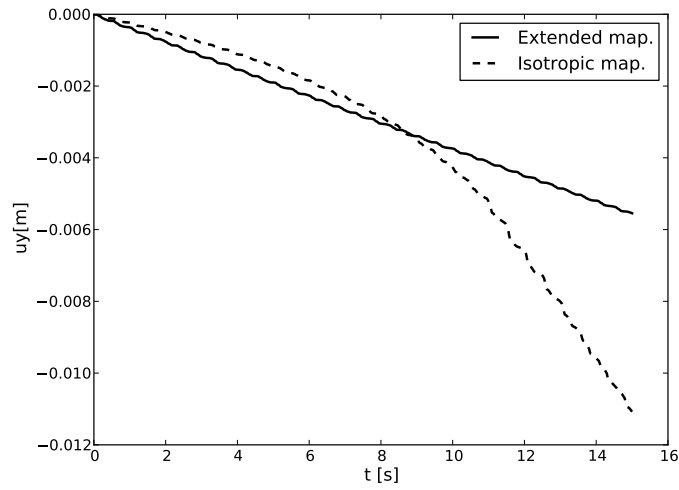
Files: `dns-shear-layer-dry-ext.inp`, `dns-shear-layer-dry-iso.inp`

This benchmark is taken from paper by Sawicki [10]. It shows the effect of settlements of 15m deep dry loose sand layer during shaking applied through the *Seismic input* option (shaking table approach) in form of assumed accelerogram $a(t) = 0.1 g \sin(4 * \pi t)$. Duration of the shaking is taken as 15s with the time step $\Delta t = 0.01s$. To model shear layer mesh consists of a single column of Q4 elements (element size is taken as 1m) with periodic BC that ties both vertical and horizontal translational degrees of freedom on both vertical walls of the domain (except the bottom edge where standard fixities are applied).

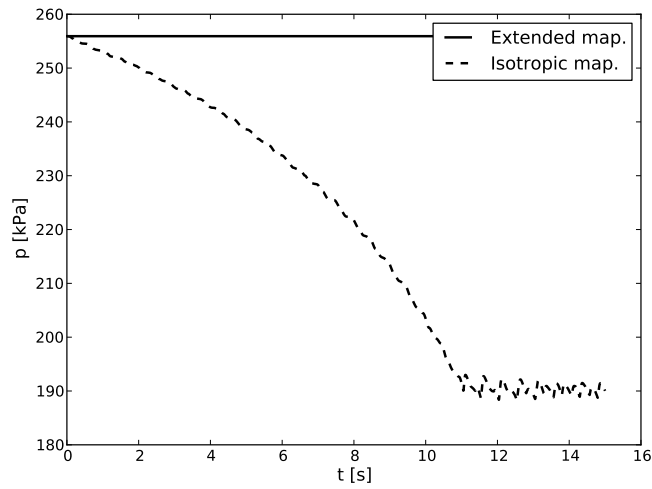
The following data is used in this benchmark: $H = 15$ m, $\rho = 1800$ kg/m³, $K_o^{insitu} = 1$, $n = 0.4$, $C_1 = 8.7 * 10^{-3}$, $C_2 = 2 * 10^5$, $\phi = 30^\circ$, $c = 0$ kPa, $\nu = 0.2$, $m = 0.5$, $\sigma_{ref} = 100$ kPa, $E_{ur}^{ref} = 216053$ kPa shear mechanism is inactive, small strain mode is inactive, accumulated strain mapping is assumed in the extended form. This test is run for two strain mapping modes to show spurious effects that can be generated when isotropic strain mapping is used. The $u_x(t)$ time histories of the point on the ground surface are shown in Fig.6.59a, the settlements of the surface are shown in Fig.6.59b while evolution of the mean stress at the bottom of the layer (last element) are presented in Fig.6.59c. The last plot shows strong variation of the mean stress during shaking that generates larger shear strain amplitudes and in consequence stronger densification. This process becomes dominant once the reduction of the horizontal normal stress activates the MC criterion that prevents further reduction of the mean stress. In the elastic case, as in the original Sawicki's model, at the end of shaking we could observe very high tensions in the horizontal direction. As we can see the proposed anisotropic mapping eliminates this serious drawback. Sawicki reports 6mm of settlement after 20 cycles (at $t = 10s$) while here we get about 4 mm. This difference is due to simplified method of calculation of the settlement used by Sawicki.



(a) Time history $u_x(t)$ on ground surface



(b) Time history $u_y(t)$ on ground surface



(c) Time history of $p(t)$ at the bottom of soil layer

Figure 6.59: Cyclic undrained test

6.6.5 Layer subject to San Fernando earthquake (dry medium)

Files: dns-ss-lay-15m-SanFernando-NW-drained-HSs.inp, dns-ss-lay-15m-SanFernando-NW-drained-HS-Brick.inp

In this example a 15m deep loose sand layer is subject to the San Fernando earthquake 1971. The acceleration time history is taken from the US data bank for Castaic Station NW. The aim of this test is to show the evolution of settlements of the layer during shaking applied through the *Seismic input* option (shaking table approach). Duration of the shaking is 30s, the applied time step is $\Delta t = 0.005s$. The following data is used: $H = 15$ m, $\rho = 1620$ kg/m³, $K_o^{insitu} = 1$, $n = 0.4$ $C_1 = 8.7 * 10^{-3}$, $C_2 = 2 * 10^5$, $\phi = 30^\circ$, $c = 0$ kPa, $\nu = 0.2$, $m = 0.5$, $\sigma_{ref} = 100$ kPa, $E_o^{ref} = 240000$ kPa, $E_{ur}^{ref} = 80000$, $\gamma_{0.7} = 0.0002$. We assume that shear mechanism is inactive and accumulated strain mapping is used in the extended form. The computed evolution of horizontal displacements and settlements for both small strain approaches is shown in figures 6.60 and 6.61 with the final value of order 3.8cm. The HSs small strain approach yields much larger horizontal residual deformations than the HS-Brick one.

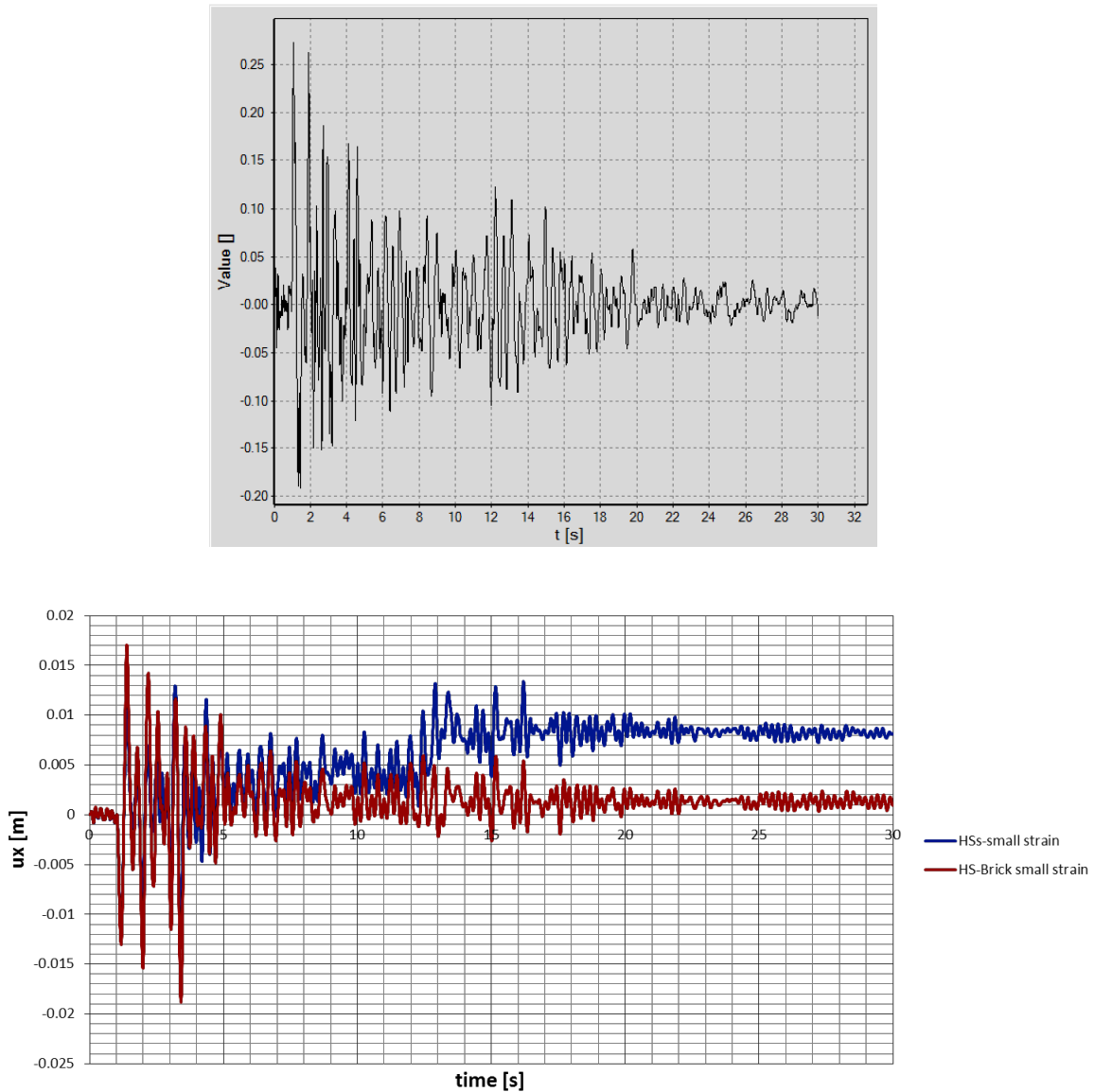


Figure 6.60: Horizontal deformation time history at the top of the layer

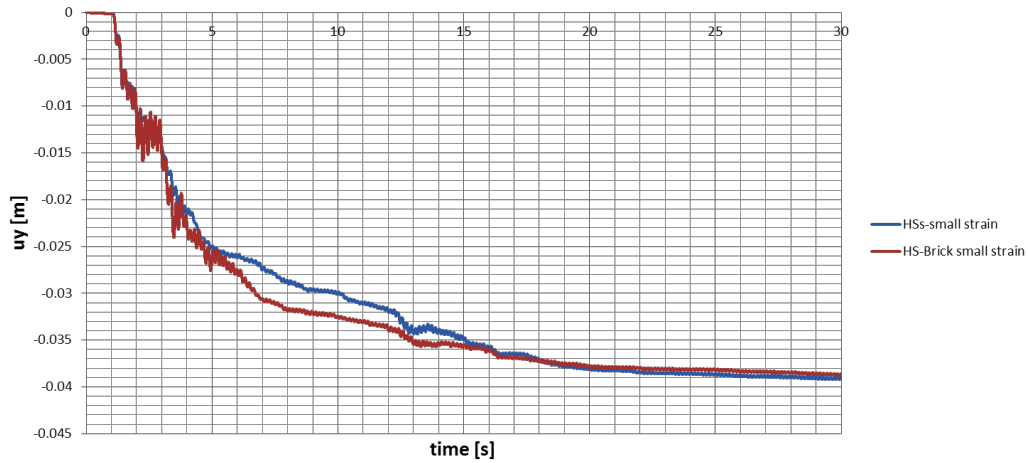
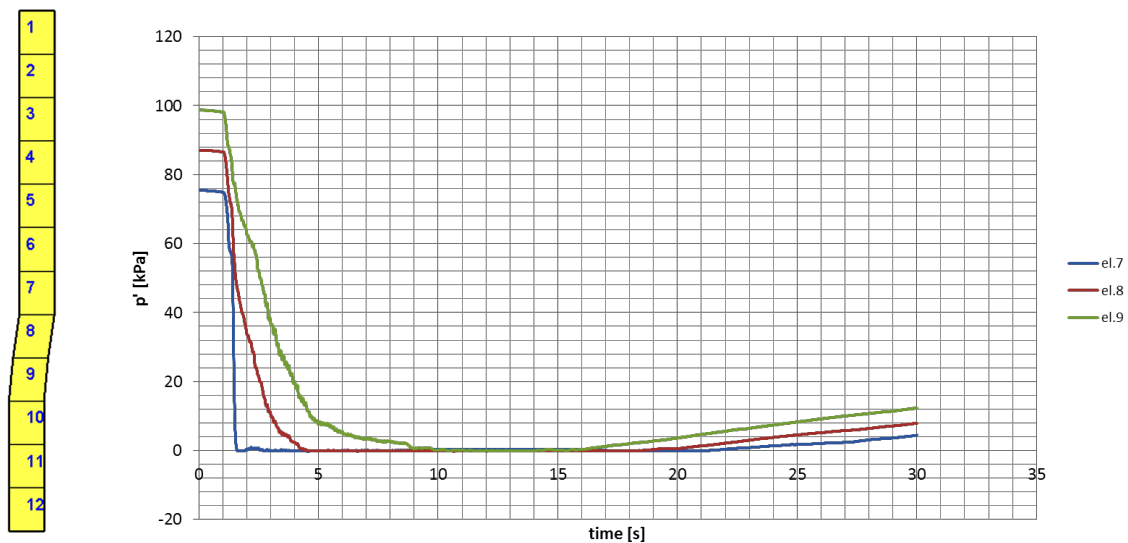


Figure 6.61: Settlements time history

6.6.6 Liquefaction of sand layer subject to San Fernando earthquake (two-phase consolidation)

Files: dns-ss-lay-15m-SanFernando-NW-2phase-HSs.inp, dns-ss-lay-15m-SanFernando-NW-2phase-HS-Brick.inp

The same example presented in the previous section for dry state is analyzed here in the two-phase format assuming full saturation of sand layer. Same geometry and material data is used ($k = 10^{-4}$ m/s). The pressure BC $p = 0$ at the top boundary is assumed. The resulting evolution of the mean effective stress in 4 selected elements is plot in the figure shown below. The interesting observation is such that the liquefaction is initiated in element 9 (about $2/3H$ from the top). Then the liquefaction front starts moving upwards. Evolution of mean effective stress for the two small strain approaches is shown in figures 6.62, 6.63.

Figure 6.62: Evolution of effective mean stress $p'(t)$ in time (HSs-small strain approach)

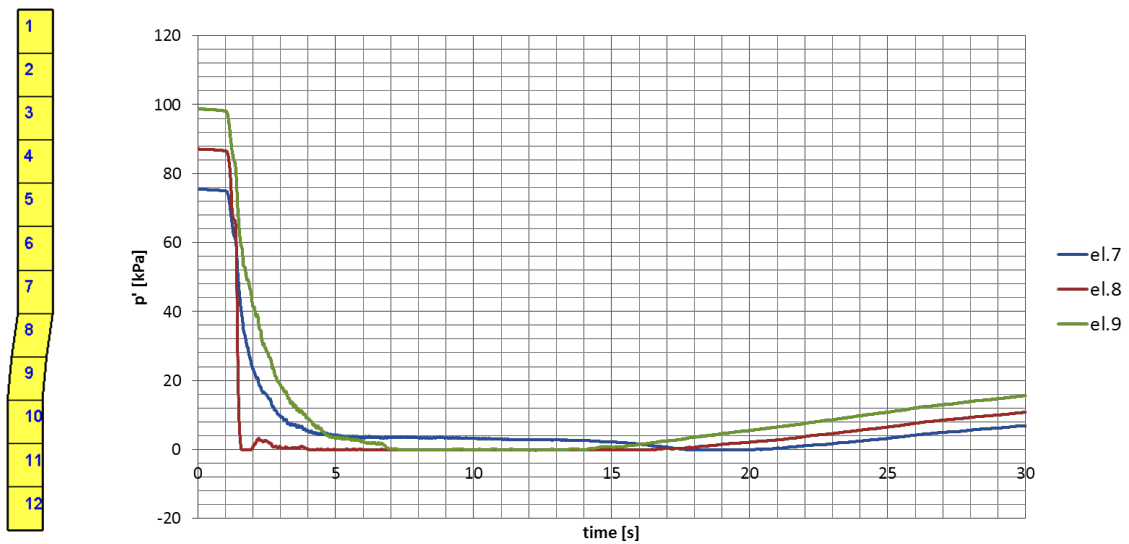


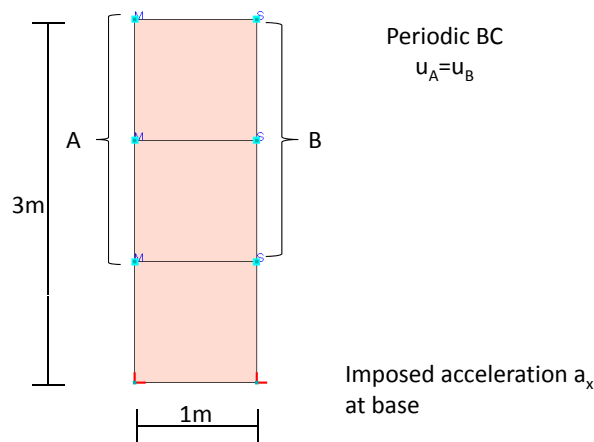
Figure 6.63: Evolution of effective mean stress $p'(t)$ in time (HS-Brick strain approach)

6.7 Baseline correction and Butterworth filtering

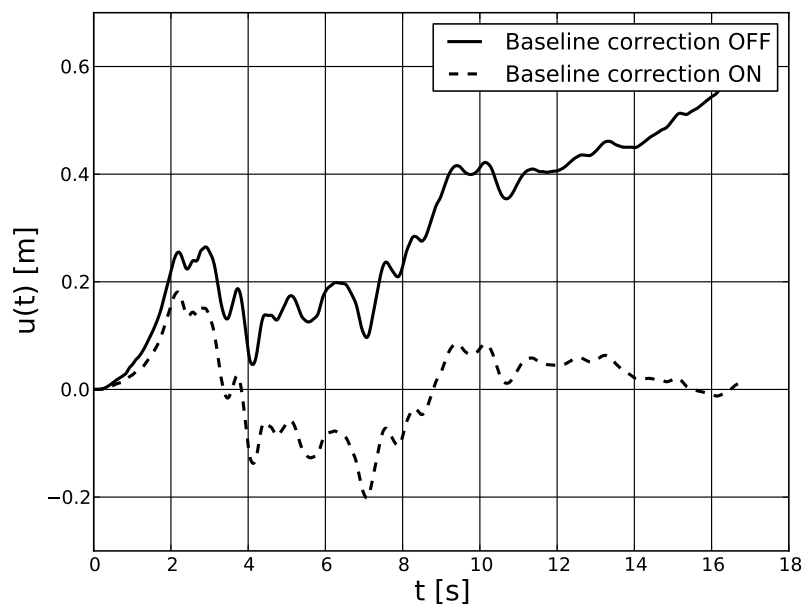
6.7.1 Example of baseline correction and Butterworth filtering

Files: DYN-TR-Layer-3m-NO-BASE-LINE.inp, DYN-TR-Layer-3m-WITH-BASE-LINE.inp

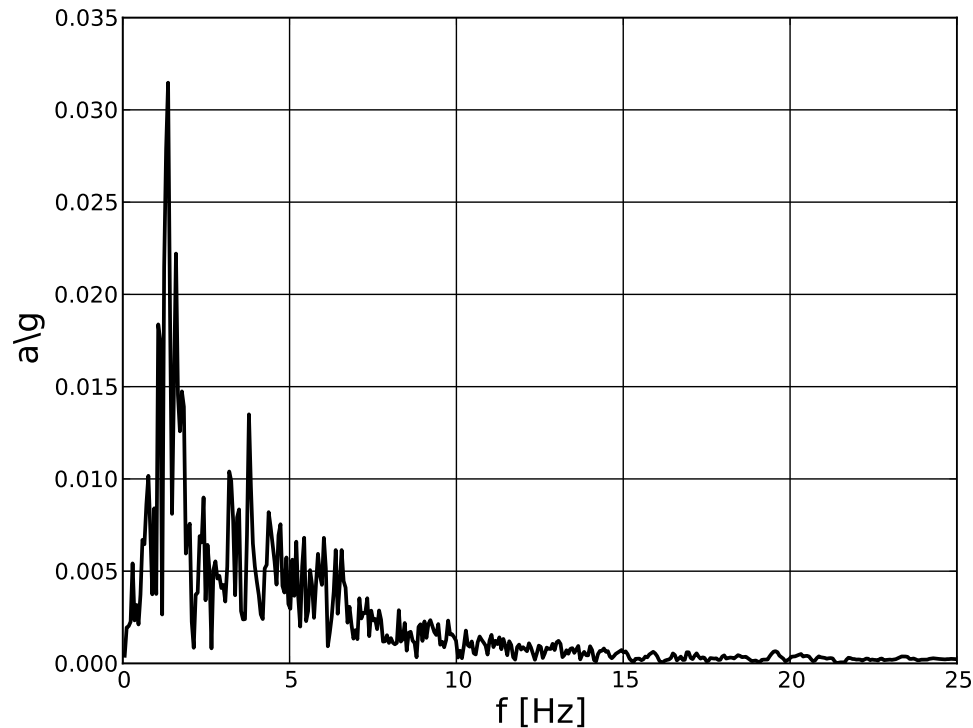
In this example a 3m deep soil layer is subject to the Loma Prieta earthquake (LomaPrieta-18-10-1989-Station-Corralitos). Material data for this example is as follows: $E = 512000$ kPa, $\nu = 0.22625$, $\gamma = 20$ kN/m³. HHT integration scheme is used with zero material damping and time step $\Delta t = 0.01$ s. Discretization and boundary conditions are shown in the figure below. Note that the earthquake is applied through the imposed accelerations at two nodal points located at the base. At other nodal points periodic boundary condition is defined to model shear layer problem.



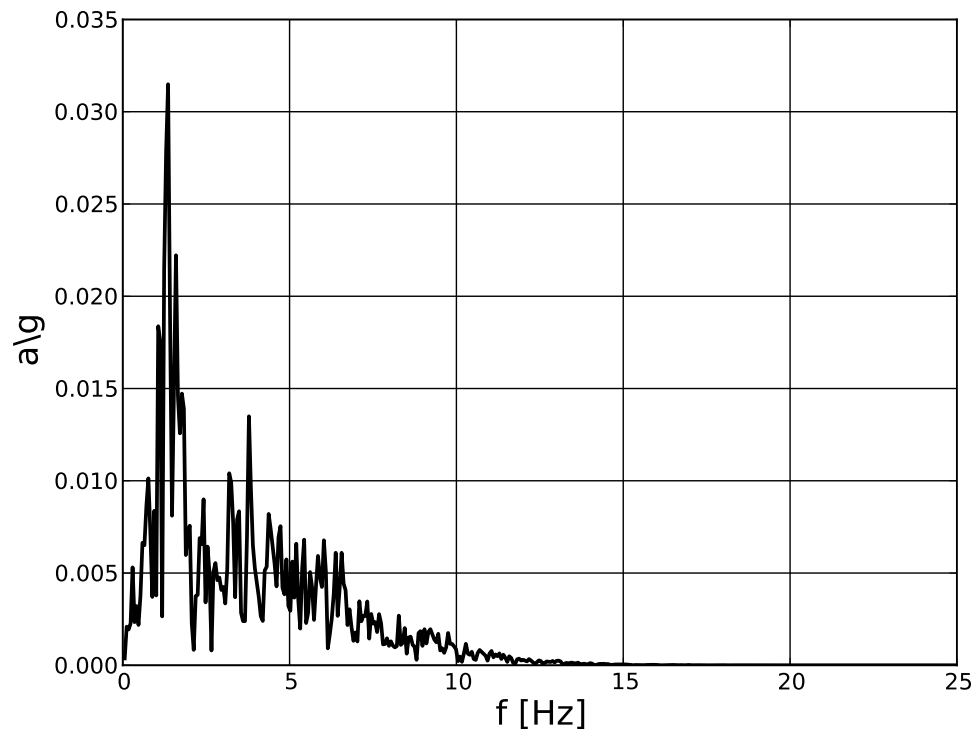
Computed horizontal displacement time history at top of the layer is shown in the next figure. One may easily notice that baseline correction procedure applied to the signal removes characteristic drift observed in $u(t)$.



Fourier amplitudes for unfiltered and filtered (using 10 Hz low pass Butterworth filter) Loma Prieta record are shown in the next two figures.



Fourier amplitudes for unfiltered signal



Fourier amplitudes for filtered signal

6.8 Linear deconvolution

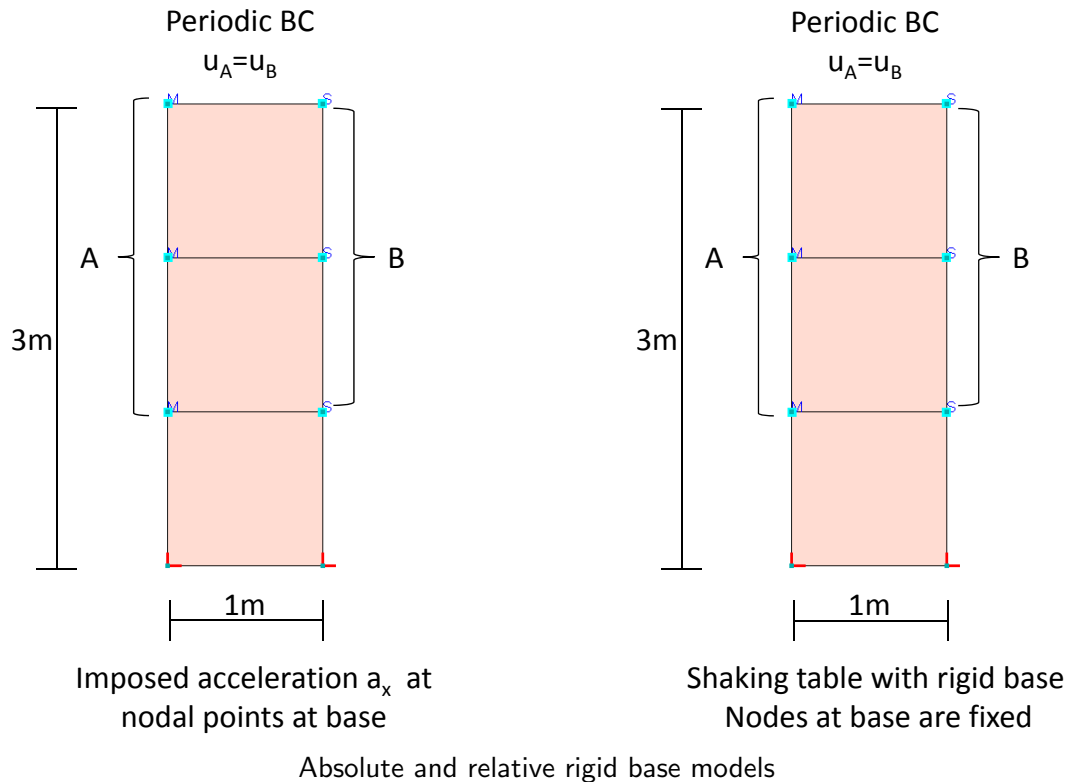
6.8.1 Convolution analysis for undamped soil layer on rigid base

Files:

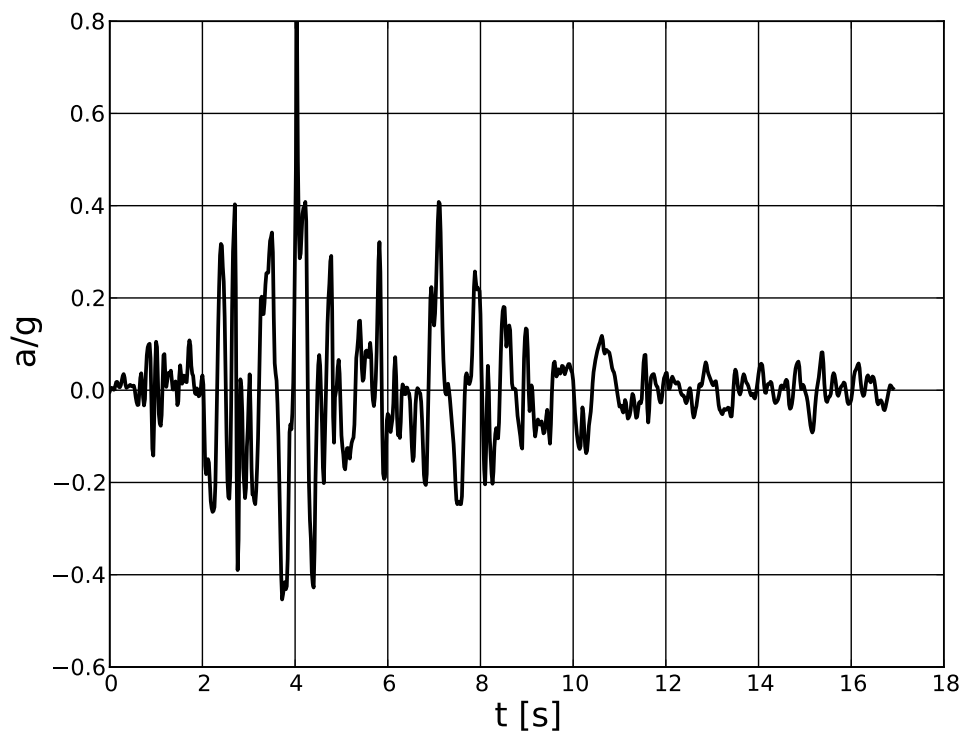
DYN-TR-Layer-3m-form-abs-no-damp-3ele.inp,

DYN-TR-Layer-3m-form-rel-no-damp-3ele.inp

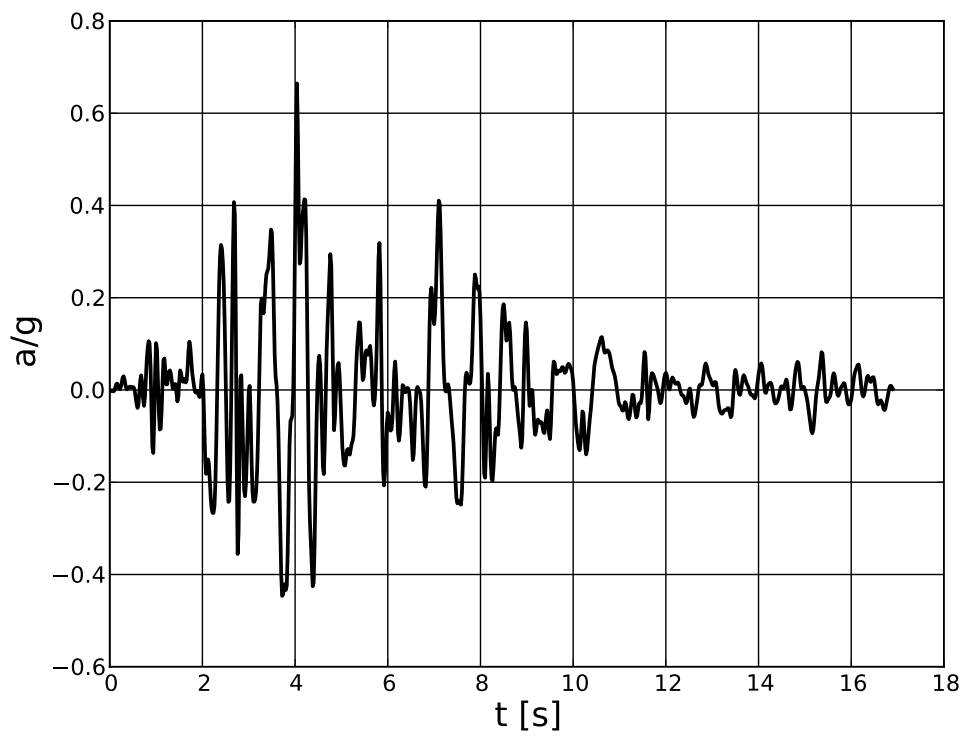
The convolution analysis (transfer of the signal from base to the surface) of Loma Prieta seismic acceleration record (LomaPrieta-18-10-1989-Station-Corralitos) for a 3m deep soil layer resting on a rigid bedrock is the aim of this benchmark. The original signal is filtered with 10 Hz low pass Butterworth filter and baseline corrected. The two ways of application of an earthquake to the finite element model are analyzed. In the first model imposed accelerations are applied at two nodes at the base (absolute format set at the level of boundary conditions) while in the second one acceleration is applied as global to the whole structure (while bottom nodes remain fixed)(relative format, set using *Seismic input* option). It should be mentioned that results of both models must properly be analyzed because first model yields total accelerations at nodes while the second one relative with respect to the rigid base. Comparizon that is made here refers to global accelerations. Material data for this example is as follows: $E = 525000$ kPa, $\nu = 0.25$, $\gamma = 20$ kN/m³. HHT integration scheme is used with zero material damping and time step $\Delta t = 0.01$ s. Discretization and boundary conditions are shown in the figure below. At all nodes, except base ones, periodic boundary condition is used to represent shear layer deformation mode.



Original signal and filtered, and baseline corrected, are shown in the next two figures.

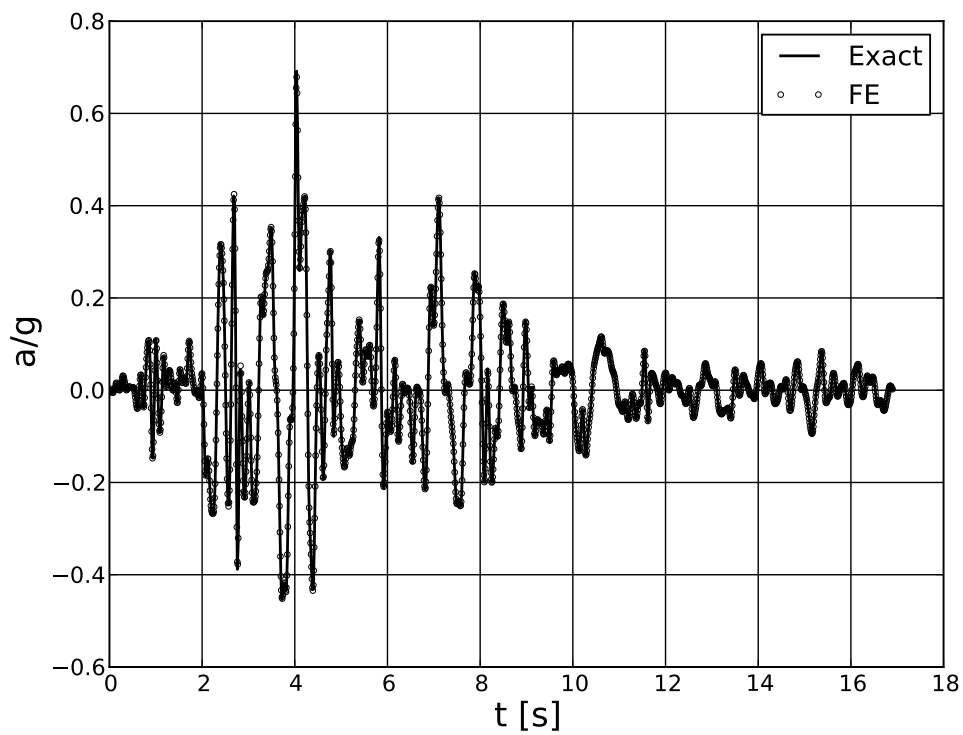


Original signal (LomaPrieta-18-10-1989-Station-Corralitos)

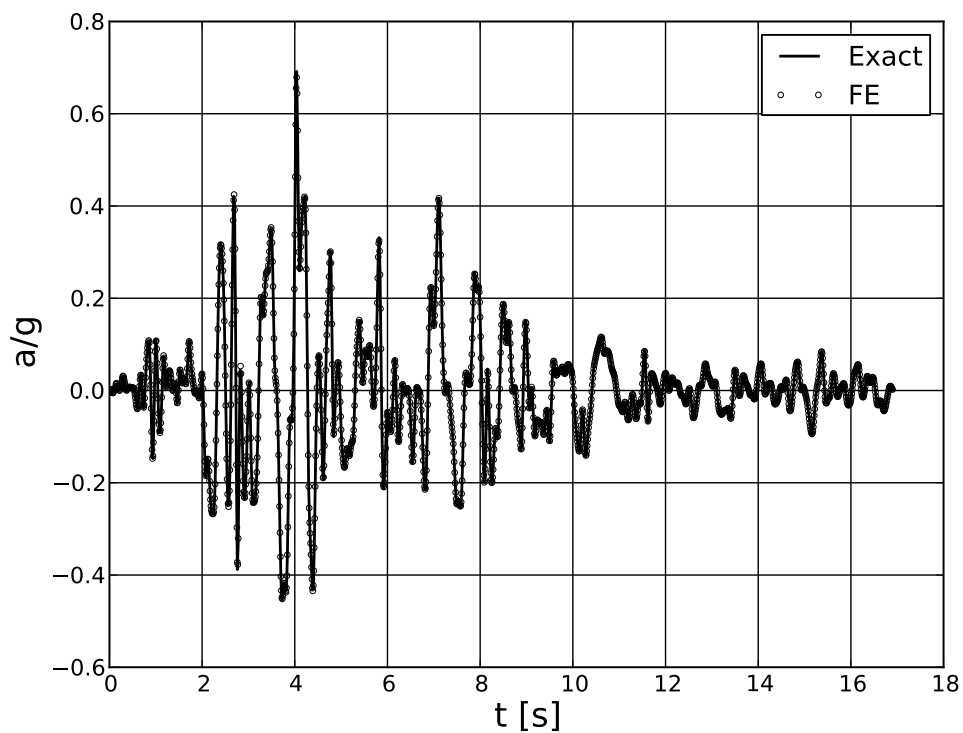


Signal after filtering and baseline correction

Comparizon of analytical and numerical solutions shows an excellent agreement.



Analytical and numerical solutions for acceleration $a_x(t)$ at free surface (absolute format)



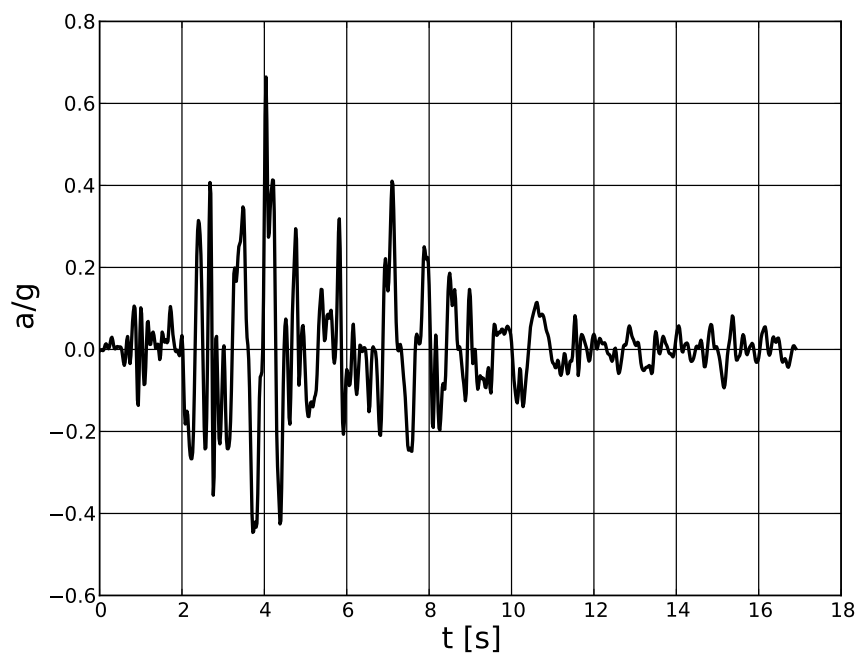
Analytical and numerical solutions for acceleration $a_x(t)$ at free surface (relative format)

6.8.2 Deconvolution analysis for undamped soil layer on rigid base

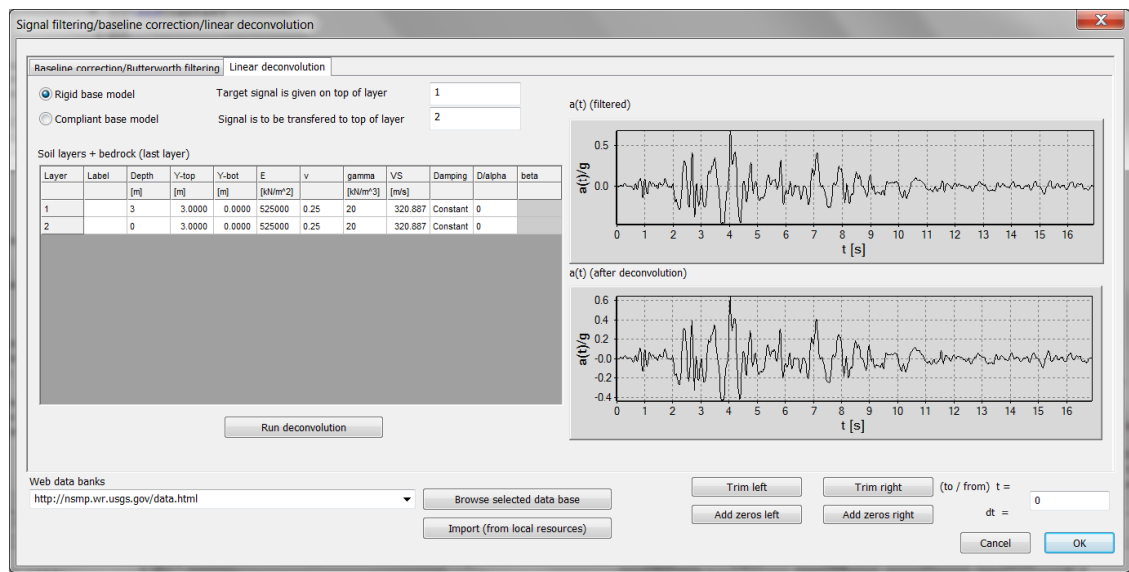
Files:

DYN-TR-deconvolution-Layer-3m-form-abs-no-damp-3ele.inp,
DYN-TR-deconvolution-Layer-3m-form-rel-no-damp-3ele.inp

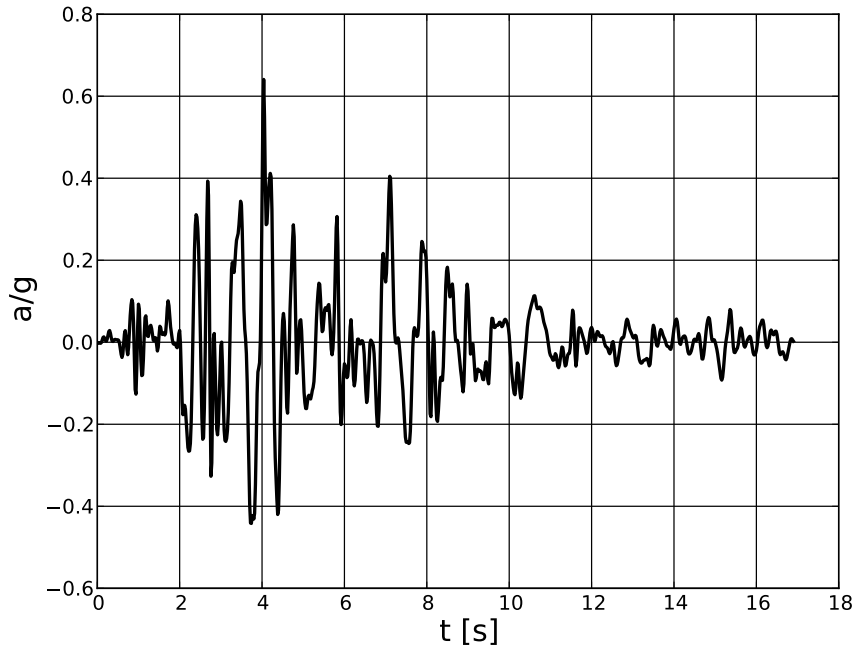
To verify procedure of deconvolution the original signal (LomaPrieta-18-10-1989-Station-Corralitos) is filtered with 10 Hz low pass Butterworth filter and baseline corrected first, then deconvolution procedure is run from Acceleration time history toolbox. Data set for deconvolution procedure is shown in the figure below (data in the second row corresponds to the bedrock, although for rigid base model it is not meaningful).



Signal after filtering and baseline correction (assumed at ground surface)

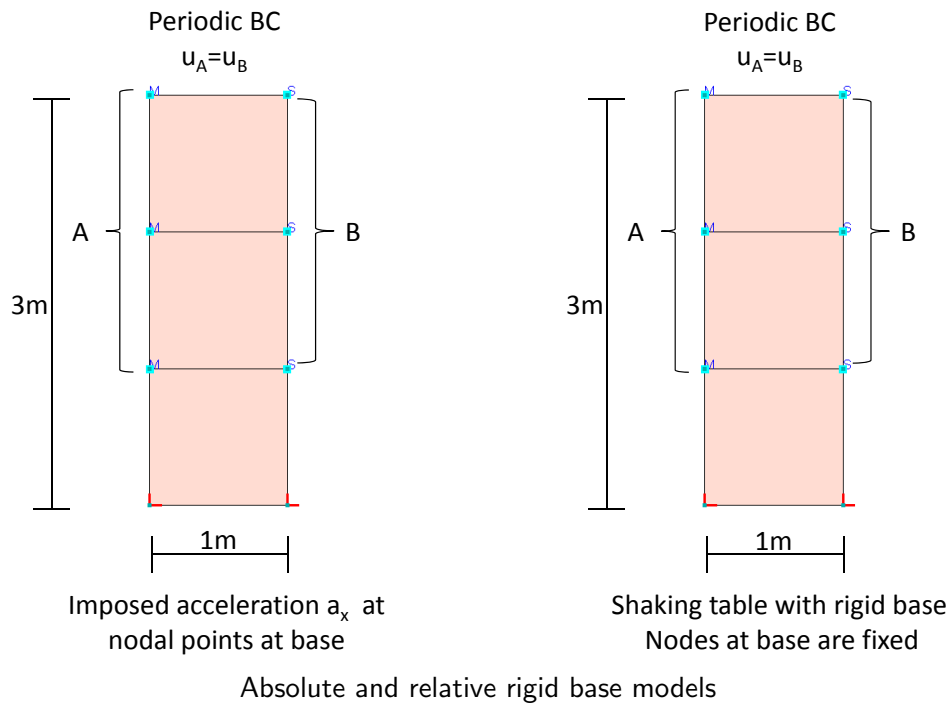


Data setup for deconvolution of Loma Prieta signal from surface to the base of FE model

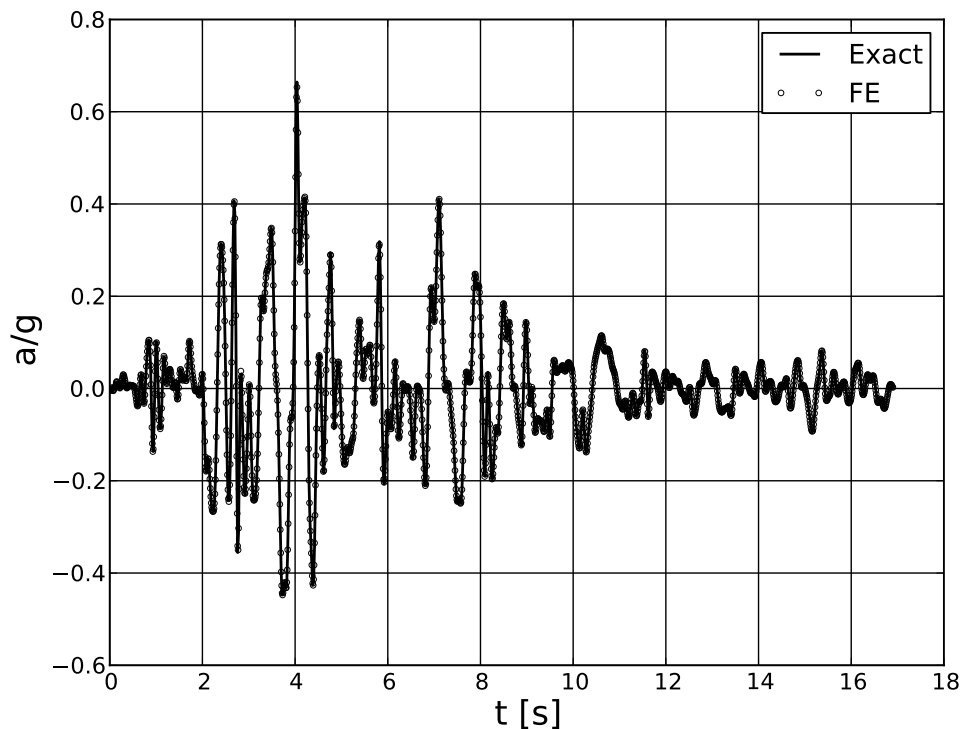


Signal transfered to the base of the model (after deconvolution procedure)

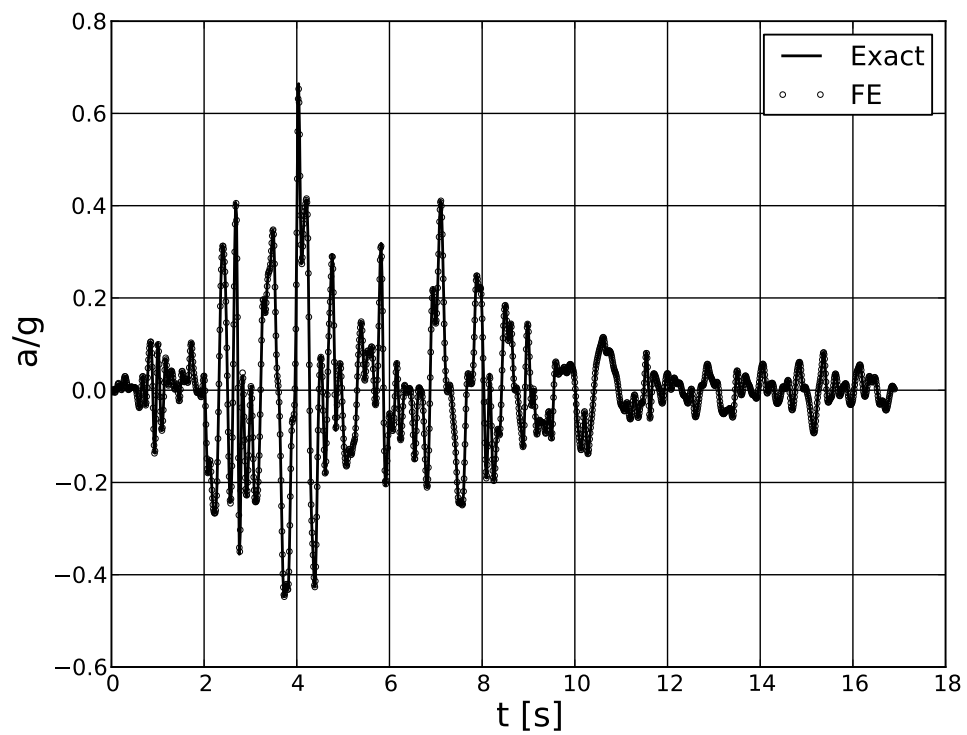
By applying the deconvoluted signal at the base we expect that the computed acceleration (at surface) will fully be compatible with the original signal. In this benchmark a 3m deep soil layer resting on a rigid bedrock is analyzed. The two ways of application of an earthquake to the finite element model are analyzed. In the first model imposed accelerations are applied at two nodes at the base (absolute format set at the level of boundary conditions) while in the second one acceleration is applied as global to the whole structure (while bottom nodes remain fixed)(relative format, set using *Seismic input* option). It should be mentioned that results of both models must properly be analyzed because first model yields total accelerations at nodes while the second one relative with respect to the rigid base. Comparizon that is made here refers to global accelerations. Material data for this example is as follows: $E = 525000 \text{ kPa}$, $\nu = 0.25$, $\gamma = 20 \text{ kN/m}^3$. HHT integration scheme is used with zero material damping and time step $\Delta t = 0.01 \text{ s}$. Discretization and boundary conditions are shown in the figure below. At all nodes, except base ones, periodic boundary condition is used to represent shear layer deformation mode.



Comparizon of analytical and numerical solutions shows an excellent agreement.



Analytical and numerical solutions for acceleration $a_x(t)$ at free surface (absolute format)



Analytical and numerical solutions for acceleration $a_x(t)$ at free surface (relative format)

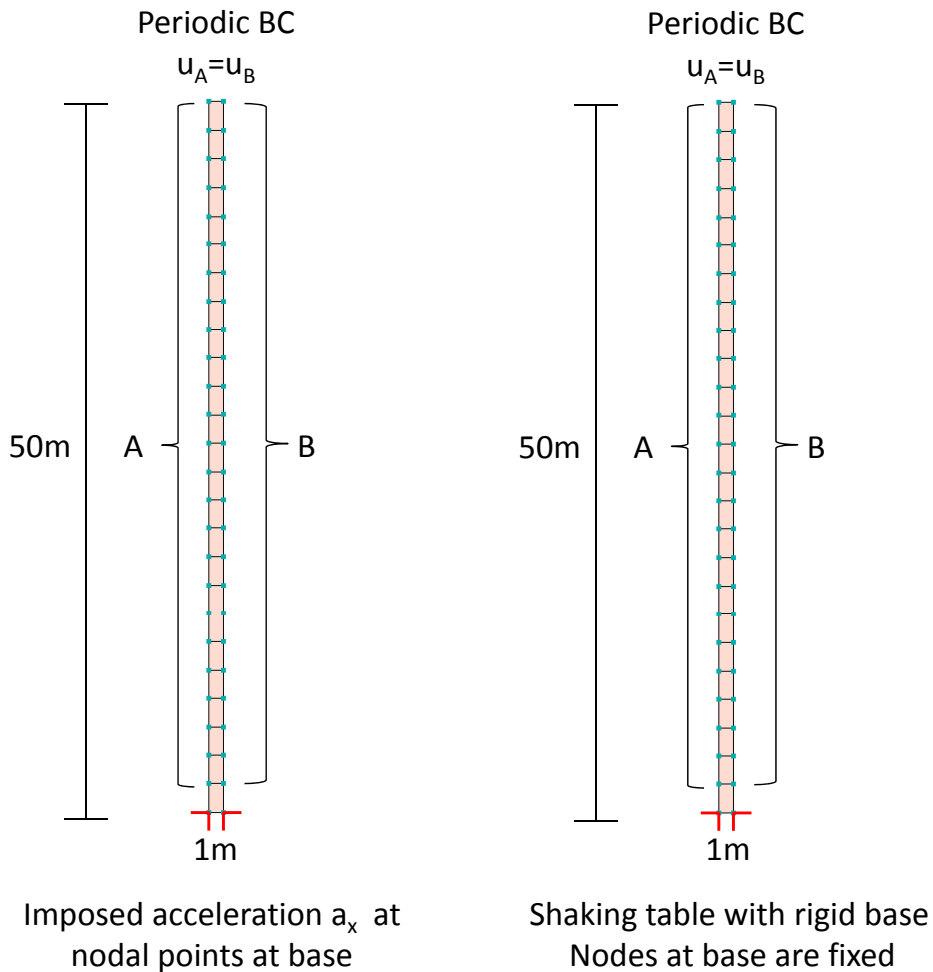
6.8.3 Convolution analysis for damped soil layer on rigid base

Files:

DYN-TR-Layer-50m-form-abs-damp.inp,

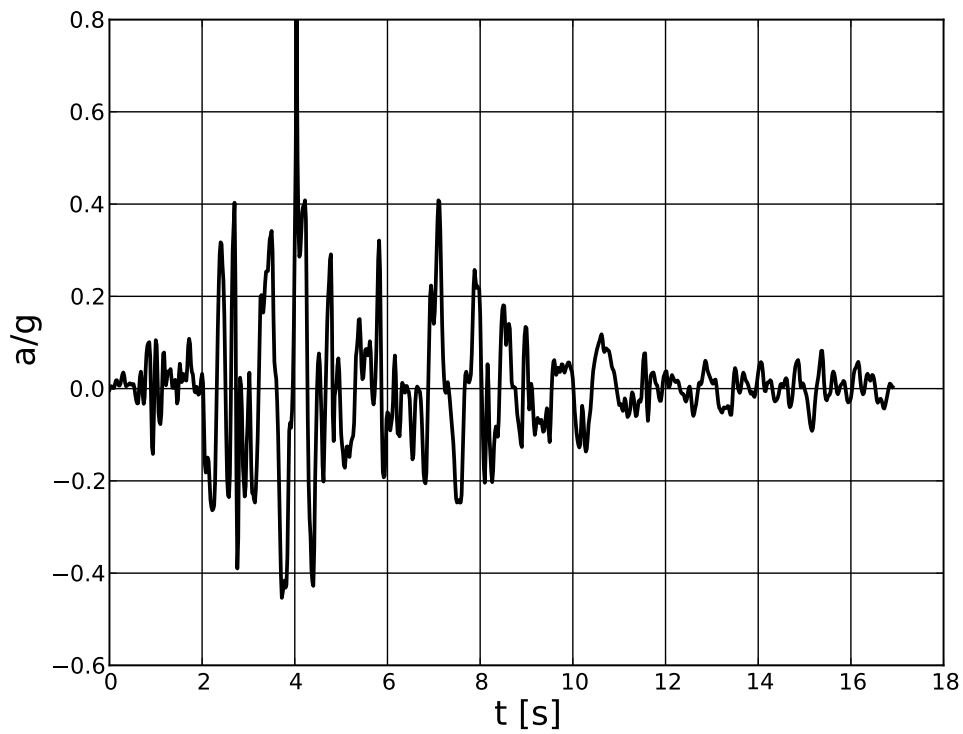
DYN-TR-Layer-50m-form-rel-damp.inp

The convolution analysis (transfer of the signal from base to the surface) of Loma Prieta seismic acceleration record (LomaPrieta-18-10-1989-Station-Corralitos) for a 50m deep soil layer resting on a rigid bedrock is the aim of this benchmark. The original signal is filtered with 10 Hz low pass Butterworth filter and baseline corrected. The two ways of application of an earthquake to the finite element model are analyzed. In the first model imposed accelerations are applied at two nodes at the base (absolute format set at the level of boundary conditions) while in the second one acceleration is applied as global to the whole structure (while bottom nodes remain fixed)(relative format, set using *Seismic input* option). It should be mentioned that results of both models must properly be analyzed because first model yields total accelerations at nodes while the second one relative with respect to the rigid base. Comparizon that is made here refers to total accelerations. Material data for this example is as follows: $E = 1250000$ kPa, $\nu = 0.25$, $\gamma = 20$ kN/m³, Rayleigh damping parameters $\alpha_o = 1.88496$ and $\beta_o = 0.00397887$. HHT integration scheme is used with time step $\Delta t = 0.01$ s. Discretization and boundary conditions are shown in the figure below. At all nodes, except base ones, periodic boundary condition is used to represent shear layer deformation mode.

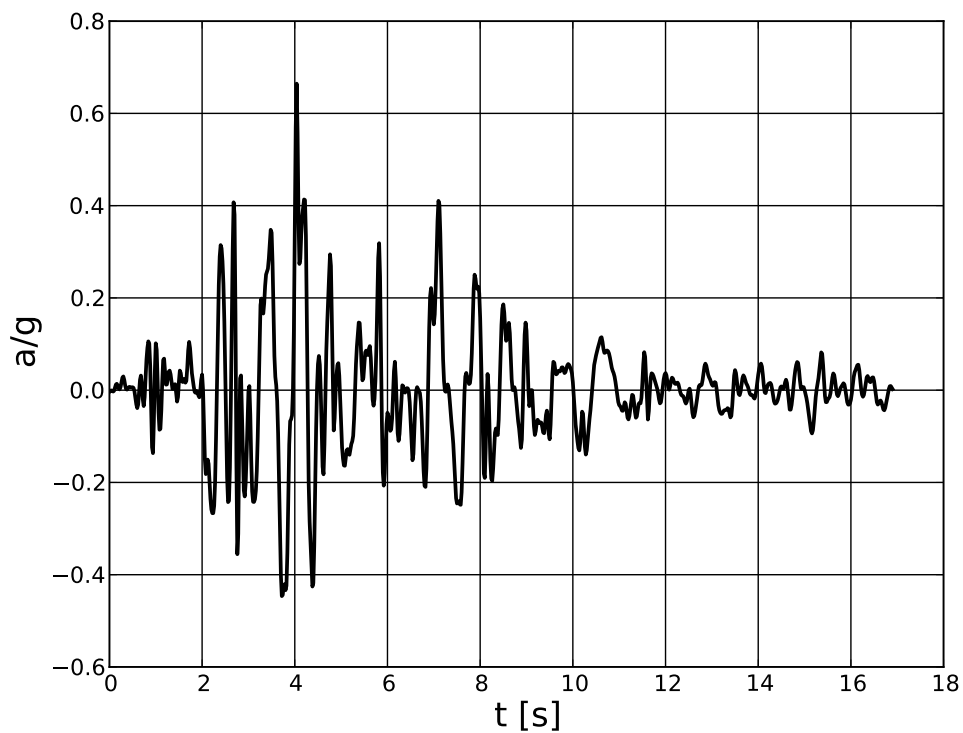


Absolute and relative rigid base models

Original signal and filtered, and baseline corrected, are shown in the next two figures.

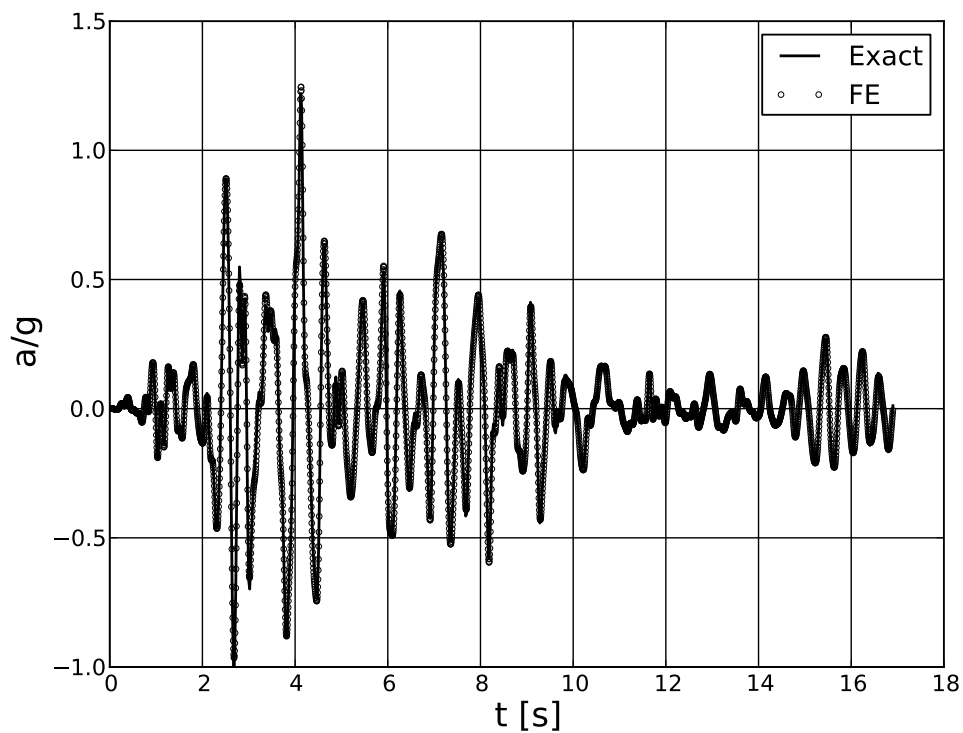


Original signal (LomaPrieta-18-10-1989-Station-Corralitos)

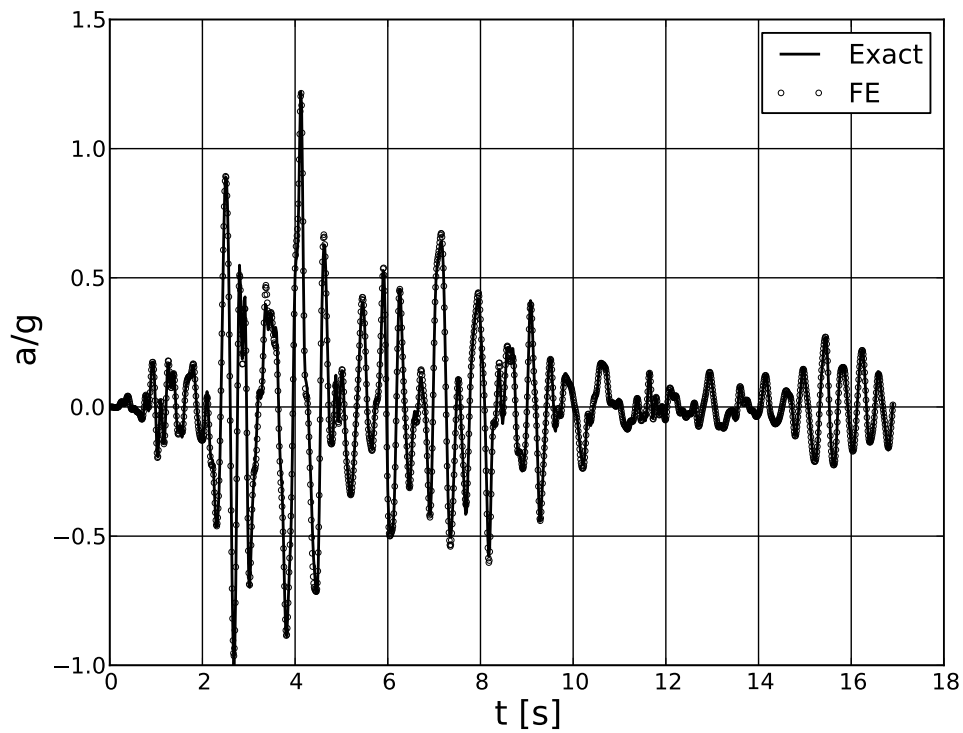


Signal after filtering and baseline correction

Comparizon of analytical and numerical solutions shows an excellent agreement.



Analytical and numerical solutions for acceleration $a_x(t)$ at free surface (absolute format)



Analytical and numerical solutions for acceleration $a_x(t)$ at free surface (relative format)

6.8.4 Deconvolution analysis for damped soil layer on rigid base

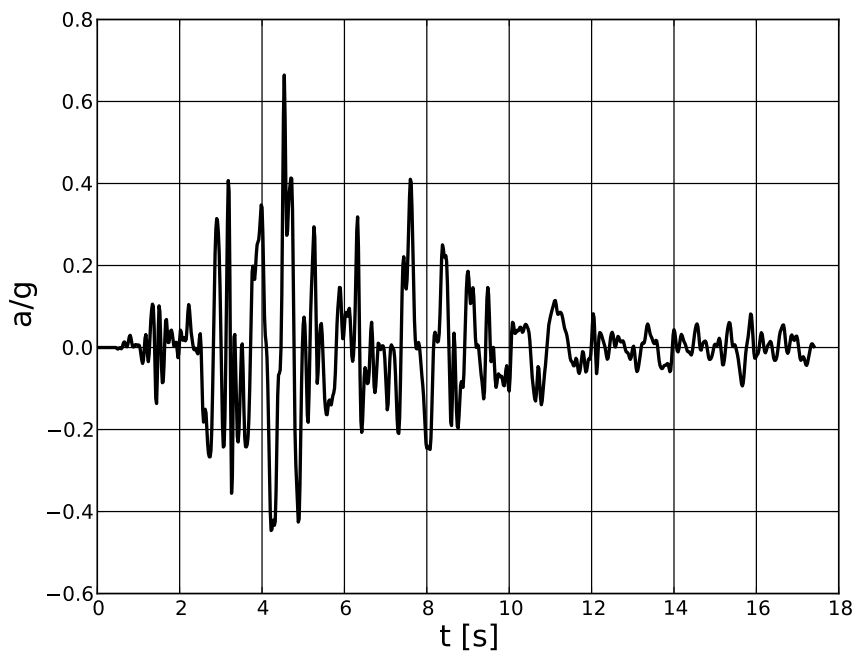
Files:

DYN-TR-DECONVOLUTION-Layer-50m-form-abs-damp.inp,

DYN-TR-DECONVOLUTION-Layer-50m-form-rel-damp.inp

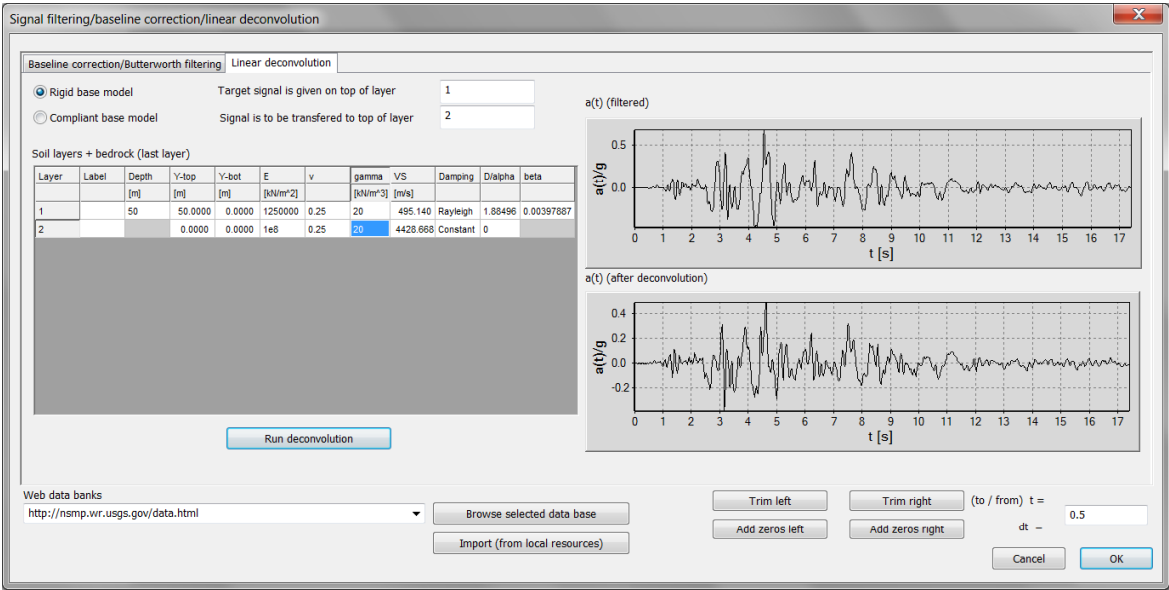
To verify procedure of deconvolution for damped system the original signal (LomaPrieta-18-10-1989-Station-Corralitos) is filtered with 10 Hz low pass Butterworth filter and baseline corrected first, then deconvolution procedure is run from Acceleration time history toolbox.

One has to mention that in the considered case acceleration record shows significant nonzero values from the very beginning. It means that such a signal cannot be deconvoluted without any loss of accuracy (so-called effect of initial transients) because shear wave velocity is bounded by a certain value. Therefore it is recommended prior running the deconvolution procedure to add a quiet zone to the acceleration record (using option **Add zeros left**). Duration of this quiet zone can easily be estimated as fraction $\frac{H}{v_s}$ (H is a subsoil depth while v_s is a shear wave velocity). In this example 0.5s was added to the record (see figure).

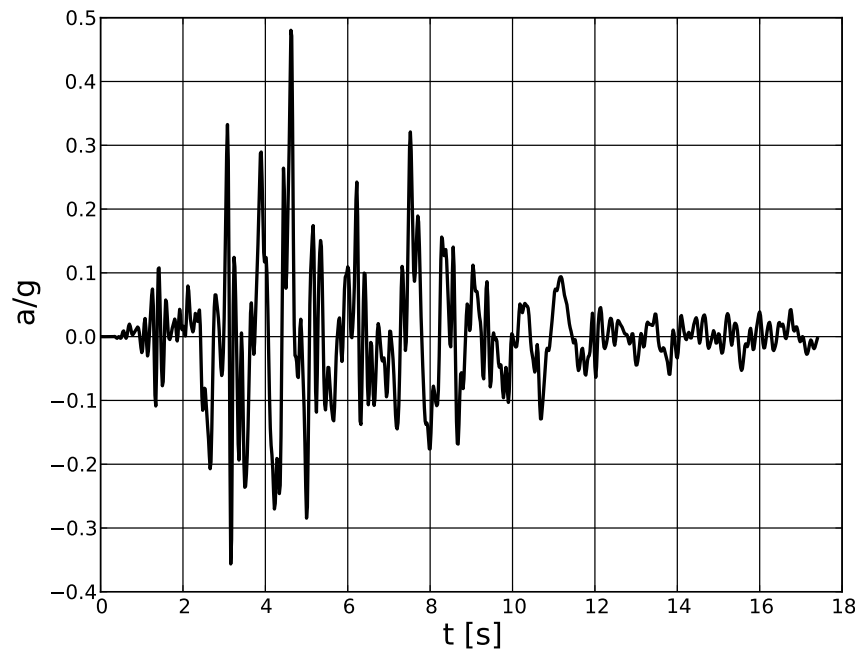


Signal after filtering and baseline correction (assumed at ground surface)

Data set for deconvolution procedure is shown in the figure below (data in the second row corresponds to the bedrock, although for rigid base model it is not meaningful).



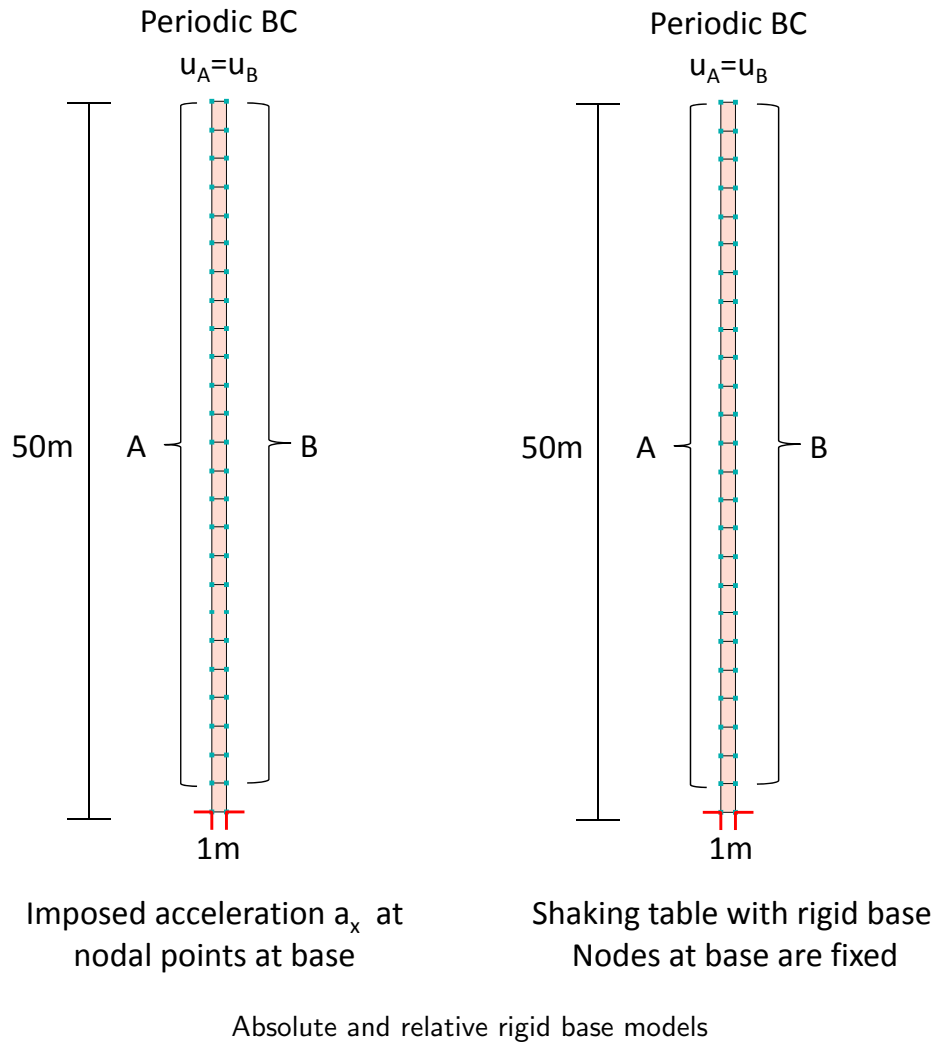
Data setup for deconvolution of Loma Prieta signal from surface to the base of FE model



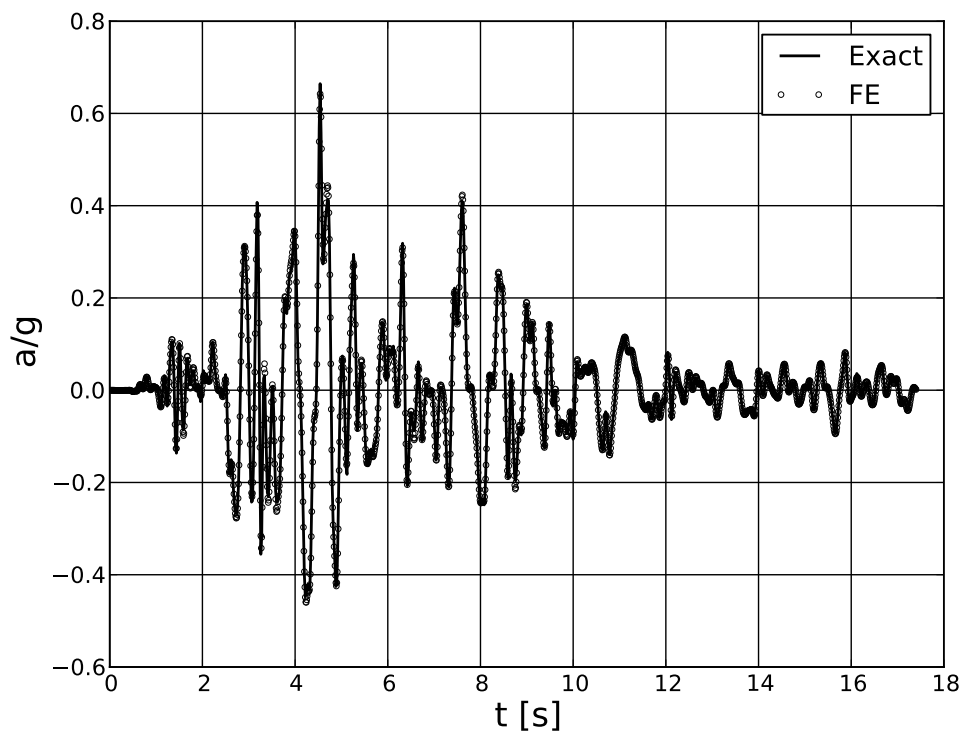
Signal transferred to the base of the model (after deconvolution procedure)

By applying the deconvoluted signal at the base we expect that the computed acceleration (at surface) will fully be compatible with the original signal. In this benchmark a 50m deep soil layer resting on a rigid bedrock is analyzed. The two ways of application of an earthquake to the finite element model are analyzed. In the first model imposed accelerations are applied at two nodes at the base (absolute format set at the level of boundary conditions) while in the second one acceleration is applied as global to the whole structure (while bottom nodes remain fixed)(relative format, set using *Seismic input* option). It should be mentioned that results of both models must properly be analyzed because first model yields total accelerations at nodes while the second one relative with respect to the rigid base. Comparizon that is made here refers to global accelerations. Material data for this example is as follows: $E = 1250000$ kPa, $\nu = 0.25$, $\gamma = 20$ kN/m³, Rayleigh damping

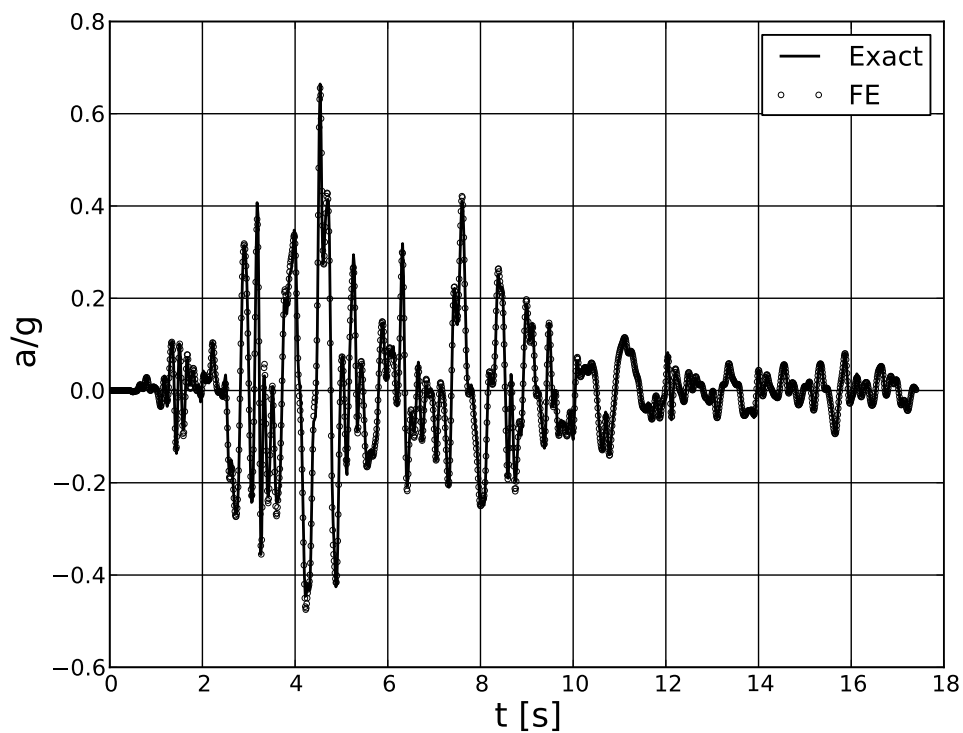
parameters $\alpha_o = 1.88496$ and $\beta_o = 0.00397887$. HHT integration scheme is used with time step $\Delta t = 0.01$ s. Discretization and boundary conditions are shown in the figure below. At all nodes, except base ones, periodic boundary condition is used to represent shear layer deformation mode.



Comparizon of analytical and numerical solutions shows an excellent agreement.



Analytical and numerical solutions for acceleration $a_x(t)$ at free surface (absolute format)



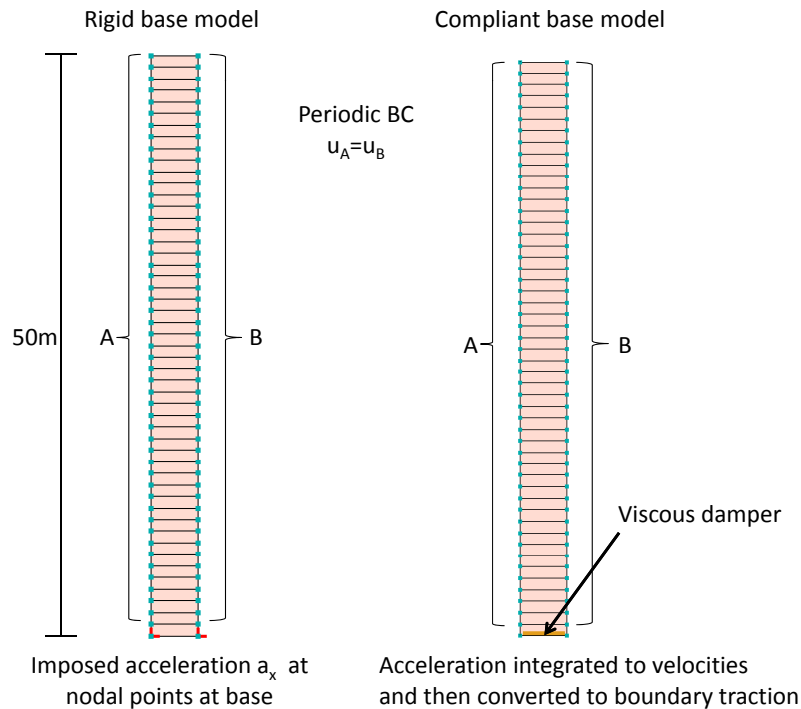
Analytical and numerical solutions for acceleration $a_x(t)$ at free surface (relative format)

6.8.5 Convolution analysis for damped soil layer on compliant base

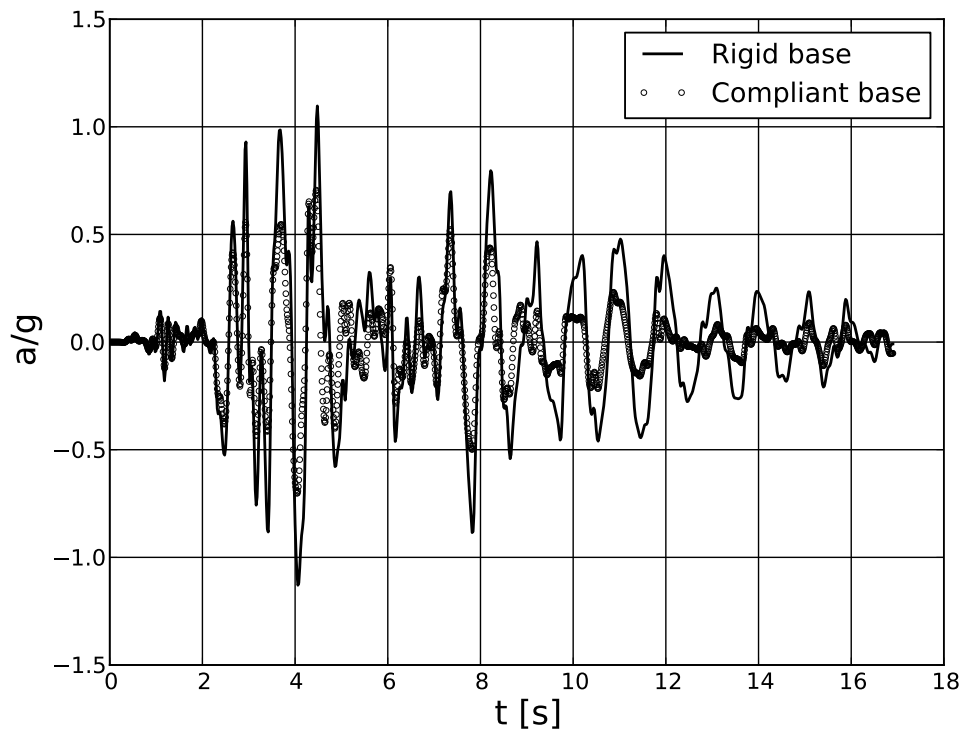
Files:

DYN-TR-Layer-50m-compliant-base-damp-E1.inp,
 DYN-TR-Layer-50m-compliant-base-damp-E2.inp,
 DYN-TR-Layer-50m-compliant-base-damp-E3.inp,
 DYN-TR-Layer-50m-rigid-base-damp.inp

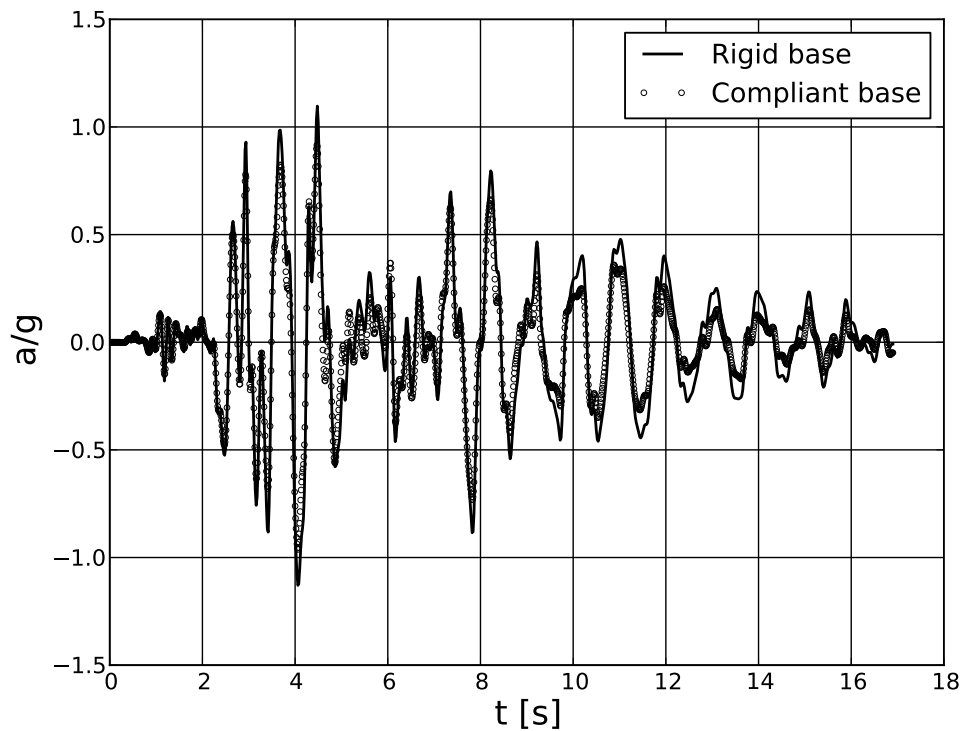
The convolution analysis (transfer of the signal from base to the surface) of Loma Prieta seismic acceleration record (LomaPrieta-18-10-1989-Station-Corralitos) for a 50m deep soil layer resting on a compliant bedrock is the aim of this benchmark. The original signal is filtered with 10 Hz low pass Butterworth filter and baseline corrected. In all these examples imposed accelerations are applied at two nodes at the base (absolute format set at the level of boundary conditions). Results comparizon that is made here refers to total accelerations. To avoid initial state computation multiplier for body forces is set to zero (at material level for subsoil in group ☐ **Unit weights**). Material data for soil layer is as follows: $E = 205000$ kPa, $\nu = 0.25$, $\gamma = 20$ kN/m³, Rayleigh damping parameters $\alpha_o = 1.88496$ and $\beta_o = 0.00397887$. HHT integration scheme is used with time step $\Delta t = 0.01$ s. Mesh and boundary conditions are shown in figure below. To check whether compliant base model converges to the rigid base one a parametric study was carried out for 3 different sets of elastic parameters for bedrock ie. $E = E1 = 2000000$ kPa, $E = E2 = 30000000$ kPa and $E = E3 = 30000000000$ kPa. In all cases bedrock Poisson's ratio $\nu = 0.25$ and $\gamma = 23$ kN/m³. Note that the elastic halfspace is represented here by the viscous damper (with bedrock properties).



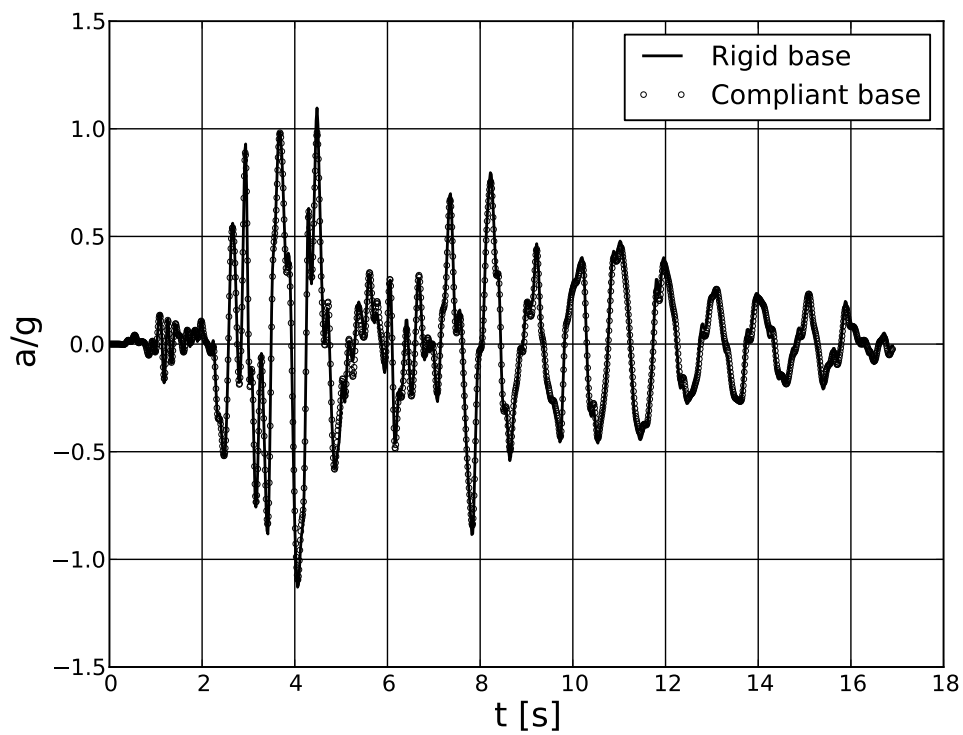
Rigid base and compliant base model



Analytical and numerical solutions for rigid base and compliant base models for $E = E1 = 2000000$ kPa in bedrock



Analytical and numerical solutions for rigid base and compliant base models for $E = E1 = 30000000$ kPa in bedrock




Analytical and numerical solutions for rigid base and compliant base models for
 $E = E1 = 300000000000 \text{ kPa}$ in bedrock

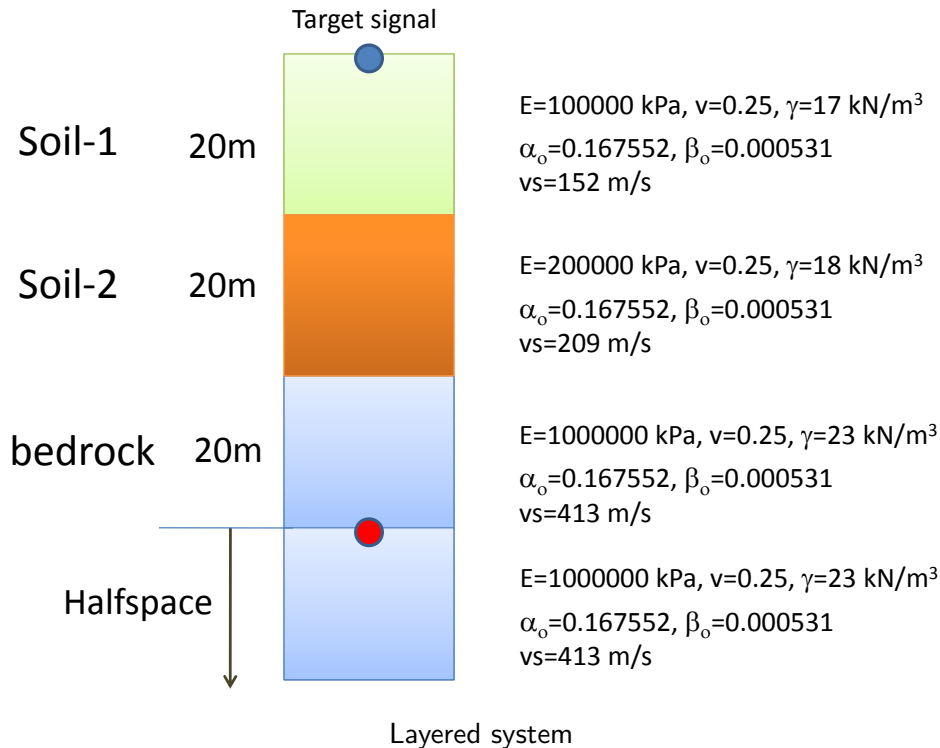
The above figures indicate that the compliant base model converges to the rigid one but for bedrock stiffness that is very large and usually far away from the real values measured in experiments.

6.8.6 Rigid vs compliant base models

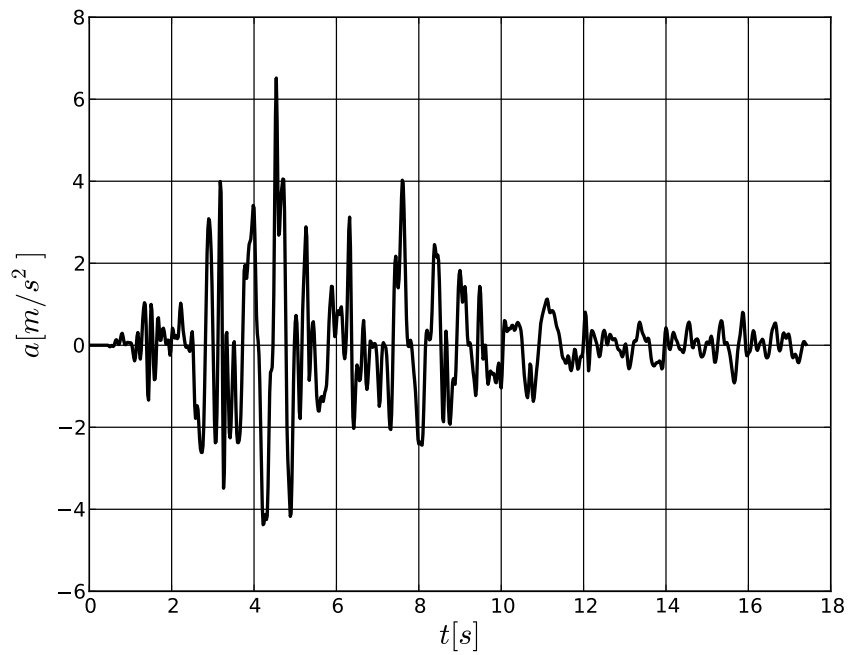
Files:

DYN-TR-3Layers-compliant-base-damp.inp,
 DYN-TR-3Layers-compliant-base-damp-spurious.inp,
 DYN-TR-3Layers-rigid-base-damp.inp,
 DYN-TR-3Layers-rigid-base-damp-spurious.inp

In this benchmark we will perform deconvolution analysis of LomaPrieta-18-10-1989-Station-Corralitos signal from surface to the base of two models ie. rigid base and compliant base one. Then this signal will be applied at the base of aforementioned two models and convolution analysis will be carried out but with small (10%) perturbation of shear wave velocity in the first soil layer. The main goal is to assess sensitivity of the two models to the introduced error. This analysis is carried out for a system shown in the figure below. Each layer is discretized using 40 Q4 elements (element size is 0.5m). Earthquake record in the rigid base model is defined through the imposed boundary conditions (imposed acceleration a_x) while in the compliant base model signal is introduced through Seismic input option and  **Compliant base model** set ON. This way computed accelerations in both cases are total ones. At all nodes, except base ones, periodic boundary condition is used to represent shear layer deformation mode.

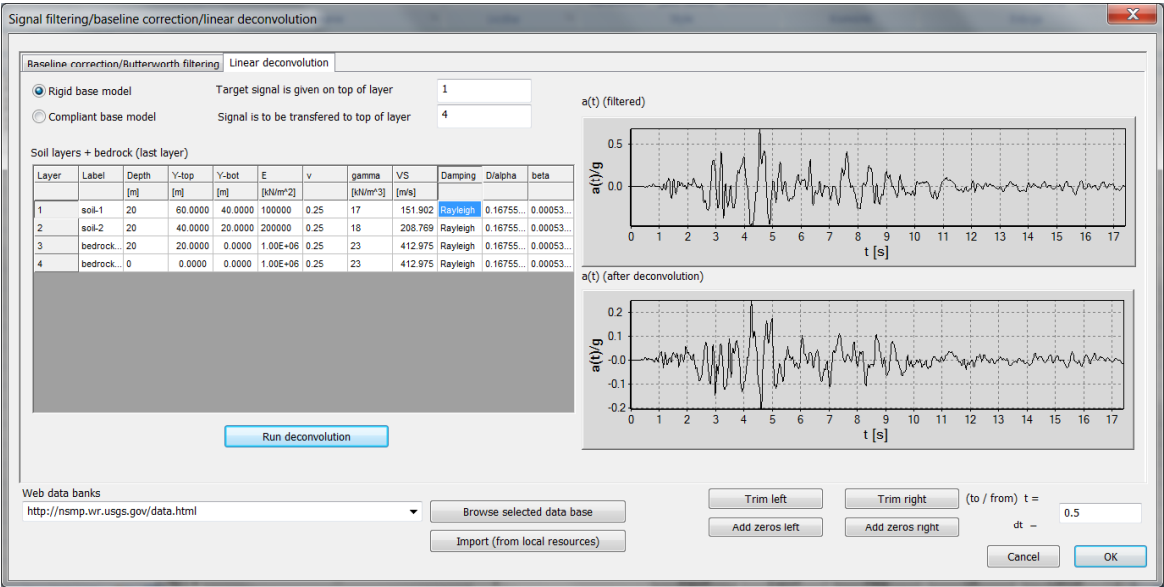


The original signal (LomaPrieta-18-10-1989-Station-Corralitos) is filtered with 10 Hz low pass Butterworth filter and baseline corrected first, then deconvolution procedure is run from Acceleration time history toolbox. As the acceleration record shows significant nonzero values from the very beginning, therefore it is recommended to add a quiet zone using option **Add zeros left**. In this example 0.5s was added to the record (see figure).

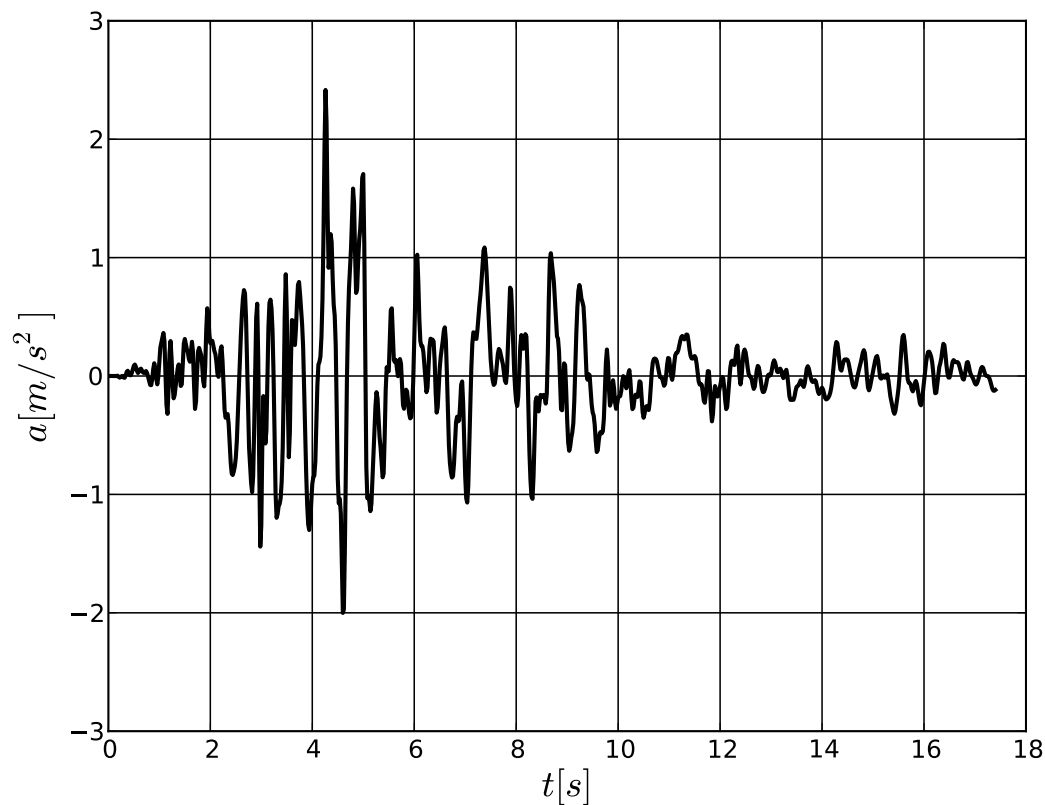


Signal after filtering and baseline correction (assumed at ground surface)(target earthquake)

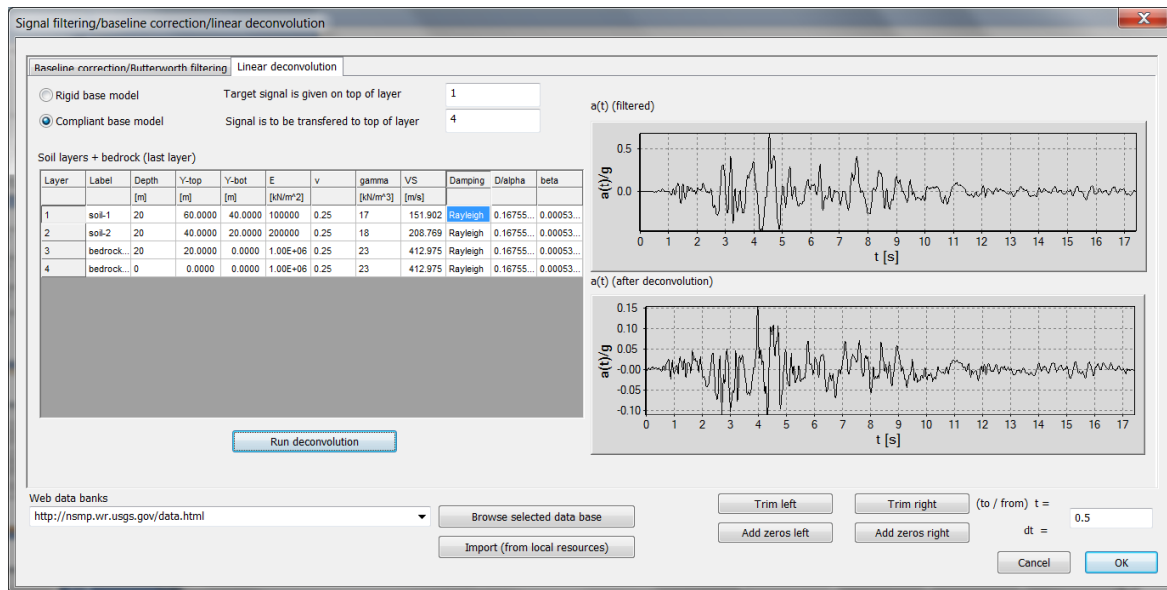
Data set for deconvolution procedure for rigid and compliant base models are shown in figures below (data in the fourth row corresponds to the elastic halfspace, although for rigid base model it is not meaningful).



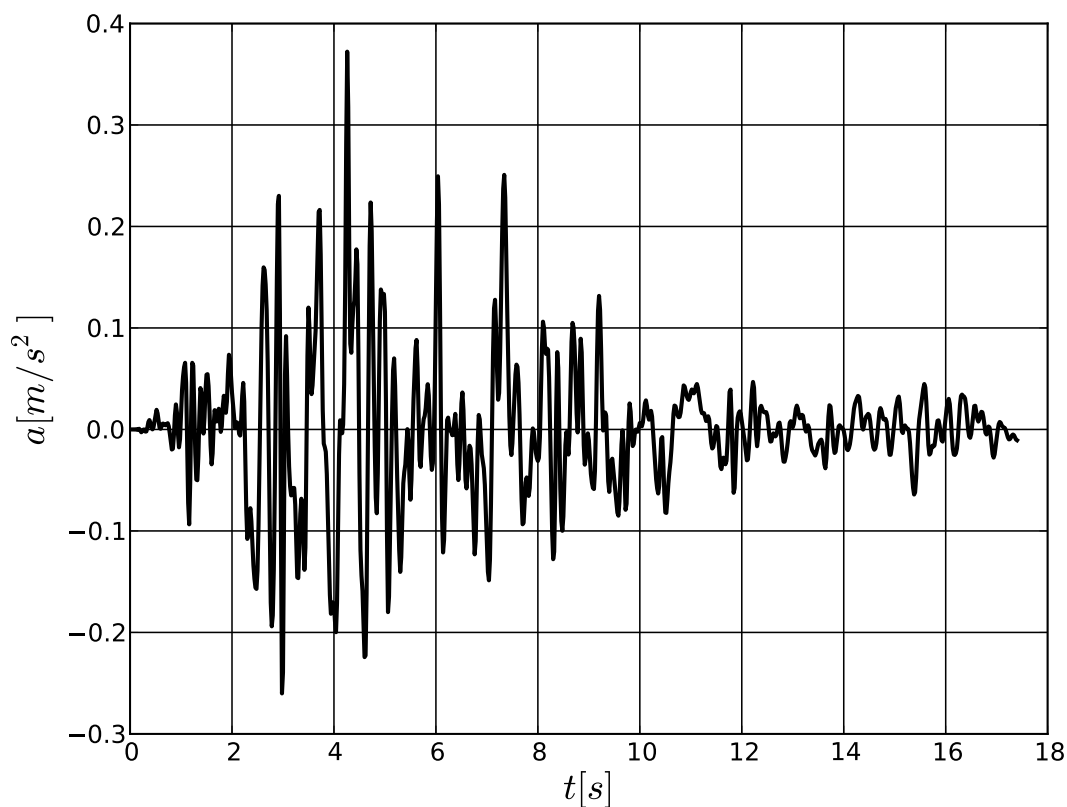
Data setup for deconvolution of Loma Prieta signal from surface to the base of rigid base FE model



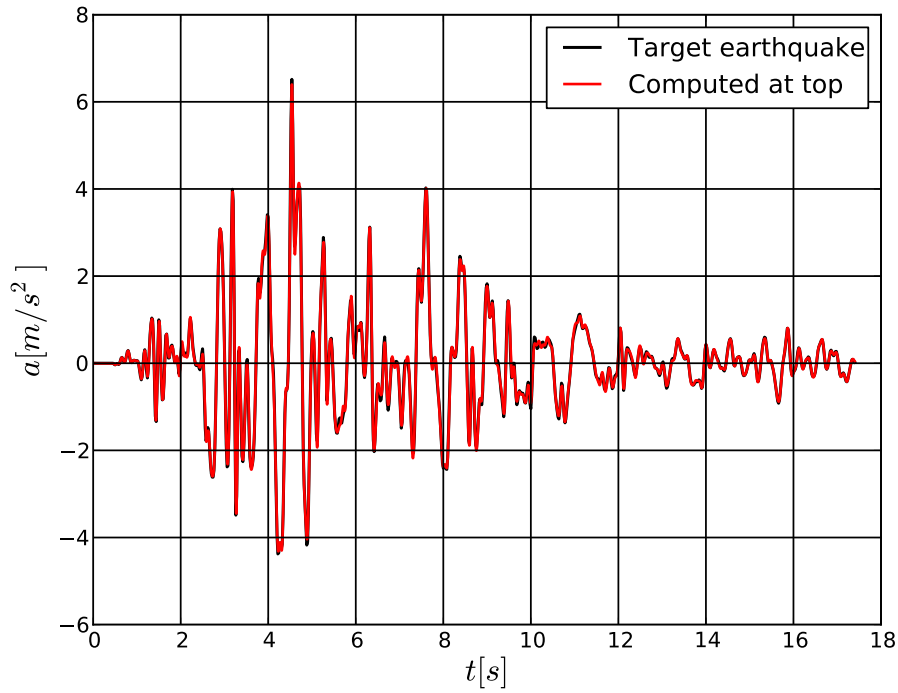
Signal after deconvolution for rigid base model



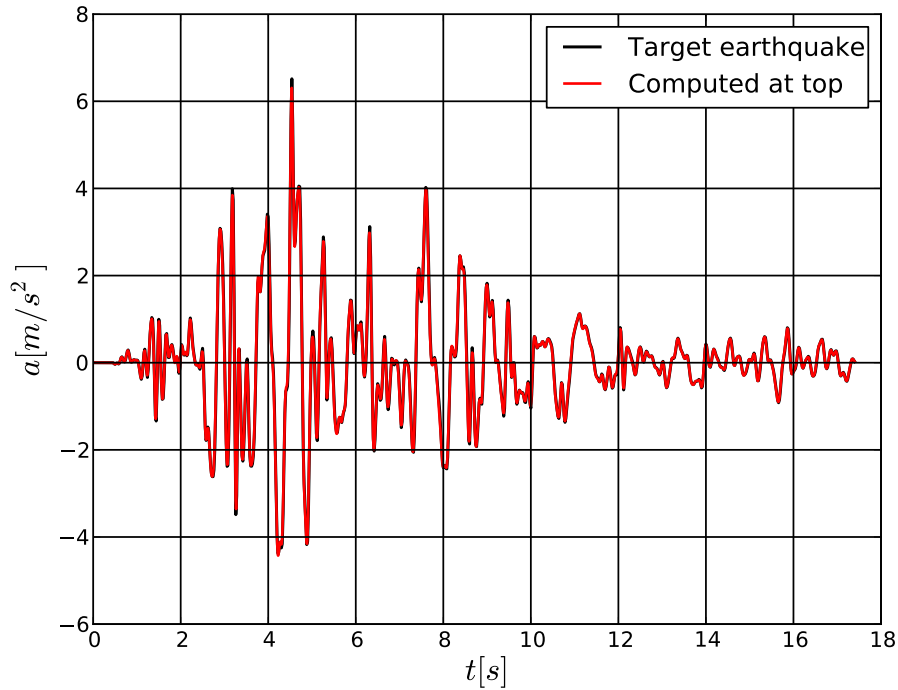
Data setup for deconvolution of Loma Prieta signal from surface to the base of compliant base FE model



Comparison of target earthquake record and computed one for rigid base and compliant base models are shown in next two figures.

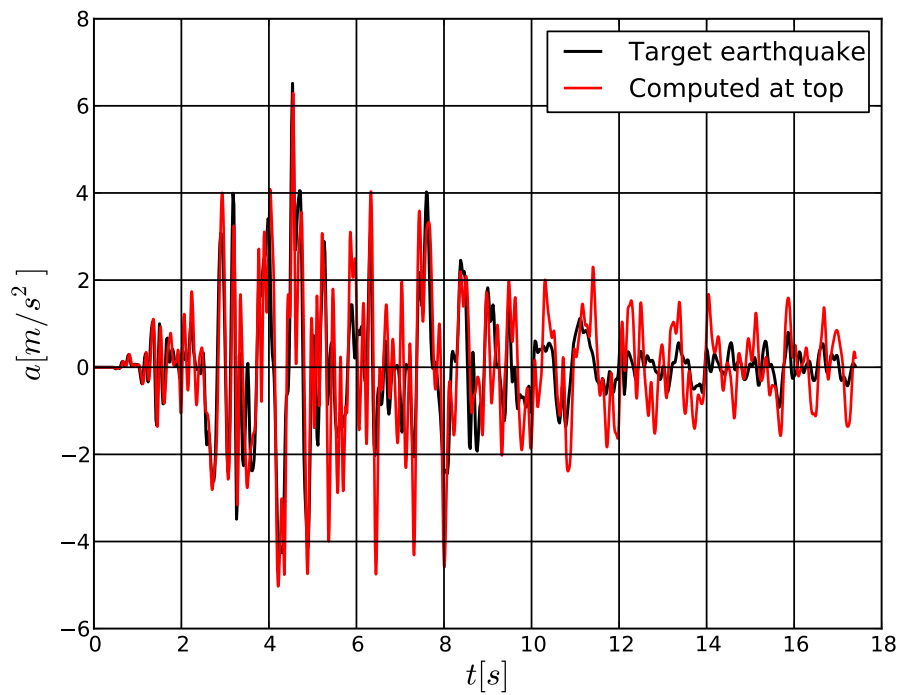


Analytical and numerical solutions for acceleration $a_x(t)$ at free surface for rigid base model

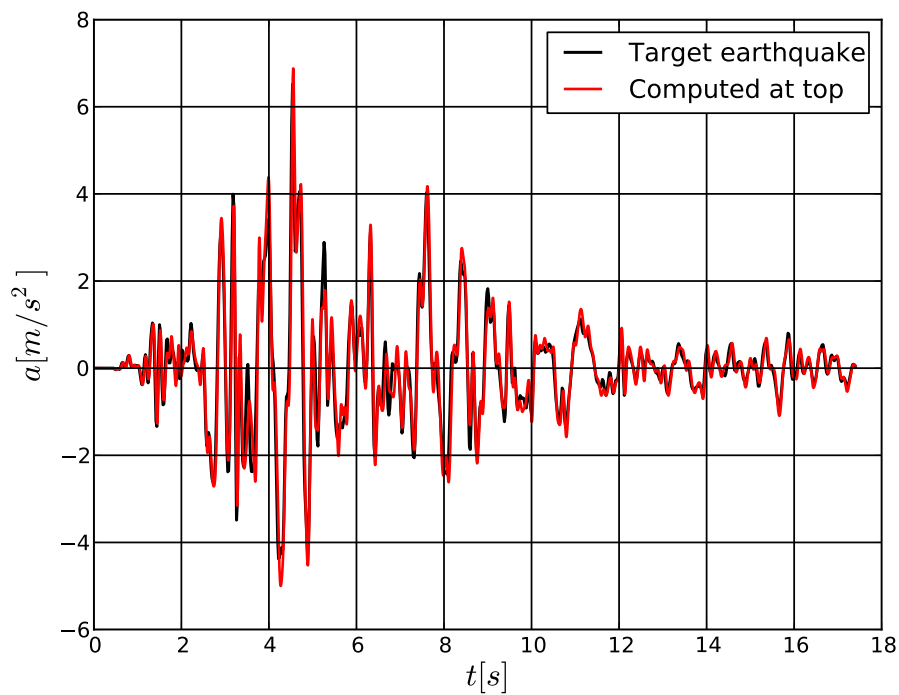


Analytical and numerical solutions for acceleration $a_x(t)$ at free surface for compliant base model

Comparison of target earthquake record and computed one for rigid base and compliant base models including stiffness perturbation in the first layer ($E_1 = 81000$ kPa) are shown in next two figures. One may observe that compliant base model is relatively insensitive to the introduced error while rigid base one shows significant discrepancies after 8s of shaking. This effect becomes very strong for low level of material damping.



Analytical and numerical solutions for acceleration $a_x(t)$ at free surface for perturbed rigid base model



Analytical and numerical solutions for acceleration $a_x(t)$ at free surface for perturbed compliant base model

Bibliography

- [1] J. Bielak, K. Loukakis, Y. Hisada, and C. Youshimura. Domain reduction method for three-dimensional earthquake modeling in localized regions. part i: Theory. *Bulletin of the seismological Society of America*, 93:817–824, 2003.
- [2] R. W. Clough and J. Penzien. *Dynamics of structures*. McGraw-Hill International Editions, 1975.
- [3] H. M. Hilber, T. J. R. Hughes, and R. L. Taylor. Improved numerical dissipation for time integration algorithms in structural dynamics. *Earthquake Engineering & Structural Dynamics*, 5:283–292, 1977.
- [4] T. J. R. Hughes. *The finite element method. Linear Static and Dynamic Finite Element Analysis*. Prentice Hall, Inc. A Division of Simon & Schuster, Englewood Cliffs, New Jersey 07632, 1987.
- [5] S. Kantoe. *Development of time integration schemes and advanced boundary conditions for dynamic analysis*. PhD thesis, Department of Civil and Environmental Engineering, Imperial College of Science, Technology and Medicine, London, SW7 2BU, May 2006.
- [6] S. L. Kramer. *Geotechnical Earthquake Engineering*. Prentice-Hall, Inc., Upper Saddle River, NJ07458, 1996.
- [7] L. Mejia and E. Dawson. Earthquake deconvolution for flac. paper 04-10. In *4th International FLAC Symposium on Numerical Modeling in Geomechanics*, pages 2–9, Minneapolis, 2006.
- [8] H. Modaressi and I. Benzenati. Paraxial approximation for poroelastic media. *Soil Dynamics and Earthquake Engineering*, 13:117–129, 1994.
- [9] M. Preisig. Nonlinear finite element analysis of dynamic soil-foundation-structure interaction, 2005.
- [10] A. Sawicki and W. Swidziński. Mechanics of sandy subsopil subjected to cyclic loadings. *International Journal for Numerical and Analytical Methods in Geomechanics*, 13:511–529, 1989.
- [11] C. Youshimura, J. Bielak, Y. Hisada, and A. Fernandez. Domain reduction method for three-dimensional earthquake modeling in localized regions. part ii: Verification and applications. *Bulletin of the seismological Society of America*, 93:825–840, 2003.
- [12] O. Zienkiewicz, A. Chan, M. Pastor, B. Schrefler, and T. Shiomi. *Computational Geomechanics with Special Reference to Earthquake Engineering*. John Wiley & Sons Ltd, 1999.
- [13] O. Zienkiewicz, A. H. C. Chan, M. Pastor, B. A. Schrefler, and T. Shiomi. *Computational Geomechanics with special Reference to Earthquake Engineering*. John Wiley & Sons, West Sussex PO19 1UD, England, 1999.